Metal-Sulfur Compounds in N_2 Reduction and Nitrogenase-Related Chemistry

Kazuki Tanifuji[1] and Yasuhiro Ohki[2]*

[1] Department of Molecular Biology and Biochemistry, University of California, Irvine, Irvine, CA 92697-3900, United States

[2] Department of Chemsitry, Graduate School of Science, Nagoya University, Furo-cho, Chikusa-ku, Nagoya 464-8602, Japan

e-mail: ohki@chem.nagoya-u.ac.jp

Abstract

Transition metal-sulfur (M-S) compounds are an indispensable means for biological systems to convert N_2 into NH_3 (biological N_2 fixation), and these may have emerged by chemical evolution from a pre-biotic N_2 fixation system. With a main focus on synthetic species, this article provides a comprehensive review of the chemistry of M-S compounds related to the conversion of N_2 and the structures/functions of the nitrogenase cofactors. Three classes of M-S compounds are highlighted here: multi-nuclear M-S clusters structurally or functionally relevant to the nitrogenase cofactors; mono- and di-nuclear transition metal complexes supported by sulfur-containing ligands in N_2 and N_2H_x (x = 2, 4) chemistry; metal sulfide-based solid materials employed in the reduction of N_2. Fair assessments on these classes of compounds revealed that our understanding is still limited in N_2 reduction and related substrate reductions. Our aims of this review are to compile a collection of studies performed at atomic to mesoscopic scales and to present potential opportunities for elucidating the roles of metal and sulfur atoms in the biological N_2 fixation that might be helpful for the development of functional materials.

A Table of contents

1 Introduction

Nitrogen is an essential element for key biomolecules such as proteins, DNAs, and RNAs. Despite the necessity of nitrogen to maintain life, readily bioavailable forms of nitrogen such as NH_3 and NO_3^- are estimated to occupy only ~$9 \cdot 10^{-3}$ % of the Earth's total atomic inventory[1] and are continuously converted into stable N_2 through nitrification and denitrification processes. As most organisms do not contain metabolic systems to utilize N_2 but simply take up ready-to-use N sources from their surroundings, the conversion of N_2 into NH_3, or N_2 fixation, is an imperative process to sustain the global nitrogen cycle. Nitrogenase is the only known enzyme that catalyzes this difficult chemical conversion by utilizing redox-active M-S cofactors and adenosine triphosphate (ATP). All three known variants, Mo-, V-, and Fe-nitrogenases, commonly consist of two independent soluble proteins, a specific electron carrier component and a catalytic component, and both protein components contain M-S clusters. As shown in an example of the best characterized variant (Mo-nitrogenase, **Figure 1**), electrons generated from cellular metabolism are transferred from the [Fe_4S_4] cluster of the homodimeric electron carrier component, the Fe protein,[2,3] to the heterotetrameric MoFe protein, which represents the catalytic component. Within the MoFe protein, the P-cluster ([Fe_8S_7] cluster)[4,5] receives electrons from the Fe protein and transfers them to the active site FeMo-cofactor,[6,7,8] which is often abbreviated as FeMoco or M-cluster. The overall electron-transfer process is ATP-dependent, and the Fe protein features two ATP-binding sites. Upon binding of two ATP molecules, the Fe protein associates with the MoFe protein[9,10] and delivers an electron to the MoFe protein. The subsequent hydrolysis of ATP has been postulated to lead to a conformational change that induces dissociation of the Fe protein from the MoFe protein.[11] Upon repetition of this electron transfer process, the MoFe protein accumulates electrons for the reduction of N_2 into two NH_3 molecules, supposedly with the obligate production of a H_2 molecule (**Figure 1**).

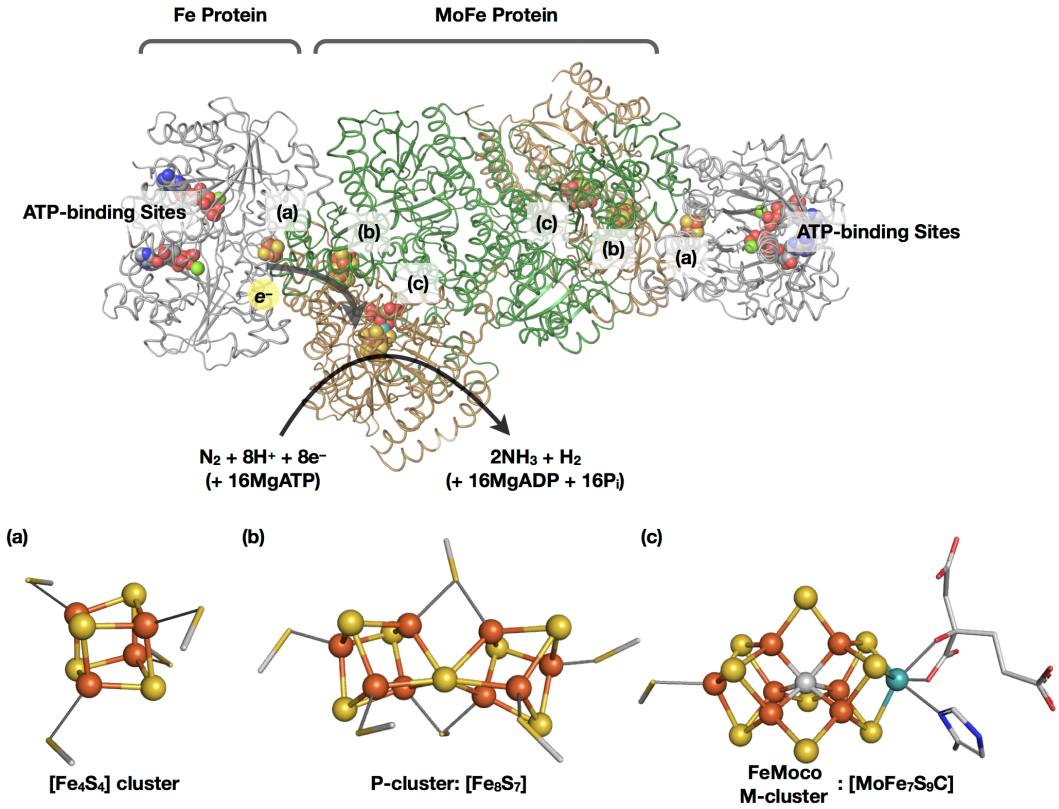

Figure 1. Schematic drawing of the association complex between Fe protein and MoFe protein of Mo-nitrogenase and their metallo-cofactors: (a) $[Fe_4S_4]$ cluster of the Fe protein, (b) P-cluster and (c) FeMoco of the MoFe protein. The cofactors and protein-bound ATP analogues in the association complex are shown as spheres. Expanded structures of the metallo-clusters are illustrated with ball-and-stick models. PDB ID: 4WZA and 3U7Q. Color legend of molecules shown in sphere and ball-and-stick descriptions: Blue, N; gray, C; green, Mg; orange, Fe; red, O; teal, Mo; yellow, S.

The structures of FeMoco and FeV-cofactor (FeVco), which are the active sites of Mo- and V-nitrogenases,[12,13] respectively, showed that they are exclusive examples of carbon-centered high-nuclearity metal-sulfur clusters (**Figure 2**). Their core compositions are $[(cit)MoFe_7S_9C]$ and $[(cit)VFe_7S_8(CO_3)C]$ (cit = *R*-homocitrate), and both clusters can be seen as fused forms of two $[M_4S_3C]$ cubes (M = Fe/Mo/V), which share the central μ_6-C atom and are additionally connected through inter-cubane ligands in the middle of the cores, *i.e.* three sulfides (for FeMoco) or two sulfides and a carbonate (for FeVco). One of the peripheral metals in FeM'co (M' = Mo or V) is Mo or V bearing

an *R*-homocitrate ligand, making the inorganic cores of FeM'co asymmetric. Environments around the inorganic cores are also asymmetric by virtue of the protein backbones and the hydrogen bonds to the cores. Each FeM'co is immobilized in the protein scaffold through a histidine on the Mo/V site and a cysteine on the opposite Fe site (**Figure 2**). Although the active site of Fe-nitrogenase is not yet crystallographically characterized, its structure has been proposed to be analogous to FeM'co but containing only Fe as transition metals.[14,15]

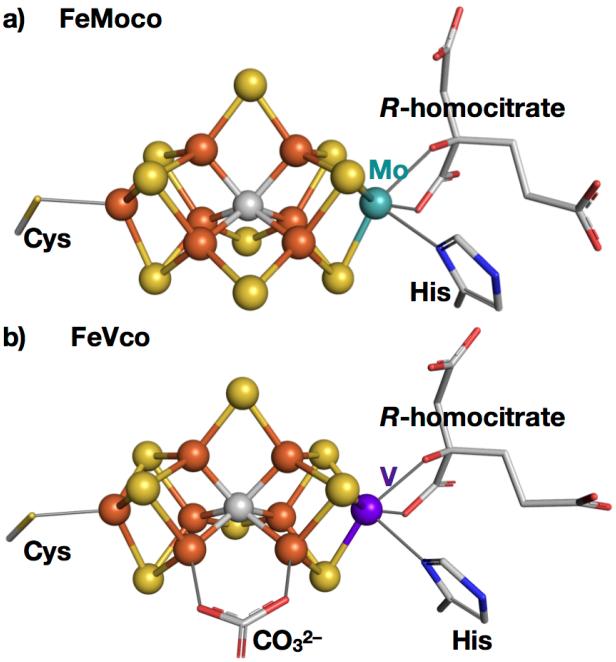

Figure 2. Structures of a) FeMoco from Mo-nitrogenase and b) FeVco from V-nitrogenase. Metal and sulfur atoms in the cores are displayed in ball-and-stick representation; protein residues and supporting ligands around the cores are shown in stick format. PDB ID: 3U7Q and 5N6Y. Color legend: Blue, N; gray, C; orange, Fe; purple, V; red, O; teal, Mo; yellow, S.

As there are only subtle differences between the structures of FeMoco and FeVco, the Mo- and V-nitrogenases have been suggested to share a mechanism for N_2 transformation to a substantial degree. Deliveries of electrons/protons during the enzymatic reactions have been postulated to follow the Thorneley-Lowe scheme, which is based upon extensive kinetic data from the catalysis of Mo-nitrogenase (**Figure 3a**).[16,17] In the latest proposal, the four-electron-reduced E_4 state of FeMoco

(also designated the *Janus intermediate*)[17] has been proposed to possess two Fe-bridging hydrides and reversibly bind N_2 with simultaneous elimination of hydrides as H_2.[17,18,19] Afterwards, four additional electrons/protons are delivered to the active site to produce two molecules of NH_3 and regenerate the starting E_0 state. The cycle therefore consists of eight electron/proton transfer steps in total.

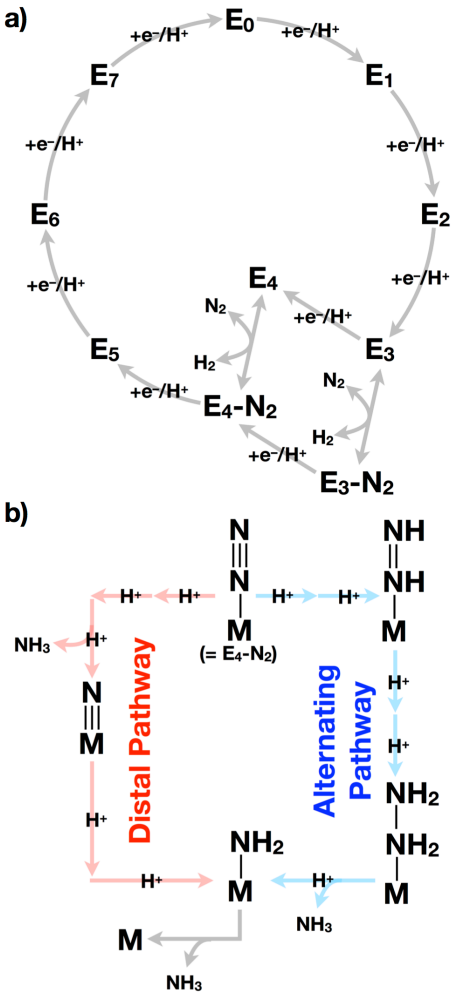

Figure 3. a) Simplified illustration of the Thorneley-Lowe scheme of nitrogenase mechanism and b) proposed "distal" and "alternating" pathways for N_2 reduction. In figure a), the protonation levels (*e.g.* E_3H_3) and relaxation pathways for H_2 evolution, included in the original Thorneley-Lowe scheme, are omitted for clarity.

With regard to a detailed reaction pathway after binding of N_2 to the E_4 state of FeMoco, there are two proposals for how N_2 is protonated and reduced to eventually produce two NH_3 molecules (**Figure 3b**). The "distal" pathway, originally proposed as the Chatt cycle for the protonation of N_2 in $[M(PMe_2Ph)_4(N_2)_2]$ (M = Mo, W),[20,21] assumes that the terminal N atom of N_2 is protonated until the first NH_3 is released. Then, the remaining metal-nitride (M≡N) species uptakes protons to yield the second NH_3. In contrast, the "alternating" pathway is based on the hypothesis that both N atoms of N_2 are alternatively protonated to gradually produce diazene (HN=NH, N_2H_2) and then hydrazine ($H_2N–NH_2$, N_2H_4) before the formation of NH_3. Given the relatively symmetric reactivity of N atoms in this pathway, interaction of both N atoms of N_2 with two (or more) metal atoms would be preferable.[22] Some experimental results are in favor of the "alternating" pathway. For instance, quenching of the pre-steady state of Mo-nitrogenase under turnover conditions gives rise to hydrazine.[16] Additional support comes from work with V-nitrogenase, which produces hydrazine in addition to NH_3 under N_2-reducing conditions particularly at elevated temperatures.[23,24] Furthermore, the Mo-nitrogenase is known to convert both diazene and hydrazine to NH_3.[16] These results are compatible with the "alternating" mechanism, but the lack of direct observation of partially reduced N_2 species on FeMoco that could distinguish between the distal and alternating pathways prevents us from concluding the discussion.

Abiochemical approaches have also been useful (a) to better comprehend the nitrogenase mechanism at the molecular level, (b) to uncover the requirements for stoichiometric and catalytic N_2 activation, or (c) to link the concepts of N_2 conversion among biological, artificial, and tentative pre-biotic systems. For example, theoretical calculations have predicted the substrate/product binding modes and reaction steps of the nitrogenase mechanism,[25,26,27,28,29,30] and various transition metal complexes have been synthesized to demonstrate N_2 activation and to understand how N_2 is captured and transformed.[22,31,32] Given the importance of metal-sulfur compounds in biological N_2 fixation and the potential significance of metal-sulfide materials in the pre-biotic chemical evolution, we summarize herein the N_2 chemistry and the nitrogenase-related chemistry of sulfur-containing inorganic compounds. Topics covered in this review include: synthetic M-S clusters modeling or mimicking nitrogenase cofactors and their properties with reactivity studies (**section 2**), transition metal complexes supported by S-based ligands in N_2 or N_2H_x (x = 2, 4) chemistry (**section 3**), and solid metal-sulfide materials promoting N_2 reduction (**section 4**).

2. Metal-Sulfur Clusters in Nitrogenase-Related Chemistry

Even though the reduction of N_2 into NH_3 by H_2 or protons and electrons is both exergonic, N_2 can be viewed as a significantly inert molecule due to its strong N–N triple bond (bond dissociation energy: 941.7 kJ/mol) and its fairly negative equilibrium potentials of one- and two-electron reduction in aqueous media.[33] In this sense, nitrogen fixation is recognized as one of the most difficult enzymatic reactions. The biological cofactors catalyzing this reaction, FeMoco and FeVco, are the largest metallo-cofactors identified thus far in proteins and have unique elemental compositions and core structures. These features provoke the idea that the complex structures of cofactors correlate with their N_2-reducing functions, and thus lead to the emergence of modeling approaches for the structures of nitrogenase cofactors. Furthermore, FeMoco,[34] FeVco,[35] and their biosynthetic precursors[36,37] are extractable from the host protein scaffolds, suggesting the stability and synthetic accessibility of these metal-sulfur clusters as molecular entities. Chemical synthesis of cofactor analogues should offer some advantageous perspectives that help to gain insight into the relationship between the structures and functions of cofactors, *e.g.* preparation of sufficient amount of materials for detailed investigation into physical properties, collection of information focusing on the target metal-sulfur cluster without obscuring noise from protein backbones or different inorganic moieties, and modification of the structures to control the properties and reactivity. The complex structures of FeMoco and FeVco have also generated a great deal of interest as synthetic targets, but their precise synthesis still remains elusive. This section covers structural mimics of nitrogenase metallo-clusters and some biomimetic metal-sulfur clusters revealing nitrogenase-related reactivity that have been previously addressed in review articles based on relevant perspectives.[38,39,40,41,42,43,44,45] Small metal-sulfur complexes mimicking the functions or local structures of nitrogenase clusters will be described in **section 3**.

2.1 Synthetic Clusters Structurally Relevant to the Nitrogenase Cofactors

Over decades, researchers have strived to develop synthetic methodologies for producing precise models of nitrogenase clusters. Major synthetic strategies for multi-nuclear metal-sulfur clusters relevant to FeMoco and FeVco can be categorized into the following three classes: (1) assembly or fusion of cuboidal clusters, (2) growth of metal-sulfur frameworks on template trisulfide complexes,

and (3) assembly reactions in non-polar media. Although more than 150 M-Fe-S (M = Mo, V) clusters have been synthesized to date, here we focus on those closely relevant to strategies (1)-(3) (**Chart 1**), while some M-Fe-S clusters mimicking the local structures of FeMoco and FeVco are also addressed. The following subsections overview these strategies and point out some issues that are still needed to reproduce the structures of FeMoco and FeVco. Unfortunately, adducts with N_2 or alkynes have not been synthesized from the M-Fe-S clusters in this section.

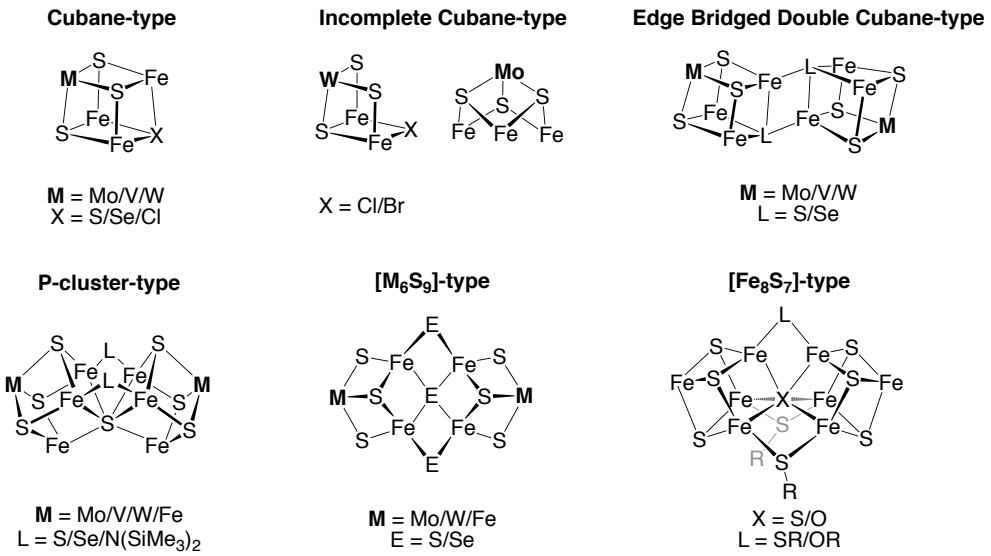

Chart 1. Core structures of representative synthetic metal-sulfur clusters in this section. Most of the terminal ligands are omitted for clarity.

2.1.1 High-Nuclearity Metal-Sulfur clusters from Cuboidal Clusters

2.1.1.1 $[MoFe_3S_4]$ and $[VFe_3S_4]$ Cubanes as Precursors or Partial Structural Analogues of Nitrogenase Cofactors

Cuboidal compounds are a representative class of metal-sulfur clusters in both synthetic chemistry and biology. In fact, early synthetic studies of Mo-Fe-S clusters, initiated in the late 1970s, provided various cubic clusters typically from assembly reactions of $[MoS_4]^{2-}/FeCl_3/NaSR$ that were developed simultaneously by the groups of Holm and Garner.[46,47,48,49,50,51] However, the exact nature of FeMoco was unknown at this point due to a lack of the relevant protein crystallography. These reactions gave rise to double-cubane $[MoFe_3S_4]_2$ clusters such as $[[MoFe_3S_4(SR)_3]_2(\mu\text{-}SR)_3]^{3-}$, $[[MoFe_3S_4(SR)_3]_2(\mu$-

$SR)_2(\mu\text{-}S)]^{3-}$, $[[MoFe_3S_4(SR)_3]_2(\mu\text{-}OMe)_3]^{3-}$, and $[[MoFe_3S_4(SR)_3]_2\{(\mu\text{-}SR)_3Fe(\mu\text{-}SR)_3\}]^{3-/4-}$ (**1**; R = Et, *Z* = 3–), in which two Mo atoms are connected through thiolate/sulfide, alkoxide, or $Fe(SR)_6$ (**Scheme 1**). The interconnected double-cubane clusters were split into two $[MoFe_3S_4]$ cubes in the presence of appropriate chelating ligands for Mo. Thus Holm *et al.* achieved the introduction of tetrachloro-catecholate (Cl_4-cat) and the substitution of thiolates to chlorides in **1** to afford a monomeric cubane, $[(Cl_4\text{-cat})(MeCN)MoFe_3S_4Cl_3]^{2-}$ (**2**) (**Scheme 2**).[52] After the first crystal structure of the MoFe protein was reported in 1992, showing a rough framework of FeMoco,[53] this approach was modified to reproduce the first coordination sphere of Mo in FeMoco: six-coordinate with $(OON)Mo(S)_3$ coordination environment. For example, Evans and coworkers added imidazole (Imi) to $[(Cl_4\text{-cat})(MeCN)MoFe_3S_4(SEt)_3]^{2-}$ to furnish $[(Cl_4\text{-cat})(Imi)MoFe_3S_4(SEt)_3]^{2-}$ (**3**),[54] while replacement of Cl_4-cat and MeCN in **2** with a tridentate *N*-methyliminodiacetate ligand (meida) was examined by Coucouvanis and Demadis to provide $[(meida)MoFe_3S_4Cl_3]^{2-}$ (**4**) (**Scheme 2**).[55] The Mo centers of both **3** and **4** interact with two O and one N atoms in addition to three sulfides and adopt a six-coordinate octahedral $(OON)Mo(S)_3$ coordination geometry. The reaction of **2** with $[NEt_4][citrate]$, which is an analogue of *R*-homocitrate on the Mo atom of FeMoco, led to the replacement of Cl_4-cat and MeCN to provide $[(citrate)MoFe_3S_4Cl_3]^{3-}$ (**5**) (**Scheme 2**).[55] While the structure of **5** was not crystallographically determined, the tridentate O,O,O-coordination of citrate employing two carboxylate groups has been suggested. Structural similarity of $[MoFe_3S_4]^{3+}$ clusters **2**, **4**, and **5** was supported by the comparable $S = 3/2$ features in the electron paramagnetic resonance (EPR) spectra, where *g*-values were 5.403, 2.463, and 1.903 for **2**, 4.467, 2.608, and 1.882 for **4**, and 5.403, 2.463, and 1.772 for **5**.

Scheme 1. One of the assembly reactions of $[MoS_4]^{2-}/FeCl_3/NaSR$ furnishing a double-cubane $[MoFe_3S_4]_2$ cluster **1** with a central $Fe(SR)_6$ moiety.

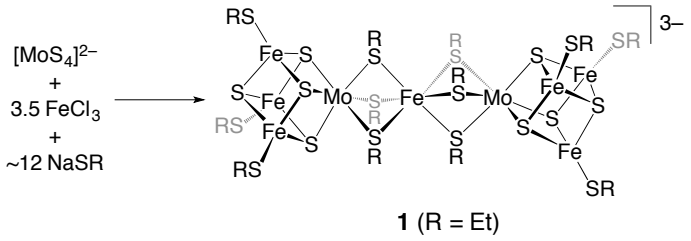

1 (R = Et)

Scheme 2. Single cubane $[MoFe_3S_4]$ clusters derived from $[(Cl_4\text{-cat})(MeCN)MoFe_3S_4Cl_3]^{2-}$ (**2**) and thiolate-supported analogues.

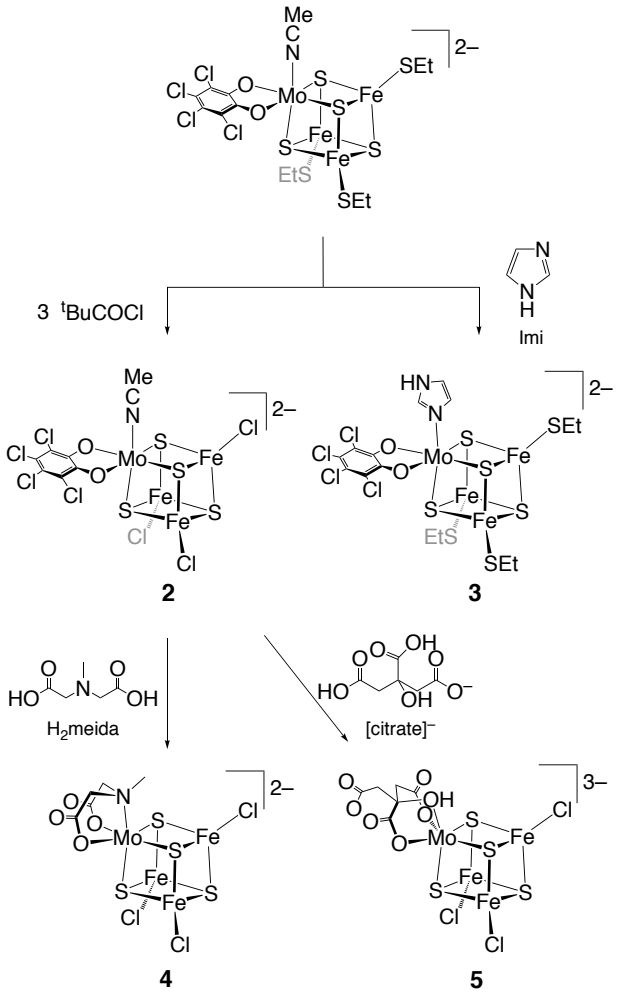

2 **3**

4 **5**

In parallel with the exploration of Mo-Fe-S clusters, V-Fe-S clusters have also been desirable synthetic targets due to the existence of the V-nitrogenase, and therefore a comparable approach to the synthesis of **1** was taken. Holm *et al.* synthesized a single cubane $[VFe_3S_4]$ cluster from sequential reactions of $[VS_4]^{3-}$ with 2 equiv. $FeCl_2$ to generate a linear trinuclear cluster $[VFe_2S_4Cl_4]^{3-}$ and the subsequent conversion into a monomeric cubane $[(DMF)_3VFe_3S_4Cl_3]^-$ (**6**; DMF = *N*,*N*-dimethylformamide) in the presence of another 2 equiv. $FeCl_2$ in DMF (**Scheme 3**).[56,57,58,59] In the latter step, $FeCl_2$ not only serves as the Fe source but also works as the reductant, which is in agreement with the requirement of a total of 4 equiv. $FeCl_2$ for incorporation of three Fe atoms of the resultant $[VFe_3S_4]$ cube. Treatment of **6** with $[S\text{-}p\text{-}C_6H_4Me]^-$ led to the selective substitution of Fe-Cl and gave $[(DMF)_3VFe_3S_4(S\text{-}p\text{-}C_6H_4Me)_3]^-$ (**7**), leaving the vanadium center unchanged (**Scheme 3**).[57] In contrast, a tridentate ONO-ligand (meida) was found to selectively bind to the V site to afford $[(meida)VFe_3S_4Cl_3]^{3-}$ (**8**) (**Scheme 3**).[60] The $[VFe_3S_4]^{2+}$ core common to **6** and **7** was suggested to be in the $S = 3/2$ configuration, based on the observation of characteristic EPR signals (g = 5.50, 3.27, and 2.04 for **7**) and temperature-dependent magnetic susceptibility of **6** that fits well with a simulated spectrum.[57] While detailed investigations were not conducted for **8**, its paramagnetism was supported by isotropically shifted methylene signals (14.9 and 6.01 ppm) in the ^{1}H NMR spectrum.

Scheme 3. Synthesis and ligand-exchange reactions of $[(DMF)_3VFe_3S_4Cl_3]^-$ (**6**).

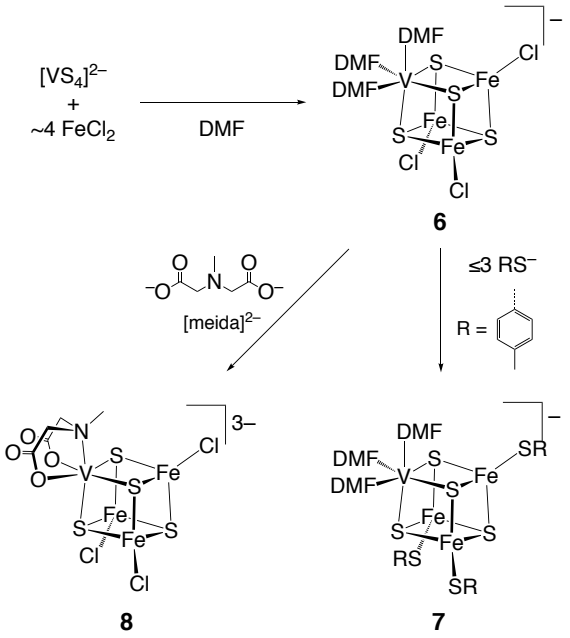

2.1.1.2 [$MoFe_3S_3$] Incomplete Cubanes

In the decade after the first crystal structure of Mo-nitrogenase was reported in 1992,[53] the core structure of FeMoco had been regarded as a center-voided [$MoFe_7S_9$] until the central light atom X was discovered in 2002 based on an improved crystallographic data set (**Figure 4**).[61] A conceptual fragmentation of the [$MoFe_7S_9$] core generates [$MoFe_3S_3$] and [Fe_4S_3] incomplete cubanes in addition to three S atoms from the inter-cubane positions, and thus the [M_4S_3]-type incomplete cubanes have been considered as suitable structural components for the FeMoco models. Even after confirmation of the [$MoFe_7S_9C$] core of FeMoco (**Figure 4**),[6] incomplete cubanes can be viewed as useful platforms for incorporation of a central μ_6-C atom.

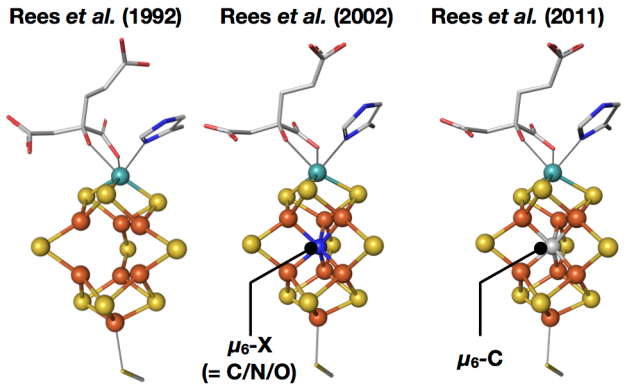

Figure 4. Chronological development of crystal structures of FeMoco. PDB ID: 1MIO, 1M1N, 3U7Q. Color legend: Blue, N; gray, C; orange, Fe; purple, V; red, O; teal, Mo; yellow, S.

A deconstructive approach was developed by Coucouvanis *et al.* for the synthesis of [$MoFe_3S_3$] incomplete cubane clusters. Treatment of an edge-bridged [$MoFe_3S_4]_2$ double-cubane cluster [{(Cl_4-cat)$MoFe_3S_4(PEt_3)_3\}_2$] (**9a**)[62] with CO under high pressure (500 psi) afforded a corner-voided [$MoFe_3S_3$] cluster [(Cl_4-cat)$MoFe_3S_3(PEt_3)_2(CO)_6$] (**10**),[63] in which the Mo atom was found to uptake an oxygen atom from Me_3NO to furnish a terminal oxo (Mo=O) moiety in [(Cl_4-cat)(O)$MoFe_3S_3(PEt_3)_2(CO)_6$] (**11**).[64] In the presence of pyridine (Pyr), the reaction of **9a** with CO produced the Pyr adduct [(Cl_4-cat)(Pyr)$MoFe_3S_3(PEt_3)_2(CO)_6$] (**12**) (**Scheme 4**),[65] which replicates the Mo coordination environment of FeMoco. From the P^nPr_3 analogue of **9a**, adducts of P^nPr_3 and

pyridine, [(Cl_4-cat)(P^nPr_3)$MoFe_3S_3$(P^nPr_3)$_2$($CO)_6$] (**13**) and [(Cl_4-cat)(Pyr)$MoFe_3S_3$(P^nPr_3)$_2$($CO)_6$] (**14**), were obtained (**Scheme 4**).[64,65] In these reactions, phosphines work as desulfurization agents to dissociate phosphine sulfides (S=PR_3) and concurrently reduce the inorganic core. The series of clusters **10**-**14** share the [$MoFe_3S_3$]-type incomplete cubane structure supported by a Mo-bound bidentate Cl_4-cat ligand. The overall [$MoFe_3S_3$] core geometry is related to those of an NO-bound [Fe_4S_3] cluster designated as *Roussin's black anion* ([$Fe_4S_3(NO)_7]^-$),[66,67] as well as a unique [Fe_4S_3] cluster found in an O_2-tolerant [NiFe] hydrogenase from *Ralstonia eutropha*.[68,69] Interestingly, the number of CO ligands on the [$MoFe_3S_3$] core varies in the 4-6 range by subtle changes in the combination of ligands and reaction conditions. For example, from the reaction mixture containing **10** as the major component, an oxo cluster **11** with a different PEt_3/CO ligand set was obtained by simple extension of the reaction time. Variation in the numbers of PR_3/CO/Pyr and oxo ligands leads to various total electron counts, *i.e.* 60 valence electrons (VE) for **14**, 62 VE for **10**, **12**, and **13**, and 66 VE for the oxo cluster **11**, that affect the metal-metal interactions in the [$MoFe_3S_3$] core. The 60 VE cluster **14** shows 3Fe-Fe(*s*) (*s* = short) and 2Mo-Fe(*s*)/1Mo-Fe(*m*) (*m* = moderate) distances, while in the 62 VE clusters one of the Fe-Fe interactions is apparently broken to reveal 2Fe-Fe(*m*) and 1Mo-Fe(*s*)/2Mo-Fe(*m*) distances. In the oxo cluster **11** with 66 VE, two Mo-Fe interactions are additionally broken to exhibit 2Fe-Fe(*s*) and 1Mo-Fe(*m*) distances. Formal oxidation states of **10** and **12**-**14** can be described as Mo^{III}-$2Fe^{II}$-Fe^{I} or Mo^{IV}-Fe^{II}-$2Fe^{I}$ containing at least one Fe^{I} center, and these should be stabilized by the CO ligands. Because of the extensive back-bonding from Fe to these ligands, the ^{57}Fe Mössbauer signals of **10** and **12**-**14** gave low isomer shift (δ) values at 0.053-0.135 mm/s. These values are within the standard range of six-coordinate, monomeric Fe-(CO, PR_3) and Fe-(NO, CO) species.

Scheme 4. Synthesis of $[MoFe_3S_3]$ incomplete cubane clusters from edge-bridged $[MoFe_3S_4]_2$ double-cubane clusters.

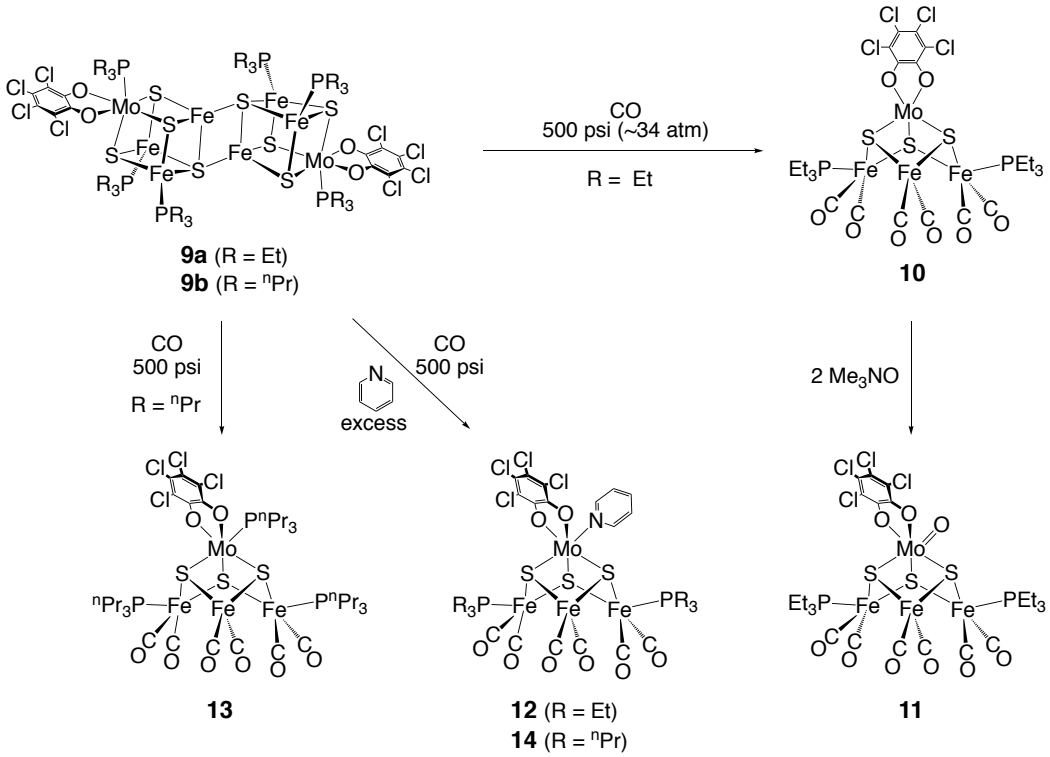

The $[M_4S_3]$ class of clusters may define the two halves of FeM'co (M' = Mo, V). Therefore, linkage of two $[M_4S_3]$ clusters with an interstitial carbide and three sulfides offers a putative synthetic route to precise FeM'co analogues. A possible future challenge we propose along this line is to apply a bio-mimetic methyl transfer from a sulfonium ion $[H_3C\text{-}SRR']^+$, by taking advantage of the reduced nature of the $[MoFe_3S_3]$ clusters **10-14** or their analogues. In an early stage of the biosynthesis of FeMoco, transfer of the CH_3 group of *S*-adenosyl-L-methionine (SAM, **Figure 5**) has been suggested to occur through an S_N2-type reaction employing one of the sulfides of the $[Fe_4S_4]$ cubes as a nucleophile.[70] Due to the cationic (sulfonium) character of SAM, clusters in the reduced states and/or with more negative charges would be suitable for this reaction. Reduced clusters can alternatively facilitate the direct addition of a CH_3 group to a metal center (nucleophilic oxidative addition). The resultant oxidation of the cluster probably leads to spontaneous dissociation of CO due to the less extent of back-bonding from Fe.

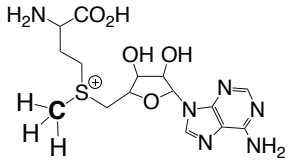

Figure 5. *S*-adenosyl-L-methionine (SAM), which is the source of the central carbide of FeMoco.

2.1.1.3 Core Fusion of Cuboidal Clusters

Metal-sulfur clusters with higher nuclearities are accessible from a modular approach employing cuboidal cores. As exemplified with an edge-bridged $[MoFe_3S_4]_2$ double-cubane cluster **9**,[62] assembly of cubic $[MFe_3S_4]$ (M = Mo, V) and $[Fe_4S_4]$ clusters sometimes occurs under reducing conditions or by the use of reduced cubic clusters. It is also interesting to note that core-fusion of two cubes is highly relevant to the recently elucidated biosynthetic pathways[71,72,73] for the nitrogenase P-cluster[74,75,76] and FeMoco.[6,36,70,77] The precursors for FeMoco are a pair of conventional $[Fe_4S_4]$ clusters, which are coupled into an intermediate $[Fe_8S_9C]$ cluster (L-cluster) via incorporation of one carbon and one sulfur atom. Then, one of the peripheral Fe atoms of the $[Fe_8S_9C]$ core is replaced by Mo to furnish the $[MoFe_7S_9C]$ core of FeMoco, which is finally transferred to the designated catalytic protein. Small molecule approaches to imitate such biological core conversion reactions are desirable not only to develop synthetic methods for FeMoco analogues but also to understand the metal-sulfur chemistry in protein scaffolds. Herein we review the core-fusion approaches with M-Fe-S (M = Mo, V) and Fe-S cubes. The resultant metal-sulfur clusters are structurally more relevant to P-cluster than FeMoco. The structures of FeMoco and P-cluster share some features such as the fused form of two cubes and the presence of a central μ_6-atom and μ_2-bridging inter-cube ligands. Despite the functional difference between the N_2 fixation site (FeMoco) and the electron mediator (P-cluster), structural analogues of P-cluster deserve to be outlined owing to their structural relevance to FeMoco.

Structural conversion of the $[MoFe_3S_4]_2$ cluster **9** to furnish the $[Mo_2Fe_6S_9]$ moiety, whose atomic arrangement resembles that of the $[Fe_8S_7]$ core of P-cluster, was discovered by Holm and coworkers.[78,79] The reaction of **9** with 2 equiv. $[NEt_4][SH]$ resulted in the rearrangement of the cluster core to give a mixture of products, from which a large $[Mo_2Fe_6S_9]$-$[Mo_2Fe_8S_{12}]$-$[Mo_2Fe_6S_9]$ cluster precipitated as crystals. An analogous reaction in the presence of a strong reductant ($KC_{14}H_{10}$:

potassium anthracenide) afforded a $[Mo_2Fe_6S_9]$-$[Mo_2Fe_6S_9]$ dimer with linkages through K^+ and μ-S atoms. The synthetic protocol using double-cubane clusters and $[NEt_4][SH]$ was extended to start with the $[MFe_3S_4]_2$ (M = Mo, V) clusters bearing hydrotris(pyrazolyl)borate (Tp) ligands on heterometals (M) and PEt_3 ligands on Fe. Thus $[TpMFe_3S_4]_2$ (M = Mo, V) clusters were converted into $[\{TpMoFe_3S_3(SH)\}_2(\mu_6\text{-}S)(\mu_2\text{-}S)_2]^{3-}$ (**15**) and $[\{TpVFe_3S_3(SH)\}_2(\mu_6\text{-}S)(\mu_2\text{-}S)_2]^{4-}$ (**16**) by treatment with $[NEt_4][SH]$ (**Scheme 5a**).[80,81,82] Analogous core conversion reactions were found to be promoted by the reactions of the $[TpMoFe_3S_4]_2$ cluster with hydroselenide (HSe^-), methoxide (MeO^-), and ethane thiolate (EtS^-), resulting in the incorporation of these ligands in place of terminal HS^- ligands and one of the μ_2-S atoms in **15**.[83,84,85] Cyanide (CN^-) also replaced the terminal HS^- ligands of **15** to afford $[\{TpMoFe_3S_3(CN)\}_2(\mu_6\text{-}S)(\mu_2\text{-}S)_2]^{3-}$ (**17**).[86] Tungsten (W) and selenium (Se) are congeners of molybdenum and sulfur, respectively, and thus the Se-containing W analogues of **15** supported by hydrotris(3,5-dimethylpyrazolyl)borate (Tp*) ligands, $[\{Tp^*WFe_3S_3(L_1)\}_2(\mu_6\text{-}S)(\mu_2\text{-}Se)(\mu_2\text{-}L_2)]^{3-}$ (L_1 = SH, L_2 = S (**18**); L_1 = SeH, L_2 = Se (**19**); $L_1 = L_2$ = SMe (**20**)), were synthesized in a similar manner from $[\{Tp^*WFe_3S_3Se(PEt_3)_2\}_2]$ (**21**) (**Scheme 5b**).[87] The precursor cluster **21** was prepared through a *trisulfide* approach, which is the subject of the next section (**section 2.1.2**).

Scheme 5. Core-fusion reactions of a) Tp-supported $[MFe_3S_4]_2$ (M = Mo, V) clusters or b) a Tp*-supported $[WFe_3S_3Se]_2$ cluster in the presence of hydrosulfide (HS^-), hydroselenide (HSe^-), or MeS^-.

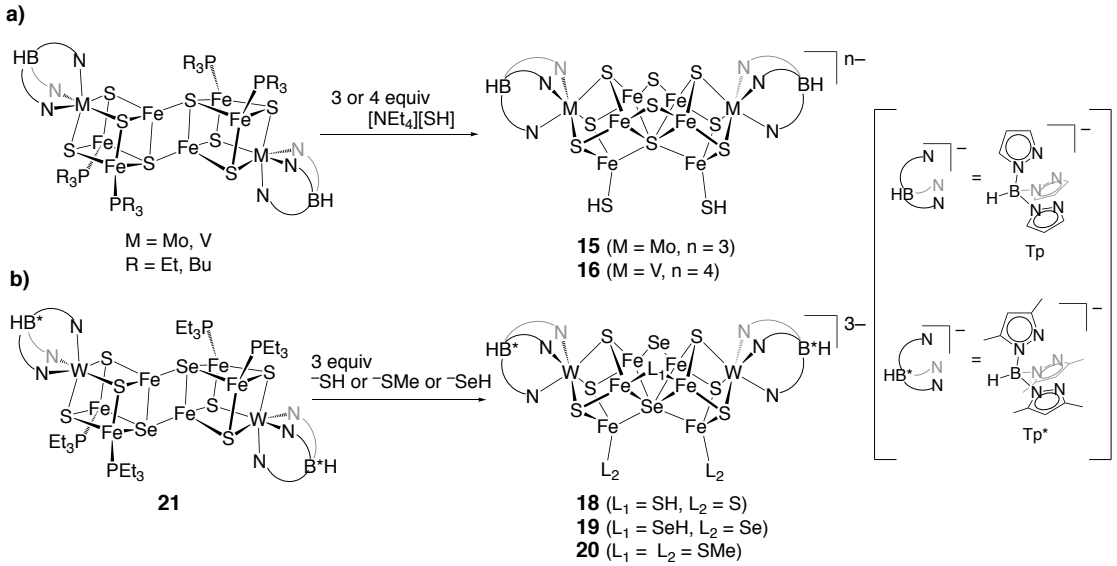

Reductive fusion of two $[Fe_4S_4]$ cubes into an $[Fe_8S_7]$ cluster, which reproduces the core of P-cluster, was developed by the present authors *et al.* Desulfurization from an all-ferric $[Fe_4S_4]$-amide cluster $[Fe_4S_4\{N(SiMe_3)_2\}_4]$ was found to proceed in the presence of PR_3 (R = Me, Et), giving rise to $[Fe_8S_7]$ clusters $[Fe_4S_3\{N(SiMe_3)_2\}(S{=}PR_3)]_2(\mu_6\text{-}S)\{\mu_2\text{-}N(SiMe_3)_2\}_2$ (R = Me (**22a**), Et (**22b**)) (**Scheme 6a**).[88] In this reaction, PR_3 abstracts a sulfur atom from an $[Fe_4S_4]$ cluster to give phosphine sulfide ($S{=}PR_3$), which is present as ligands in the product. Removal of a sulfur atom from the $[Fe_4S_4]$ core generates a transient $[Fe_4S_3]$ intermediate, in which vacant sites on iron atoms presumably capture another $[Fe_4S_4]$ cluster through a sulfur atom to provide the $[Fe_8S_7]$ core with a central μ_6-S atom (**Scheme 6a**). This speculated pathway may reflect the biosynthesis of P-cluster, as the maturation process has been proposed to proceed through the coupling of two $[Fe_4S_4]$ clusters under reducing conditions.[74-73] An analogous $[Fe_8S_7]$ cluster $[Fe_4S_3\{N(SiMe_3)_2\}(SC(NMe_2)_2)]_2(\mu_6\text{-}S)\{\mu_2\text{-}N(SiMe_3)_2\}_2$ (**23**) has been synthesized from a one-pot assembly reaction of an Fe-amide complex $Fe\{N(SiMe_3)_2\}_2$ with HSTip (Tip = 2,4,6-tri(isopropyl)phenyl), tetramethylthiourea ($SC(NMe_2)_2$), and elemental sulfur in toluene.[89,90] While the $[Fe_8S_7]$ core of **23** is not supported by cysteine analogs (*i.e.* thiolates), the terminal amide and thiourea ligands in **23** could be replaced to thiolates by addition of HSR and ^-SR, respectively (**Scheme 6b**).[89]

Scheme 6. Synthesis of $[Fe_8S_7]$ clusters from a) core-fusion reaction of $[Fe_4S_4\{N(SiMe_3)_2\}_4]$ in the presence of phosphines (PR_3) or b) an assembly reaction using an Fe^{II} amide complex $Fe\{N(SiMe_3)_2\}_2$, HSTip (Tip = 2,4,6-tri(isopropyl)phenyl), tetramethylthiourea ($SC(NMe_2)_2$), and elemental sulfur in toluene.

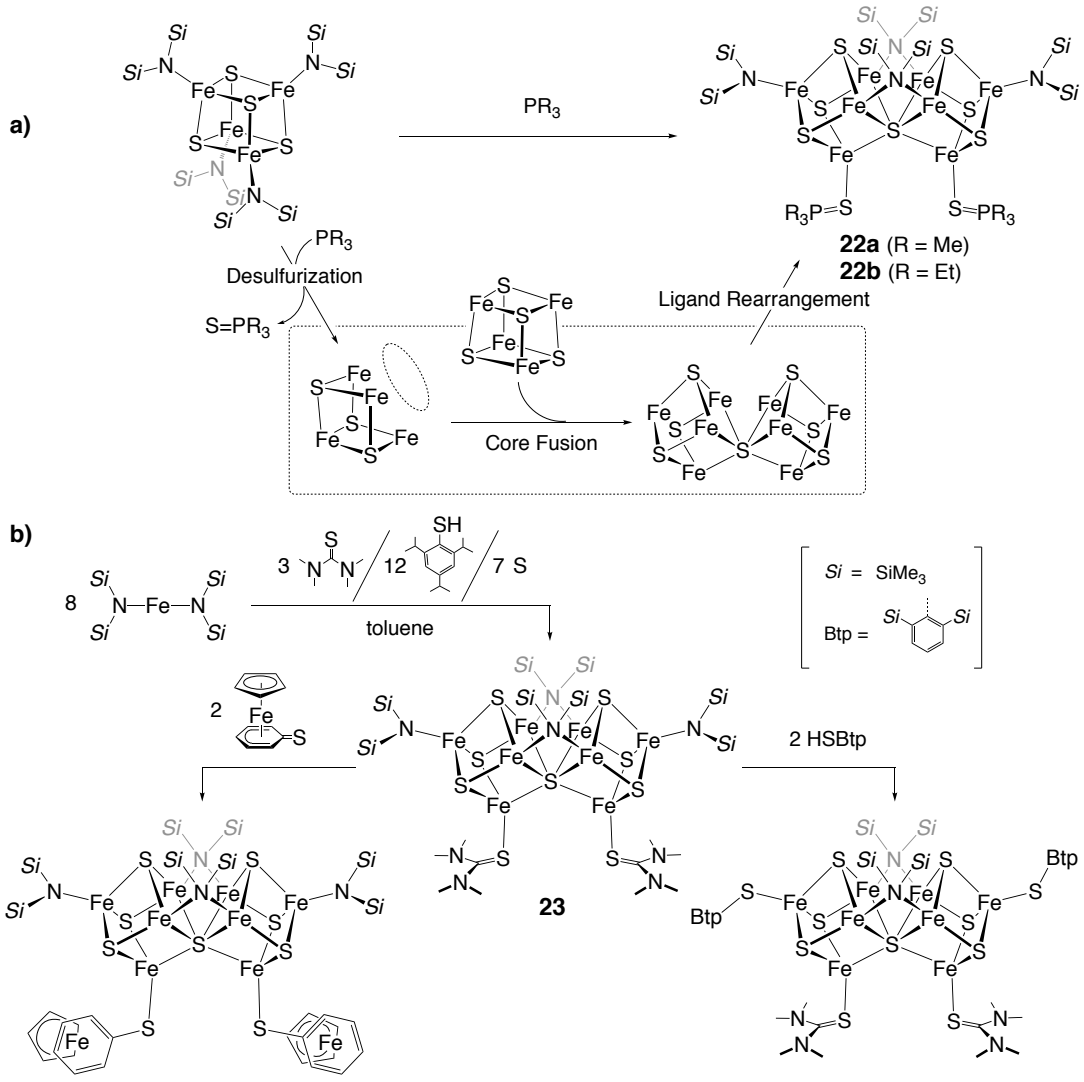

Comparisons of structures and spectroscopic features of the aforementioned core-fusion products with those of P-cluster would be valuable to gain insight into the physicochemical properties of high-nuclearity metal-sulfur clusters. In the MoFe protein, P-cluster has been reported to undergo redox-dependent structural changes over three states (**Figure 6**). The first one is the *reduced* P^N state with a relatively symmetric [Fe_8S_7] core, and is identical to those of **22a**-**23** but supported by two bridging and four terminal cysteines.[4,5] The second one is the *2 electron-oxidized* P^{OX} (P^{2+}) state, which reveals a relatively "open" core configuration because two inner Fe atoms of the [Fe_8S_7] core move away from the central μ_6-S atom and instead interact with an oxygen atom of a serine residue and a backbone amide nitrogen of a bridging cysteine residue. The last one is the *1 electron-oxidized* P^{1+} state, the structure of which could be considered an intermediate between the P^N and P^{OX} states and loses one of the Fe-(μ_6-S) bonds in the P^N-cluster and instead forms an Fe-O bond with a serine residue.[91] A series of core-fusion cluster products in this section, which contain [$M_2Fe_6S_9$]-type (M = Mo, V) or [Fe_8S_7] cores, commonly feature a P^N-like framework with a μ_6-S atom and two μ_2-bridging ligands (*e.g.* S^{2-}, $\{N(SiMe_3)_2\}^-$) in the middle of their cores. The overall structural similarity is confirmed by comparison of the [$\{M_4S_3\}_2(\mu_6\text{-}S)(\mu_2\text{-}X)_2$] core (X = S^{2-}, $\{N(SiMe_3)_2\}^-$) of **15**, **16**, and **23** with the [$Fe_8S_7(\mu\text{-}S\text{-}Cys)_2$] core of the P^N-cluster, which can be represented by weighted root mean square deviation values (RMSDs) of 0.38 Å (**15**), 0.33 Å (**16**),[80] and 0.34 Å (**23**)[92] vs. P^N-cluster. These values were calculated by including all atoms of inorganic cores and inter-cubane bridging atoms. The RMSDs for the W/Se-containing clusters appeared to be lower, **18** (0.29 Å), **19** (0.33 Å), and **20** (0.25 Å).[92] The Mössbauer spectra of **15**, **16**, and **18**-**20** displayed one or two doublets with similar δ values, which denote relatively reduced Fe^{II} centers. The assignments are consistent with isomer shifts observed for the P^N-cluster, and those shifts were attributed to an $8Fe^{II}$ state.[93] In contrast, the δ values of two doublets in the spectrum of **23** are indicative of the $2Fe^{III}$-$6Fe^{II}$ oxidation state, which is consistent with the P^{OX} state (or *2 electron-oxidized* form of the P^N state).[94] The two Fe^{III} sites are assigned as the peripheral Fe atoms based on the comparison of the Mössbauer spectra of derivatives of **23** (**Scheme 6b**).[90]

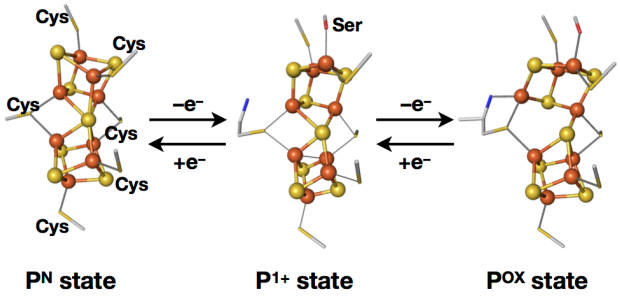

Figure 6. Redox-dependent structural change of P-cluster across P^N, P^{1+}, and P^{ox} states. The inorganic core of P-cluster reveals more "open" core configurations upon oxidation. In the P^{1+} and P^{OX} states, some inner Fe atoms lose interaction with the central S atom (*i.e.* μ_6-S atom in the P^N state) and instead interact with a serine residue and an amide N atom from a bridging cysteine. Protein residues are shown in stick format. PDB ID: 3U7Q, 6CDK.

2.1.2 Template Mo/W Trisulfides for Growth of Metal-Sulfur Clusters

While the Mo atom in FeMoco occupies one of the peripheral positions, the Mo-Fe-S clusters prepared from assembly reactions using $[MoS_4]^{2-}$ usually situate the Mo atoms at inner positions (see **section 2.1.1**). A major reason for this placement is the change in the coordination geometry of Mo during the cluster synthesis, from four-coordinate and tetrahedral in $[MoS_4]^{2-}$ to six-coordinate and nearly octahedral for most of the Mo atoms in Mo-Fe-S clusters. Owing to the high affinities of Mo toward sulfur and oxygen atoms, the extra coordination sites of Mo generated by the geometry change (and rearrangement of sulfides) are occupied either by thiolates, sulfides, or alkoxides, which are prone to bridge metals to incorporate the corresponding Mo atom inside the resultant clusters. This situation changes by replacing $[MoS_4]^{2-}$ with relevant complexes with higher coordination numbers, such as $[(L)MS_3]$-type (M = Mo, W) trisulfides supported by a strongly binding multi-dentate ligand L. For instance, half-sandwich complexes $[Cp^*MS_3]^-$ (M = Mo, W; $Cp^* = C_5Me_5$)[95] use three terminal sulfides to accommodate noble metals (*e.g.* Cu, Ag, and Au) and provide various metal-sulfur clusters surrounded by Cp*M units.[96] Likewise, this class of trisulfide complexes can serve as templates and capture Fe atoms through terminal sulfide ligands to grow M-Fe-S clusters in the presence of appropriate sulfur reagents, as described below. In this protocol, the $[(L)MS_3]$ (M = Mo, W) structure is retained in the cluster products. Even though tungsten and selenium are irrelevant to the nitrogense cofactor, this section describes W-Fe-S and W-Fe-Se clusters as well

owing to their structural relevance to the Mo-Fe-S clusters.

2.1.2.1 $[M_6S_9]$-type Clusters Derived from $[(L)MS_3]$ Precursors

A tungsten complex $[Tp^*WS_3]^-$ (**24**)[97] made by Mizobe, Hidai, *et al*. was the first $[(L)MS_3]$ trisulfide template used in M-Fe-S cluster synthesis, while the biologically more relevant molybdenum analogue was obtained not as a trisulfide complex but as a sulfide/tetra-sulfide complex $[TpMoS(S_4)]^-$,[97] which can be used as a precursor for a cubane cluster $[TpMoFe_3S_4Cl_3]^-$.[98] Holm *et al.* examined an assembly reaction of **24** with 2 equiv. each of $FeCl_2$ and HS^- and obtained a $[M_6S_9]$-type cluster $[Tp^*_2W_2Fe_4S_9]^-$ (**25**),[87] which can be reduced to $[Tp^*_2W_2Fe_4S_9]^{2-}$ (**26**) upon treatment with $[BH_4]^-$ (**Scheme 7**). An analogous reaction using Se^{2-} instead of HS^- provided $[Tp^*_2W_2Fe_4S_6Se_3]^{2-}$ (**27**), whereas addition of a slight excess $FeCl_2$ led to the formation of the 2-electron oxidized form of **27**, $[Tp^*_2W_2Fe_4S_6Se_3]^0$ (**28**) (**Scheme 7**). Similar $[M_6S_9]$-type clusters, such as $[Fe_6S_9(SR)_2]^{4-}$,[99,100,101,102] $[Fe_6Se_9(SR)_2]^{4-}$,[103] and $[(edt)_2Mo_2Fe_4S_9]^{3-/4-}$ (edt = ethane-1,2-dithiolate),[104] have previously been reported by the groups of Holm and Henkel (**Figure 7**). These syntheses have been accomplished without $[(L)MS_3]$ platforms but rather from one-pot or stepwise reactions of $FeCl_3$ with thiolates and sulfides/selenides, while $[MoS_4]^{2-}$ should be present to obtain the $[Mo_2Fe_4S_9]$ cluster.

The formal oxidation states of W^{IV}-$3Fe^{III}$-$1Fe^{II}$ (**25**) and W^{IV}-$2Fe^{III}$-$2Fe^{II}$ (**26**) were suggested from the ^{57}Fe Mössbauer spectra, which showed averaged signals at δ = 0.37 (**25**) and 0.42 (**26**) mm/s with quadrupole splittings (ΔE_Q) = 1.21 and 0.98 mm/s, respectively. The trend of a more reduced Fe site exhibiting a higher isomer shift was also observed for the Se-containing clusters (δ = 0.43 (**27**) vs. 0.41 (**28**) mm/s). Comparison of redox behaviors between **26** and **27** revealed that the substitution of core S atoms for Se leads to the positive shift of the [2–/3–] redox couple, *i.e.* $E_{1/2}$ = –1.91 V (**27**) and –1.97 V (**26**) in DMF vs. SCE (saturated calomel electrode). Thus the $[W_2Fe_4S_6Se_3]$ core favors lower oxidation states compared to the $[W_2Fe_4S_9]$ core, whereas a further reduced [4–] state of **27** was found to be kinetically unstable. The [3–/4–] couple of **27** ($E_{1/2}$ = –2.19 V vs. SCE) became nearly irreversible; in contrast, **26** showed the reversible corresponding couple ($E_{1/2}$ = –2.38 V vs. SCE).

Scheme 7. Synthesis of W-Fe-S and W-Fe-Se clusters from a template trisulfide complex $[Tp^*WS_3]^-$ (**24**).

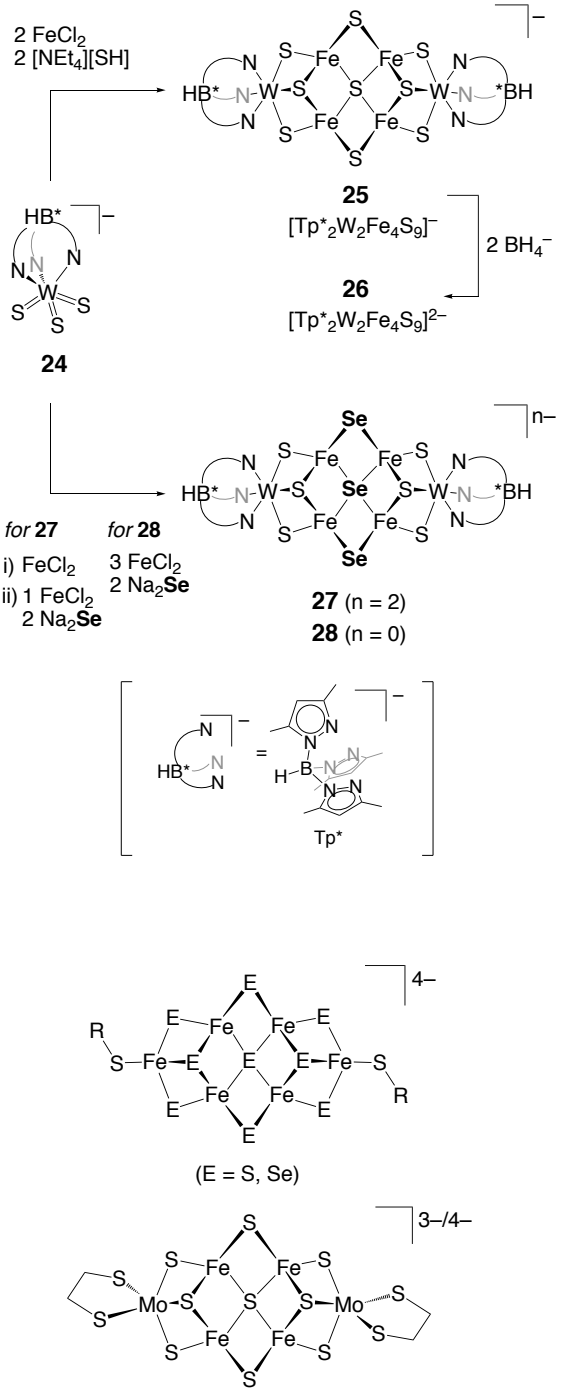

Figure 7. $[Fe_6E_9(SR)_2]^{4-}$ (E = S, Se) and $[(edt)_2Mo_2Fe_4S_9]^{3-/4-}$ (edt = ethane-1,2-dithiolate) clusters.

Another tridentate N-donor ligand 1,3,5-tri-(*tert*-butyl)-1,3,5-triazacyclohexane (^{t}Bu$_3$tach) has been used by Holm *et al*. for stabilization of the [(L)MS$_3$]-type precursors [(^{t}Bu$_3$tach)MS$_3$] (M = Mo (**29**), W (**30**)).[105] Although synthesis of [M$_6$S$_9$]-type clusters has not been accomplished with these trisulfide complexes, their reactions with FeCl$_2$, RS$^-$, and Q^{2-} (S^{2-} or Se^{2-}) were found to afford [MFe$_3$S$_4$] cubanes or [MFe$_3$S$_3$Se] heterocubanes (**31**-**32**; M = Mo, W) (**Scheme 8**).[106] The Se atoms in [MFe$_3$S$_3$Se] heterocubanes selectively occupy the corner opposite to M, suggesting the retention of the (L)MS$_3$ structure during the cluster formation.

Scheme 8. Schematic depiction of the synthesis of cubic [MFe$_3$S$_3$Se] (M = Mo, W) clusters from trisulfide complexes [(^{t}Bu$_3$tach)MS$_3$] (^{t}Bu$_3$tach = 1,3,5-tri-(*tert*-butyl)-1,3,5-triazacyclohexane).

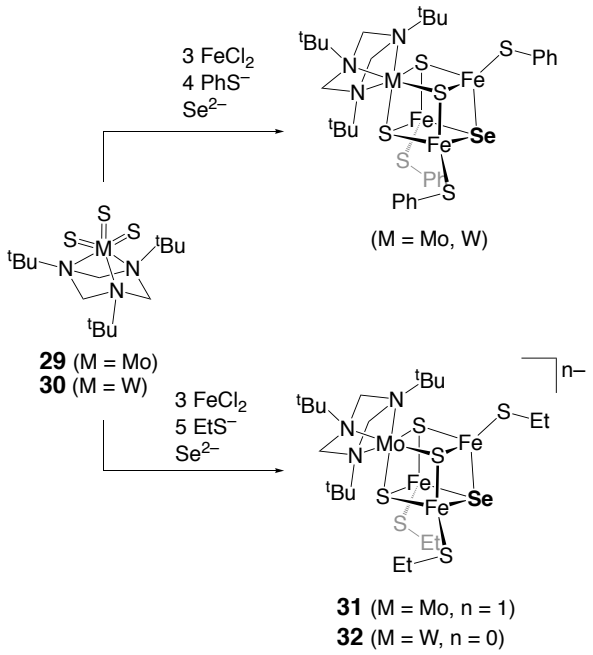

2.1.2.2 Asymmetric [MoFe$_5$S$_9$] Cluster Derived from [Cp*MoS$_3$]$^-$ Precursor

One of the remaining challenges of FeMoco model chemistry was to mimic the asymmetric arrangement of metal atoms, and this was recently achieved by the present authors *et al.* A half-sandwich Mo trisulfide [Cp*MoS$_3$]$^-$ (**33**)[95] was found to serve as a suitable Mo source in an assembly reaction with 5 equiv. FeCl$_2$ and 20 equiv. HS$^-$ to afford an asymmetric Mo-Fe-S cluster [Cp*MoFe$_5$S$_9$(SH)]$^{3-}$ (**34**) (**Scheme 9**),[107] which works as a catalyst for the reduction of CO$_2$ and CO

as will be described in **section 2.2.2.2**. Consistent with the odd number of d-electrons in the inorganic core, the ^{1}H NMR spectrum of **34** in CD_3CN exhibited a broadened, upfield-shifted signal of Cp* at –9.36 ppm. Cluster **34** is redox active and its cyclic voltammogram exhibited reversible redox processes at $E_{1/2}$ = –0.91 V ([2–]/[3–] couple) and –2.06 V ([3–]/[4–] couple) vs. $Ag/AgNO_3$ in CH_3CN. The $[MoFe_5S_9]$ core of **34** can be viewed as a FeMoco analog that lacks one of three Fe-(μ_2-S)-Fe bridges and has a μ_4-S atom instead of the interstitial μ_6-C atom. The long Fe-(μ_4-S) distances of **34** (2.3131(12)-2.3338(12) Å) relative to the Fe-(μ_6-C) distances of FeMoco (1.984-2.018 Å) result in a more *open* and less compact structure of $[MoFe_5S_9]$ than the $[MoFe_7S_9C]$ core of FeMoco, as indicated by the elongated distance between the peripheral Mo and Fe atoms (7.473(1) Å for **34** vs. 6.997 Å for FeMoco) (**Figure 8**). The *open* conformation of **34** is further supported by the smaller dihedral angles between two Fe-(μ_3-S)-Fe planes facing across the μ_4-S atom in **34** (58.87(5)˚) relative to the angles in FeMoco derived from the corresponding planes opposing the μ_6-C atom (83.1-86.6˚). The *open* conformation also induces an almost coplanar arrangement of the six metals in **34**, with atomic deviations of ≦ 0.1223(4) Å from the least square plane.

Scheme 9. An assembly reaction of $[Cp^*MoS_3]^-$ (**33**) with $FeCl_2$ and $[NEt_4][SH]$ affording an asymmetric Mo-Fe-S cluster $[Cp^*MoFe_5S_9(SH)]^{3-}$ (**34**).

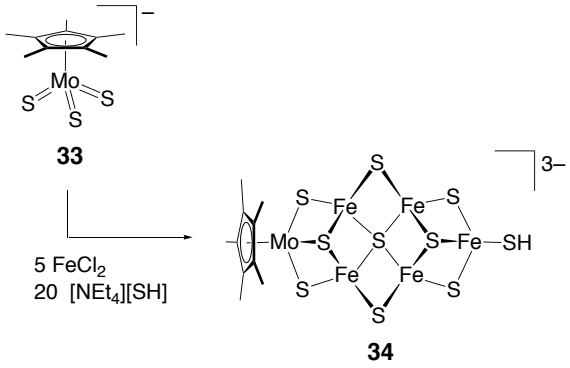

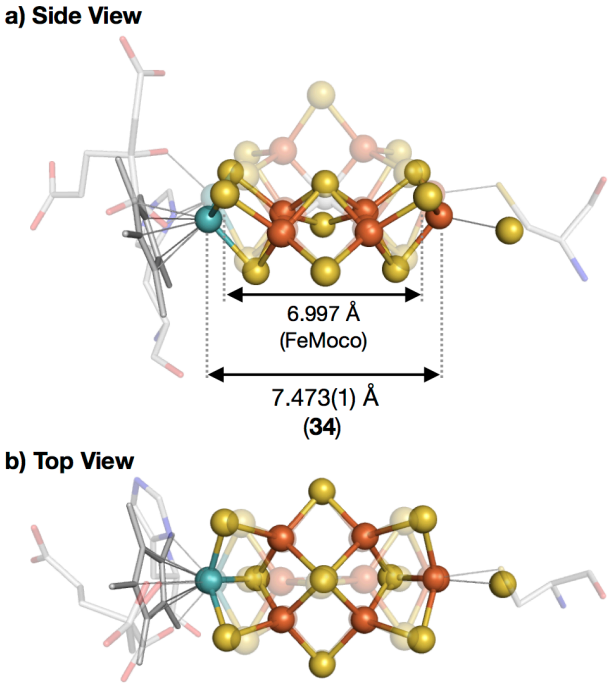

Figure 8. a) Side view and b) top view of $[Cp^*MoFe_5S_9(SH)]^{3-}$ (**34**) overlaid with FeMoco (PDB ID: 3U7Q). Organic ligands are shown in stick format, while hydrogen atoms are omitted for clarity. Color legend: Blue, N; gray, C; orange, Fe; red, O; teal, Mo; yellow, S.

In **sections 2.1.2.1** and **2.1.2.2**, we addressed three classes of ligands (L) for trisulfide templates $[(L)MS_3]$, *i.e.* Tp-, Cp-, and ^{R}tach-based ligands, which are typical *facially*-coordinating ligands. There remains other possible *fac*-ligand candidates for $[(L)MS_3]$ or variants, such as tri-phosphines, tris-N-heterocyclic-carbenes, tris(thioimidazolyl)borates, and tris(2-pyridyl)alkanes, although some cautions need to be discussed. For instance, the former two classes have propensities to uptake elemental sulfur and sulfides on metals to form P=S or C=S bonds, and thereby these ligands would need to be tightly attached to metals prior to sulfurization reactions. The latter two classes sometimes exhibit less robust M-L interactions, which may limit the reaction conditions for cluster synthesis. The charges and steric properties of L also need to be considered upon usage. Among Tp, Cp, and ^{R}tach ligands, the former two are negatively charged and allow more robust M-L interactions than neutral ^{R}tach. Steric properties are analogous between Tp and ^{R}tach in metal-sulfur clusters, and when it comes to $[(L)MFe_3S_4]$ cubes, the 3-positions of pyrazolyl groups in Tp and the N-substituents of ^{R}tach point to terminal ligands on tetrahedral Fe (**Figure 9**). On the other hand,

substituents of Cp ligands are coplanar with ring carbons and thus they are away from terminal ligands on Fe and instead impose less steric protection around M. Even though these notes point out some complexities, the further application of *fac*-ligands in metal-sulfur cluster chemistry would be beneficial, not only to synthesize more precise structural analogues of FeMoco by taking advantage of locating the (L)M unit at outer positions of clusters, but also to activate N_2 with synthetic M-S clusters (to be discussed in **Section 2.2.1**).

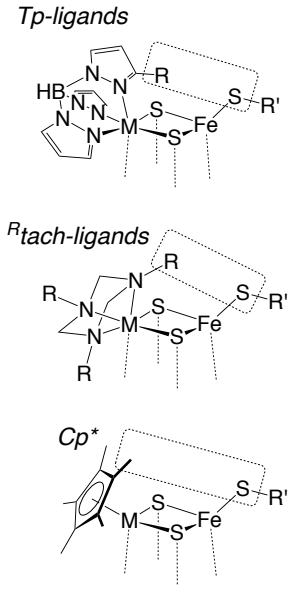

Figure 9. Steric properties of Tp-, ^{R}tach, and Cp* ligands in [(L)MFe_3S_4] cubes.

2.1.3 Incorporation of a Light Atom into M-S Cores as a Bridging Vertex

Although the presence of an interstitial atom within FeMoco was theoretically predicted soon after the first structural characterization of Mo-nitrogenase,[25] it took a decade to find the corresponding μ_6-X light atom, and another decade was needed to finally confirm that X = C. Discovery of the central atom X of FeMoco generated significant research interest in the synthesis of Mo-Fe-S and Fe-S clusters incorporating a light atom, whereas the light atoms thus far incorporated into Fe-containing metal-sulfur clusters have been typically N or O because the corresponding studies have been mainly carried out or initiated before the confirmation of the μ_6-C atom of FeMoco. Therefore, this subsection mainly deals with M-S clusters having N or O atoms as bridging vertices, as clues for future synthetic work. This area remains primitive and leaves two major synthetic challenges: (a) the

formation of a carbide from an external source and (b) incorporation of the carbide, not as a vertex but as an interstitial atom. Future studies can refer to the biosynthesis of FeMoco, which has been shown to involve the transfer of a CH_3 group of SAM (**Figure 5**) to an Fe-S cluster.[71] As discussed earlier in **section 2.1.1.2**, one can design bio-mimetic pathways starting from the S_N2-type reactions of methyl-sulfonium ions induced by M-S clusters.

Chen, Holm, and their coworkers reported the cubic $[WFe_3S_3X]$ (X = Cl, Br) clusters, in which the halide atom, X, in the core is expected to be replaceable. The W trisulfide complex **24** ($[Tp^*WS_3]^-$)[97] reacted with FeX_2 (3 equiv.), $[Et_4N][X]$ (1 equiv.), and then with sodium benzophenone ketyl (3 equiv.) as the reductant, giving rise to cubic clusters $[Tp^*WFe_3S_3(\mu_3\text{-}X)X_3]^{2-}$ (X = Cl (**35**), Br (**36**)) (**Scheme 10**).[108] In an analogous reaction of **24** with 2 equiv. FeX_2 and 1 equiv. sodium benzophenone ketyl, tri-nuclear clusters $[Tp^*WFe_2S_3(\mu_2\text{-}X)X_2]^-$ (X = Cl (**37**), Br (**38**)) were obtained (**Scheme 10**). These reactions are extensions of those described in section 2.1.2.1, and so the reactions proceeded similarly, with retention of the $[Tp^*WS_3]$ structure to place a halide X at the positions most distant from W in the $[WFe_3S_3X]$ and $[WFe_2S_3X]$ cores. The $[WFe_3S_3X]^+$ cores of **35** and **36** are $2e^-$ more reduced than typical $[MFe_3S_4]^{2+}$ cubes (M = Mo or W), and electrons required to adjust the stoichiometry to the $[WFe_3S_3X]^+$ state are provided from benzophenone ketyl in this reaction system. A comparative experiment using a sulfide/tetra-sulfide complex $[TpMoS(S_4)]^-$ instead of a trisulfide complex **24** led to the formation of the $[MoFe_3S_4]$ core, suggesting that sulfides are preferably incorporated into the cubic core rather than halides.

In contrast to an unsuccessful salt-metathesis strategy for replacement of the μ_3-Cl ligand of the $[WFe_3S_3Cl]$ cube to incorporate a light atom, oxidative reactants Me_3SiN_3 and S_8 were found to trigger redox metathesis reactions to replace the core chloride of **35**, providing $[Tp^*WFe_3S_3(\mu_3\text{-}X)Cl_3]^-$ (X = Me_3SiN^{2-} (**39**), S^{2-} (**40**)) (**Scheme 10**). The $[WFe_3S_3N]$ core of **39** reveals a close topological analogy to the $[MoFe_3S_3C]$ subunit of FeMoco. While the μ_3-Cl in the $[WFe_3S_3Cl]$ core of **35** is relatively inert, the μ_2-Cl in the trinuclear $[WFe_2S_3Cl]$ cluster **37** appeared to be more labile and exchangeable through salt metathesis reactions to afford $[WFe_2S_3]$ clusters bearing μ_2-N_3^- (**41**) or μ_2-OMe (**42**) ligands (**Scheme 10**). A similar approach might also be applicable to incorporate carbon atom to the M-S core by selecting suitable ligands instead.

Scheme 10. Synthesis and ligand-replacement reactions of halide-containing cubic [WFe_3S_3X] and trinuclear [WFe_2S_3X] clusters (X = Cl, Br).

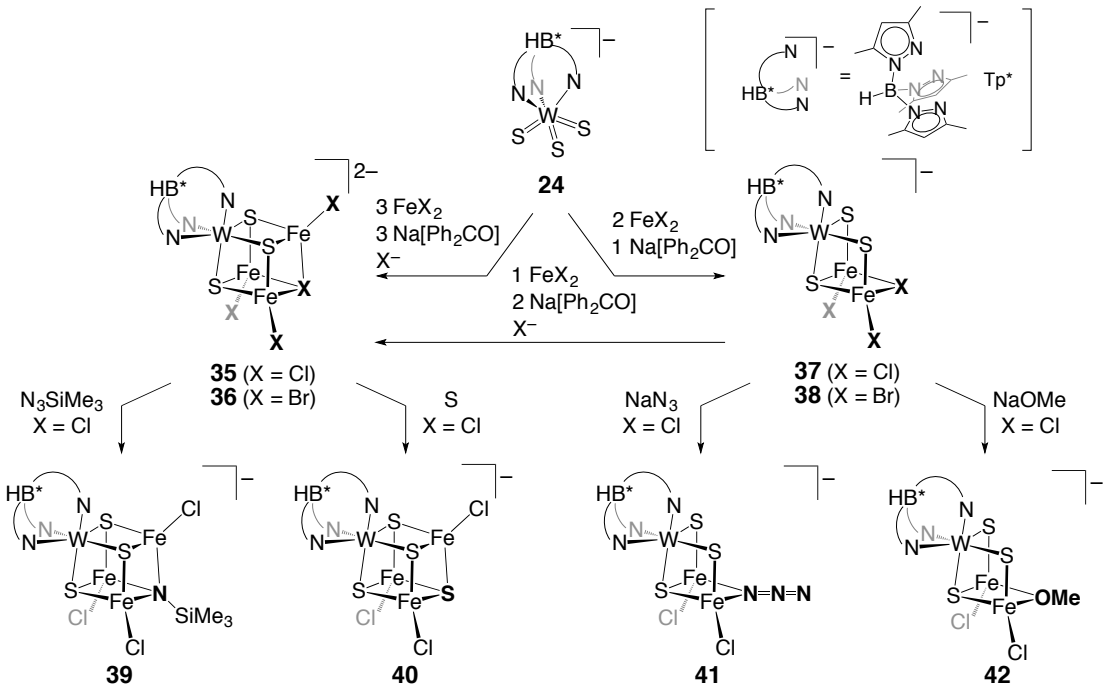

Methods to incorporate light atoms to metal-sulfur clusters are not limited to those utilizing the [(L)MS_3] templates. Lee *et al.* synthesized a series of amide- or imide-bridged Fe_2 complexes $Fe_2(\mu\text{-}N^tBu)_2Cl_2(NH_2{}^tBu)_2$, $[Fe_2(\mu\text{-}N^tBu)(\mu\text{-}S)Cl_4]^{2-}$, $Fe_2(\mu\text{-}NH^tBu)_2(\mu\text{-}S)(N\{SiMe_3\}_2)_2$, and $Fe_2(\mu\text{-}NH^tBu)_2(N\{SiMe_3\}_2)_2$, and used them as precursors for imide-sulfide mixed $[Fe_4(N^tBu)_xS_{4-x}]$ (x = 1-3) cubanes (**Figure 10**).[109,110] For example, a binary equimolar reaction of $[Fe_2(\mu\text{-}N^tBu)(\mu\text{-}S)Cl_4]^{2-}$ with $Fe_2(\mu\text{-}NH^tBu)_2(\mu\text{-}S)(N\{SiMe_3\}_2)_2$ formed the $[Fe_4(N^tBu)_2S_2]$ cluster, while a mixture of $Fe_2(\mu\text{-}NH^tBu)_2(\mu\text{-}S)(N\{SiMe_3\}_2)_2$ and $[Fe_4S_4Cl_4]^{2-}$ provided the $[Fe_4(N^tBu)S_3]$ cube, which is nearly isometric with the $[Fe_4S_3C]$ subunit of FeMoco. An imide-selenide cube $[Fe_4(N^tBu)Se_3Cl_4]^{2-}$ was also synthesized in a similar manner from $Fe_2(\mu\text{-}NH^tBu)_2(\mu\text{-}Se)(N\{SiMe_3\}_2)_2$.[109] In these reaction systems, partial reduction of the $Fe^{III}{}_2$ precursors occurs, and the oxidative formation of an azo-compound as a byproduct was proposed to compensate the electrons, but the possibility of other redox couplings cannot be excluded. Pure samples of $[Fe_4(N^tBu)_xS_{4-x}]$ (x = 1-3) clusters are stable in solution with respect to disproportionation of core ligands. Their cyclic voltammograms revealed that replacement of each

sulfide by imide leads to an incremental shift of the redox potentials by *ca.* –400 mV, indicating the greater donor ability of the N^{t}Bu ligand relative to sulfide.

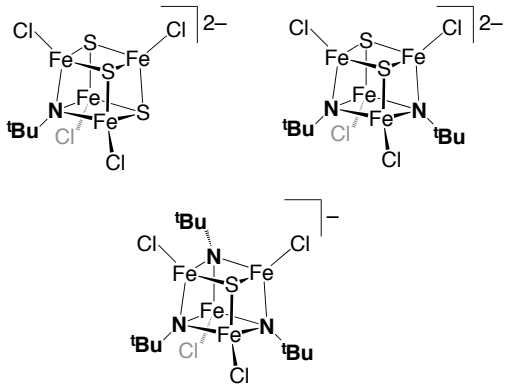

Figure 10. Structures of imide-sulfide mixed cuboidal clusters $[Fe_4(N^tBu)_xS_{4-x}]^{n-}$ (x = 1-3; n = 2 or 1).

Although incorporation of an interstitial carbide into Fe-S or Mo-Fe-S clusters remains a challenge, an $Fe_6(\mu_6\text{-}C)$ carbide cluster without sulfur, $[Fe_6C(CO)_{16}]^{2-}$,[111,112] was synthesized from $Fe(CO)_5$ and has been known over 40 years. Sulfurization of this Fe-carbide cluster would offer alternative synthetic pathways to FeMoco models, and this idea prompted Rauchfuss *et al.* to examine the reactions of $[Fe_6C(CO)_{16}]^{2-}$ with various sulfurization agents.[113] However, incorporation of sulfur atoms from oxidizing sulfur sources such as elemental sulfur and ethylene sulfide were unsuccessful because $[Fe_6C(CO)_{16}]^{2-}$ is susceptible to oxidative degradation. On the other hand, SO_2 was known to replace one of the CO ligands of $[Fe_6C(CO)_{16}]^{2-}$ to furnish $[Fe_6C(CO)_{15}(SO_2)]^{2-}$ as reported by Shriver *et al.*,[114] and thus Rauchfuss *et al.* converted its SO_2 into S via methylation and reduction to obtain $[Fe_6C(CO)_{14}(S)]^{2-}$ (**Scheme 11**).[113] This reductive route for generation of a sulfide from SO_2 is relevant to one of the biosynthetic steps of FeMoco, where a core sulfur atom is incorporated via reduction of external $[SO_3]^{2-}$.[77] Even though one might envision the repetition of several cycles to incorporate sufficient number of sulfides, fragility of the Fe-CO-carbide species eventually terminates the sulfide incorporation. Since the single S incorporation couples with 2-electron oxidation of the $[Fe_6C]$ core (**Scheme 11**), cycles of this process should cause oxidation of the Fe centers to the level where the cluster cannot maintain CO ligands and decomposes.

Scheme 11. Stepwise conversion of SO_2 into μ_3-S on an $Fe_6(\mu_6\text{-C})$ carbonyl cluster.

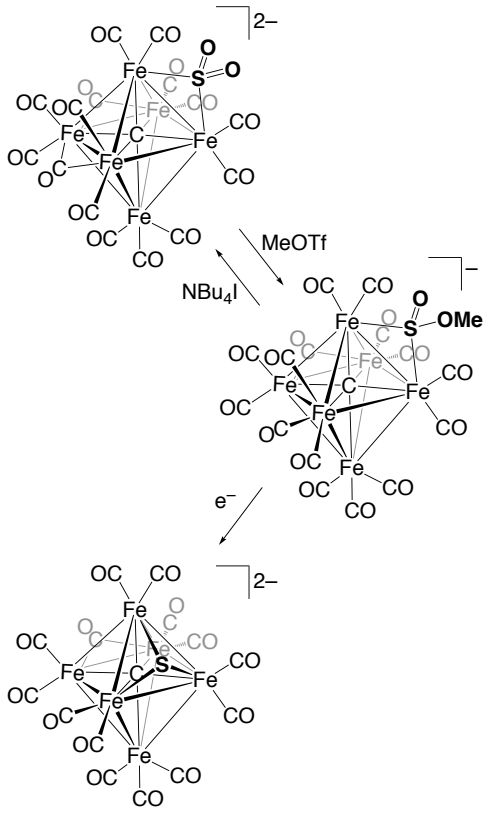

2.1.4 Assembly in Non-Polar Media

Metal-sulfur clusters are typically synthesized from ionic reactants in polar organic solvents, where salt-metathesis strategies are mainly applied. On the other hand, the use of non-ionic reactants in a non-polar solvent (toluene) turned out to be a key strategy to obtain non-traditional Fe-S clusters with high nuclearities, such as topological analogues of FeMoco.

Non-ionic self-assembly was reported by Ohki, Tatsumi, *et al.* and resulted from the reactions of an Fe-thiolate complex, $[Fe(STip)(\mu\text{-SDmp})]_2$ (Tip = 2,4,6-tri(isopropyl)phenyl, Dmp = 2,6-di(mesityl)phenyl), or an Fe-thiolate-mesityl complex, [(DME)Fe(SDmp)(Mes)] (DME = 1,2-dimethoxyethane; Mes = mesityl), with elemental sulfur in toluene. These reactions furnished $[Fe_8S_7]$ clusters $[\{Fe_8S_7(SDmp)_2\}(\mu\text{-SDmp})_2(\mu\text{-SR})]$ (R = Tip (**43a**), Mes (**43b**)) (**Scheme 12a**),[115,116] whose inorganic cores topologically reproduce the framework of FeMoco as described below. This reaction system was designed to prevent the formation of thiolate-supported conventional $[Fe_4S_4]$

clusters, which are usually most stable as the dianionic form $[Fe_4S_4(SR)_4]^{2-}$ in the $2Fe^{II}$-$2Fe^{III}$ state. The one-electron oxidized form $[Fe_4S_4(SR)_4]^{-}$ in the $3Fe^{III}$-$1Fe^{II}$ state has limited precedence,[117,118,119] and the further oxidized form $[Fe_4S_4(SR)_4]^{0}$ in the all-ferric $4Fe^{III}$ state has been unknown until recently,[120] indicating the instability of the neutral $[Fe_4S_4(SR)_4]^{0}$ cluster. As the reactions depicted in **Scheme 12** deal with non-ionic compounds in toluene, the resultant Fe-S clusters are expected to be neutral in charge. In principle, the neutral $[Fe_4S_4(SR)_4]^{0}$ may be generated in **Scheme 12** as an intermediate, but its instability should instead allow the construction of Fe-S cores without going through $[Fe_4S_4]$ species or the further assembly from $[Fe_4S_4]$ intermediates, leading to higher nuclearity clusters such as **43a** and **43b**. The bulky thiolate ligands are also important, as they not only enable the compounds to dissolve into toluene but also circumvent extensive aggregation by encapsulating the Fe-S core at the appropriate size.

Scheme 12. Non-ionic assembly reactions in toluene to furnish a) $[Fe_8S_7]$ and b) $[Fe_8S_6O]$ topological analogues of FeMoco.

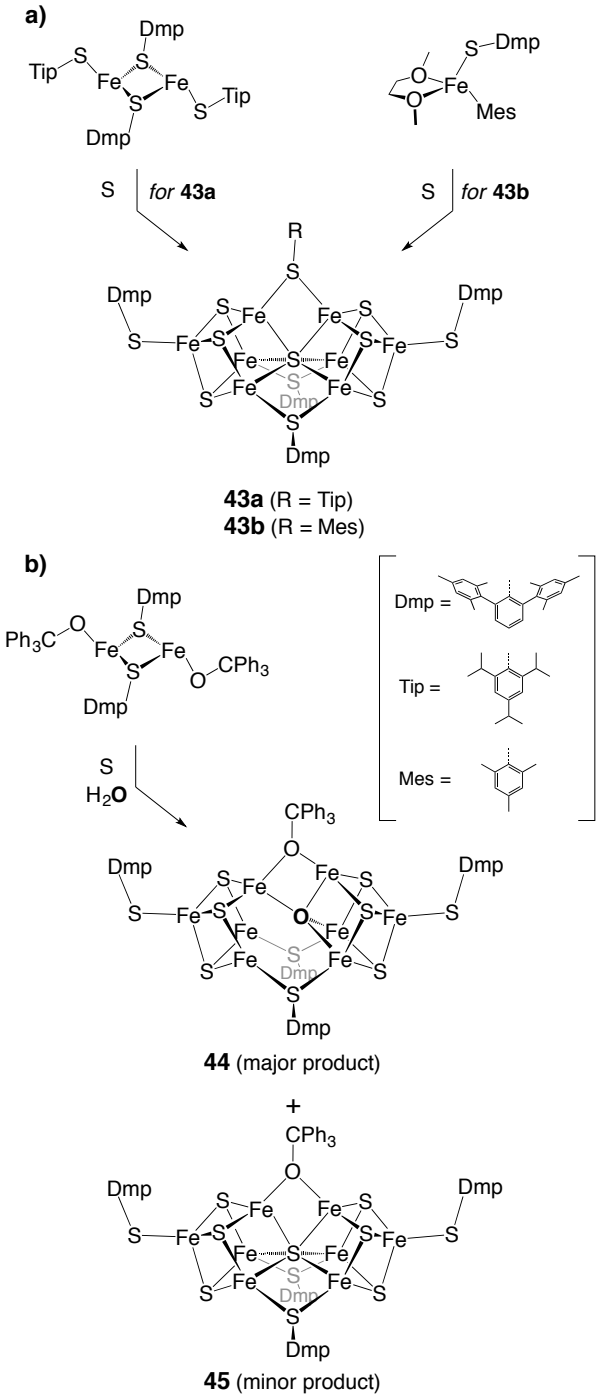

As determined by X-ray crystallography, the common $[Fe_8S_7]$ core of **43a** and **43b** is comprised of two $[Fe_4S_4]$ cubanes sharing one of the core S as the central μ_6-S atom. Around the $[Fe_8S_7]$ core, two terminal SDmp thiolates are bound to the peripheral Fe atoms, while three SR ligands (R = Dmp, Tip, mesityl) doubly bridge the inner Fe atoms. The inner Fe atoms encapsulate a μ_6-S atom and are arranged in a trigonal-prismatic fashion, which makes the $[Fe_8S_7]$ core resemble the $[MoFe_7S_9C]$ core of FeMoco. On the other hand, the Fe-Fe distances between inner Fe atoms of **43a** (2.9103(10)-3.7050(10) Å) and **43b** (2.9212(7)-3.6506(6) Å) are inconsistent with and longer than the corresponding Fe-Fe distances in FeMoco (2.58-2.62 Å), mainly due to the larger radius of central S atom relative to the C atom of FeMoco. In the context of structural models, the homometalic feature of **43a** and **43b** also relates to the biosynthetic precursor of FeMoco (L-cluster), which contains only Fe as metal centers.[36,37]

The $[Fe_8S_7]^{5+}$ net charge of **43a** and **43b** is in agreement with the formal oxidation state of $3Fe^{III}$-$5Fe^{II}$. This is relevant not only to the recent Mo^{III}-$4Fe^{III}$-$3Fe^{II}$ assignment of the resting state of FeMoco based on spatially resolved anomalous scattering in protein crystallography[121] but also to the lower end of previously proposed oxidation states for the resting state (Mo^{III}-$2Fe^{III}$-$5Fe^{II}$/Mo^{IV}-$1Fe^{III}$-$6Fe^{II}$).[122,123] In accordance with the odd number of d-electrons in **43a** and **43b**, their EPR spectra displayed rhombic S = 1/2 signals at g = 2.19, 2.07, 1.96 (**43a**) and g = 2.21, 2.07, 1.95 (**43b**), which are analogous to a rhombic S = 1/2 signal (g = 2.22, 2.05, 1.86) from the Fe-only nitrogenase (FeFe protein) under weakly acidic conditions (pH = 6.4).[124] In contrast, the resting state of FeMoco shows a S = 3/2 feature (g = 4.3, 3.7, 2.01),[16,125,126,127] and the oxidized L-cluster reveals an isotropic S = 1/2 feature (g = 1.92).[128] Consistent with the redox-active nature of FeMoco, the cyclic voltammogram of **43a** in THF exhibited three redox processes at $E_{1/2}$ = –0.74 ($[Fe_8S_7]^{5+}$/$[Fe_8S_7]^{4+}$), –1.15 ($[Fe_8S_7]^{4+}$/$[Fe_8S_7]^{3+}$), and –2.00 V ($[Fe_8S_7]^{3+}$/$[Fe_8S_7]^{2+}$) vs. $[Cp_2Fe]$/$[Cp_2Fe]^+$.[115]

In order to incorporate a light atom into FeMoco-analogues, the non-ionic assembly has been extended to use an oxygen source. An $[Fe_8S_6O]$ cluster, $[\{Fe_8S_6O(SDmp)_2\}(\mu\text{-}SDmp)_2(\mu\text{-}OCPh_3)]$ (**44**), was obtained from the reaction of $[Fe(OCPh_3)(\mu\text{-}SDmp)]_2$ with elemental sulfur and a small amount of water (**Scheme 12b**).[129] While water is the most accessible O source in this reaction, the $OCPh_3$ ligand could also provide the interstitial O atom by cleavage of its relatively weak O–C bond. In this reaction, the sulfur-centered analogue $[\{Fe_8S_7(SDmp)_2\}(\mu\text{-}SDmp)_2(\mu\text{-}OCPh_3)]$ (**45**) was also generated as a minor byproduct and it co-crystallized with **44**. Therefore, crystals of **44** were often

contaminated with **45**, which appeared as a compositional disorder in X-ray crystallographic analysis. The occupancy ratio of **44** to **45** fluctuated from 100:0 to 75:25 (**44**:**45**). In the [Fe_6O] core of **44**, the central O atom interacts with four Fe atoms out of six inner Fe atoms and exhibits the Fe-O bonds of 1.910(6)-2.190(5) Å. The two inner Fe atoms, which are distant from the μ_4-O atom (3.361(5) Å), interact with the mesityl rings of the μ_2-SDmp ligands (2.505(2) Å for the shortest Fe-C distance), and this interaction allows two Fe atoms to position themselves away from the central oxygen (**Figure 11**). In other words, cleavage of Fe-(central atom) bonds creates vacant sites on two inner Fe atoms, which are filled by aromatic substituents. Thus the Fe-mesityl interaction mimics a proposed substrate binding mode of FeMoco.

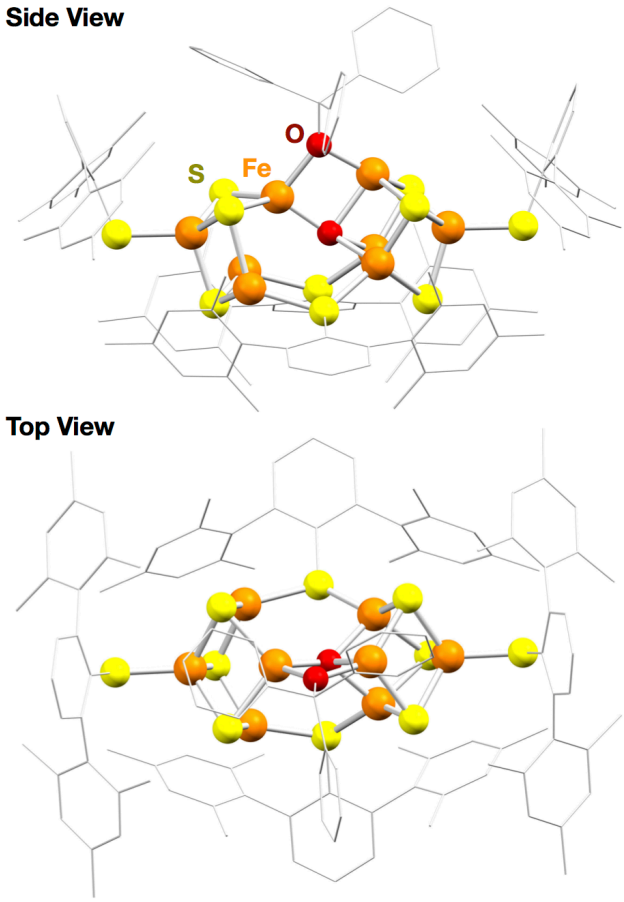

Figure 11. Side view and top view of [{$Fe_8S_6O(SDmp)_2$}(μ-SDmp)$_2$(μ-$OCPh_3$)] (**44**). Hydrogen and disordered atoms are omitted for clarity. Carbon atoms are shown as wireframe.

2.2 Nitrogenase-Related Reactions of Biomimetic Metal-Sulfur Clusters

While substrate selectivity is one of the textbook features of enzymatic reactions, this criterion should not be applied to nitrogenase, as its substrate (N_2) is too small to be specifically recognized at the binding pocket. Combined with its strong reducing activity, nitrogenase is expected to be promiscuous toward small molecules that are more reactive than N_2 and small enough to pass through the substrate channel extending from the protein surface to the metal-sulfur cofactor. The extracted forms of cofactors were also shown to catalyze some reduction reactions, but not N_2 fixation.[130] **Table 1** summarizes the known small-molecule substrates of nitrogenases except for $>C_2$ organic compounds.[131] With regard to the functional analogues of nitrogenase cofactors, we describe herein the activation and reduction of nitrogenase-related substrates facilitated by biomimetic metal-sulfur clusters. It should be noted that intermediate clusters and cluster degradation processes have rarely been characterized in the reactions addressed below. Future studies in this field are expected to address the mechanistic insights, *e.g. in-situ* identification of the substrate binding sites and the electronic states of possible intermediates, through spectroscopic techniques, alongside seeking higher catalytic activities.

Table 1. Reduction of small-molecule substrates catalyzed by nitrogenases and extracted cofactors. N_2H_2 = diazene, N_2H_4 = hydrazine, N_3^- = azide, N_2O = nitrous oxide, NO_2^- = nitrite, C_2H_2 = acetylene, COS = carbonyl sulfide, NH_2CN = cyanamide, CH_3NC = methyl-isocyanide, SCN^- = thiocyanate, OCN^- = cyanate, RCHO = aldehydes. *Kp* = *Klebsiella pneumoniae*, *Ac* = *Azotobacter chroococcum*, *Av* = *Azotobacter vinelandii*, *Rc* = *Rhodobacter capsulatus*, *Rp* = *Rhodopseudomonas palustris*.

Catalyst	Substrate	Product(s)	Reductant	Rate[l]	TON[l, s]	Ref.
Mo-nitrogenase	N_2	NH_3	Fe protein	990 (*Kp*), 1040 (*Av*), 470 (*Rc*)[m]	-	14, 16
	N_2	NH_3	CdS nanocrystals[h]	315 (*Av*)	$1.1\cdot10^4$ (*Av*)[t]	132
	N_2H_2	NH_3[e]	Fe protein	400 (*Av*)[m]	-	133
	N_2H_4	NH_3	Fe protein	320 (*Av*)[m]	-	134, 135
	N_2H_4[a]	NH_3	Eu-DTPA[i]	~490 (*Av*)[m, n]	156 (*Av*)[n, t, u]	135, 136,
	N_3^-	NH_3, N_2H_4,[f] N_2	Fe protein	350/57 (for NH_3/N_2H_4, *Kp*), 225/45/104 (for $NH_3/N_2H_4/N_2$, *Av*)[m]	1709/561/1070 (for $NH_3/N_2H_4/N_2$, *Kp*)[t]	137, 138
	N_3^-[a]	NH_3	Eu-DTPA,[i] Eu-EGTA, Eu-EDTA[j]	-	39 (*Av*)[t, u]	135
	N_2O	N_2	Fe protein	1700 (*Kp*)[m]	-	139
	NO_2^-	NH_3	Fe protein	~120-130 (*Av*)[m, o]	-	140
	CO_2	CO, CH_4[g]	Fe protein	-	0.0073 (for CH_4, *Av*)[t, o]	141
	CO_2, C_2H_2[b]	CH_2=$CHCH_3$	Fe protein	-	~0.9 (*Av*)[t, o]	142
	COS	CO	Fe protein	37.2 (*Av*)[m]	-	143
	CO	C_2-C_4 hydrocarbons[g]	Fe protein	~0.021 (for C_2H_4, *Av*)[m, o, p]	-	144
	CN^-	CH_4,C_2H_4, C_2H_6, NH_3	Fe protein	-	-	145
	CN^-	CH_4, NH_3	$[Ru(bpy)_3]^+$[k]	0.4 (for CH_4, *Av*)[m, o]	-	146
	NH_2CN	CH_4, CH_3NH_2, NH_3	Fe protein	68 (for CH_4, *Kp*)[m, o]	128/90/345 (for $CH_4/CH_3NH_2/NH_3$, *Kp*)[t]	147
	CH_3NC	CH_4, CH_3NH_2	Fe protein	-	-	148
	SCN^-	CH_4, NH_3, S^{2-}, CN^-	Fe protein	31 (for CH_4, *Av*)[q]	-	149
	OCN^-	CO	Fe protein	116 (*Av*)[q]	-	149
	CS_2	S^{2-}	Fe protein	157 (*Av*)[q]	-	149
	C_2H_2	C_2H_4	Fe protein	1693 (*Kp*), 2000 (*Av*), 1200 (*Rc*)[m]	-	14, 16
	CH_3CN	C_2H_6, NH_3	Fe protein	-	-	131, 150
	H^+	H_2	Fe protein	2100 (*Kp*), 2220 (*Av*), 1300 (*Rc*)[m]	-	14, 16
	H^+[c]	H_2	Eu-EDTA	-	262 (*Av*)[t]	135

V-nitrogenase	N_2	NH_3, N_2H_4	Fe protein	350 (*Ac*), 660 (*Av*) [m]	-	14, 16, 151
	CO_2	CO, CH_4, C_2H_2, C_2H_6 [g]	Fe protein	-	0.3/0.02/0.04/0.002 (for CO/ CH_4/C_2H_2/C_2H_6, *Av*) [t]	141
	CO	C_1-C_4 hyhydrocarbons	Fe protein	~31 (for C_2H_4, *Av*) [m, o, p]	-	144, 152
	C_2H_2	C_2H_4, C_2H_6	Fe protein	608/15 (for C_2H_4/C_2H_6, *Ac*), 560/16 (for C_2H_4/C_2H_6, *Av*) [m]	-	14, 151
	NH_2CN	CH_4, CH_3NH_2, NH_3	Fe protein	7.5 (for CH_4, *Ac*) [m, o]	-	147
	CH_3CN	C_2H_6, NH_3	Fe protein	-	-	131, 150
	H^+	H_2	Fe protein	1348 (*Ac*), 1725 (*Av*) [m]	-	14, 151
Fe-nitrogenase	N_2	NH_3	Fe protein	110 (*Av*), 350 (*Rc*) [m]	-	14, 153
	CO_2(?)	CH_4	Fe protein	-	1 (*Rp*)[t]	154
	C_2H_2	C_2H_4, C_2H_6	Fe protein	58/26 (for C_2H_4/C_2H_6, *Av*), 260/5 (for C_2H_4/C_2H_6, *Rc*) [m]	-	14, 153
	H^+	H_2	Fe protein	350 (*Av*), 2400 (*Rc*) [m]	-	14, 153
Extracted FeMoco	CO_2	C_1-C_3 hydrocarbons	SmI_2	-	68 [m, v]	107, 155
	CO	C_1-C_5 hydrocarbons	Eu-DTPA,[i] SmI_2	-	~0.06 (Eu-DTPA reductant, for CH_4), 225 (SmI_2 reductant) [m, v]	107, 155, 156, 157
	CN^-	C_1-C_7 hydrocarbons	Eu-DTPA,[i] SmI_2	-	~0.4 (Eu-DTPA reductant, for CH_4), 914 (SmI_2 reductant) [m, v]	107, 155, 156, 157
	RCHO, CO[d]	C_1-C_4 hydrocarbons	Eu-DTPA[i]	-	41 (CH_2O and CO substrates), 84 (CH_3CHO and CO substrates) [m, v]	158
	RCHO, CN^- [d]	C_1-C_4 hydrocarbons	Eu-DTPA[i]	-	64 (CH_2O and CN^- substrates), 84 (CH_3CHO and CN^- substrates) [m, v]	158
	RCHO[d]	C_1-C_4 hydrocarbons	Eu-DTPA[i]	-	67 (CH_2O substrate), 112 (CH_3CHO substrate) [m, v]	158
	C_2H_2	C_2H_4, C_2H_6	$NaBH_4$, Zn/Hg, Eu/Hg, Na/Hg,	34 ($NaBH_4$ reductant), 2-3	190 (Na/Hg reductant)	159, 160,

			electrochemical reduction	(Zn/Hg reductant), 40-50 (Eu/Hg reductant) [r]		161, 162, 163
Extracted FeVco	CO_2	C_1-C_3 hydrocarbons	SmI_2	-	1.8 [m, v]	155
	CO	C_1-C_5 hydrocarbons	Eu-DTPA,[i] SmI_2	-	~0.02 (Eu-DTPA reductant, for CH_4), 2.7 (SmI_2 reductant) [m, v]	155, 156, 157
	CN^-	C_1-C_5 hydrocarbons	Eu-DTPA,[i] SmI_2	-	~0.6 (Eu-DTPA reductant, for CH_4), 13 (SmI_2 reductant) [m, v]	155, 156, 157

[a] Using *α*-Y64H, *β*-Y98H, or *β*-F99H mutant of MoFe protein. [b] Using *α*-V70A/*α*-H195Q mutant of MoFe protein. [c] Using *β*-Y98H mutant of MoFe protein. [d] R = H, CH_3. [e] N_2 production was not evaluated. [f] Produced from HN_3. [g] Nearly stoichiometric or substoichiometric products. [h] Using photoexcited materials. [i] DTPA = diethylenetriaminepentaacetic acid. [j] EGTA = ethylene glycol-bis(β-aminoethyl ether)-*N*,*N*,*N*′,*N*′-tetraacetic acid; EDTA = ethylenediaminetetraacetatic acid. [k] Photogenerated covalently linked species; bpy = bipyridine. [l] Best values reported in references are shown. [m] Normalized by (nmol product)·(mg catalytic component)$^{-1}$·(min)$^{-1}$. When specifc activities were reported as (nmol product)·(nmol catalytic component)$^{-1}$·(min)$^{-1}$, the values were converted based on formula weights of the corresponding proteins. [n] Using α-Y64H mutant of MoFe protein. [o] Exact values were not shown and/or values for all products were not described. [p] Values only for major products are shown. [q] Described as (nmol product)·(nmol Fe protein)$^{-1}$·(min)$^{-1}$. [r] Normalized by (nmol product)·(nmol catalytic component)$^{-1}$·(min)$^{-1}$. [s] TON = turnover number. [t] Normalized by (nmol product)·(nmol catalytic component)$^{-1}$. Reported values were converted based on formula weights of the corresponding proteins, when necessary. [u] Using Eu-EDTA as a reductant. [v] Calculated based on total reduced substrates.

2.2.1 Metal-Sulfur Clusters in N_2 Chemistry

Among the wide variety of substrates in the nitrogenase reactions, N_2 is of particular interest. However, none of the M-S clusters in **section 2.1** have been found to bind N_2. Before describing a few successful N_2-clusters, to be discussed below, here we first discuss a major reason for difficult N_2 binding —the facile aggregation of M-S clusters. A vacant metal site is a prerequisite for N_2 binding, but the site can readily become occupied by a sulfur atom of a different cluster. This phenomenon is exemplified with edge-bridged $[MoFe_3S_4]_2$ clusters (precursors in **Schemes 4** and **5**), which were prepared by the removal of terminal ligands on Fe from $[MoFe_3S_4]$ cubes and the formation of inter-cubic Fe-S interactions. Even though N_2 can coordinate to the vacant site, replacement of the N_2 by a sulfur atom can follow due to the typically strong metal-sulfur bonds relative to metal-N_2 interactions, which lead to a short lifetime of the tentative N_2-bound species. As is the case for many isolated N_2 complexes (*e.g.* **section 3**), steric protection around the vacant metal site is one of the ways to hinder the exchange of trapped N_2. Another possible way to extend the lifetime of N_2-bound species is to prevent cluster aggregation by immobilization to a matrix or a support, and this would provide one reason why FeMoco works only in the protein matrix.

In the context of functional mimics, a seminal compound is the first N_2-cluster reported by Mizobe *et al*, $[Cp^*_3Ir_3S_4Ru(N_2)(tmeda)]$ (**46**; tmeda = $Me_2NCH_2CH_2NMe_2$),[164] which was synthesized by chemical reduction of a heterometallic Ir-Ru-S cube $[Cp^*_3Ir_3S_4Ru(tmeda)(MeCN)]^{2+}$ (**47**) with $[Cp_2Co]$ and $[Cp^*_2Co]$ (1 equiv. each) under N_2 (**Scheme 13**). The proposed Ru^{II} assignment of **46** is consistent with the major oxidation state of isolated Ru-N_2 complexes bearing S-based ligands (see **section 3.1.2**). Although the N–N distance of the Ru-N_2 moiety in **46** (1.06(1) Å) is comparable to that of *free* N_2 (1.098 Å), the N-N stretching band of **46** (ν_{N2} = 2019 cm^{-1}) appeared at a lower frequency than *free* N_2 (2358.6 cm^{-1}) and is slightly lower than that of a phosphine-supported Ru^0–N_2 complex $[Ru(N_2)\{P(CH_2CH_2PPh_2)_3\}]$ (ν_{N2} = 2080 cm^{-1}).[165] A certain extent of back-donation therefore occurs in **46** from the d-orbitals of Ru to the π*-orbitals of N_2, which might result from the π-donor ability of three sulfides as well as their strong σ-donation. However, neither protonation nor silylation of the Ru-bound N_2 in **46** has been achieved so far.

Scheme 13. Accommodation of N_2 on the Ru site of [Ir_3S_4Ru] cube to furnish **46**.

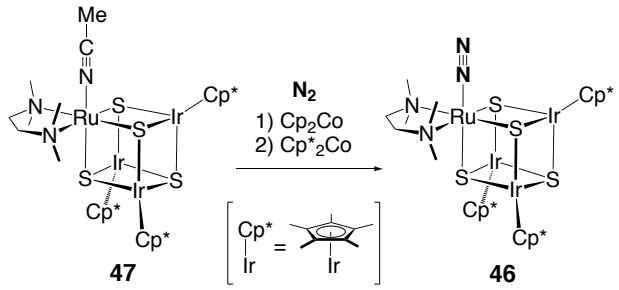

Activation and protonation of N_2 on a metal-sulfur cluster was recently accomplished by Ohki *et al.* with a double-cubane type N_2-cluster [{Cp*$_3$Mo$_3$S$_4$Ti}$_2$(μ-N_2)]$^{2-}$ (**48**) (**Scheme 14**),[166] which was prepared from the reaction of a cubic cluster [Cp*$_3$Mo$_3$S$_4$TiCl$_2$] with 4 equiv. KC_8 under N_2. Addition of an excess of KC_8 in this reaction led to the formation of the 1-electron reduced form of the N_2-cluster, [{Cp*$_3$Mo$_3$S$_4$Ti}$_2$(μ-N_2)]$^{3-}$ [**48**]$^-$, which was obtained in a trace amount. Formation of the central Ti-N=N-Ti moiety in **48** through N_2 uptake was corroborated by physical measurements of **48** and ^{15}N-labeled **48**. For instance, the ^{15}N NMR of the ^{15}N-labeled **48** exhibited the signal of bridging N_2 at –75.4 ppm (relative to CH_3NO_2) in THF-d_8. In the resonance-Raman spectrum, the N-N stretching band was found at ν_{N2} = 1240 cm^{-1}, which shifted to 1200 cm^{-1} upon isotope labeling with $^{15}N_2$. The fact that the N-N stretching frequency of **48** falls in between those of $H_3CN{=}NCH_3$ (1575 cm^{-1})[167] and $H_2N{-}NH_2$ (1111 cm^{-1})[168] indicates a character between N=N double and N-N single bonds for the Ti-N=N-Ti moiety. This fact was further endorsed by the crystallographically determined N–N distance (1.294(7) Å) of **48**, which is slightly longer than the N=N double bond of $H_3CN{=}NCH_3$ (1.25 Å)[169]. The 1-electron reduced form [**48**]$^-$ exhibits a comparable N-N bond distance (1.293(5) Å), whereas its Mo–Ti and Mo–Mo distances differ from those of **48** (Mo–Ti = 3.0242(8) Å for [**48**]$^-$ vs. 3.0487(12) Å for **48**; Mo–Mo = 2.8668(6) Å for [**48**]$^-$ vs. 2.8150(8) Å for **48**), indicating a relatively large contribution by the metals in the storage of the additional electron.

A high degree of N_2 reduction in **48** enabled the formation of NH_3 and N_2H_4 from the Ti-N=N-Ti moiety. Simple protonation of **48** with H_2O furnished 0.12(3) equiv. NH_3 as well as 0.60(3) equiv. N_2H_4, and the amount of NH_3 increased to 0.47(27) equiv. in the presence of 6 equiv. KC_8. The maximum NH_3 yield of 1.20(19) equiv. was generated when 100 equiv. KC_8 was added prior to the protonation with H_2O. No detection of N_2H_4 in this case implies that the N≡N bond cleavage occurs prior to the

complete protonation. Exclusive formation of $^{15}NH_3$ from the ^{15}N-enriched **48** under a $^{14}N_2$ atmosphere confirmed the conversion of the Ti-^{15}N=^{15}N-Ti moiety and showed that the N_2 conversion is not catalytic. Detection of the trinuclear $[Mo_3S_4]$ species in the mass spectrum after hydrolysis suggested the dissociation of the Ti atom from the cubic $[Mo_3S_4Ti]$ core. Dissociation of the Ti atom indicates a relatively low affinity between a *hard* and *early* transition metal (Ti) and *soft* sulfur atoms. Nevertheless, it is noteworthy that the Cp-supported $[Mo_3S_4]$ clusters serve as versatile precursors for cubanes and accommodate various transition metals at the voided corner.[170,171,172,173,174,175,176,177,178,179,180,181,182] Hence, the synthetic methodology of employing $[Mo_3S_4]$ clusters and heterometals may help to develop superior functional mimics of FeMoco.

Scheme 14. Synthesis of metal-sulfur-N_2 clusters **48** and [**48**]$^-$ featuring a Ti-N=N-Ti moiety and the formation of NH_3 from **48**.

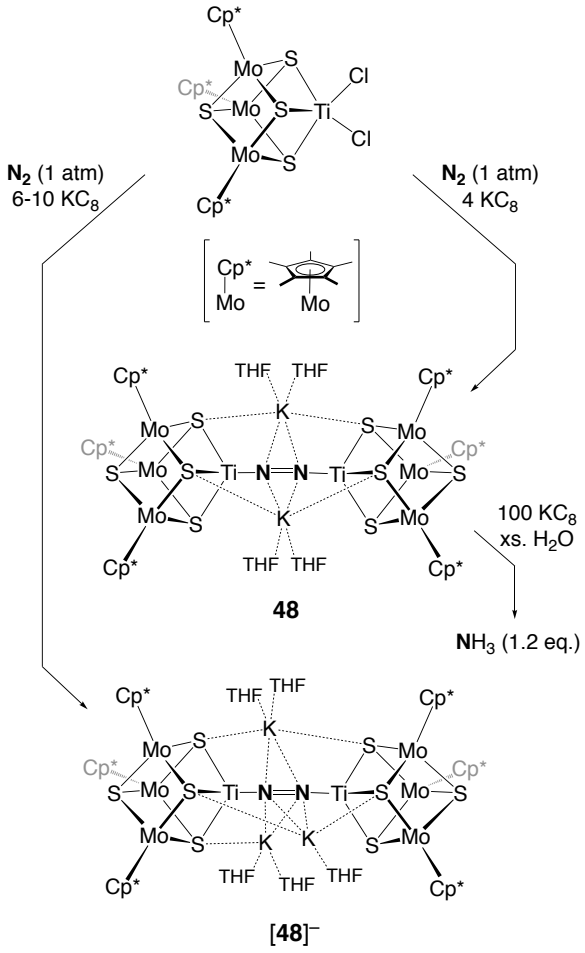

A common feature of the currently known N_2-clusters (**Schemes 13** and **14**) is the three Cp* ligands on a cube. These ligands work as protecting groups for metals, owing to the multidentate character of Cp* leading to the robust Cp*-M (M = Mo, Ir) bonding. Such site-differentiation induced by ancillary ligands is important to generate the vacant metal site at a specific metal center (Ti or Ru) to leave other metals (Mo or Ir) intact during the reaction. Steric hindrance imposed by three Cp* ligands would also offer an advantage to slow or terminate the cluster aggregation. Generation of more than one vacant metal site in a metal-sulfur cluster is often problematic, because multiple sites facilitate the aggregation even more. Furthermore, multiple sites in a cluster are usually not arranged for cooperative activation of a substrate (**Figure 12a**). An exceptional cluster is FeM'co (M'

= Mo, V, Fe), which features μ_2-S atoms in the middle. Putative removal of a μ_2-S from FeM'co generates two neighboring vacant Fe sites, which can interact with the same substrate, and may lead to efficient N_2 activation (**Figure 12b**). A recent crystallographic analysis of the VFe protein exemplifies the possibility of the removal of μ_2-S for substrate activation, while it does not reveal a N_2-bound species.[13] Another important factor for N_2 activation by synthetic metal-sulfur clusters is their stability under reducing conditions, because N_2 complexes are typically synthesized via treatment of precursor metal complexes with strong reducing agents under N_2 (*e.g.* **section 3**). Typical biomimetic $[Fe_4S_4]$ clusters are not very stable under highly oxidizing/reducing conditions, and for instance, a highly-oxidized $[Fe_4S_4]^{4+}$ cluster bearing amide ligands was found to split into 2 x $[Fe_2S_2]$ clusters in the presence of pyridines.[183] Notably, isolated super-reduced $[Fe_4S_4]^0$ clusters have been limited to those supported by CN^-, N-heterocyclic carbenes, CO, or NO,[184,185,186] indicating that a π-acidic property is crucial to stabilize the super-reduced state. Rigidity of the cluster cores would also be important for FeM'co (M' = Mo, V, Fe), as typical lifetimes of nitrogenases are hours and may imply degradation of the clusters. In this regard, the strength of M'-S bonds[187] may contribute to the degradation resistance of FeM'co and to help retaining their catalytic activities, while electronic effect of M' is important in the reductive elimination of H_2 from FeM'co and the accompanying N_2 binding/reduction.[188] Robustness of Mo-S bonds relative to Fe-S bonds may be exemplified with a suggested intermediary step of the biosynthesis of FeMoco, where the Fe-S bonds of a peripheral Fe atom of L-cluster ($[Fe_8S_9C]$ cluster) are cleaved for incorporation of a Mo atom to furnish M-cluster (**Figure 13**).[71]

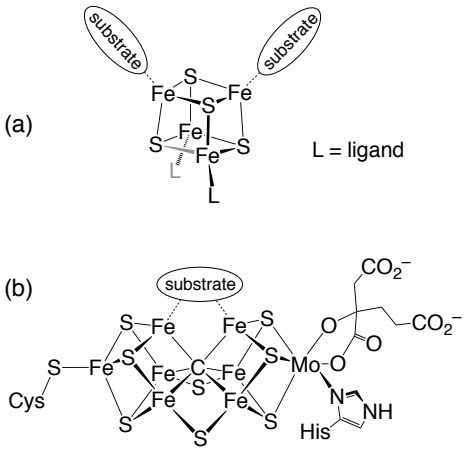

Figure 12. Speculative drawings of (a) $[Fe_4S_4]$ cluster and (b) FeMoco with two vacant Fe sites, to which substrates are bound. The two sites in (a) cannot sustain intramolecular cooperativity, while those in (b) can cooperate to activate a substrate.

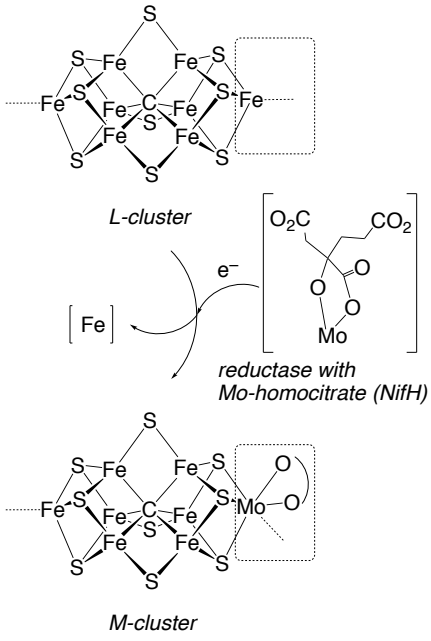

Figure 13. Schematic drawing of an intermediary step of the proposed biosynthesis of FeMoco. A peripheral Fe atom of L-cluster is replaced by a Mo atom.

Besides the synthesis and reactions of N_2-bound metal-sulfur clusters, the use of $[Fe_4S_4]$ clusters as additives in N_2-reducing systems has been investigated. Soon after the first synthesis of the $[Fe_4S_4]$ cluster as a ferredoxin model in 1972,[189] this class of compounds was brought into N_2 reduction chemistry as potential electron mediators. The groups of Schrauzer and van Tamelen independently reported N_2 reduction using Mo complexes in the presence of $[Fe_4S_4]$ clusters. In Schrauzer's system, a mixture of $[MoO_4]^{2-}$/cysteine or a cyano complex $[Mo(O)(H_2O)(CN)_4]^{2-}$ were utilized as precursors of reactive species in the presence of $[Fe_4S_4(S^nPr)_4]^{2-}$ as a possible electron mediator.[190,191] The N_2-fixation reaction performed with a mixture of $[Mo(O)(H_2O)(CN)_4]^{2-}$, the $[Fe_4S_4]$ cluster, BH_4^-, and ATP, was reported to give 6.3 x 10^{-6} equiv. NH_3 and 0.63 x 10^{-6} equiv. N_2H_4 after incubation for 6 h at 10˚C, and without $[Fe_4S_4]$, the total yield of fixed nitrogen dropped to *ca.* 60% of original amounts. It should be noted that the $[Fe_4S_4]$ cluster does not participate in the N_2 reduction.[192] In the mid-1970s, van Tamelen and coworkers examined NH_3 synthesis from the Mo–N_2 complex $[Mo(N_2)_2(dppe)_2]$ (dppe = diphenylphosphanoethane), by mixing with $[Fe_4S_4(L)_4]^{n-}$ (L = $S_2C_2Ph_2$, n = 0 or L = SEt, n = 2) and excess reducing agents (sodium naphthalenide (NaNp) or sodium fluoranthenide (NaFl)) followed by quenching with HCl, that generated up to 0.27 equiv. NH_3.[193,194] It is to be noted that the same group later reported NH_3 production in a higher yield (up to 0.37 equiv.) from the same Mo–N_2 complex $[Mo(N_2)_2(dppe)_2]$ upon treatment only with aqueous acids (*i.e.* HCl, HBr, *p*-toluene sulfonic acid, trifluoroacetic acid).[195] The authors also suggested the formation of up to 0.27 equiv. NH_3 by a mixture of $[Fe_4S_4(S_2C_2Ph_2)_4]$ and *ca.* 300 equiv. NaNp.[193] Whereas the formation of $[Fe_4S_4(S_2C_2Ph_2)_4]^{4-}$ was considered in the literature, this system would likely involve degradation products of the $[Fe_4S_4]$ cluster because the $[Fe_4S_4(S_2C_2Ph_2)_4]^{4-}$ oxidation level is out of the range of electrochemical measurements.[196] As discussed above, super-reduced $[Fe_4S_4]$ clusters are usually unstable unless π-acidic ligands are attached.

Electrocatalytic N_2 reduction in the presence of metal-sulfur clusters has been also investigated. Tanaka *et al.* electrochemically generated the reduced species by controlled potential electrolysis of homo- and hetero-metallic cubane clusters $[Fe_4S_4(SPh)_4]^{2-}$ (**49**) and $[\{MoFe_3S_4(SPh)_3\}_2(\mu\text{-}SPh)_3]^{3-}$ (**50**), and then tested the N_2-fixation reactions.[197] In the presence of **49** or **50** in a mixture of MeOH and THF, electrolysis at –1.30 V vs. SCE (standard caromel electrode) for 24 h yielded NH_3 up to 0.21 equiv. (with **49**, MeOH/THF = 3/7) or 0.16 equiv. (with **50**, MeOH/THF = 7/3), respectively (**Scheme 15a**). Under the applied potential, **49** and **50** are reduced to levels of $[Fe_4S_4(SPh)_4]^{3-}$ ([**49**]$^-$) and

[{$MoFe_3S_4(SPh)_3$}$_2$(μ-$SPh)_3$]$^{5-}$ ([**50**]$^{2-}$). The ratio of solvents appeared to affect the efficiency. In the reactions employing **49**, the MeOH/THF ratio of 3/7 provided the maximum NH_3 yield (0.21 equiv.) and the highest current efficiency (1.6%), while for the reactions using **50** the 3/7 ratio of MeOH/THF gave the highest current efficiency (0.51%) but the 7/3 ratio led to the maximum yield (0.16 equiv.). At a lower potential of –1.70 V vs. SCE in MeOH/THF = 1/1, where **49** is further reduced to the super-reduced state [$Fe_4S_4(SPh)_4$]$^{4-}$ ([**49**]$^{2-}$), the current efficiency went down to <0.1%. The reactions were further examined in an aqueous medium, in which clusters are not well-dissolved but rather suspended. Cluster **49** dispersed in an NaOH solution (pH 12.5) containing Triton X-100 (0.8 mM) as a surfactant and promoted the generation of 0.26 equiv. NH_3 upon electrolysis at –1.40 V vs. SCE for 4 days. Under the same conditions with a suspension of **50**, the NH_3 yield rose to 1.95 equiv. after 4 days, which may imply that metal-containing species derived from **50** were responsible for the reaction (**Scheme 15b**). Gradual degradation of **50** for generation of the reactive species can be corroborated by the significant increase in the NH_3 yield after 4 days (1.95 equiv.) relative to the reaction after 2 days (0.33 equiv.), exhibiting nearly 6 times higher NH_3 yield with double reaction time (**Scheme 15b**). The current efficiencies of these aqueous reactions were ~0.07%, and thus most of electrons transferred from the electrode were consumed for H_2 evolution.

Scheme 15. Electrochemical N_2 reduction in the presence of metal-sulfur clusters: a) in MeOH/THF solutions, b) in aqueous solutions where clusters are dispersed.

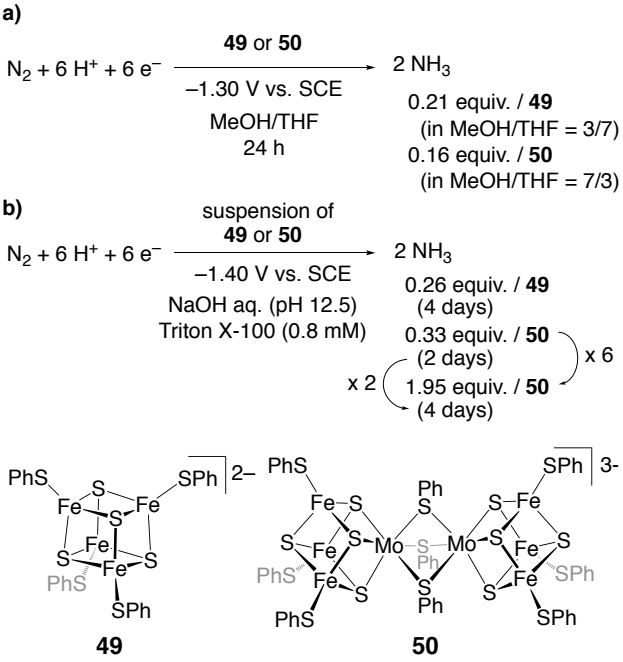

Given the reaction time of ~4 days, the instability of reduced metal-sulfur clusters, and the increased activity over the time course of the reaction, the species responsible for N_2 reductions were probably distinct from clusters **49** and **50**. In this context, the results referred to above, particularly for **50**, have relevance to the electrocatalytic N_2 reduction by solid metal-sulfides (**section 4.3**) or an N_2 reduction system using phospholipid-modified sodium amalgam (Na/Hg) and Mo complexes (**Scheme 16**).[198,199] In the presence of Na/Hg, a phospholipid (phosphatidylcholine), and additives (Mg^{2+} and phosphines), Shilov *et al*. reported that Mo species that were generated in a mixed MeOH/H_2O solvent catalyzed reduction of N_2 into N_2H_4 and NH_3 up to 1000 turnovers under ambient pressure and >10000 turnovers under high pressure (70 atm). The authors proposed that the reduced Mo species are located near the surface of Na/Hg, the phospholipid covers the surface of Na/Hg to control the H^+ flow, and the phosphines attach to Mo to prevent catalyst deactivation. Some Mo clusters, $[Mo^{V}(O)Mg(MeOH)_2(OMe)_5]_2$, $[Mo^{VI}(O)_2Mg(MeOH)_2(OMe)_4]_2$, and $[Mg_2Mo_8O_{22}(OMe)_6(MeOH)_4]^{2-}$, can be crystallized from the catalytic systems. They were found to serve as pre-catalysts for N_2 reduction, exhibiting the highest activity with the largest cluster

$[Mg_2Mo_8O_{22}(OMe)_6(MeOH)_4]^{2-}$.

Scheme 16. Reduction of N_2 by Mo species generated in a mixed MeOH/H_2O solvent in the presence of Na/Hg. Additives such as phosphatidylcholine, Mg^{2+}, and phosphines, were found to improve the catalytic activity.

$$N_2 + 6\,H^+ + 6\,e^- \xrightarrow[Na/Hg]{Cat.,\ MeOH/H_2O} 2\,NH_3$$

Cat.	additive	p_{N2}/ atm	TON[c] per Mo N_2H_4 + 0.5NH_3
$MoCl_5$	-	70	0.5
$MoCl_5$	Mg^{2+}	70	2.5
$MoCl_5$	PL[b]	70	25
$Mo_8Mg_2^{2-}$ [a]	PL, PPh_3	1	100-200
$Mo_8Mg_2^{2-}$ [a]	PL, PPh_3	70	10000

[a] $Mo_8Mg_2^{2-}$ = $[Mg_2Mo_8O_{22}(OMe)_6(MeOH)_4]^{2-}$. [b] PL = phospholipid. [c] TON = turnover number.

2.2.2 Catalytic Reduction of Nitrogenase-Related Substrates by Metal-Sulfur Clusters

Catalytic reduction of N_2 by biomimetic metal-sulfur clusters still remains challenging, and this is underscored by the inability of extracted FeMoco to perform N_2 reduction outside the protein scaffold.[130] On the other hand, the extracted FeMoco has been shown to catalyze the reduction of nitrogenase-related substrates such as C_2H_2 (acetylene), CO_2, CO, CN^-, and aldehydes (Table 1), while the acetylene reduction has been commonly used in biochemical studies as a benchmark to evaluate the catalytic activity of nitrogenase proteins. Furthermore, catalytic reduction of N_2H_4 may also provide some clues into understanding the relationship between the structural features and the functions of clusters. While mechanistic studies on stoichiometric reactions of Fe-S-based clusters[200] and catalytic functions of $[M_4S_4]$ clusters[38] have been summarized elsewhere, here we address the catalytic reduction of some nitrogenase-related substrates promoted by biomimetic metal-sulfur

clusters. The fate of the cluster precatalysts remains unclear in most of the reactions in this section, and it remains to be seen if one can isolate substrate-bound clusters or identify M-S clusters during/after catalytic reactions. Thus far, some protonated clusters and hydrazine adducts have been characterized.

2.2.2.1 Reduction of Acetylene and Nitrogen-Containing Substrates by Cuboidal [MFe_3S_4] Clusters (M = Mo, V, Fe)

From the late 1970s through the 1980s, FeMoco has been the subject of intensive spectroscopic studies both in the protein-bound and extracted forms. As suggested from an early extended X-ray absorption fine structure (EXAFS) study of the Mo atom in FeMoco,[201] a cuboidal [$MoFe_3S_4$] core had been one of the prominent candidates for a model of FeMoco, until the crystal structure of Mo-nitrogenase indicated that FeMoco was more complicated than a cuboidal [$MoFe_3S_4$] cluster.[202] In this context, cuboidal [M_4S_4] clusters were the first and most common class of metal-sulfur clusters examined in the activation of small molecules. The synthetic accessibility and thermodynamic stability of cuboidal clusters have additional advantages in catalytic applications. Hence, this section considers reactivity studies of the cuboidal clusters that contain Fe, Mo, and V atoms, in monomeric [M_4S_4] or dimeric [$M_4S_4]_2$ forms.

Because acetylene (C_2H_2) reduction is a typical assay utilized to evaluate enzymatic activity, the initial functional modeling of nitrogenases was attempted with the reduction of C_2H_2 by synthetic metal-sulfur clusters. In a report by Holm *et al.* in 1979, C_2H_2 was added to a mixture of reduced $[Fe_4S_4]^+$ clusters $[Fe_4S_4(SR)_4]^{3-}$ (R = Ph ([**49**]$^-$), *p*-MeC_6H_4), acetic acid (AcOH), and acetic anhydride (Ac_2O) in *N*-methylpyrolidinone (NMP), which led to the oxidation of the $[Fe_4S_4]^+$ clusters to the $[Fe_4S_4]^{2+}$ state and the concurrent formation of C_2H_4.[203] When acetic acid-d_4 and 1% v/v D_2O were used as proton sources in the reaction, *cis*-1,2-$C_2H_2D_2$ appeared as the predominant product, as was the case with the C_2H_2 reduction by nitrogenase. Electron transfer from the $[Fe_4S_4]^+$ cluster to C_2H_2 was supported by the UV-vis spectral changes of the reaction mixtures, as well as the inactivity of the $[Fe_4S_4]^{2+}$ clusters in the C_2H_2 reduction under the assay conditions. The maximum yield of C_2H_4 reached 64% relative to the amount of the $[Fe_4S_4]^+$ clusters after 200 min at 25˚C, which is in agreement with eq 1.

$$2[Fe_4S_4(SR)_4]^{3-} + 2H^+ + C_2H_2 \rightarrow 2[Fe_4S_4(SR)_4]^{2-} + C_2H_4 \text{ (eq 1)}$$

A related system using cluster [**49**]$^-$ and 2,6-lutidinium cation ([LutH]$^+$, H^+ source) in MeCN was later investigated in detail by Henderson *et al*.[204] Based on the kinetic analysis under various H^+ and ligand additive (PhSH) concentrations, it was proposed that [**49**]$^-$ is converted into a hydride/hydrosulfide cluster $[Fe_4HS_2(SH)_2(SPh)_3]^+$ and that this intermediate binds and eventually reduces C_2H_2. As reported by Shilov and coworkers, the 1-electron oxidized form of [**49**]$^-$, $[Fe_4S_4(SPh)_4]^{2-}$ (**49**), was found to function as a pre-catalyst for the reduction of C_2H_2 into C_2H_4 in the presence of Zn/Hg (an electron donor) in MeOH (**Scheme 17**), and the turnover number (TON) per **49** reached 20.[160] The catalytic activity is dependent on the redox potentials of the clusters, and so the TON using a different cluster $[(DMF)_3VFe_3Cl_3]^-$ (**6**) was only 0.7 with Zn/Hg reductant, but remarkably, improved up to 1000 with a stronger Na/Hg reductant (**Scheme 17**). Otsuka and Nakamura, *et al.* found that $NaBH_4$ works as a reductant in the catalytic reduction of phenylacetylene to styrene mediated by [**49**]$^-$,[205] while Ogo and coworkers reported analogous reductions of C_2H_2 and phenylacetylene catalyzed by an incomplete cuboidal cluster $[Mo(O)Fe_2S_3Cl_4]^{2-}$ in the presence of $NaBH_4$ as the reducing agent and H_2O as the proton source.[206]

Scheme 17. Reduction of C_2H_2 catalyzed by $[Fe_4S_4]$ or $[VFe_3S_4]$ clusters in the presence of Zn/Hg or Na/Hg.

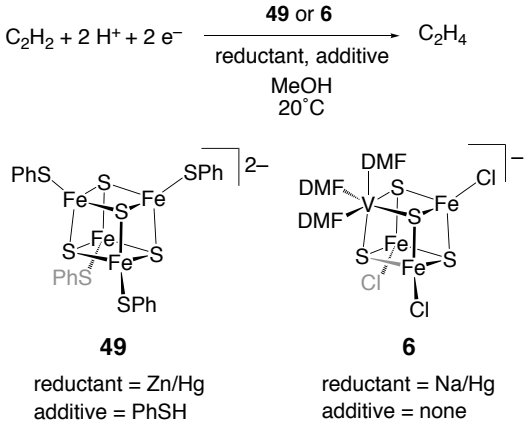

49

reductant = Zn/Hg
additive = PhSH

6

reductant = Na/Hg
additive = none

Tanaka and his colleagues employed **49** for electrochemical reduction of C_2H_2 in a mixed MeOH/THF solution containing LiCl electrolyte.[207] The observed reaction rate was 0.012 mol/(mol_{cat}·min) under the applied voltage at –1.25 V vs. SCE and was accelerated to 0.069 mol/(mol_{cat}·min) at –1.60 V (**Scheme 18**). The authors also assessed the catalytic activity of $[\{MoFe_3S_4(SPh)_3\}_2(\mu\text{-}SPh)_3]^{3-}$ (**50**), which exhibited 0.011 mol/(mol_{cat}·min) for C_2H_4 production at –1.25 V vs. SCE. The bathochromic shift of C-C stretches in the presence of the clusters, *i.e.* ν_{CC} = 1960 (free C_2H_2), 1890 (C_2H_2 with reduced **49**), and 1900 (C_2H_2 with reduced **50**)), suggests that C_2H_2 binds to the reduced forms of **49** and **50**.[208] An aqueous NaOH-H_3PO_4 solution was also utilized as the medium for the reactions promoted by $[Fe_4S_4(SR)_4]^{2-}$ (R = Ph (**49**), CH_2CH_2OH (**51**)) or $[\{MoFe_3S_4(SR)_3\}_2(\mu\text{-}SR)_3]^{3-}$ (R = Ph (**50**); R = CH_2CH_2OH (**52**)), although **49** and **50** were merely dispersed in this medium.[209] Turnover frequencies for C_2H_2 reduction were lower than 3 h^{-1} at pH 7.0-12.0 under potentials of –1.25 V or –1.40 V vs. SCE. A significant amount of H_2 was simultaneously produced at pH 7.0, where the produced H_2/C_2H_4 ratios were 1.50 - 18.34, but the ratios became lower to 0.14 - 1.86 at pH 12.0, indicating that the higher proton concentration facilitates the competing H_2 evolution.[207] In relation to the H_2 production, **49** and **50** have been shown to catalyze the H-D exchange reaction between H_2 and D_2 under reducing conditions, either in the presence of sodium acenaphthylenide or by electrolysis at –1.90 V for **49** or at –1.70 V for **50** vs. SCE.[210]

Scheme 18. Electrochemical reduction of C_2H_2 catalyzed by metal-sulfur clusters.

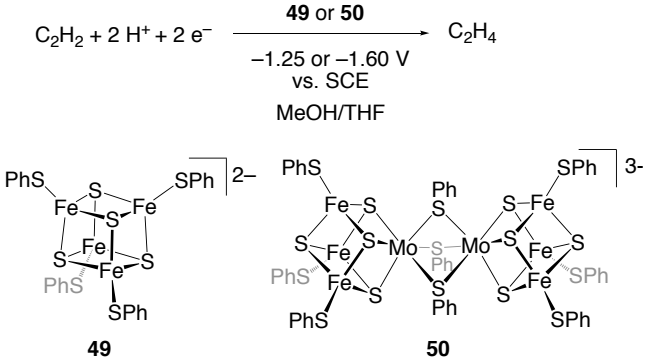

Electrochemical reduction of hydrazine (N_2H_4) to ammonia (NH_3) has also been achieved in the presence of **49**-**52** (**Scheme 19**).[211] In a mixed MeOH/THF solvent, 16 μmol of $[Fe_4S_4]$ cluster **49** or

$[MoFe_3S_4]_2$ cluster **50** catalyzed the conversion of 1.4 mmol of N_2H_4 into 790 or 1450 μmol of NH_3, respectively, after electrolysis at –1.25 V vs. SCE for 4 h. A high current efficiency of 97% was attained by **50** for NH_3 production in MeOH/THF, while the current efficiency decreased in an aqueous medium to 36% (pH 12.0) or 16% (pH 7.0) at –1.30 V vs. SCE. Under any conditions tested, the Mo-Fe-S clusters **50** and **52** outperformed the Fe-S clusters **49** and **51** in N_2H_4 reduction. Additionally, clusters **49** and **50** were also found to catalyze the reductions of CH_3NC and CH_3CN to produce CH_3NH_2, CH_4, C_2H_6, and C_2H_4 (from CH_3NC) and C_2H_6, C_2H_4, and NH_3 (from CH_3CN), respectively.[212]

Scheme 19. Electrochemical reduction of N_2H_4 to NH_3 catalyzed by metal-sulfur clusters.

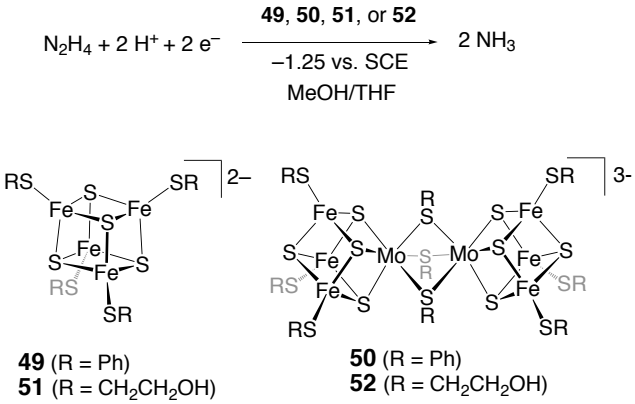

The electrochemical system developed by Tanaka and coworkers was further extended to the reduction of azide (N_3^-) by clusters **51** and **52**: a reaction that provided N_2 and NH_3 in roughly a 2:1 ratio, with a concomitant formation of a large amount of H_2 (≥15 fold excess relative to NH_3) and a small amount of N_2H_4 (up to 0.21 ratio to NH_3) (**Scheme 20**).[213] Turnover frequencies based on the NH_3 production were 2.8 and 5.0 h^{-1} for **51** and **52**, respectively, in H_2O at pH 7.0 under a controlled potential at –1.25 V vs. SCE. The authors proposed the intermediary formation of N_2H_2 in this system on the basis of the observation of N_2H_4 in the products and an experiment to trap N_2H_2 with stilbene to furnish N_2 and dibenzyl (1,2-diphenylethane). Suppression of H_2 evolution for the higher NH_3 yield can be accessed by a heterogeneous approach using a glassy carbon (GC) electrode modified with the $[MoFe_3S_4]_2$ cluster **50**,[214] and the amount of NH_3 produced after 150 min reduction of N_3^- was comparable to that of H_2 (83 μmol of NH_3 vs. 58 μmol of H_2) at pH 7.0 and –1.25 V vs. SCE. This GC electrode was further utilized in the reductions of alkyl azides (RN_3, R = CH_3, $HOCH_2CH_2$),[215,216] NO_3^-,

NO_2^-, and NH_2OH.[217]

Scheme 20. Electrochemical reduction of N_3^- catalyzed by metal-sulfur clusters.

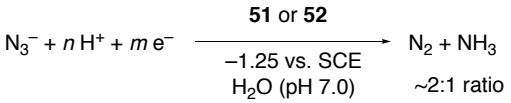

Coucouvanis *et al.* have investigated catalysis by cubane-type clusters in the presence of reducing agents. Some cuboidal $[MoFe_3S_4]$ clusters such as $[(Cl_4\text{-cat})(MeCN)MoFe_3S_4Cl_3]^{2-}$ (**2**) and $[(citrate)MoFe_3S_4Cl_3]^{3-}$ (**5**) (see **section 2.1.1.1**) were found to efficiently catalyze the reduction of N_2H_4, where cobaltocene (Cp_2Co) and lutidinium cation ($[LutH]^+$) were used as electron and proton sources, respectively (**Scheme 21a**).[218, 219] This reaction system attained almost quantitative conversion of 10 equiv. N_2H_4 and >71% conversion of 40 equiv. N_2H_4 into NH_3. The authors suggested that the generation of a Mo-NH_2-NH_2 moiety followed by protonation of the terminal NH_2 group is a prerequisite for the formation of the first NH_3 molecule from N_2H_4. The significantly lower catalytic activity of $[Fe_4S_4Cl_4]^{2-}$ under the same reaction conditions indicated that the Mo atom captures N_2H_4.[219] The suggested generation of a Mo-NH_2-NH_2 moiety during catalysis was reinforced by the formation of an analogue of **2** bearing phenylhydrazine ($PhHNNH_2$) and its catalytic activity. A recent theoretical study also suggested the formation of the Mo-NH_2-NH_2 moiety and proposed the N–N cleavage from the protonated Mo-NH_2-NH_3 species as the rate-determining step.[220] Even though a bridging form of N_2H_4 has been achieved with dimers of cubes, $[\{(Cl_4\text{-cat})MoFe_3S_4Cl_3\}_2(\mu\text{-}N_2H_4)]^{4-}$ (**53**)[221] and $[\{(Cl_4\text{-cat})MoFe_3S_4Cl_2\}_2(\mu\text{-}N_2H_4)(\mu\text{-}S)]^{4-}$ (**54**) (**Scheme 21b**),[222,223] conversion of their Mo-NH_2-NH_2-Mo units into NH_3 was unsuccessful after a 2 h incubation with Cp_2Co and $[LutH]^+$. In contrast to $[(Cl_4\text{-cat})(L)MoFe_3S_4Cl_3]^{2-}$ (L = MeCN, CH_3NH_2, etc.) with a relatively labile ligand L, the Mo site of **5** is occupied by a tridentate citrate. Although chelation may hinder generation of the Mo-based binding site, **5** and analogues of **5** with tridentate polycarboxylates worked as catalysts. The variation of carboxylates showed a limited impact on the catalytic activity,[224] which was attributed to the lability of a part of the polycarboxylate ligands on Mo in the presence of proton sources. All of the above results demonstrated by Coucouvanis *et al.* are in agreement with the generation of the Mo reaction site, to which N_2H_4 is terminally bound by one of the nitrogen atoms. Although the results of the experiments using synthetic clusters can be extended to imply that the Mo atom of

FeMoco works as the reaction site, recent biochemical studies indicated that the inner Fe atoms of FeMoco serve as the substrate binding site,[17] particularly in the reaction with CO.[225] The direct observation of N_2-derived species on FeMoco is necessary to clarify this point, and the possible reasons behind the suggested discrepancy between synthetic clusters and FeMoco would be a matter of future debate.

Scheme 21. a) Catalytic reduction of N_2H_4 mediated by [$MoFe_3S_4$] clusters in the presence of electron and proton sources. b) Synthesis of dimers of cubes with bridging N_2H_4 from a cubic [$MoFe_3S_4$] cluster **2**.

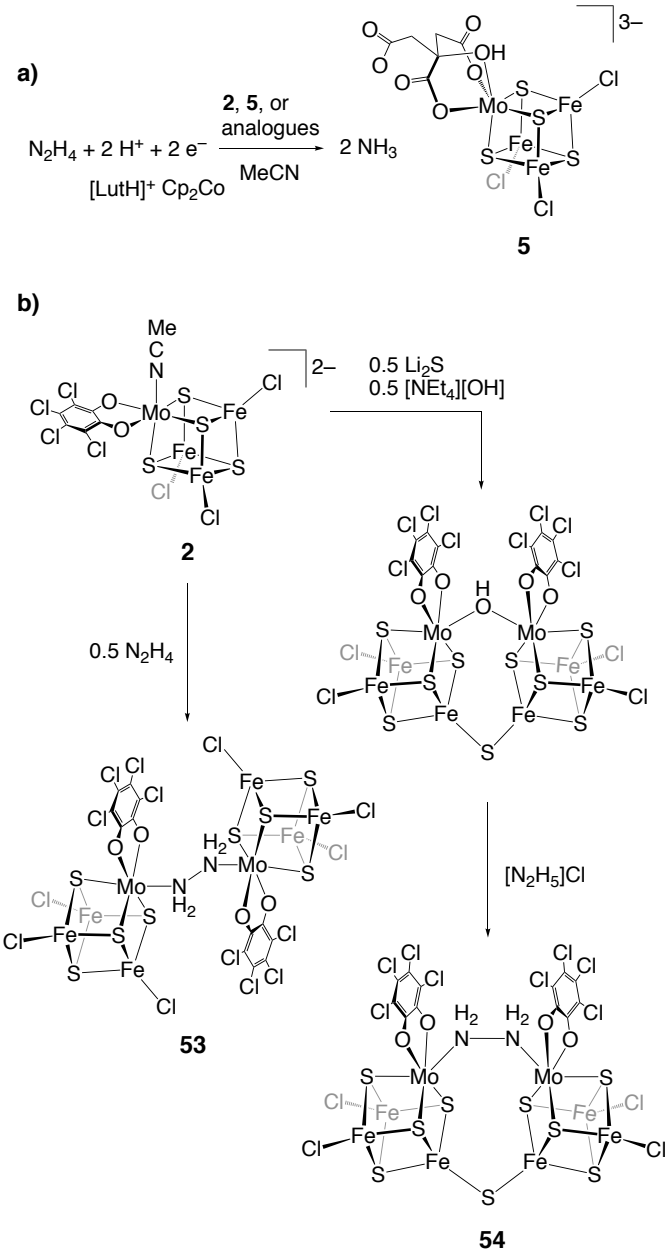

The importance of a heterometal (M) in the catalytic N_2H_4 reduction by synthetic [MFe_3S_4] cubes was further corroborated by studies with [VFe_3S_4] clusters. Coucouvanis *et al.* applied a series of

[VFe_3S_4] clusters with chlorides on Fe, $[(DMF)_l(L)_mVFe_3S_4Cl_3]^{n-}$ (l = 3, m = 0, n = 1, L = none (**6**); l = 2, m = 1, n = 1, L = PEt_3 (**55**); l = 1, m = 1, n = 1, L = 2,2'-bipyridine (**56**); and l = 0, m = 1, n = 2, L = tris(pyrazolyl)hydroborate (Tp) (**57**)), and analogues of **6** with different halides on Fe, $[(DMF)_3VFe_3S_4X_3]^-$ (X = Br (**58**), I (**59**)) (**Scheme 22**).[219, 226] The number of DMF ligands in $[(DMF)_l(L)_mVFe_3S_4Cl_3]^{n-}$ significantly affected the catalytic activity, as demonstrated by the conversion rates of 100% for **6**, 47% for **55**, and 17% for **56**, with no detectable product for **57** after a 2 h reaction in the presence of 10 equiv. N_2H_4, 20 equiv. Cp_2Co, and 40 equiv. $[LutH]^+$. On the other hand, the variation of halides on Fe did not lead to notable change in the catalytic activity. These results are consistent with the participation of the V atom as the substrate binding site, which is in contrast to a recent crystallographic analysis of FeVco suggesting the involvement of inner Fe atoms in the reactions.[13]

Scheme 22. N_2H_4 reduction catalyzed by [VFe_3S_4] clusters in the presence of $[LutH]^+$ and Cp_2Co as proton and electron sources.

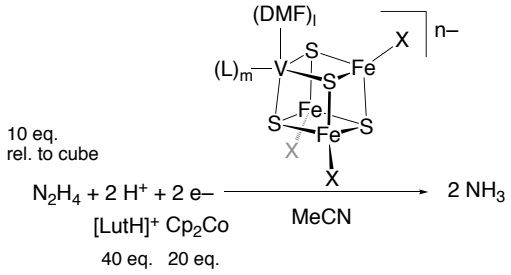

Complex No.	l	m	n	L	X	NH_3 Yield (%)
6	3	0	1	-	Cl	100
55	2	2	1	PEt_3	Cl	47
56	1	1	1	bpy[a]	Cl	17
57	0	1	2	Tp[b]	Cl	n.d.[c]
58	3	0	1	-	Br	-[d]
59	3	0	1	-	I	-[d]

[a] bpy = 2,2'-bipyridine. [b] Tp = hydrotris(pyrazolyl)borate. [c] n.d. = not detected. [d] Values not reported. Described as "virtually identical" to the yield from **6**.

A tetrarchlorocatecholate-supported [$MoFe_3S_4$] cluster **2** was further utilized as a catalyst precursor by Coucouvanis *et al.* for the reduction of *cis*-dimethyldiazene (*cis*-MeN=NMe)[227] and C_2H_2.[228] The catalytic reduction of 15 equiv. *cis*-MeN=NMe by **2** gave $MeNH_2$ as the sole product in 80% yield in 1 h (**Scheme 23**). The robust nature of **2** was supported by the EPR spectrum after the catalytic reaction, where a diagnostic $S = 3/2$ signal of the $[MoFe_3S_4]^{3+}$ core was integrated to 82% of the original value prior to the reaction. Exclusive involvement of the Mo site in the activation of *cis*-MeN=NMe was suggested by inhibition of catalysis by Mo-binding PEt_3 and the catalytic inertness of $[Fe_4S_4Cl_4]^{2-}$ under the same reaction conditions. A theoretical analysis proposed alternate protonation of two nitrogen atoms of MeN=NMe on Mo during the conversion into $MeNH_2$.[220] C_2H_2 was also catalytically reduced by **2**, affording C_2H_4 and a small amount of C_2H_6, and the TON reached 15 over 24 h (**Scheme 24**). A detailed kinetic analysis of the catalytic C_2H_2 reduction provided a moderate activation enthalpy ($\Delta H^{\ddagger}$ = 9(1) kcal/mol) and a large activation entropy ($\Delta S^{\ddagger}$ = –32(2) cal/(K·mol)), leading to a significant Gibbs free energy of activation ($\Delta G^{\ddagger}$ = 19(1) kcal/mol). The large negative $\Delta S^{\ddagger}$ value suggests the involvement of the catalyst, substrate, and one or more of the proton source ($[LutH]^+$) to form an ordered transition state. Apparent inconsistency between the catalytic reductions of *cis*-MeN=NMe and C_2H_2 can be found in the low but evident C_2H_2 reduction activities of the PEt_3-inhibited form of **2** and $[Fe_4S_4Cl_4]^{2-}$. These observations are indicative of the involvement of Fe atoms in C_2H_2 reduction at a slower rate.

Scheme 23. Reduction of *cis*-MeN=NMe catalyzed by a [$MoFe_3S_4$] cube **2**.

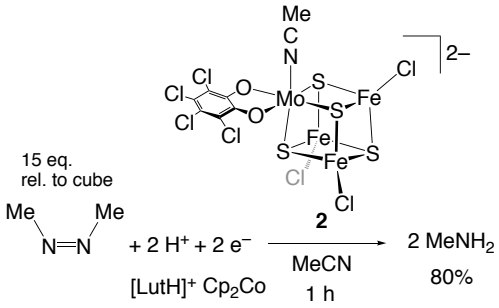

Scheme 24. Reduction of C_2H_2 catalyzed by a [$MoFe_3S_4$] cube **2**.

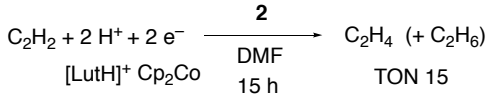

2.2.2.2 Reduction of CO_2, CO, and $[CN]^-$ Promoted by Metal-Sulfur Clusters

While reduction of carbon dioxide (CO_2) was recently discovered to be a nitrogenase-related reaction (Table 1), early studies were driven by interest in the formation of useful organic substances from CO_2. The first example of CO_2 reduction by metal-sulfur clusters was reported by Tezuka, Hidai, and their coworkers in 1982.[229] Controlled potential electrolysis at as low as –1.7 V vs. SCE was performed in a CO_2-saturated DMF solution of $[Fe_4S_4(SR)_4]^{2-}$ (R = Ph (**49**), CH_2Ph (**60**)) and $[NBu_4][BF_4]$ (0.1 M as a supporting electrolyte), from which formate (HCO_2^-) and a small amount of CO were generated (**Scheme 25**). The current efficiency of HCO_2^- production mediated by **49** reached 93% at –2.0 V vs. SCE. Although the reduction of CO_2 without catalyst occurred at –2.4 V vs. SCE under the same setup to afford a mixture of oxalate, formate, and CO, the $[Fe_4S_4]$ catalyst positively shifted the required potential by approximately 0.7 V. The authors suggested $[NBu_4]^+$ ion as the source of the hydrogen atom of formate, at least in part. Okuno *et al.* reported an analogous electrochemical reduction of CO_2 to formate, and achieved initial current efficiencies of up to 40% by employing macrocyclic tetrathiolate ligands in place of four –SR ligands of $[Fe_4S_4(SR)_4]^{2-}$.[230]

Scheme 25. Electrochemical reduction of CO_2 to HCO_2^- mediated by $[Fe_4S_4]$ clusters **49** and **60**.

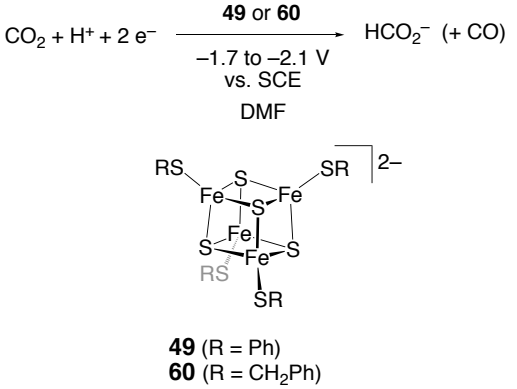

49 (R = Ph)
60 (R = CH_2Ph)

As an extension of the work of Tanaka and coworkers on electrochemical reduction of NO_2^-/NO_3^- to NH_3 mediated by glassy carbon electrodes modified with $[\{MoFe_3S_4(SPh)_3\}_2(\mu\text{-}SPh)_3]^{3-}$ (**50**) or $[\{(Cl_4\text{-cat})MoFe_3S_4(SPh)_2\}_2(\mu\text{-}SPh)_2]^{4-}$ (**61**),[231,232] the Tanaka group coupled the reduction of NO_2^- with carboxylation of acetophenone ($PhCOCH_3$) that was promoted by $[Fe_4S_4(SPh)_4]^{2-}$ (**49**) and **50** under electrolysis at –1.25 V vs. SCE in a CO_2-saturated MeCN solution.[233,234] While the reactions

were kept under dry conditions, the electrolysis provided N_2 and N_2O (minor product) through proton-coupled reduction of NO_2^- (eqs 2 and 3). In this system, $PhCOCH_3$ supplies protons to generate a carbanion ($PhCOCH_2^-$, in equilibrium with the enolate form), which traps CO_2 to afford $PhCOCH_2CO_2^-$. The overall reaction was described as **Scheme 26**, and the current efficiencies for N_2 and $PhCOCH_2CO_2^-$ productions were 70 and 78% for **49** and 98 and 50% for **50**. Based on these findings, Tanaka *et al*. further investigated C-C bond forming reactions with CO_2 by using organic molecules alternative to $PhCOCH_3$. Since the pKa values are comparable among $PhCOCH_3$ (p*K*a = 19), phenylacetylene (PhC≡CH, p*K*a = 21), and cyclohexanone (p*K*a = 18), carboxylated products derived from PhC≡CH or cyclohexanone were similarly obtained in the presence of **49**. An overall 2-electron reduction of CO_2 was also coupled with the reactions with RCOSEt (R = Me, Et, Ph) that afforded *α*-keto carboxylates ($RCOCO_2^-$).[235,236] These reactions were performed under electrolysis at –1.55 V (R = Me, Ph) or –1.60 V (R = Et) vs. SCE in a CO_2-saturated solution containing $[\{MoFe_3S_4(SEt)_3\}_2(\mu\text{-}SEt)_3]^{3-}$ (**62**), RCOSEt, and 3-Å molecular sieves (**Scheme 27**). Current efficiencies of the production of $RCOCO_2^-$ reached 27, 49, and 13% for R = Me, Et, and Ph, respectively. It is intriguing to note that an analogue of **62** bearing –SPh ligands (**50**) was not active. The difference has been speculated to associate with the lability of terminal –SEt ligands via protonolysis by an aqueous Triton X-100 solution, owing to the greater basicity of –SEt relative to –SPh. The use of CH_3COX (X = Cl, OC_2H_5, $SC(O)CH_3$, $OC(O)CH_3$) instead of CH_3COSEt was also unsuccessful. In contrast, a relevant C-C coupling between CO_2 and methyl acrylate ($H_2C{=}CHCO_2CH_3$) was observed in the electrolysis at –1.6 to –1.7 V vs. SCE.[237] While the CO_2-binding site has not been unequivocally identified due to the lack of direct observation, Tanaka *et al.* proposed the nucleophilic attack of one of the sulfides of $[MoFe_3S_4]$ cubes, on the basis of the higher p*K*a values of core sulfur atoms than those of thiolate ligands. Despite mechanistic uncertainty, the concept of capturing CO_2 with pre-activated molecules (*i.e.* deprotonated $PhCOCH_3$, RCOSEt, and $H_2C{=}CHCO_2CH_3$) has relevance to natural carbon fixation systems and may deserve further investigations.

$$2NO_2^- + 6H^+ + 4e^- \rightarrow N_2O + 3H_2O \text{ (eq 2)}$$

$$N_2O + 2H^+ + 2e^- \rightarrow N_2 + H_2O \text{ (eq 3)}$$

Scheme 26. Proton-coupled reduction of NO_2^- catalyzed by metal-sulfur clusters leading to the formation of $PhCOCH_2CO_2^-$ from $PhCOCH_3$ and CO_2.

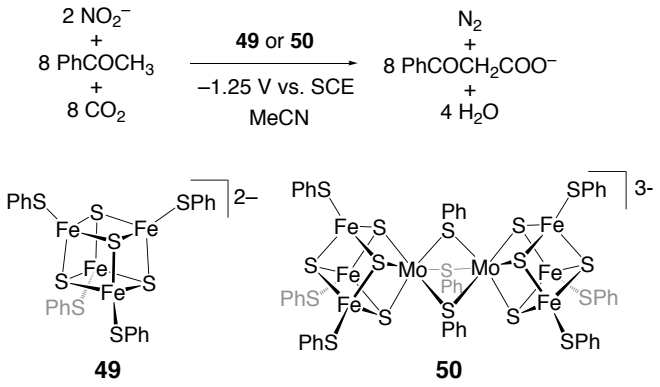

Scheme 27. Electorochemical coupling of RCOSEt and CO_2 promoted by a $[MoFe_3S_4]_2$ double cubane cluster **62**.

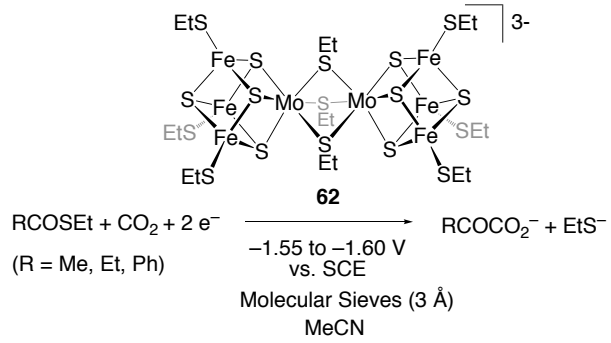

Direct conversions of CO_2 to hydrocarbons (and CO) by metal-sulfur clusters have emerged in recent studies. Soon after the discovery of the carbon-fixation abilities of the nitrogenase VFe and MoFe proteins and the cofactors extracted therefrom,[141,155] Hu *et al.* achieved the reduction of CO_2 to CO catalyzed by the $[Fe_4S_4]$ clusters in the Fe proteins of Mo-nitrogenase and V-nitrogenase from *Azotobacter vinelandii*, with a TON of up to 8 in the presence of a Eu^{II}-based reductant (Eu-DTPA, DTPA = diethylenetriaminepentaacetate) (**Scheme 28a**). [238] From further investigations, a homologous Fe protein from *Methanosarcina acetivorans* was found to reduce CO_2 not only to CO but also to C_1-C_4 hydrocarbons (CH_4, C_2H_4, C_2H_6, C_3H_6, C_3H_8, C_4H_8, and C_4H_{10}) (**Scheme 28b**).[239] The maximum TON based on total produced hydrocarbons per Fe protein was ~6 for CO_2 reduction, while

the TON for the reduction of CO reached up to ~30. The TONs were improved for both CO_2 and CO reductions to 16 and 90, respectively, with the use of a synthetic $[Fe_4S_4]$ cluster catalyst $[Fe_4S_4(SCH_2CH_2OH)_4]^{2-}$ (**51**) [240, 241] in DMF, in the presence of samarium iodide (SmI_2) and triethylammonium cation ($[Et_3NH]^+$) as the electron and proton sources (**Scheme 28c**).[239] Among the C_1-C_4 hydrocarbon products produced by **51**, CH_4 was predominant and accounted for >50%, and the second major product was C_2H_4 with a ratio of ~20%. This product profile was slightly different from those of the protein-based reactions, where the percentage of C_2H_4 in the products did not surpass 15%. Based on density functional theory (DFT) calculations, a mechanism for CO_2/CO reduction was proposed as follows: (1) CO_2 binds to an Fe atom of the $[Fe_4S_4]^0$ cluster and is reduced to CO via proton coupled electron transfer, (2) Fe-CO is converted to Fe-CH_3 through formyl (Fe–CH=O) and carbene (Fe=C(OH)H and Fe=CH_2) intermediates, (3) for the CH_4 evolution, a supply of a proton and an electron to the Fe-CH_3 group generates CH_4, and (4) for the C-C bond formation, CO inserts into the Fe-CH_3 bond (termed as *migratory insertion*) to generate an acetyl (Fe–$COCH_3$) group that can be further reduced to an ethyl (Fe–C_2H_5) species. The Fe–C_2H_5 species produced by process (4) releases ethane, or accommodates CO for further C-C bond formation to furnish C_3 and C_4 hydrocarbons. A related $[Fe_4S_4]$ cluster featuring an Fe-C_2H_5 moiety has been isolated.[242]

Scheme 28. Reduction of CO_2 catalyzed by $[Fe_4S_4]$ clusters: a) Fe-proteins from *Azotobacter vinelandii*, b) Fe-protein from *Methanosarcina acetivorans*, c) $[Fe_4S_4(SCH_2CH_2OH)_4]^{2-}$ (**51**).

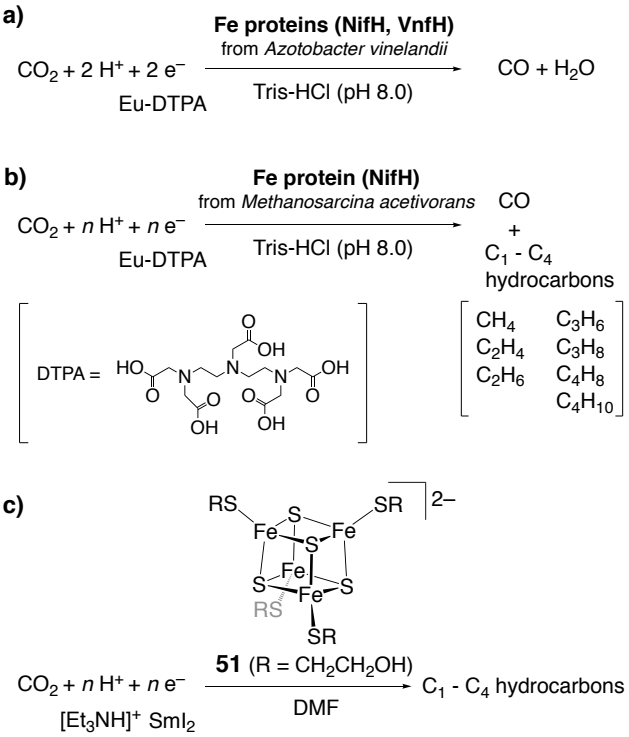

A joint research team including the present authors, Tatsumi, Ribbe, and Hu found that an asymmetric and non-cuboidal Mo-Fe-S cluster $[Cp^*MoFe_5S_9(SH)]^{3-}$ (**34**) and a symmetric Fe_6 analogue $[Fe_6S_9(SEt)_2]^{4-}$ (**63**)[243] also catalyze the direct conversion of CO_2/CO into hydrocarbons (**Scheme 29**).[107,244] The TONs were 24 and 14 for CO_2 reduction and 73 and 92 for CO reduction by clusters **34** and **63**, respectively, in the presence of SmI_2 and $[Et_3NH][BF_4]$ as the reductant and the proton source in DMF. In an analogous manner, clusters **34** and **63** also catalyzed the reduction of cyanide $[CN]^-$ into hydrocarbons (and NH_4^+ ions) with TONs of 282 and 409, respectively. The TONs for CO_2/CO/cyanide reductions by these synthetic clusters were around 1/2 - 1/3 of those for the extracted form of FeMoco, which gave TONs of 68 (CO_2), 225 (CO), and 914 (cyanide). The superiority of FeMoco in catalysis may be ascribed to its most idiosyncratic trait, the central μ_6-C atom. Nevertheless, the product profiles are similar among the catalytic reactions by **34**, **63**, and the extracted FeMoco with approximately 40% selectivity for the C-C coupling products, implying a shared mechanism in the C-C bond forming steps. A relevant but yet relatively new approach

reported by the joint research team is the combination of a synthetic cluster **63** and a nitrogenase protein lacking the catalytic component (*apo*-NifDK protein).[245] This combination, which can be described as an *artificial enzyme*, was found to catalyze the Eu-DTPA-driven reduction of $[CN]^-$, furnishing C_1-C_3 hydrocarbons (and NH_4^+ ions) with a TON of 37. The authors proposed the formation of unidentified carbon-containing products as well, because the total carbon amount of C_1-C_3 products accounted for only a 44% molar ratio of the concomitantly formed NH_4^+ ion. This *artificial enzyme* also achieved C_2H_2 reduction with a TON of 1213 under an analogous reaction condition using the Eu-DTPA reductant, and the TON dropped to 36 upon introducing the synthetic cluster into the standard ATP-dependent nitrogenase assay conditions. The abilities of synthetic metal-sulfur clusters **34** and **63** to reduce CO_2 to hydrocarbons, as well as the catalysis by the *artificial enzyme*, suggest the feasibility of developing nitrogense-based biomimetic approaches for fuel production.

Scheme 29. Direct conversion of a) CO and b) CO_2 into hydrocarbons catalyzed by non-cuboidal metal-sulfur clusters $[Cp^*MoFe_5S_9(SH)]^{3-}$ (**34**) or $[Fe_6S_9(SEt)_2]^{4-}$ (**63**).

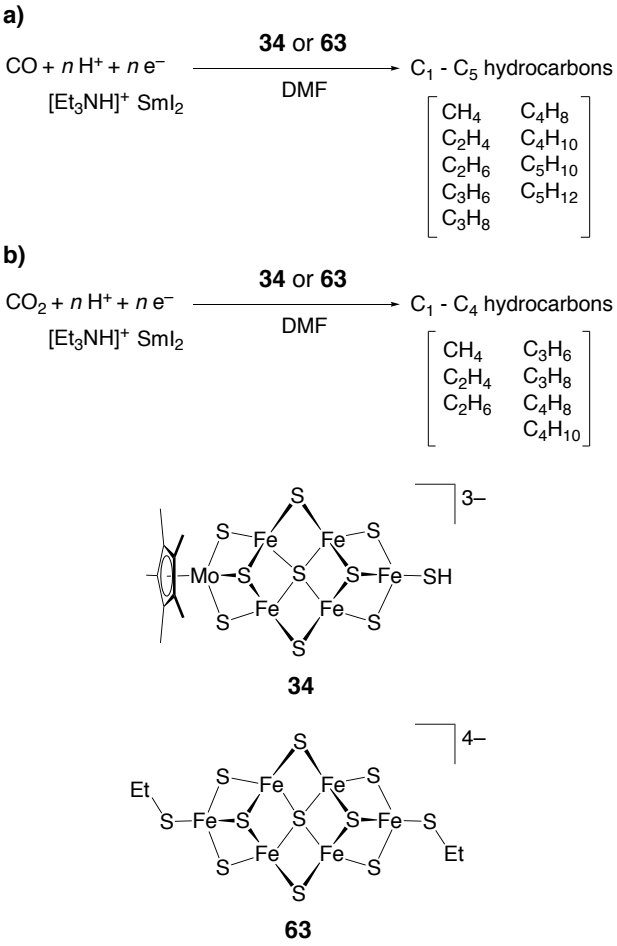

2.2.2.3 Cuboidal Clusters without Fe for Nitrogenase-Related Reactions

Conversion of nitrogenase-related substrates by cuboidal clusters containing Mo and S, but without Fe, has been studied by a joint research group led by Hidai and Mizobe. As described in **section 2.2.1**, trinuclear $[Mo_3S_4]$ clusters can be used as platforms to accommodate a metal atom (M) to furnish cuboidal $[Mo_3S_4M]$ clusters,[246, 247, 248] including the Ru-containing variants $[Cp^*{}_3Mo_3S_4RuH_2(PR_3)]^+$ (R = Ph (**64**), cyclohexyl (**65**)).[174] Disproportionation of N_2H_4 was examined with $[Mo_3S_4Ru]$ clusters **64** and **65**, which reacted with 20 equiv. anhydrous N_2H_4 in THF at ambient temperature to provide $[Cp^*{}_3Mo_3S_4Ru(NH_3)(PPh_3)]^+$ (**66**, 50% yield) as well as NH_3 (1.2 equiv.) and N_2 (0.45 equiv.) (**Scheme 30**). When heated to 60˚C in the presence of 20 equiv. N_2H_4, the reaction

proceeded catalytically, and converted 11.5 equiv. (by **64**) and 15.2 equiv. (by **65**) of N_2H_4 to give NH_3 and N_2 in a *ca.* 4:1 ratio. This result is consistent with the proposed chemical equation for N_2H_4 disproportionation (eq 4). Cluster **64** also catalyzes the disproportionation of phenylhydrazine ($PhNHNH_2$). In this case, treatment of **64** with 20 equiv. $PhNHNH_2$ in THF at 60˚C afforded aniline ($PhNH_2$, 2.3 equiv.), N_2 (1.6 equiv.), benzene (PhH, 2.1 equiv.), NH_3 (1.2 equiv.) and the NH_3 cluster **66** (0.35 equiv.).

$$3N_2H_4 \rightarrow 4NH_3 + N_2 \text{ (eq 4)}$$

Scheme 30. Reaction of $[Cp^*_3Mo_3S_4RuH_2(PPh_3)]^+$ (**64**) with an excess of N_2H_4.

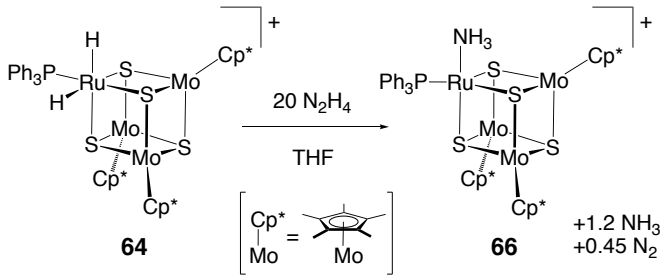

Catalytic reduction of an organohydrazine ($MePhNNH_2$) was attained by $[Cp^*_2M_2S_4\{Mo(O)Cl_2\}\{MoCl_2(DMF)\}]$ (M = Ir (**67**), Rh (**68**)), and these were prepared from the reactions of $[(Cp^*MCl)_2(\mu\text{-}SH)_2]$ (M = Ir, Rh) with $[\{(DMF)_3(O)Mo\}_2(\mu\text{-}S)_2]^{2+}$ and $[NMe_4][Cl]$ (**Scheme 31a**).[249] In the presence of 10 mol % of **67** or **68**, Cp_2Co (2 equiv.), and [LutH][Cl] (2 equiv.), $MePhNNH_2$ was converted into MePhNH (and NH_3), and the yield of MePhNH was quantified as 64% (by **67**) and 31% (by **68**), respectively (**Scheme 31b**). Partial substitution of sulfides to selenides led to comparable or increased catalytic activities, yielding 70% and 56% MePhNH by $[Cp^*_2Ir_2S_2Se_2\{Mo(O)Cl_2\}\{MoCl_2(DMF)\}]$ and $[Cp^*_2Rh_2S_2Se_2\{Mo(O)Cl_2\}\{MoCl_2(DMF)\}]$, respectively. In a stoichiometric reaction of **68** with $MePhNNH_2$, the Mo=O moiety was replaced by a Mo=NNMePh unit with concomitant liberation of water, giving rise to $[Cp^*_2Ir_2S_4\{Mo(NNMePh)Cl_2\}\{MoCl_2(DMF)\}]$ (**69**) (**Scheme 31a**). Treatment of **69** with 2 equiv. each of Cp_2Co and [LutH][Cl] resulted in the liberation of MePhNH in 21% yield.

Scheme 31. a) Synthesis of $[Cp^*_2M_2S_4\{Mo(O)Cl_2\}\{MoCl_2(DMF)\}]$ (M = Ir (**67**), Rh (**68**)) and the reaction of **67** with $MePhNNH_2$. b) Reduction of $MePhNNH_2$ catalyzed by **67** or **68** in the presence of Cp_2Co and $[LutH]^+$.

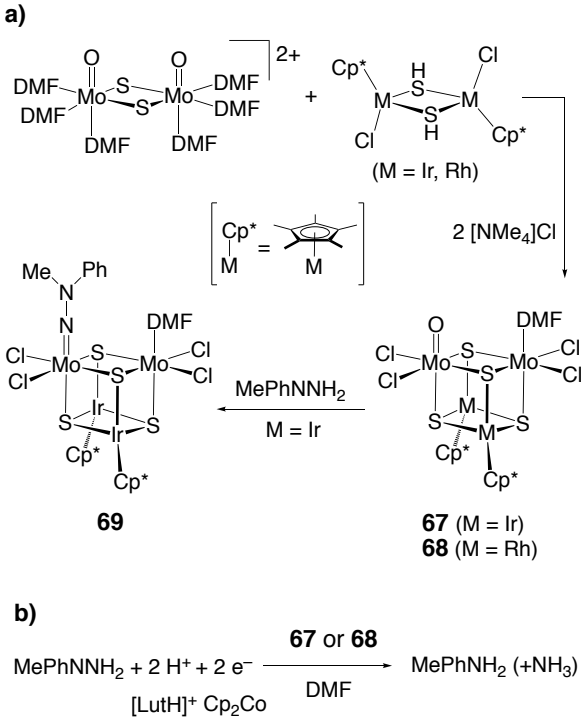

3 Sulfur-supported Transition Metal Complexes in N_2 Chemistry

Due to the importance and intrinsic difficulty of N_2 fixation, mechanistic study of N_2 reduction by nitrogenases was and still is a challenge to inorganic and biological chemists. In this regard, one advantage of using transition metal complexes is their ability to probe the behavior of N_2 at the molecular level, *e.g.* providing insights on how N_2 is bound and transformed through multiple steps.[31,32] Efforts devoted to the N_2 chemistry of transition metal complexes were recently rewarded with discoveries and development of small-molecule catalysts that reduce N_2 under ambient pressure and at room temperature or lower.[250,251,252,253,254,255,256] Moreover, a variety of transition metals have been found to furnish N_2 complexes and their reactivities have been investigated;[31,32] however, they are typically coordinated by P-, N- and/or C-based ligands that can stabilize low-valent metals in the pre-N_2-binding or N_2-bound forms, which are often in the low-spin state. In contrast, Fe atoms in the nitrogenase cofactors are in a sulfur-rich environment and adopt a tetrahedral

geometry, which leads to high-spin states. It is also noteworthy that sulfur-based ligands remain scarce in the N_2 chemistry of transition metals. This section addresses sulfur-supported transition metal complexes that bind, and in some cases activate, N_2 and N_2H_x (x = 2, 4) species.

3.1 N_2 Complexes Supported by Sulfur-based Ligands

Sulfur-based ligands, such as sulfide/thiolate/thioether, are known to exhibit various modes of interactions with metals, *i.e.* σ-donor, σ-donor/π-accepter,[257] and σ-donor/π-donor (**Figure 14**),[258] leading to variable spin states. Variation is also found in the number of interacting metals, as the high affinity of sulfur ligands toward a range of transition metals and the lone pairs on the sulfur atom not only allow the production of mono-nuclear complexes but also facilitate the formation of a doubly bridging M–S–M mode or even triply (μ_3) or quadruply (μ_4) bridging modes.[259,260] Although these features often lead to complexity in sulfur-supported transition metal complexes and clusters, the natural N_2-fixation system employs sulfur-supported metal centers. A possible advantage of sulfur-based ligands is proton-accepting ability. Protonation of some sulfur atoms of FeMoco has been suggested to occur in the N_2-fixation cycle,[17] possibly to balance the net charge of FeMoco in the reduced states and to accumulate protons for NH_3 production. N_2 complexes supported by sulfur-based ligands may contribute to a better understanding of the enzymatic system, as detailed roles of sulfur atoms in FeM'co (M = Mo, V) still remain elusive. Based on the relevance to the enzymatic reactions, the following subsections are categorized by transition elements, *i.e.* Fe as the most biologically relevant element, Ru as a congener of Fe, and other metals.

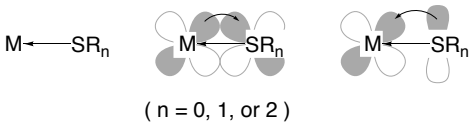

Figure 14. Typical modes of interactions between S-based ligands and metals.[255,256]

3.1.1 Fe

Efforts to elucidate the coordination behaviors of N_2 on Fe centers have been devoted (1) to modeling the N_2 binding mode(s) of the nitrogenase cofactors, (2) to modeling the reaction of iron-based catalysts in the Haber-Bosch process, and (3) to developing molecular catalysts for N_2 reduction under mild conditions by taking the advantage of the high natural abundance of Fe. In particular, great progress has been made recently for the chemical conversion of N_2 with the discoveries of N≡N bond cleavage[261] and catalytic N_2 reduction[250-256] by Fe complexes that are summarized elsewhere.[31,262] Due to the sulfur-rich environment of the relevant enzymatic active sites, here we summarize N_2 complexes of Fe supported by thiolate ($^-$S-R) or thioether (R-S-R) ligands. To the best of our knowledge, sulfide-supported N_2 complexes categorized in this class so far remain elusive.

Since the first report of Fe-N_2 complexes $[(RPh_2P)_3Fe(H)_2(N_2)]$ (R = Et, Bu) by Sacco and Aresta in 1968,[263] it took almost 40 years until an Fe-N_2 complex with a sulfur ligand was synthesized. Chirik *et al.* found that an Fe^0 bis-N_2 complex supported by a tridentate bis(imino)pyridine ligand $[(^{iPr}PDI)Fe(N_2)_2]$ (^{iPr}PDI = 2,6-(2,6-^{i}Pr$_2$C$_6$H$_3$CNMe)$_2$C$_5$H$_3$N) exchanges one of the N_2 ligands with tetrahydro-thiophene (THT) to afford $[(^{iPr}PDI)Fe(N_2)(THT)]$ (**70**) (**Scheme 32**).[264] While the structure of **70** was determined by X-ray crystallography, its C_{2v} symmetry in solution suggested facile dissociation of THT under ambient conditions. Peters and coworkers designed silyl-tethered phosphine-thioether hybrid ligands $[(2\text{-}^i Pr_2PC_6H_4)_2(2\text{-}AdSC_6H_4)Si]^-$ and $[(2\text{-}^i Pr_2PC_6H_4)(2\text{-}AdSC_6H_4)_2Si]^-$, which are designated as $[SiP^{iPr}_{3-n}S^{Ad}_n]$ (n = 1 or 2), for the synthesis of a cationic and trigonal-bipyramidal Fe^{II}-N_2 complex $[(SiP^{iPr}_2S^{Ad})Fe(N_2)]^+$ (**71**) (**Scheme 33**) from protonation of the Fe-CH_3 precursor under N_2.[265] The thioether group in this Fe complex is a weaker electron donor than phosphine groups, as indicated by the higher N-N stretching frequency of **71** (ν_{N2} = 2156 cm^{-1}) relative to $[(SiP^{iPr}_3)Fe(N_2)]^+$ (ν_{N2} = 2143 cm^{-1}) bearing three phosphine moieties.[266] Thus the N_2 on thioether-bound Fe is less activated and more labile. In fact, the analogue of the N_2 complex **71** with a $[SiP^{iPr}S^{Ad}_2]$ ligand featuring two thioether groups was inaccessible. The Fe center instead captured the solvent (Et_2O) to furnish $[(SiP^{iPr}S^{Ad}_2)Fe(Et_2O)]^+$, whereas this complex showed the paramagnetic (S = 1) character similar to complex **71**. Generation of electron-rich Fe centers increases the N_2 binding affinities, and treatment of the cationic Fe complexes with a hydride reagent led to the formation of hydride-N_2 complexes $[(SiP^{iPr}_{3-n}S^{Ad}_n)Fe(H)(N_2)]$ (**72**, n = 1; **73**, n = 2) (**Scheme 33**), whose

N-N bands reveal bathochromic shifts relative to **71** (ν_{N2} = 2055 cm^{-1} for **72** and ν_{N2} = 2060 cm^{-1} for **73**). Chemical reduction of $[(SiP^{iPr}S^{Ad}_2)Fe(Et_2O)]^+$ produced an unusual Fe^{I}/Fe^{II} mixed-valent N_2 complex $[[(SiP^{iPr}S^{Ad}_2)Fe]_2(\mu\text{-}N_2)]^+$ (**74**) (**Scheme 33**), which exhibited a low N-N frequency at ν_{N2} = 1881 cm^{-1} as a result of the bimetallic interaction to the bridging N_2. The Fe-N_2-Fe bridging mode can be also seen in a dinuclear Cp^*Fe^{II} complex (Cp^* = C_5Me_5) supported by a bidentate phosphine-thiolate ligand ($^{-}SC_6H_4PPh_2$), which has been applied as a pre-catalyst for the hydroboration of *N*-heteroarenes owing to the lability of bridging N_2.[267]

Scheme 32. Ligand exchange reaction of an Fe^0 bis-N_2 complex with tetrahydro-thiophene (THT).

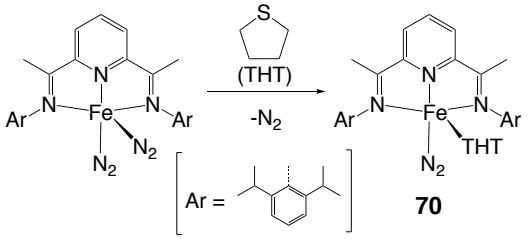

Scheme 33. Synthesis of Fe^{II}-N_2 complexes and an Fe^{II}-N_2-Fe^{I} complex supported by thioether-phosphine-silyl hybrid ligands.

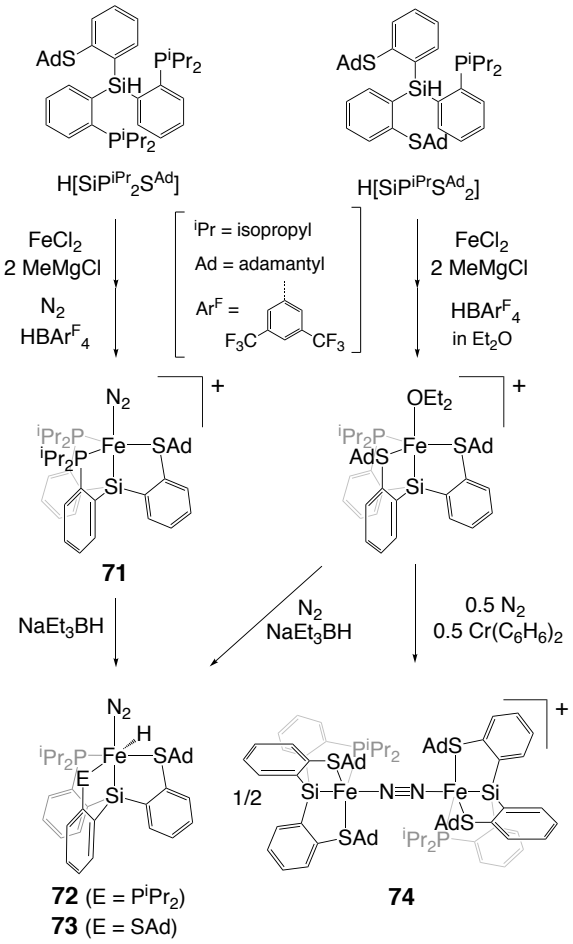

The [$SiP^{iPr}_2S^{Ad}$] ligand was later modified to replace the thioether moiety by a thiolate to provide the [SiP_2S] ligand.[268] The [SiP_2S] ligand was then used for the synthesis of a N_2-bridging dinuclear Fe^{II} complex [$(SiP_2S)Fe]_2(N_2)$ (**75**) (**Scheme 34**), which contains a short N-N length of 1.138(2) Å and a weak N-N stretch (1888 cm^{-1}). Chemical reduction of **75** by Na(Hg) or K led to the formation of monomeric anions [$(SiP_2S)Fe^{I}(N_2)]^-$ (**76**) and [$(SiP_2S)Fe^{0}(N_2)]^{2-}$ (**77**), respectively, while hydride incorporation to **75** afforded a diamagnetic Fe^{II} complex [$(SiP_2S)Fe(H)(N_2)]^-$ (**78**) (**Scheme 34**). Subsequent oxidation of **78** by $[Cp_2Co]^+$ provided the first observed Fe^{III}–N_2 complex [$(SiP_2S)Fe(H)(N_2)$] (**79**) (**Scheme 34**). A significantly higher N-N stretching frequency of the Fe^{III} complex **79** (ν_{N2} = 2123 cm^{-1}) relative to the Fe^{II} complex **78** (1971 cm^{-1}) results from the metal-

centered oxidation, leading to weakened back-donation from Fe to N_2, which is also corroborated by comparisons of the Fe–N bonds (1.882(3) Å for **79** vs. 1.810(4) Å for **78**) and the N-N bonds (1.077(4) Å vs. 1.117(6) Å, respectively). As oxidation of the Fe center leads to smaller ionic radius, the Fe-S distance becomes shorter by oxidation from **78** (2.339(2) Å) to **79** (2.2182(7) Å). A spin density map of complex **79** exhibited a partial leakage of the spin onto the sulfur atom (0.18 e^-, 11%). Spontaneous conversion of **79** to **75** was found to occur via loss of H_2, and the kinetic analysis revealed a second-order scheme of the reaction, as well as an unexpectedly positive activation entropy ($\Delta S^{\ddagger}$ = 39(13) cal/(mol·K)). This implies a bimolecular H_2 elimination via pre-equilibrium between an N_2-bound and N_2-dissociated state followed by dimerization (**Figure 15**). This H_2 elimination accounts for the reduction of Fe centers and generates N_2 binding sites on the Fe atoms, which may be relevant to the concurrent H_2 production with N_2 binding proposed for the nitrogenase cofactors.

Scheme 34. Reactions of an Fe-N_2-Fe complex **75** supported by a thiolate-phosphine-silyl hybrid ligand.

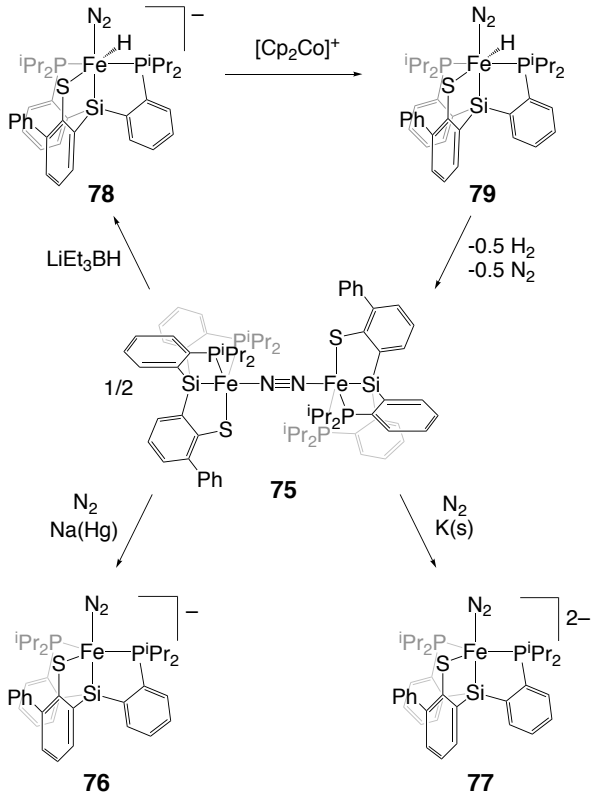

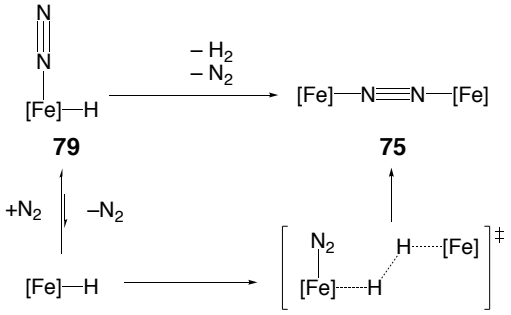

Figure 15. Proposed mechanism of spontaneous conversion from **79** to **75**.

The concept of a sulfur-phosphine-silyl hybrid ligand system was also extended to a dinucleating scaffold featuring a bridging thiolate (μ-SAr).[269] The resultant $Fe^{I}Fe^{I}$ N_2 adduct, $[N_2\text{-}Fe^{I}(\mu\text{-SAr})Fe^{I}\text{-}N_2]^{-}$ (**80**), possesses two terminal N_2 ligands on each Fe atom, and can be oxidized by one or two electrons to afford $[N_2\text{-}Fe^{I}(\mu\text{-SAr})Fe^{II}\text{-}N_2]$ (**81**) or $[N_2\text{-}Fe^{II}(\mu\text{-SAr})Fe^{II}\text{-}N_2]^{+}$ (**82**), respectively (**Scheme 35a**). Although these complexes show little difference in their crystal structures, their N-N stretches systematically shifted to higher frequencies upon oxidation, ν_{N2} = 2017, 1979 cm^{-1} (**80**), 2070, 1983 cm^{-1} (**81**), and 2129 cm^{-1} (**82**). A hydride complex $[N_2\text{-}Fe(\mu\text{-SAr})Fe\text{-}N_2(H)]^{n-}$ (**83,** n = 0; $[\mathbf{83}]^{-}$, n = 1) is also accessible from treatment of the precursor of **80**, an Fe^{II}/Fe^{II} dichloride complex, with excess sodium amalgam (**Scheme 35b**). Biomimetic reactivities, *i.e.* the conversions of N_2 or N_2H_4 (hydrazine), have been tested with the dinuclear complexes $[N_2\text{-}Fe(\mu\text{-SAr})Fe\text{-}N_2]^{n-}$. Treatment of the anionic $Fe^{I}Fe^{I}$ complex **80** with excess KC_8 (reducing agent) and $HBAr^{F}_4\cdot(Et_2O)_2$ (proton source, Ar^{F} = 3,5-$(CF_3)_3C_6H_3$) under an N_2 atmosphere at –78 °C generated 1.8 ± 0.3 equiv. NH_3 to **80**. The corresponding cationic $Fe^{II}Fe^{II}$ complex **82** was found to serve as an efficient catalyst for the disproportionation of hydrazine to NH_3 and N_2 in the presence of $[LutH][BAr^{F}_4]$ (1 equiv. to **82**, LutH = lutidinium) as an acid-cocatalyst, and thus hydrazine (50 equiv. to **82**) was converted to generate NH_3 (29 equiv.) after 1 h incubation at room temperature.[269]

Scheme 35. Redox reactions of thiolate-bridged $Fe_2(N_2)_2$ complexes; a) without hydride, b) with a hydride on one of the Fe atoms.

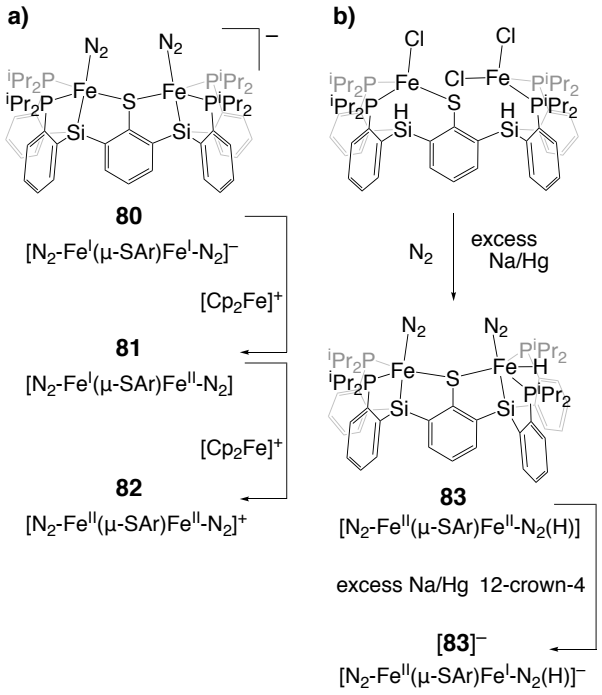

An Fe-N_2 complex mimicking the postulated coordination environment of a proposed N_2-bound form of the nitrogenase cofactor was synthesized. Holland and coworkers designed a sterically encumbering bis(thiolate) ligand (L^{2-}) to coordinate an Fe center with two sulfur atoms and an aromatic group, and synthesized the corresponding Fe^0 complex $[LFe(N_2)]^{2-}$ (**87**) (**Figure 16**) through complexation of an Fe^{II} center followed by treatment with KC_8 at low temperature.[270,271] This thermally unstable N_2 complex **87** reveals a pseudo-tetrahedral coordination geometry consisting of one N_2, two thiolates, and one aromatic ring. The nitrogenase cofactor has been suggested to activate N_2 with the inner Fe atom(s), which are surrounded only by sulfur and carbon atoms, and therefore, **87** might reflect the local structure of the enzyme in the active state. Involvement of a C-based ligand in **87** made a step toward better modeling the μ_6-C atom of the cofactor, while the Fe^0 state of **87** is more reduced than the operative oxidation states of nitrogenase. The low-frequency N-N stretching band of **87** (ν_{N2} = 1880 cm^{-1}) verifies the strong electron donating ability of the thiolates, enabling an effective π-back bonding from the d orbital of Fe to the π^* orbital of N_2.

Further reduction of the N_2 complex to the formally Fe^{-I} state enabled the authors to protonate the Fe-bound N_2 to furnish NH_3 and N_2H_4 in low yields.[271]

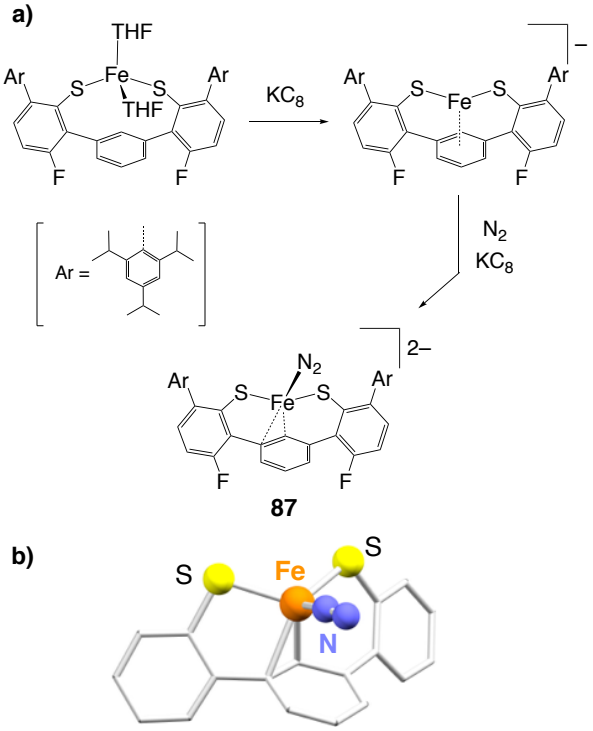

Figure 16. a) Synthesis of $[LFe(N_2)]^{2-}$ (**87**) bearing a bis(thiolate) ligand (L^{2-}). b) Crystal structure of **87**. Substituents of L^{2-} and hydrogen atoms are omitted for clarity.

Although homogeneous N_2 reduction systems usually employ N_2 complexes as catalyst precursors,[250-256] hydride complexes without N_2 have also been found to catalyze the reduction of N_2. As far as sulfur-supported complexes are concerned, Ohki *et al.* reported an $[Fe_4]$ hydride cluster $[Fe_4(\mu\text{-}H)_4(\mu_3\text{-}H)_2(SDmp)_2(PMe_3)_4]$ (**84**; Dmp = 2,6-(mesityl)$_2C_6H_3$)[272] and $[Mo_2Fe_2]$ hydride clusters supported by bulky thiolate ligands $[\{Cp^*Mo(PMe_3)\}_2\{Fe(SR)\}_2(H)_8]$ (**85**, R = 2,4,6-^{i}Pr$_3C_6H_2$ (Tip); **86**, R = 2,6-(SiMe$_3$)$_2C_6H_3$ (Btp))[273] (**Figure 17**), which were found to catalyze the conversion of N_2 into $N(SiMe_3)_3$ in the presence of Na and Me_3SiCl. The yields of $N(SiMe_3)_3$ were 104 ± 5 equiv. by the $[Fe_4]$ cluster **84**, and 65 ± 16 equiv. (STip) and 69 ± 9 equiv. (SBtp) by the $[Mo_2Fe_2]$ clusters **85** and **86**, respectively. Although structures of the N_2-bound forms remain uncertain, the $[Fe_4]$ hydride cluster has been speculated to use the inner two Fe atoms, based on the formation of the Ph_2SiH_2 adduct

from an analogue of **84**. Generation of mono-nuclear fragments or aggregated nano-particles as catalytically active species has been suggested to be less likely, due to the low or negligible catalytic activities of mono-nuclear analogues and the homogeneity test[274] on the [Mo_2Fe_2] cluster.

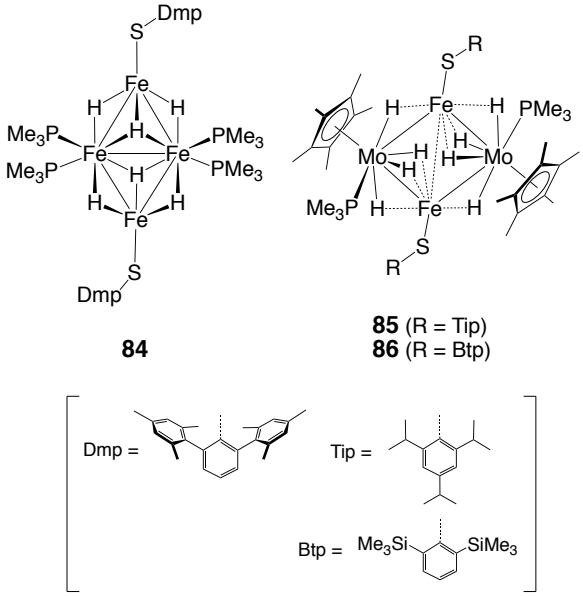

84

85 (R = Tip)
86 (R = Btp)

Figure 17. Thiolate-supported [Fe_4] and [Mo_2Fe_2] hydride clusters which serve as pre-catalysts for the conversion of N_2 to $N(SiMe_3)_3$.

3.1.2 Ru, Os, and Co

Ru and Os are congeners of Fe, and therefore their N_2 complexes have also received attention in the context of potential nitrogenase models. Some examples of Ru- and Os-N_2 complexes with S-based ligands were reported earlier than the corresponding Fe compounds, suggesting the relative stability of metal-N_2 interaction with the heavier group 8 metals. Nevertheless, as discussed above in **section 2.2.1**, the synthesis of sulfur-supported N_2 complexes shares a common difficulty, which lies in the facile formation of sulfur bridges to occupy the coordinatively unsaturated site generated on the metal center rather than accommodation of an N_2 molecule.

The first S-supported Ru-N_2 complex was reported in 2001. With a diamine-dithiolate tetradentate ligand ('$N_2Me_2S_2$'), Sellmann and coworkers synthesized an acetonitrile precursor [Ru(MeCN)(P^iPr_3)('$N_2Me_2S_2$')] and found its ligand exchanged with N_2 to afford

[Ru(N_2)(P^iPr_3)('$N_2Me_2S_2$')] (**88**) under a stream of N_2 at ambient temperature (**Scheme 36**).[275] Due to weak back-bonding from the Ru^{II} center, the N_2 ligand in **88** reveals a relatively high N-N stretching frequency (ν_{N2} = 2113 cm^{-1}) and a typical N≡N bond length (1.110(4) Å). A derivative bearing PCy_3 (Cy = cyclohexyl) instead of P^iPr_3 was reported to show nearly the same properties of the N_2 ligand (ν_{N2} = 2115 cm^{-1}; N-N distance = 1.108(8) Å).[276] Consistent with the weak Ru-N_2 interaction, a part of the N_2 ligand in **88** was found to dissociate from a gently warmed toluene solution under an Ar atmosphere to give an N_2-bridging dinuclear complex [{Ru(P^iPr_3)('$N_2Me_2S_2$')}$_2$(μ-N_2)] (**89**) (**Scheme 36**).[277] Formation of the Ru-N_2-Ru structure led to a slight decrease in the N-N stretching frequency (ν_{N2} = 2047 for **89** vs. 2113 cm^{-1} for **88**). Complex **88** (and **89**) can be alternatively prepared from an ammonia adduct [Ru(NH_3)(P^iPr_3)('$N_2Me_2S_2$')].[278] This result indicates that the Ru center in this system has higher affinity to N_2 than NH_3. Later, we will describe this Ru system in more detail with the hydrazine adducts.

Scheme 36. Synthesis of Ru^{II}-N_2 and Ru^{II}-N_2-Ru^{II} complexes supported by a diamine-dithiolate tetradentate ligand.

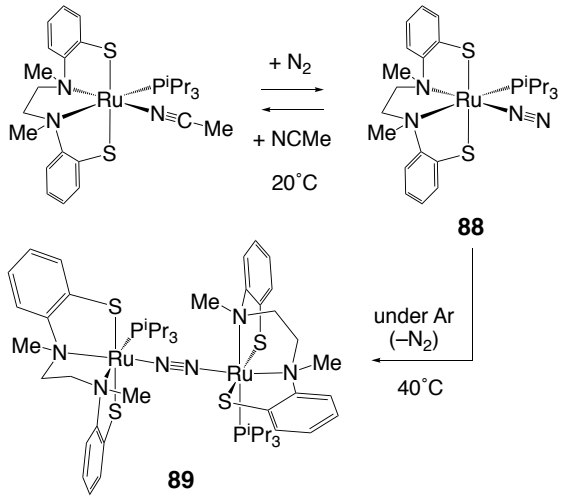

The first S-supported Os-N_2 complex was reported in 1983 and was synthesized by Cruz-Garritz, Richards, and their coworkers from a salt metathesis reaction of [$OsCl_2(N_2)(PMe_2Ph)_3$] with $Pb(SC_6F_5)_2$, that resulted in the formation of [$OsCl(SC_6F_5)(N_2)(PMe_2Ph)_3$] (**90**) (**Scheme 37**).[279] Analogues with different thiolates –SR (R = Me, Ph, CF_3) were later synthesized in a similar manner,

while attempts to incorporate bidentate dithiocarbamate ($[S_2CNMe_2]^-$) led to the dissociation of N_2.[280] The stretching frequency of **90** at ν_{N2} = 2080 cm^{-1} is comparable to those of analogues with bromide or different thiolates, which reveal their ν_{N2} stretches in the range of 2077-2094 cm^{-1}.[280] In a series of the N_2 complexes, only **90** was structurally characterized. Its N≡N distance (1.112(5) Å) is typical of less activated N_2 complexes and comparable to those in the Fe^{II}-N_2 complexes (**section 3.1.1**).

Scheme 37. Incorporation of a thiolate ligand from the reaction of $[OsCl_2(N_2)(PMe_2Ph)_3]$ with $Pb(SC_6F_5)_2$.

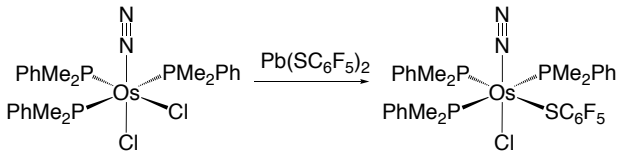

90

The formation of the Ru-N_2 complex **88** in the presence of a large excess of MeCN (solvent) highlights the stability of this complex, because MeCN can bind to metals in a similar manner with N_2 and thus MeCN and N_2 often compete in the coordination to metals. Moreover, the Ru- and Os-N_2 complexes in **Schemes 36** and **37** resist the displacement of their N_2 ligands to induce aggregation through the formation of bridging thiolates, indicating the stability of their M-N_2 interactions under ambient conditions. The apparent affinity toward N_2 is not ascribed to π-back-donation from the Ru/Os center, because the activation levels of the N_2 ligands in complexes **88**-**90** are not significantly high (ν_{N2} = 2047-2113). The fact that the strong π-back-donation is not necessary to form stable M-N_2 complexes is intriguing, if it also happens in Fe-N_2 complexes. Interaction of N_2 with Ru/Os as a σ donor ligand should be the key to understand such unusual behavior, which requires more physical and theoretical investigations. As for the competition between N_2 binding and sulfur bridging, an intriguing instance is a Co^{II} species supported by a tridentate phosphine-thiolate ligand ($[PhP(C_6H_4S\text{-}2)_2]^{2-}$) and 2,2'-bipyridine (bpy), $[Co\{PhP(C_6H_4S\text{-}2)_2\}(bpy)]$. This complex was found to take up N_2 to furnish an N_2-bridged $[Co_2\{PhP(C_6H_4S\text{-}2)_2\}_2(bpy)_2(\mu_2\text{-}N_2)]$, while a related reaction in the absence of bpy afforded a thiolate-bridged dinuclear complex without N_2, $[Co_2\{PhP(C_6H_4S\text{-}2)_2\}_2]$.[281]

3.1.3 Groups 5-7 Metals

While recent structural studies of Mo- and V-nitrogenases provided persuasive evidence of the substrate binding to Fe, the N_2 binding site in the cofactors has been under discussion since the discovery of these heterometallic clusters. In this regard, Mo-N_2 complexes, including non-S-supported ones, have been of interest. Furthermore, Mo has been, thus far, the most successful transition element in stoichiometric and catalytic N_2 reductions.[250-256, 282, 283] By extending the context of N_2 fixation beyond biologically relevant transition metals, this section covers S-supported N_2 complexes of *hard* and *early* metals from groups 5-7. Examples mainly appear with heavier 4d- or 5d-block elements because the S-based ligands are considered to be relatively *soft* and thus their interactions with *hard* metals are less robust than those with *soft* and *late* and/or *heavier* metals.

In 1974, Chatt and his colleagues reported the syntheses of Re-N_2 complexes bearing bidentate S-based ligands, dithiocarbamate ($[S_2CNR_2]^-$, R = alkyl), O-ethyldithiocarbonate ($[S_2COEt]^-$), and diphenyldithiophosphinate ($[S_2PPh_2]^-$), as *mer*-$[Re(S_2CNR_2)(N_2)(PMe_2Ph)_3]$ (R = Me, Et), *mer*-$[Re(S_2COEt)(N_2)(PMe_2Ph)_3]$, and *mer*-$[Re(S_2PPh_2)(N_2)(PMe_2Ph)_3]$, respectively.[284] The precursor for these Re-N_2 complexes was *trans*-$[Re(Cl)(N_2)(PMe_2Ph)_4]$, in which N_2 derives from an organo-diazenide ($[N_2COPh]^-$).[285] As observed in other Re-N_2 complexes, the low N-N frequencies in these complexes (ν_{N2} = 1940-1964 cm^{-1}) are indicative of the effective π-back-donation from the Re center to the π^* orbital of N_2. The same group later determined the crystal structure of an isocyanide (CNMe) adduct of one of these N_2 complexes as *mer*-$[Re(S_2PPh_2)(N_2)(CNMe)(PMe_2Ph)_3]$ (**91**), verifying the binding of an N_2 molecule (N≡N distance = 1.126(13) Å) (**Scheme 38**).[286] Since isocyanides are good π-accepting ligands, addition of one more CNMe to furnish $[Re(S_2PPh_2)(N_2)(CNMe)_2(PMe_2Ph)_2]$ (**92**) was accompanied by a remarkable increase in the N-N frequency (ν_{N2} = 1980 cm^{-1} for **91** and 2010 cm^{-1} for **92**).

Scheme 38. Addition of CNMe to *mer*-$[Re(S_2PPh_2)(N_2)(PMe_2Ph)_3]$.

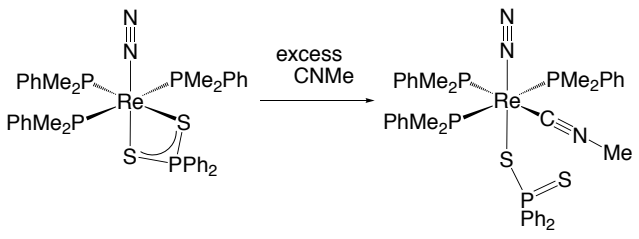

91

Coordination of atmospheric N_2 to S-supported Re was achieved by Dilworth and coworkers from the reaction of $[ReH_7(PPh_3)_2]$ with 3 equiv. bulky thiol, TipSH (Tip = 2,4,6-triisoproplylphenyl), which led to the formation of $[Re(N_2)(STip)_3(PPh_3)]$ (**93**) (**Figure 18a**).[287] Analogous reactions with less bulky DmtSH (Dmt = 2,6-dimethylphenyl) and DmoSH (Dmo = 2,6-dimethoxyphenyl) did not generate the corresponding N_2 complexes. Complex **93** represents a rare example of a Re^{III}-N_2 complex, in which the Re center seems to be kinetically stabilized through steric protection imposed by the bulky Tip groups. The crystal structure of **93** reveals a trigonal bipyramidal coordination geometry with N_2 and PPh_3 residing at the axial positions. The Tip groups of the equatorial STip ligands form an umbrella-like cavity for the binding of N_2 (**Figure 18b**). Another example later appeared as $[Re(N_2)(SDipb)_3(PPh_3)]$ (**94;** Dipb = 2,6-isopropyl-4-bromophenyl) (**Figure 18a**),[288] suggesting the importance of isopropyl groups at the 2,6-positions of the aryl-thiolate ligands for isolation of the N_2 adducts. In accordance with the relatively high Re^{III} oxidation state, complex **93** showed an N-N frequency (ν_{N2} = 2130 cm^{-1}) near the high end of those observed for transition metal-N_2 complex, and consistent with this finding, the N_2 ligand is readily replaced by two-electron donors, *e.g.* CO, MeCN, CN^tBu, and NH_3.[288] A cyclic voltammogram of **93** showed an irreversible oxidation at E_{pa} = 0.753 V vs. standard caromel electrode (SCE); however, no reduction process was observed even at –1.7 V vs. SCE.

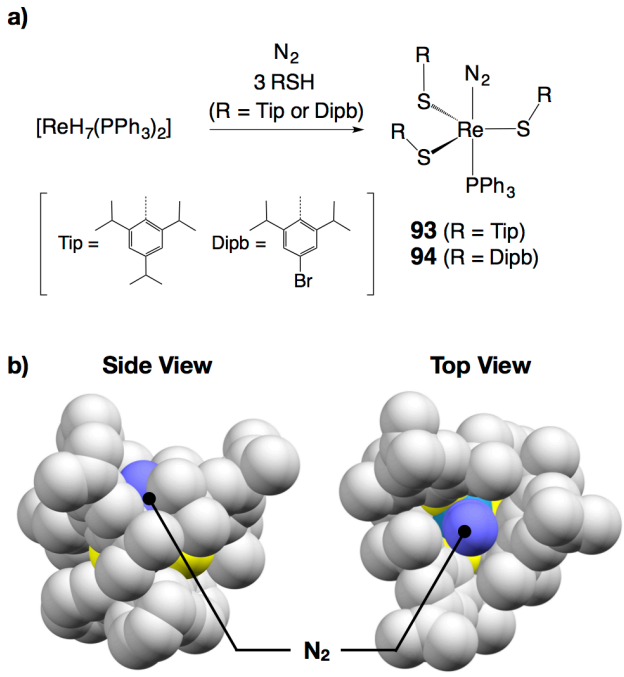

Figure 18. a) Synthesis of [Re(N_2)(SR)$_3$(PPh_3)] (**93** (R = Tip), **94** (R = Dipb)). b) Space-filling model of complex **93**. Color legend: Gray, C; orchid, N; teal, Re; yellow, S.

The first reported sulfur-supported Mo-N_2 complex was a thermally unstable thioether adduct [Mo(N_2)$_2$($PMePh_2$)$_2$($PhSCH_2CH_2SPh$)], synthesized by Aresta and Sacco through ligand substitution of *cis*-[Mo(N_2)$_2$(PMe_2Ph)$_4$] at –70 °C. [289] The structurally identified analogue *trans*-[Mo(N_2)$_2$($PMePh_2$)$_2$($PPh_2CH_2CH_2SMe$)] (**95**) was synthesized by Morris *et al.* from *trans*-[Mo(N_2)$_2$($PMePh_2$)$_4$] (**Figure 19**).[290] *Trans*-coordination of two N_2 molecules was confirmed by X-ray crystallography, and the IR spectrum of **95** displayed two N-N stretches (ν_{N2} = 2014, 1942 cm^{-1}). Intriguingly, treatment of **95** with H_2SO_4 in methanol generated a sub-stoichiometric amount of NH_3 concomitant with the formation of H_2, suggesting bifurcation of the reducing equivalents of the Mo^0 center into N_2 and H^+ reductions.

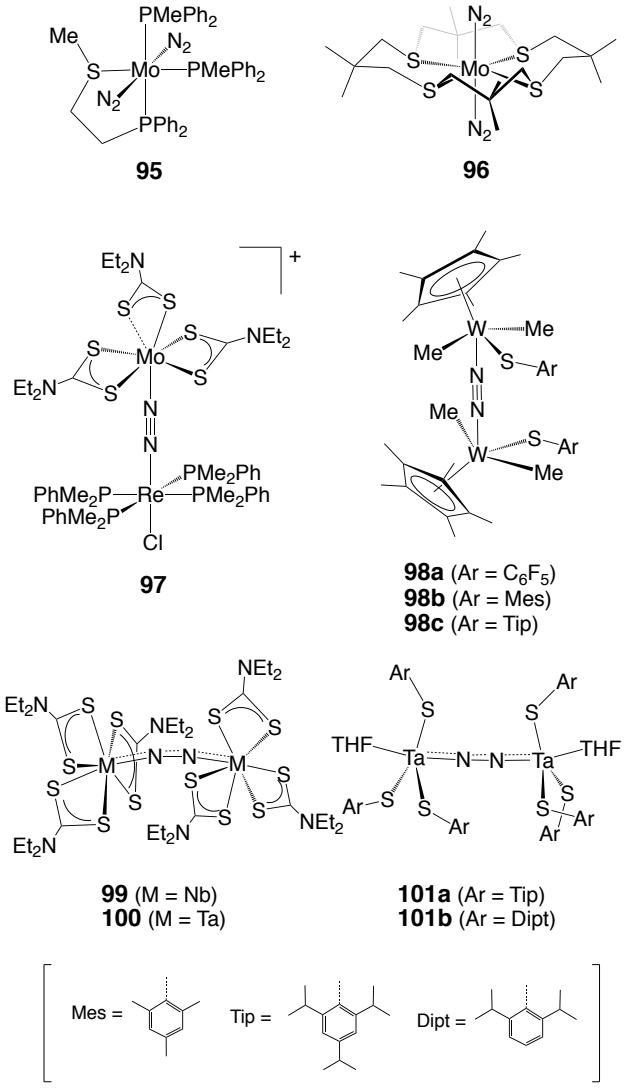

Figure 19. Sulfur-supported N_2 complexes containing groups 5 and 6 metals, *trans*-$[Mo(N_2)_2(PMePh_2)_2(PPh_2CH_2CH_2SMe)]$ (**95**), $[Mo(N_2)_2Me_8[16]aneS_4]$ (**96**), $[Re(Cl)(PMe_2Ph)_4(\mu\text{-}N_2)Mo(S_2CNEt_2)_3]^+$ (**97**), $[Cp^*WMe_2SAr]_2(\mu\text{-}N_2)$ (**98a** (Ar = C_6F_5), **98b** (R = Mes), **98c** (R = Tip)), $[\{M(S_2CNEt_2)_3\}_2(\mu\text{-}N_2)]$ (**99** (M = Nb), **100** (M = Ta)), and $[\{Ta(SAr)_3(THF)\}_2(\mu\text{-}N_2)]$ (**101a** (Ar = Tip), **101b** (Ar = Dipt)). Abbreviations: $Me_8[16]aneS_4$ = 3,3,7,7,11,11,15,15-octamethyl-1,5,9,13-tetrathiacyclohexadecane; Mes = mesityl; Tip = 2,4,6-$^{i}Pr_3C_6H_2$; Dipt = 2,6-$^{i}Pr_2C_6H_3$.

A crown-thioether, 3,3,7,7,11,11,15,15-octamethyl-1,5,9,13-tetrathiacyclohexadecane (Me_8[16]aneS_4), was also found to stabilize an N_2 complex of Mo^0 in the form of [$Mo(N_2)_2Me_8$[16]aneS_4] (**96**) (**Figure 19**) as reported by Yoshida and coworkers.[291] The Mo atom of **96** is coordinated only by S atoms, except the N atoms from the binding N_2 ligands, making **96** stand out among the S-supported metal-N_2 complexes. The N-N distances (1.108(7) and 1.105(7) Å) are within the typical range of metal-N_2 complexes. Nevertheless, the low N-N frequencies (ν_{N2} = 1955, 1890 cm^{-1}) display a high degree of activation compared to those of an analogue of **95** with 1,2-bis(diphenylphosphino)ethane (dppe) ligands (ν_{N2} = 2020, 1970 cm^{-1}). Molecular orbital calculations on simplified models with four SH_2 ligands in place of Me_8[16]aneS_4 suggested that destabilization of Mo d-orbitals caused by antibonding interactions with S p_π-orbitals leads to the stronger d_π(Mo)-p_π*(N_2) backbonding.[291] The strong activation of N_2 was also confirmed by the formation of the Mo=N-NMe_2 complex upon treatment of **96** with 2 equiv. MeBr.

To work toward a higher degree of activation of metal-bound N_2, Brown *et al*. utilized a heterometallic system. A Re^{I}-N_2 complex [Re(Cl)(N_2)(PMe_2Ph)$_4$] reacted with a half equivalent of a S-supported dinuclear Mo complex [$Mo_2(S_2CNEt_2)_6$]$^{2+}$ (S_2CNEt_2 = diethyldithiocarbamate) to afford the N_2-bridged Re/Mo complex [Re(Cl)(PMe_2Ph)$_4$(μ-N_2)Mo(S_2CNEt_2)$_3$]$^+$ (**97**) (**Figure 19**).[292] Consistent with its low N-N frequency (ν_{N2} = 1818 cm^{-1}), the N-N distance observed in the crystal structure of **97** (1.167(6) Å) is significantly longer than that of free N_2 (1.098(1) Å). Although the authors expected further cleavage of the N≡N bond of **97** to obtain a 1:1-mixture of the Re- and Mo-nitride complexes [Re(Cl)(N)(PMe_2Ph)$_4$]$^+$ and [Mo(N)(S_2CNEt_2)$_3$], this was not the case possibly due to a high kinetic barrier. It is notable that these nitride complexes were accessible from alternative synthetic routes. Simple mixing of these complexes, however, did not furnish **97** through the coupling of Re/Mo-nitrides, which indicates that a back reaction of the N≡N bond scission of **97** is not favorable either. Nevertheless, the nitride coupling to form gaseous N_2 was found to occur in a 32-42% yield from the reaction of [TpOs(N)Cl_2] with [Mo(N)(S_2CNEt_2)$_3$],[293] suggesting the importance of fine-tuning the electrophilicity and Lewis acidity of metals when designing effective nitride coupling in these systems.

Dinuclear N_2-bridged tungsten complexes [Cp*WMe_2X]$_2$(μ-N_2) (X = Me, OTf, or Cl) were found to be converted into derivatives with aryl thiolates, [Cp*WMe_2SAr]$_2$(μ-N_2) (Ar = C_6F_5 (**98a**), Mes (**98b**; Mes = mesityl), Tip (**98c**)) (**Figure 19**), as demonstrated by Schrock and coworkers.[294] In the infrared

spectra of $^{14}N_2$ and $^{15}N_2$ labeled **98c**, medium strength peaks assignable to the W-N stretching appeared at 901 and 870 cm^{-1}, respectively. These frequencies are indicative of the 4e-reduced form of the bridging N_2, which is in accordance with the molecular structure of **98b** where a short W=N distance of 1.774(8) Å and a long N-N distance of 1.27(2) Å are found.

With regard to the synthesis of sulfur-supported N_2 complexes of group 5 metals, Henderson *et al.* examined the reactions of $[\{MCl_3(THF)_2\}_2(\mu\text{-}N_2)]$ (M = Nb, Ta) with $Me_3Si\text{-}S_2CNEt_2$ and isolated $[\{M(S_2CNEt_2)_3\}_2(\mu\text{-}N_2)]$ (M = Nb (**99**), Ta (**100**)) (**Figure 19**),[295,296] and Schrock *et al.* reported an analogous reaction of $[\{TaCl_3(THF)_2\}_2(\mu\text{-}N_2)]$ with LiSAr (Ar = Tip or 2,6-$^{i}Pr_2C_6H_3$ (Dipt)) to give $[\{Ta(SAr)_3(THF)\}_2(\mu\text{-}N_2)]$ (**101a**; Ar = Tip, **101b**; Ar = Dipt) (**Figure 19**).[297] In the crystal structures, the Nb atoms of **99** adopt a pentagonal bipyramidal geometry, while the Ta atom of **101a** is in a trigonal bipyramidal geometry. Their bridging N_2 ligands reveal significantly elongated N-N distances (1.25(2) Å for **99** and 1.29(6) Å for **101a**), which can be categorized into hydrazido complexes of the M=N-N=M type. Significant reduction of the bridging N_2 was supported by the formation of hydrazine in >90% yield upon treatment of **99** and **100** with HCl, HBr, or HI. Complex **101a** was found to slowly react with PhCHO at 50-60 °C to give PhCH=N-N=CHPh in about 25% yield.

3.2 Behavior of N_2H_x on S-supported Transition Metal Complexes

One of the difficulties of elucidating the N_2-fixation pathways is the detection and characterization of intermediates, because the first bond cleavage from N_2 is more difficult than the cleavage of the N=N and N-N bonds in the subsequent intermediates.[198] Behaviors of partially reduced N_2-derived species with N=N or N-N bonds should be informative for the thorough comprehension of N_2-reducing reactions, as well as the nitrogenase mechanism, and thus this subsection deals with S-supported complexes of Fe (and Ru) with diazene (N_2H_2), hydrazine (N_2H_4), and their derivatives or analogues.

3.2.1 N_2H_x Species on Fe

3.2.1.1 Diazene Complexes

Diazene is an unstable molecule that decomposes in the solid state at temperatures above –180 °C,[298] and the activation parameters for the bimolecular decomposition are $\Delta H^{\ddagger}$ = 13.8 ± 0.6 kJ/mol and $\Delta S^{\ddagger}$ = –116 ± 2 J/mol·K at pH 4.4 in aqueous solutions.[299] It is therefore surprising to find some

isolated examples of Fe-diazene complexes.

Sellmann and coworkers have designed Fe complexes supported by a pentadentate amine-thioether-thiolate ligand [‘N_HS_4’]$^{2-}$ (dianion of bis{(2-mercaptophenylthio)ethyl}amine), that bind CO, NH_3, and N_2H_4.[300] Oxidation of the dinuclear hydrazine adduct by exposure to O_2 at –60 °C resulted in the formation of the first reported sulfur-supported Fe-diazene complex [{Fe(‘N_HS_4’)}$_2$(μ-N_2H_2)] (**102**) (**Scheme 39a**),[301] in which two octahedral Fe centers are bridged by *trans*-N_2H_2. Structural determination of **102** revealed that the diazene moiety forms N-H···S(thiolate) hydrogen bonding networks, as suggested from the H···S distances of 2.201 and 2.780 Å. Direct trapping of diazene, which is generated *in-situ* from thermolysis of $PhSO_2N_2H_3$ or acidification of $K_2N_2(CO_2)_2$, is possible with analogous Fe complexes carrying different S-based supporting ligands, [Fe(P^nPr_3)(‘S_4’)] (‘S_4’ = 1,2-bis(2-sulfanylphenylthio)ethane dianion)[302,303] and [Fe(PR_3)(‘tpS_4’)] (R = ^{n}Pr, ^{n}Bu; ‘tpS_4’ = 1,2-bis(2-mercaptophenylthio)phenylene dianion) (**Scheme 39b**).[304] The resultant Fe-diazene complexes [{Fe(P^nPr_3)(‘S_4’)}$_2$(μ-N_2H_2)] (**103**) and [{Fe(PR_3)(‘tpS_4’)}$_2$(μ-N_2H_2)] (R = ^{n}Pr (**104**), ^{n}Bu) also contain bridging *trans*-N_2H_2 and exhibit N-N bond distances comparable among this class of complexes, *e.g.* 1.300(7) Å for **102**, 1.288(15) Å for **103**, 1.234(7)/1.284(4) Å for **104**. These Fe-diazene complexes showed diagnostic strong absorption bands in the visible region (λ_{max} = 574-623 nm, ε = 10500-15100 $M^{-1}cm^{-1}$), which were assigned to the π-π transitions in the 4-center 6-electron π-system of the Fe-NH=NH-Fe chromophore (**Figure 20**).[302,303] In the electrochemical measurement, **104** displayed four quasi-reversible redox couples in an anodic sweep, which were observed at +34 mV ([**104**]$^{0/+}$), +545 mV ([**104**]$^{+/2+}$), and +1130 mV ([**104**]$^{2+/3+}$) vs normal hydrogen electrode (NHE). In the case of complex **103**, the corresponding three redox couples were observed only at low temperatures (between –40 and –70˚C).[305] Chemical oxidation of **103** by the ferrocenium ion at –78˚C yielded a deep purple solution. This unstable compound immediately turned olive-green once the solution was warmed up above –40˚C, concomitantly evolving N_2. While the solution structure of the 2 electron-oxidized form of **103** ([{Fe(P^nPr_3)(‘S_4’)}$_2$(μ-N_2H_2)]$^{2+}$) remains unclear, the reversible electrochemical behavior and the release of N_2 implies tautomerization, forming an N_2 complex with protonated ligands (**Scheme 40**). Oxidation of the metal-bound diazene to N_2 and protons may relate to the reversed first step of the N_2 reduction on the nitrogenase cofactors.

Scheme 39. Synthesis of Fe_2-diazene complexes. a) from oxidation of a [‘N_HS_4’]Fe-hydrazine complex. b) trapping *in-situ* generated diazene by Fe complexes carrying tetradentate thiolate-thioether hybrid ligands.

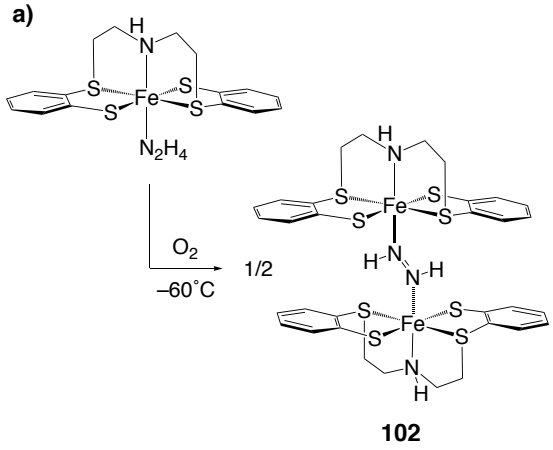

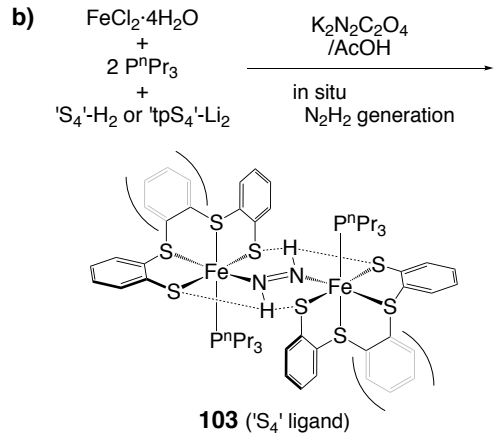

103 ('S_4' ligand)
104 (‘tpS_4' ligand)

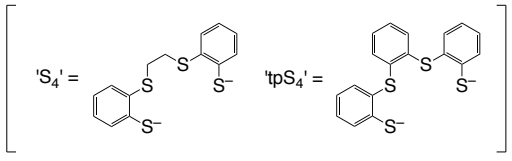

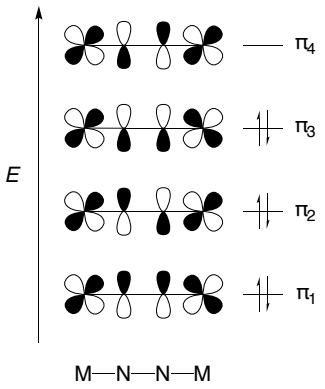

Figure 20. Qualitative description of a 4 center-6 electron π-bond system of a [M–N=N–M] fragment.

Scheme 40. Proposed tautomeric structures of the 2-electron oxidized form of **103**.

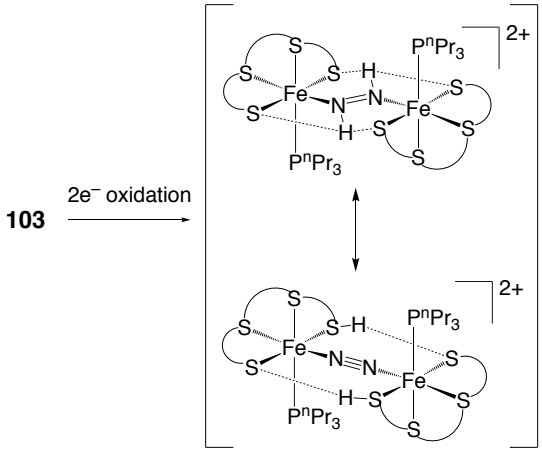

Qu and his colleagues discovered that dinuclear $Cp^*_2Fe_2$ ($Cp^* = \eta^5$-C_5Me_5) complexes with three bridging thiolates (μ-SR^1) can convert phenyl- or methyl-hydrazine (H_2N-NHR^2) to *cis*-diazenes via release of one of the thiolates as HSR^1 to furnish [$Cp^*Fe(\mu$-$SR^1)_2(\mu$-η^2-$R^2N{=}NH)FeCp^*$] (R^1 = Et, R^2 = Ph (**105a**); R^1 = Me, R^2 = Ph (**105b**); R^1 = Et, R^2 = Me (**105c**)) (**Scheme 41a**).[306] Their short N-N distances ranged from 1.307(10) Å to 1.337(2) Å and are consistent with the N=N double bond. The same group later synthesized this class of diazene complexes supported by two –SEt groups (**106a-b**, **107a**-**b**) (**Scheme 41b**) or a benzene-dithiolate (bdt) (**108a**-**b**, **109a**-**b**) (**Scheme 42**) similarly through the conversion of hydrazines on the [$Cp^*_2Fe_2$] or [$(C_5Me_4H)_2Fe_2$] frameworks,[307,308] while Nishibayashi *et al.* obtained a side-on methyl-diazenido complex with a bulky aryl thiolate (SC_6H_4-2-

$SiMe_3$), $[Cp^*_2Fe_2\{\mu\text{-}S(C_6H_4\text{-}2\text{-}SiMe_3)\}(\mu\text{-}\eta^2\text{:}\eta^2\text{-}NNMe)]$ (**110**), from the reaction of $Cp^*_2Fe_2\{\mu\text{-}S(C_6H_4\text{-}2\text{-}SiMe_3)\}_2$ with $MeHN\text{-}NH_2$.[309] Preparation of these diazene or diazenido complexes was concomitant with the formation of RNH_2 and NH_3, suggesting that these Fe-bound diazene moieties resulted from the disproportionation of hydrazines into $RNH_2 + NH_3$ and diazene. Furthermore, a series of $Cp^*_2Fe_2$ complexes have been found to catalyze the reduction of hydrazines into $RNH_2 + NH_3$ in the presence of proton sources and reducing agents, where coordinatively unsaturated $Cp^*_2Fe_2$ complexes with one or two thiolates have been proposed as intermediates. Protonation of the side-on NNMe moiety in **110** was found to give an isolable side-on methyl-diazene ($\mu\text{-}\eta^2\text{:}\eta^2$-HNNMe) complex,[309] and a CO adduct of one of the proposed intermediates has been prepared as $[Cp^*Fe(\mu\text{-}SEt)(CO)]_2$.[307] In contrast to the relatively robust $Cp^*Fe(\mu\text{-}SR)_2$ frameworks, the $Cp^*_2Fe_2(\mu\text{-}bdt)$ scaffold exhibited flexibility in the bridging mode of bdt, which allowed the formation of a $\eta^1\text{:}\eta^2\text{-}N_2H_3$ complex (**111**) by protonation of the $\eta^1\text{:}\eta^1\text{-}N_2H_2$ complex as well as the subsequent reduction/protonation to transform the N_2H_3 moiety into a bridging NH_2 ligand and a molecule of NH_3 (**Scheme 42**).[308] DFT calculations suggested a detailed reaction pathway for the conversion of the $\eta^1\text{:}\eta^2\text{-}N_2H_3$ complex into a $\mu\text{-}NH_2$ complex via liberation of NH_3 (**Scheme 42**).

Scheme 41. Synthesis of diazene-bridged dinuclear $Cp^*_2Fe_2$ ($Cp^* = \eta^5$-C_5Me_5) complexes via disproportionation of hydrazines.

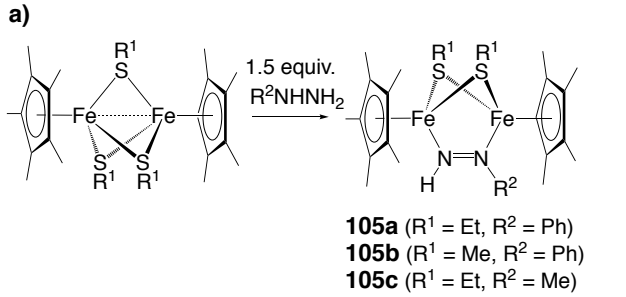

105a (R^1 = Et, R^2 = Ph)
105b (R^1 = Me, R^2 = Ph)
105c (R^1 = Et, R^2 = Me)

106a (R = Me, n = 1.5, m = 1)
106b (R = H, n = 1.5, m = 1)
107a (R = Me, n = 5, m = 0)
107b (R = H, n = 5, m = 0)

Scheme 42. Transformation of diazene on a benzene-dithiolate supported $Cp^*_2Fe_2$ framework.

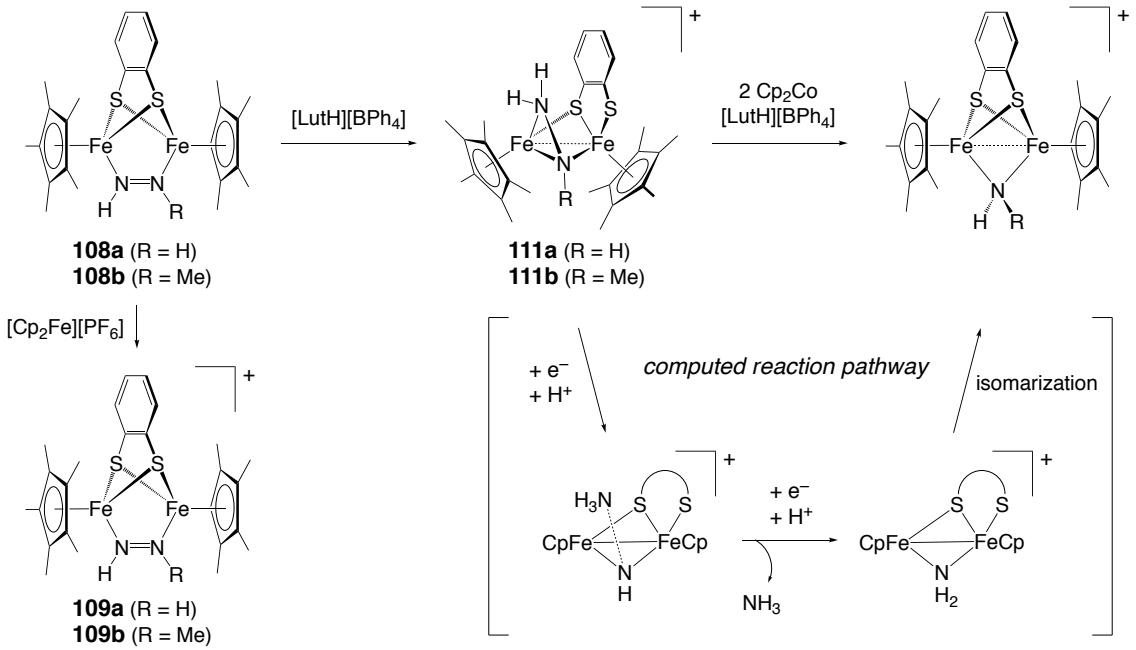

108a (R = H)
108b (R = Me)

111a (R = H)
111b (R = Me)

109a (R = H)
109b (R = Me)

The fact that the inherently unstable diazene becomes isolable via coordination to Fe provides some implications for the nitrogenase mechanism. Increased stability of the Fe-diazene species could lower the activation energy of the first reduction step in the N_2-fixation, assuming that this step proceeds through a late transition state to generate the unstable compound. The protonation/deprotonation behaviors of Fe-diazene species may mimic early N_2-fixation steps. Insights into possible involvement of sulfur atoms in these steps are desirable in future studies.

3.2.1.2 Hydrazine Complexes

Hydrazine (N_2H_4) is more stable than diazene, and therefore, the synthesis of hydrazine complexes is less complicated. Sellman and coworkers synthesized square-pyramidal Fe^{II} and Fe^{III} complexes with bridging [310] and teminal [311] hydrazine, $[\{Fe(S_2C_6H_4)_2\}_2(\mu\text{-}N_2H_4)]^{2-}$ and $[Fe(S_2C_6H_4)_2(N_2H_4)]^-$, respectively, by the addition of hydrazine to bis(1,2-benzenedithiolate) complex. The same group also synthesized the aforementioned hydrazine complexes ($[Fe(`N_HS_4')(N_2H_4)]$[301, 312] and $[Fe(PR_3)('S_4')(N_2H_4)]$[303]) and a terminally bound Fe-hydrazine complex with a pyridine-centered pentadentate ligand, $[Fe(`pyS_4')(N_2H_4)]$ (‘pyS_4’ = dianionic form of 2,6-bis(2-mercaptophenylthiomethyl)pyridine), [313] via simple treatment of the precursors with hydrazine (**Figure 21**). As demonstrated by Hsu and coworkers, a tripodal tris(thiolate)phosphine ligand (PS_3” = $P(C_6H_3\text{-}3\text{-}Me_3Si\text{-}2\text{-}S)^{3-}$) is useful for the synthesis of a mononuclear Fe^{II} hydrazine complex $[Fe(PS_3")(N_2H_4)]^-$ (**112**) (**Figure 21**) and ammonia complex $[Fe(PS_3")(NH_3)]^-$ (**113**).[314] The N–N and Fe-N bond distances of **112** are 1.451(5) and 2.036(4) Å, respectively, which are comparable to the corresponding distances in the above-mentioned Fe(‘N_HS_4’) and Fe(‘pyS_4’) complexes (N–N distances: 1.439(10) and 1.450(5) Å, Fe-N distances: 2.255(6) and 2.042(3) Å, respectively) and consistent with that of free N_2H_4 (N–N distance: 1.45-1.46 Å).[315,316] High lability of N_2H_4 and NH_3 ligands from **112** and **113** made detailed characterization difficult, but this lability should be advantageous for a release of products (*i.e.* NH_3 and N_2) from catalysts in N_2H_4 disproportionation. In the presence of 2 equiv. Cp_2Co and $[LutH]^+$, $[Fe(PS_3")(CH_3CN)]$ pre-catalyst facilitated disproportionation of N_2H_4 into NH_3 and N_2 (eq 5) up to a TON of 5.5.[314]

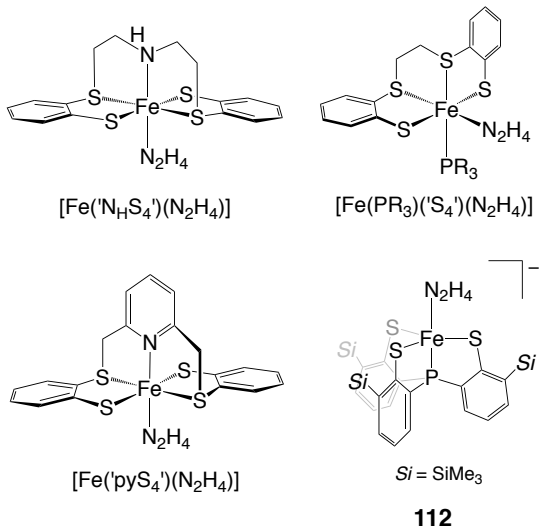

112

Figure 21. Fe-N_2H_4 complexes supported by multi-dentate thiolate-containing ligands.

$$3N_2H_4 \rightarrow 4NH_3 + N_2 \text{ (eq 5)}$$

Coordinatively unsaturated Fe centers supported by sulfides mimic possible reactive forms of the nitrogenase cofactors. This idea prompted Holland and coworkers to synthesize a sulfide-bridged Fe_2 complex $[(L^1Fe)_2(\mu\text{-S})]$ (**114**, L^1 = $[HC\{CMeN(2,6\text{-diisopropylphenyl})\}_2]^-$), in which two Fe^{II} atoms are three-coordinate and supported by β-diketiminate ligands (**Scheme 43**).[317] A closely related Fe^{II}_2 complex $[(L^2Fe)_2(\mu\text{-S})]$ (**115**, L^2 = $[MeC\{CMeN(2,6\text{-diisopropylphenyl})\}_2]^-$) was prepared via the β-hydride elimination from an isobutyl complex $[L^2Fe(^iBu)]$ followed by reductive elimination of H_2 and sulfide abstraction from $SPMe_3$.[318] The supporting β-diketiminate ligand L^2 of **115** contains an additional methyl group on the metallacycle. While an Fe^{II}_2 complex **114** reveals a bent Fe-S-Fe structure (Fe–S–Fe = 101.70(7)˚), 2e$^-$ reduction of the analogue **115** led to the formation of a linear Fe^I-S-Fe^I arrangement in $[M]_2[(L^2Fe)_2(\mu\text{-S})]$ (**116**, Fe–S–Fe = 179.70(4)˚ for M = K and 180˚ for M= Na). It should be noted that the Fe^I state is unusual in iron-sulfur cluster chemistry and only **116** and $[\{(PhBP_3)Fe\}_2(\mu\text{-S})]^{2-}$ ($PhBP_3$ = $PhB(CH_2PPh_2)_3$)[319] are unambiguously identified examples of sulfide-bridged Fe^I_2 complexes, with the excception of NO complexes for which assignment depends on the formalism of the NO ligands.[320,321,322] A relevant Fe^{II}_2 complex with one bridging sulfide and one bridging hydride, $[Na][(L^1Fe)_2(\mu\text{-S})(\mu\text{-H})]$ (**117**), was synthesized from the reaction of a hydride complex $[L^1FeH]_2$ with sodium dodecanethiolate ($NaSC_{12}H_{25}$), where homolytic cleavage of a C-S

bond took place to generate the bridging sulfide.[323] This C-S bond cleavage reaction was suggested to proceed through the generation of a short-lived alkyl radical which abstracts a hydrogen atom from Fe, based on a radical-clock experiment using a cyclopropyl-methanethiolate anion.[324] The hydride ligand in **117** was found to function as a base to deprotonate a terminal alkyne (*m*-tolyl)CCH to furnish a terminal acetylide complex or as a hydride donor to insert into CO_2 to give a bridging formate complex.[323]

As anticipated from the coordinative unsaturation in **114**, its Fe centers were found to accommodate various N-donor ligands, *e.g.* hydrazines, ammonia (NH_3), and NCMe.[317,325] The numbers of N-donors and their coordination modes were found to vary by the substrates, and the adducts of hydrazine (N_2H_4), methyl- and dimethyl-hydrazine ($MeRNNH_2$; R = H, Me), and NH_3 were obtained in the form of $[(L^1Fe)_2(\mu\text{-}S)(L^N)_2]$ (L^N = N_2H_4 (**118**), $MeHNNH_2$ (**119**), Me_2NNH_2 (**120**), NH_3 (**121**)), and were structurally characterized. On the other hand, the product from the reaction of **114** with phenylhydrazine ($PhHNNH_2$) was an $Fe^{II}Fe^{III}$ mixed-valence complex with a μ-phenylhydrazide ligand, $[(L^1Fe)_2(\mu\text{-}S)(\mu\text{-}PhNNH_2)]$ (**122**) (**Scheme 43**).[317] Requirement of 1.4 ± 0.2 equiv. $PhHNNH_2$ to **114** in the high-yield synthesis of **122**, where the concomitant generation of up to 0.5 equiv. each $PhNH_2$ and NH_3 was observed, indicated the disproportionation of $PhHNNH_2$ accompanying the transfer of a proton and an electron from the putative Fe_2-$PhHNNH_2$ intermediate. A mono-NCMe adduct relevant to the putative intermediate was isolated and structurally identified. The $Fe^{II}Fe^{III}$ mixed-valence state of **122** was supported by the Mössbauer spectrum exhibiting two doublets at ΔE_Q = 1.93 mms^{-1}, δ = 0.82 mms^{-1} for the Fe^{II} site and ΔE_Q = 0.74 mms^{-1}, δ = 0.41 mms^{-1} for the Fe^{III} site. A rhombic EPR signal appeared at g = 1.99, 1.92, 1.65 (at 9 K), which suggests an anti-ferromagnetically coupled S = 1/2 ground state.

Scheme 43. Representative reactions of β-diketiminate-supported Fe-S-Fe complexes **114** and **115**.

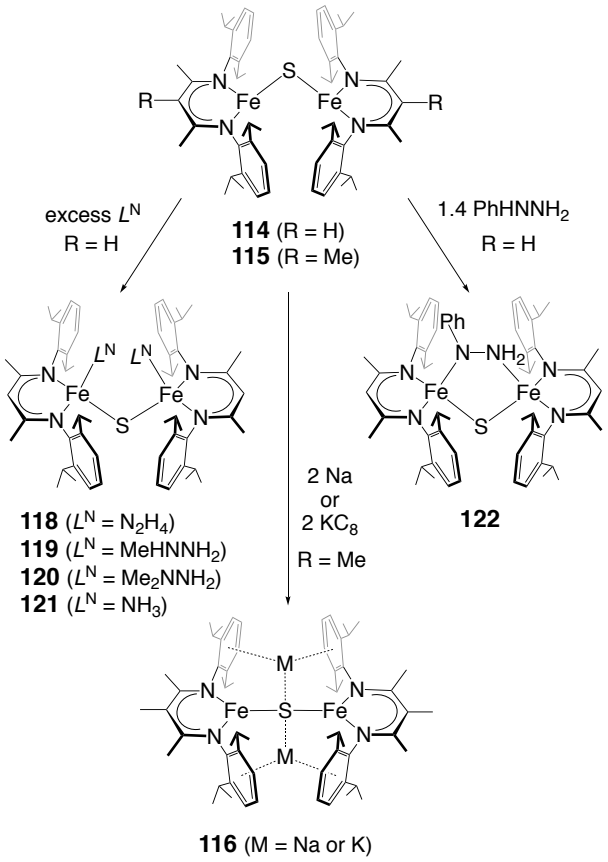

The bulkiness of the N-substituents of a β-diketiminate ligand alters the accessibility of Fe sites and lability of the ligands. Replacement of the 2,6-diisopropylphenyl groups of L^2 ligand by less bulky 2,6-dimethylphenyl groups furnishes the L^3 ligand [MeC{CMeN(2,6-dimethylphenyl)}$_2$]$^-$, which enabled Holland and coworkers to extend the structural diversity of iron-sulfur clusters.[326] An analogue of **115** was obtained as the THF adduct [{L^3Fe(THF)}$_2$(μ-S)] (**123**), in which Fe centers are four-coordinate owing to the reduced steric hindrance. This Fe-S-Fe complex **123** was found to serve as a versatile precursor for [2Fe-2S], [4Fe-3S] (**124**), and [10Fe-8S] (**125**) clusters, which were synthesized through desulfurization from ethylene sulfide, reduction with KC_8, and thermolysis, respectively (**Scheme 44**). Disproportionation of β-diketiminates and sulfides is required for the formation of [10Fe-8S] and [4Fe-3S] clusters, implying that the less hindered L^3 ligand facilitates inter-molecular interactions. The central component of [10Fe-8S] cluster **125** can be viewed as a fused form of two [4Fe-4S] cubes sharing a [2Fe-2S] face, in which each cube is decorated by a

[($L^3Fe)_2$(μ-S)] moiety. This structure leads to a formal all-ferrous $10Fe^{II}$ state, and the mean Fe-S distance (2.34(7) Å) is within the range of those in other all-Fe^{II} iron-sulfur clusters. The [$Fe_{10}S_8$] cluster **125** may engage in the activation of small molecules, as its THF ligands are labile and readily exchange with Et_2O, while difficulties remain in the high-yield synthesis of pure materials. Although the isolated yield of the [Fe_4S_3] cluster **124** from **123** was low (22%), alternative synthetic reaction of an Fe^{I} complex [(L^3Fe)(C_6H_6)] with KC_8 and $SPMe_3$ furnished a better yield (66%) of **124**, which is in the formal $3Fe^{II}1Fe^{I}$ oxidation state (**Scheme 44**).[327] Crystallographic analysis of **124** revealed a planar arrangement of the [Fe_4S_3] core with a central three-coordinate Fe site, which was tentatively assigned as the low-spin Fe^{I} state. The 1-electron oxidized all-Fe^{II} form [**124**]$^+$ was found to use the central Fe site in the reaction with N_2H_4, leading to the N-N bond cleavage and the formation of the terminal –NH_2 moiety (**Scheme 44**). The resultant amide cluster **126** is in the formal $1Fe^{III}$-$3Fe^{II}$ oxidation state, where the Fe^{III} site has been suggested to delocalize over the outer three Fe atoms. Acid treatment of **126** produced 0.81 equiv. NH_3, further confirming the presence of the –NH_2 moiety.

Scheme 44. Synthesis of a high-nuclearity [$Fe_{10}S_8$] cluster **125** and a planar [Fe_4S_3] cluster **124** from [{$L^3Fe(THF)$}$_2$(μ-S)] (**123**) and reactivity of **124**.

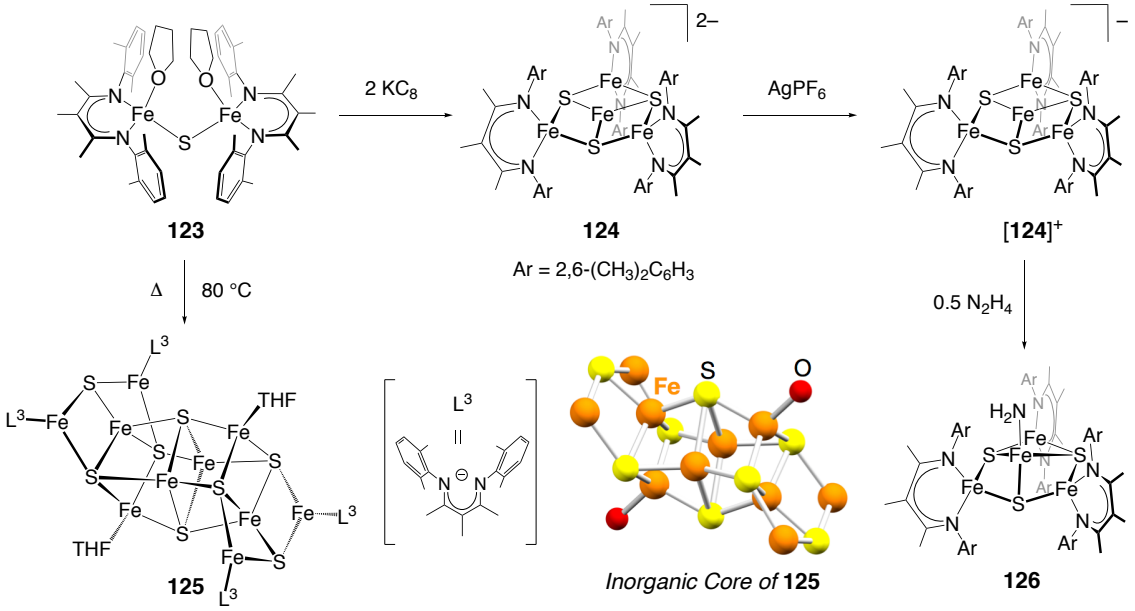

Lee *et al.* reported an Fe_2 complex supported by sterically hindered thiolates [Fe_2(μ-STriph)$_2$(STriph)$_2$] (**127**; STriph = 2,4,6-triphenylbenzenethiolate), which reacted with hydrazines in various manners dependent on the substituents on the nitrogen atoms (**Scheme 45**).[328] Addition of N_2H_4 to **127** gave rise to a hydrazine-bridged complex [Fe_2(μ-η^1:η^1-N_2H_4)$_2$(N_2H_4)$_4$(STriph)$_4$] (**128**), while no reaction took place with tetra-substituted hydrazines. The same complex **127** catalyzed the disproportionation of diphenylhydrazine (6 equiv.) into a 2:1 mixture of $PhNH_2$ and PhN=NPh (**eq 6**). After this catalytic reaction, the Fe_2 complex was transformed into the $PhNH_2$ adduct [Fe_2(μ-STriph)$_2$(STriph)$_2$($PhNH_2$)$_2$]. Treatment of **127** with PhMeNNHPh led to the formation of a deep blue solution of unidentified material,[328] which was converted in the presence of activated alumina to a purple solution containing a five-coordinate complex [Fe(STriph){MeN(C_6H_4)NPh}$_2$]. As such, combinations of **127** and diaryl-hydrazines or their derivatives exhibited complicated chemistry involving catalytic disproportionation and structural rearrangement. The same group also found the N-N bond cleavage of 1,2-diarylhydrazines (Ar'NHNHAr'; Ar' = Ph or *p*-Tol) by an amide-thiolate complex [Fe_2(μ-SMes)$_2${$N(SiMe_3)_2$}$_2$] (**129**) or its THF adduct that afforded all-ferric Fe-imide cubanes [Fe_4(μ_3-NAr')$_4$(SMes)$_4$] (Ar' = Ph (**130a**), *p*-tol (**130b**)) (**Scheme 46**).[329,330] Although the mechanism

for the formation of cubanes remains ambiguous, Lee and coworkers proposed (1) the initial deprotonation of diarylhydrazines by the $-N(SiMe_3)_2$ ligands of **129** to produce a dinuclear Fe^{II} complex bridged by a side-on ArNNAr, which undergoes (2) the reductive N-N bond cleavage to give bridging imide (NAr) ligands concomitant with the 2-electron oxidation of two Fe^{II} centers to give a tentative Fe^{III}_2 intermediate $[Fe_2(\mu\text{-NAr'})_2(SMes)_2]$ followed by (3) its dimerization to form a cubane core (**Scheme 46**).

Scheme 45. Reactions of a dinuclear iron thiolate complex **127** with nitrogen-containing substrates.

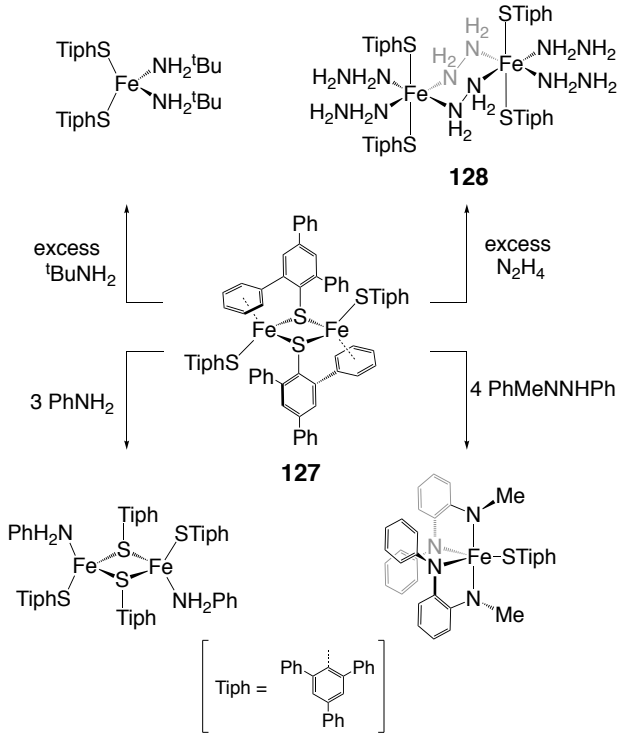

$$2PhHNNHPh \rightarrow 2PhNH_2 + PhN{=}NPh \quad (\textbf{eq 6})$$

Scheme 46. N-N bond cleavage of diaryl-hydrazines by an Fe^{II}-thiolate/amide complex **129** furnishing Fe^{III}-imide cubes.

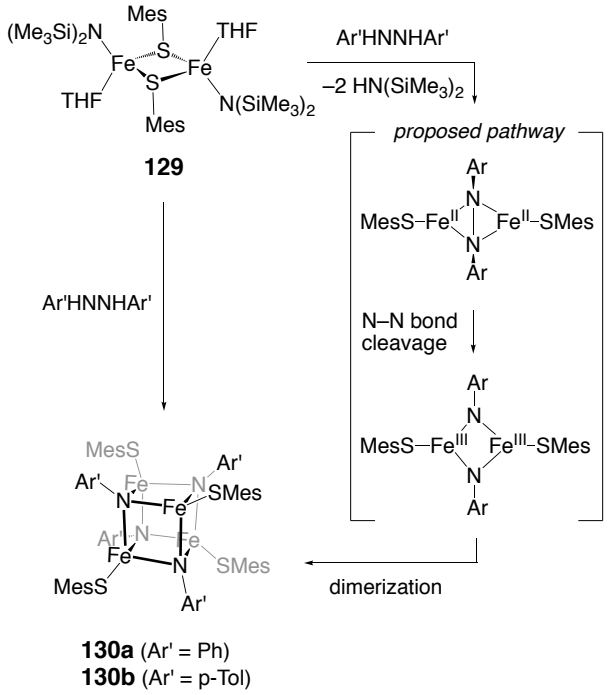

3.2.2 N_2H_x Species on Ru

In regard to the behaviors of N_2H_x on S-supported transition metals, Ru complexes have also been extensively studied. Ru is a congener of Fe, but its 4d orbital leads to larger ionic radius than Fe. The coordination number and geometry are thus often different between Fe and Ru. As far as sulfur-rich environments are concerned, a tetrahedral $M(S)_4$ geometry is typical for M = Fe but unprecedented for M = Ru. A few related $Ru(S)_4$ complexes to be noted are $Ru(STip)_4$ (Tip = 2,4,6-$^{i}Pr_3C_6H_2$)[331] with an agostic Ru··H-C interaction and a cyclic hexamer of $Ru(S^tBu)_2$ in a nearly square-planar geometry.[332] It should be noted that these are small fractions of differences between Ru and Fe complexes, and insights from Ru chemistry cannot simply be extrapolated to Fe chemistry. Notwithstanding, the difference in coordination chemistry between Fe and Ru and the behaviors of N_2H_x species on Ru can be beneficial, owing to the generally higher stability of Ru complexes that enables the formation of a wider variety of compounds.

Sellmann used the 'S_4' ligand, which is described on its Fe complexes of N_2H_2 and N_2H_4 in **section**

3.2.1, to investigate the synthesis and reactivity of the Ru analogue [{Ru(PPh_3)('S_4')}$_2$(μ-N_2H_2)] (**131**).[333] Its analogues with slightly different supporting ligands, [{Ru(PPh_3)('tpS_4')}$_2$(μ-N_2H_2)] (**132**; see **section 3.2.1** for 'tpS_4')[334] and [{Ru(PPh_3)('$^{bu}S_4$')}$_2$(μ-N_2H_2)]] (**133**; '$^{bu}S_4$' = l,2-Bis((2-mercapto-3,5-di-tert-butylphenyl)thio)ethane dianion(2–)),[335] have also been synthesized through air oxidation of the corresponding mononuclear hydrazine complexes or treatment of monomeric complexes with *in situ* generated N_2H_2 (**Figure 22**). The latter method gave the products in higher yields. Additionally, the '$N_2Me_2S_2$' ligand (**section 3.1.1**) was also found to stabilize a diazene complex as [{Ru(P^iPr_3)('$N_2Me_2S_2$')}$_2$(μ-N_2H_2)] (**134**) (**Figure 22**).[278]

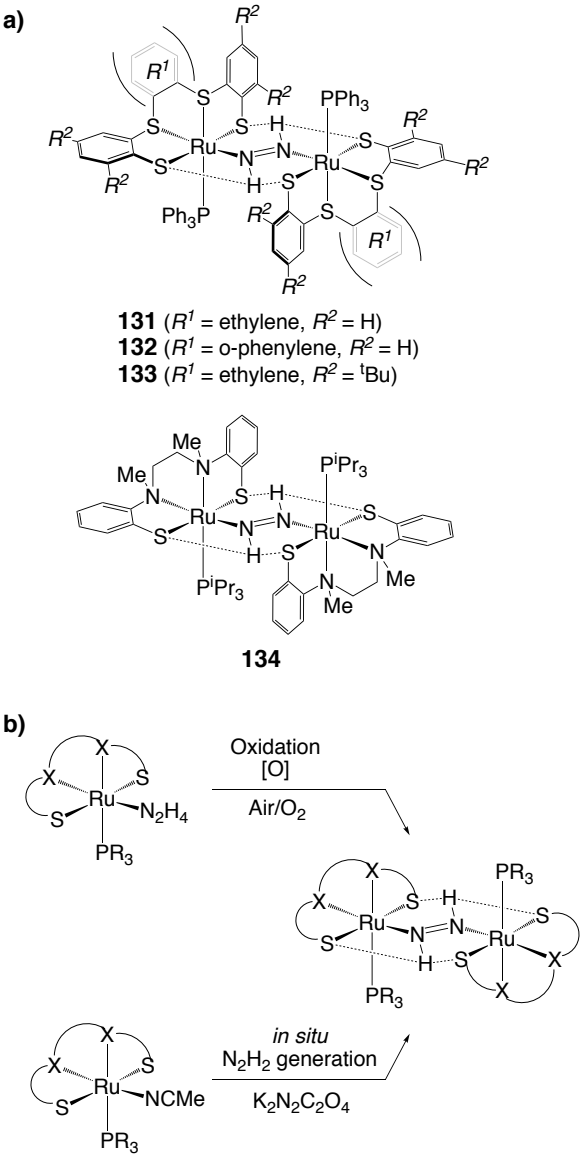

Figure 22. a) Structures of [{Ru(PPh$_3$)('S$_4$')}$_2$(μ-N$_2$H$_2$)] (**131**), [{Ru(PPh$_3$)('tpS$_4$')}$_2$(μ-N$_2$H$_2$)] (**132**), [{Ru(PPh$_3$)('^{bu}S$_4$')}$_2$(μ-N$_2$H$_2$)]] (**133**), and [{Ru(P^{i}Pr$_3$)('N$_2$Me$_2$S$_2$')}$_2$(μ-N$_2$H$_2$)] (**134**). b) Representative reactions to prepare diazene complexes of Ru.

As is the case with Fe analogues, the bridging N_2H_2 ligands in the Ru_2 complexes are in a *trans* configuration and exhibit highly organized intramolecular hydrogen bonding networks with the sulfur atoms of the thiolate moieties. For example in **134**, the Ru and S atoms in the ('N$_2$Me$_2$S$_2$')Ru moiety as well as the N and H atoms of bridging N_2H_2 are nearly coplanar in the crystal structure

(**Figure 22**). The central $Ru_2(\mu\text{-}N_2H_2)$ groups in **131**-**134** reveal short Ru-N distances (1.994(5)-2.030(7) Å) and long N-N bonds (1.270(1)-1.301 Å) relative to free *trans*-N_2H_2 (1.252 Å)[336], suggesting a partial contribution of back-bonding from Ru to N_2H_2. In accordance with this notion, these Ru_2-diazene complexes displayed an intense absorption band in the visible region, *i.e.* λ_{max} = 480 nm (**131**; ε = 6.98 x 10^2 $M^{-1}\cdot cm^{-1}$), 478 nm (**133**; ε = 1.55 x 10^3 $M^{-1}\cdot cm^{-1}$), 463 nm (**132**; ε = 8.16 x 10^2 $M^{-1}\cdot cm^{-1}$), and 502 nm (**134**; ε = 1.43 x 10^3 $M^{-1}\cdot cm^{-1}$), which is characteristic of the 4 center-6 electron π-bond system of [M–N=N–M] fragments (**Figure 20**).[302,334]

Monomeric Ru species $[Ru(PPh_3)(L)]$ (L = 'S_4', '$^{bu}S_4$', or 'tpS_4') were reported to bind hydrazine to give $[Ru(PPh_3)(L)(N_2H_4)]$.[333,334,337] These complexes were stable enough to be isolated but were not crystallographically identified, perhaps due to the lability of the hydrazine ligand. In fact, spontaneous loss of a part of N_2H_4 from $[Ru(PPh_3)('tpS_4')(N_2H_4)]$ and the subsequent dimerization generated $[\{Ru(PPh_3)('tpS_4')\}_2(\mu\text{-}N_2H_4)]$ (**135**).[334] Complexes **132** and **135** are, to our best knowledge, the only pair of structurally characterized μ-N_2H_2 and μ-N_2H_4 complexes of Ru. Crystal structures of **132** and **135** exhibited organized hydrogen bonding networks in both complexes. The coplanarity of the μ-N_2H_2 ligand with Ru and S atoms in **132** is lost in the hydrazine analogue **135** due to the presence of S('tpS_4')···H–N(hydrazine) interactions with sp^3-NH_2 groups **Figure 23**). It is notable that **135** displays hydrogen bonds between H(hydrazine) atoms and S(thioether) atoms, although the protons of diazene in **131**-**134** only interact with S(thiolate) atoms in their solid state structures. A series of mono- and di-nuclear Ru complexes with N_2 (**89** in **section 3.1.2**), N_2H_2 (**131**-**134** in this section), N_2H_4 (**135** and $[Ru(PPh_3)(L)(N_2H_4)]$ in this section), and NH_3 ($[Ru(NH_3)(P^iPr_3)('N_2Me_2S_2')]$ (**136**)) may represent intermediates of a pseudo catalytic cycle for the reduction of N_2 by two Ru centers (**Figure 24**).[278] Although neither the conversion of N_2 nor the reduction of N_2H_x have been demonstrated with these Ru complexes, the hydrogen bonding networks found in **131**-**134** and **135** could be relevant to enzymatic nitrogen fixation in terms of the possible participation of sulfur atoms.

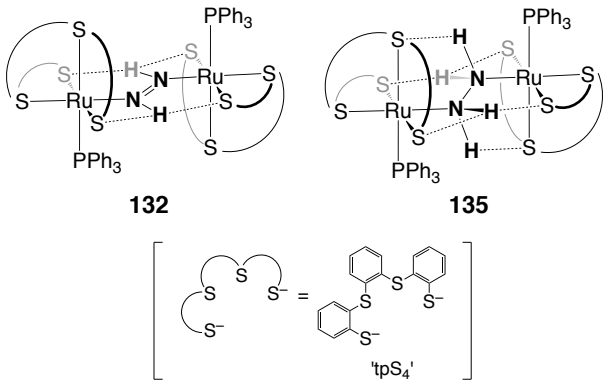

Figure 23. Hydrogen bonding interactions between sulfur atoms and bridging N_2H_x (x = 2, 4) ligands.

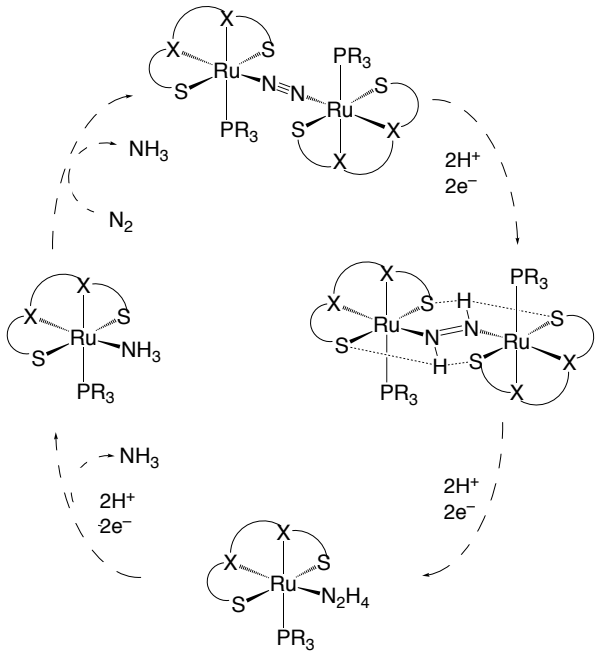

Figure 24. A pseudo catalytic cycle for the reduction of N_2 by two Ru centers speculated based on the reactivity studies of Ru complexes supported by thiolate-containing tetradentate ligands.

Ru_2 complexes with a bridging sulfide or an oligo-sulfide, which were reported by Matsumoto *et al.*, have been found to bind N_2H_4. A disulfide-bridged Ru^{III}_2 complex, $[\{RuCl\mathit{P}_2\}_2(\mu\text{-}Cl)_2(\mu\text{-}S_2)]$ (P = $P(OMe)_3$), reacted with hydrazine to give a Ru^{III}-Ru^{II} complex $[\{RuCl\mathit{P}_2\}_2(\mu\text{-}Cl)(\mu\text{-}N_2H_4)(\mu\text{-}S_2)]$ (**137**),[338] which can be transformed into $[\{RuCl\mathit{P}_2\}_2(\mu\text{-}Cl)(\mu\text{-}N_2H_4)(\mu\text{-}S_2)]^+$ ([**137**]$^+$), $[\{RuCl_2\mathit{P}_2\}_2(\mu\text{-}N_2H_4)(\mu\text{-}S)]$ (**138**), and $[\{RuCl\mathit{P}\}_2]_2(\mu\text{-}S_2O_5)(\mu\text{-}N_2H_4)]$ (**139**) upon exposure to oxygen (**Scheme 47**).[339] Detailed mechanisms for the formation of [**137**]$^+$, **138**, and **139** are discussed in the literature.[339] A related disulfide-bridged dinuclear Ru complex $[\{Ru(MeCN)_3\mathit{P}_2\}_2(\mu\text{-}S_2)]^{4+}$ appeared to take up two N_2H_4 molecules in the bridging positions to give $[\{Ru(MeCN)\mathit{P}_2\}_2(\mu\text{-}N_2H_4)_2(\mu\text{-}S_2)]^{3+}$ (**140**), upon treatment with 3.25 equiv. hydrazine (**Figure 25a**).[340] Analogous reactions of oligo-sulfide complexes $[Ru_2(\mu\text{-}S_n)(\mu\text{-}S_2CNMe_2)(S_2CNMe_2)(CO)_2(PPh_3)_2]$ (n = 5 or 6) with hydrazine led to the accommodation of N_2H_4 and the conversion of the bridging oligo-sulfide into μ-S_4 to give $[\{Ru(S_2CNMe_2)(CO)(PPh_3)\}_2(\mu\text{-}S_4)(\mu\text{-}N_2H_4)]$ (**141**) (**Scheme 48**).[341] In this reaction, PPh_3 promotes desulfurization from the bridging oligo-sulfide, and thereby the addition of PPh_3 improved the product yield. All of these $Ru_2(\mu\text{-}N_2H_4)$ complexes exhibit an octahedral coordination geometry, and their N-N distances (1.442(1)-1.48(2)

Å) are typical of hydrazine complexes. On the other hand, the Ru-S bonds are affected by the oxidation states of the Ru centers, *e.g.* the Ru-S distances follow in the order of Ru^{III}_2 complexes [**137**]$^+$ (2.191(2) and 2.204(2) Å) and **138** (2.199(2) and 2.194(2) Å), Ru^{II}-Ru^{III} complexes **137** (2.266(2) and 2.296(2) Å) and **140** (2.306(4) and 2.299(4) Å),[340] and a Ru^{II}_2 complex **141** (2.389(3) and 2.407(3) Å), because electrons from d^6 (Ru^{II}) centers occupy an orbital which is π-anti-bonding with respect to the Ru-S interaction, as suggested by a qualitative MO description.[342] Reduction of the bridging N_2H_4 remains difficult, as exemplified by the generation of only 8.4% yield of NH_3 from **141** in the presence of Na/Hg and a lutidinium salt.[341] An additional feature of **138** is the crystallographically identified intramolecular H(hydrazine)···O(in $P(OMe)_3$) hydrogen bonds that resulted in the appearance of two distinct N*H*$_2$ and *P*(OMe)$_3$ signals in the ^{1}H and ^{31}P{^{1}H} NMR spectra, respectively. A related hydrogen bond between H(hydrazine)···O(dimethylsulfoxide) is present in a mono-nuclear Ru hydrazenium complex [$RuCl_3(N_2H_5)(Me_2SO$-*S*$)_2$] (**142**) (**Figure 25b**), in which the Ru center interacts with the sulfur atom of dimethylsulfoxide.[343]

Scheme 47. Accommodation of N_2H_4 on a $Ru_2(\mu$-$S_2)$ moiety and subsequent oxidation.

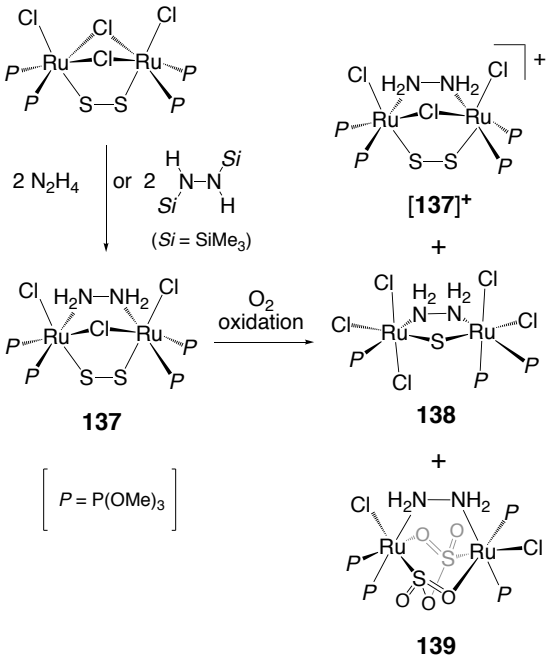

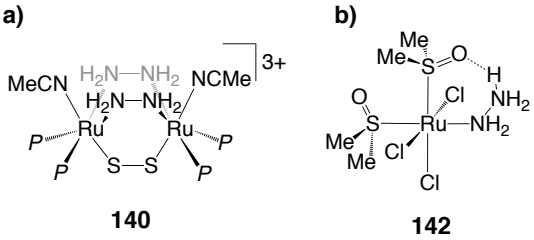

Figure 25. a) A disulfide-bridged dinuclear Ru complex **140** with two bridging N_2H_4 ligands. b) Hydrogen-bonding interaction between N_2H_4 and dimethylsulfoxide in complex **142**.

Scheme 48. Reaction of a oligosulfide-bridged dinuclear ruthenium complex with N_2H_4.

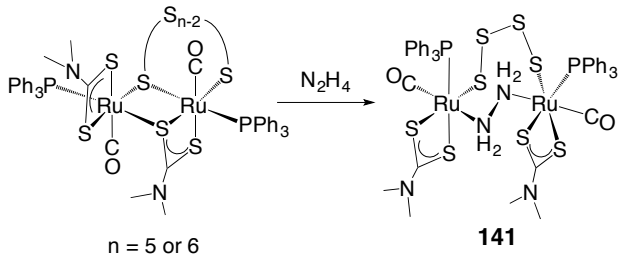

Some coordinatively unsaturated and sulfur-supported (arene)Ru platforms have been found to bind hydrazine. Mashima, Nakamura, and their coworkers synthesized 16-electron Ru complexes, $[(C_6H_6)Ru(S\text{-}2,6\text{-}Me_2C_6H_3)_2]$[344,345] and $[(C_6Me_6)Ru(S_2C_6H_4)]$ ($S_2C_6H_4$ = 1,2-benzenedithiolate),[346] while Herberhold *et al.* used *ortho*-carborane-dithiolate and Leung *et al.* used iminobis(phosphinesulfide) to prepare analogues (*p*-cymene)Ru$\{S_2C_2(B_{10}H_{10})\}$[347] and $[(C_6Me_6)Ru\{N(Ph_2PS)_2\}]^+$,[348] respectively. Their N_2H_4 adducts appeared as mono- or di-nuclear complexes $[(C_6H_6)Ru(N_2H_4)(S\text{-}2,6\text{-}Me_2C_6H_3)_2]$ (**143**), $[\{(C_6Me_6)Ru(S_2C_6H_4)\}_2(\mu\text{-}N_2H_4)]$ (**144**), $[\{(p\text{-cymene})Ru[S_2C_2(B_{10}H_{10})]\}_2(\mu\text{-}N_2H_4)]$ (**145**), and $[(C_6Me_6)Ru\{N(Ph_2PS)_2\}(N_2H_4)]^+$ (**146**) (**Figure 26**), in which Ru centers are in the 18-electron configuration and adopt a three-legged piano stool geometry. The crystal structure of **144** revealed hydrogen bonds between H(hydrazine)···S(thiolate) (3.18 and 3.22 Å), consistent with the red-shifted N-H stretches in the IR spectra of solid samples (ν_{NH} = 3160 and 3080 cm^{-1} for **144** vs. 3300, 3200 cm^{-1} for **143**). In complex **146**, the average P-S distance (2.0215 Å) is shorter than that of the precursor $[(C_6Me_6)Ru\{N(Ph_2PS)_2\}]^+$ (2.0391 Å), as the $[N(Ph_2PS)_2]^-$ ligand can be described in two resonance structures (**Scheme 49a**) of which extreme **A** prefers to bind to a saturated metal center in **146** and extreme **B** is suitable for stabilization of an unsaturated metal center. The $[N(Ph_2PS)_2]^-$

ligand can also stabilize a square pyramidal complex [Ru{N($Ph_2PS)_2$}$_2$(PPh_3)], which forms hexa-coordinate adducts of hydrazines as [Ru{N($PPh_2PS)_2$}$_2$(PPh_3)(L)] (L = N_2H_4 (**147a**), $^tBuNHNH_2$ (**147b**), $C_5H_{10}NNH_2$ (**147c**)) (**Scheme 49b**).[349] Upon exposure to air, **147a** generated an orange compound, analyzed as a diazene complex [Ru{N($Ph_2PS)_2$}(PPh_3)(N_2H_2)] (**148**) along with an uncharacterized material. While the crystal structure of **148** did not definitively confirm the Ru-NH=NH formulation, the N-H and N=N stretching bands in the IR spectrum (ν_{N-H} = 3341, 3330 cm^{-1}; $\nu_{N=N}$ = 1572 cm^{-1}) validated this assignment.

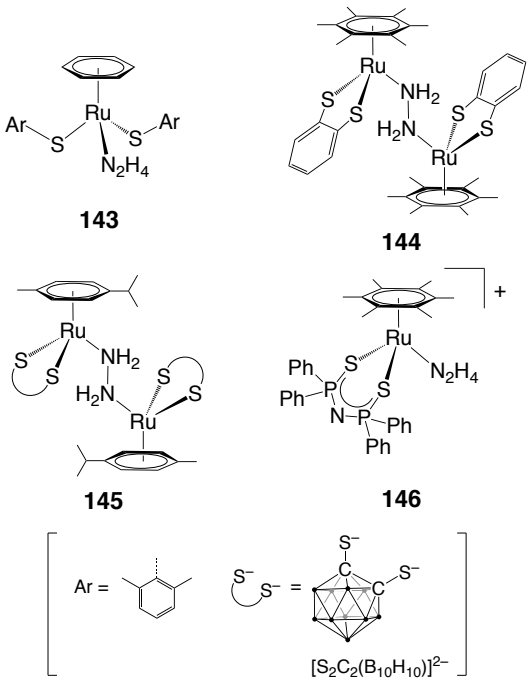

Figure 26. Thiolate-supported N_2H_4 complexes of (arene)Ru.

Scheme 49. a) Resonance structures of $[N(Ph_2PS)_2]^-$ ligand. b) Ru-N_2H_4 complexes supported by two $[N(Ph_2PS)_2]$ ligands.

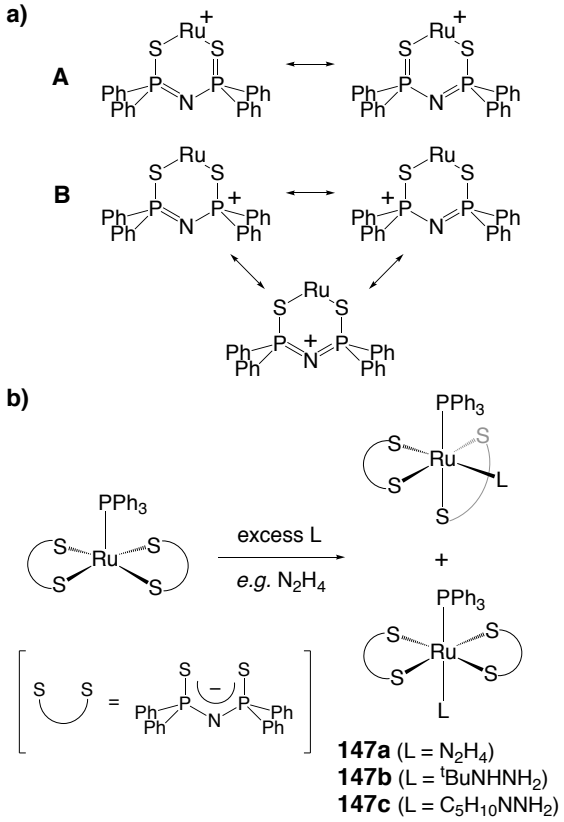

4 Solid-State Metal-Sulfides in N_2 Chemistry

Fe-S clusters, sometimes containing heterometals, are proposed as some of the most ancient cofactors in biological systems,[350] and this coincides with a bioinformatic observation of an enrichment of Fe-S enzymes involved in phosphate-independent metabolism.[351] As this process is proposed to be a *metabolic fossil*[351] of early nonenzymatic biochemistry even prior to the *last universal common ancestor* (LUCA), Fe-S cofactors were perhaps built into biological systems at their initial stage. Such antiquity of Fe-S enzymes can be correlated with one theory of the origin of life: the iron-sulfur world hypothesis. Based on an assumption that the transition from an abiotic to biotic system occurred in close proximity to a location where essential organic molecules were synthesized, an active surface of iron sulfide is proposed to be the origin of chemoautotrophic systems.[352,353] By using model conditions of hydrothermal vents providing metals, inorganic gases, and heat under

high pressure,[352-354] Wächtershäuser and others have demonstrated that nickel and/or iron sulfide converts inorganic gases (*e.g.* CO, CO_2, H_2S) and/or simple organic and inorganic compounds into, for example, carboxylic acids,[355,356] pyruvate,[357] amino acids,[356,358,359] and dipeptides.[360] These abiotic processes operating under model conditions imply that pre-biotic syntheses of nitrogen-containing compounds may have given rise to the emergence of life. Biological nitrogen fixation has been suggested to emerge as early as 3.2 billion years ago in the mid Archaean,[361] when the atmosphere was weakly reducing with N_2 as a major component.[362,363] As a high percentage of the Earth's total nitrogen supply consisted of N_2, abiotic conversion of N_2 into NH_3 facilitated by metal-sulfide materials might be a key to better understand pre-biotic chemical evolution. As current biological systems utilize M-S clusters as enzymatic cofactors to facilitate the N_2 conversion, such M-S cofactors could be considered relics of metal-sulfide materials that performed pre-biotic N_2 reduction. This section summarizes the reduction of N_2 mediated by metal sulfides, with a focus on Fe-based examples. Some photoactive metal sulfide semiconductors in the photoinduced N_2 reduction and the electrochemical reduction of N_2 to NH_3 on metal sulfide electrodes will be also addressed later in this section as an emerging area of N_2 chemistry employing metal-sulfur compounds.

4.1 Reduction of N_2 Mediated by FeS

Fe and Fe-containing minerals have received attention as potential N_2-reducing materials due to the natural abundance of iron. An early example of these investigations is the reduction of N_2 by Fe_3O_4/HCOOH or Fe/H_2O systems, where high temperatures (300-800˚C) and pressures (0.1-0.4 GPa) were required.[364] In a variety of Fe minerals, iron sulfides (Fe_xS_y)[365] are of interest due to their potential relevance to the chemical and biological evolution of N_2 fixation. As summarized in the previous sections, nitrogenases utilize metal-sulfur clusters as their active site cofactors, in which Fe atoms are currently proposed as the substrate binding sites. Reduction of N_2 mediated by iron sulfides can potentially be linked to the origin of N_2 fixation, based on a speculation that ancient N_2-reducing cofactors[366] emerged from fragments or extracts of naturally accessible iron-sulfur materials through evolutionary modifications.

With regard to the notion that the redox couple between FeS/H_2S and FeS_2 is applicable in H_2 formation[367] and has potential to convert N_2 into NH_3 (**eqs 7** and **8**) in thermodynamic calculations,

Schoonen and coworkers investigated N_2 reduction in the presence of FeS and H_2S under high pressure (5 MPa) and moderately high temperature (120 ˚C).[368]

$$N_2 + 3FeS + 3H_2S \rightarrow 2NH_3 + 3FeS_2 \text{ (**eq 7**)}$$

$$N_2 + 2H^+ + 3FeS + 3H_2S \rightarrow 2NH_4^+ + 3FeS_2 \text{ (**eq 8**)}$$

Although the stainless steel surface of a reactor can possibly mediate the ammonia formation even without FeS, the presence of FeS significantly accelerated ammonia production. The final concentration of ammonium ion was theoretically estimated to be between 0.1 and 1 mol/L. However, the observed values merely reached 10^{-5} mol/L. Due to the low ammonia yield, Schoonen *et al.* concluded that this process is not appropriate to produce enough ammonia to sustain pre-biotic synthesis of nitrogen-containng hydrocarbons.

An analogous redox system appeared to work for the reduction of N_2 in aqueous solutions under milder conditions. Weigand, Kreisel, and their coworkers tested N_2 reduction under continuous N_2 flow at pH 3-4 and 80˚C in the presence of freshly prepared FeS precipitate.[369] The yield of NH_4^+ after 2 weeks was small (0.1%, *i.e.* 3 mmol NH_3 from 3 mol FeS), but the origin of the resultant NH_4^+ was confirmed as gaseous N_2 based on an isotope labeling experiment with $^{15}N_2$. Interestingly, freshly prepared FeS precipitate is required for this reaction, and commercial or aged FeS materials did not show the N_2-fixing activity. Based on the scanning electron microscope (SEM) observation of a highly rugged surface in the *active* materials, the authors proposed that a library of different FeS surfaces could provide some local structures that would be well-tailored for the reaction. Recently, this reaction system was revisited to better understand the mechanism.[370] X-ray photoelectron spectroscopy (XPS) measurements of the N 1s region revealed that a surface of pyrrothite (Fe_8S_7) exposed to N_2 (total 2700-L volume at a pressure of 1 x 10^{-9} bar for 45 min) adsorbs nitrogen even at room temperature. A 35% decrease of the total area of the S 2p region in the XPS was attributed to the formation of a nitrogen layer on the surface. Subsequent exposure to H_2S resulted in the significant decrease of the N 1s signal, implying the conversion of the adsorbed nitrogen into NH_3. Detection of NH_3 after full exposure of H_2S to the N_2-incorporated sample, based on the thermal desorption spectrum coupled with mass spectrometry, further supported the occurrence of N_2 reduction. Based on these results, N_2 reduction in this system has been proposed to proceed through

the initial activation of N_2 to form surface N atoms, which are subsequently converted into NH_3 by protonation with H_2S (**Figure 27**).

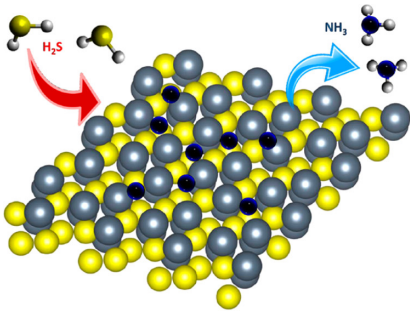

Figure 27. Representation of the reaction of nitrogen-adsorbed pyrrothite (Fe_8S_7) with H_2S to furnish NH_3. Color legend: Gray, Fe; yellow, S; black, N. Reprinted with permission from Niño, M. A.; Flores, E.; Sánchez, C.; Rojo, J. M. *J. Phys. Chem. B* **2018**, *122,* 705–712. Copyright 2018 American Chemical Society.

4.2 Metal Sulfide Semiconductors in Photocatalytic N_2 Reduction

Due to the huge energy demand of the current industrial process to produce NH_3 from N_2, photocatalytic N_2 reduction has recieved increasing attention as a potentially complementary approach.[371,372] Although photocatalysis has no direct relevance to biological nitrogen fixation, some metal sulfide materials have been employed as photocatalysts or photoactive semiconductors in the light-induced reduction of N_2.

Light excitation of photoactive semiconductors leads to the generation of an electron-hole pair (**Figure 28**), which readily recombines by emission of light or heat to regenerate the original state. Alternatively, the excited electron can be transferred to catalytic sites or substrates to trigger reduction reactions, depending on the efficiency of electron transfer and the energy level of the conduction band relative to the required reduction potential for the target reaction. In this scenario, the hole generated in the valence band needs to be filled by oxidation of a sacrificial reagent, which is often a weak reductant and preferably H_2O. Therefore, an advantage of the photocatalytic systems is the ability to generate highly reducing species without strong reducing agents. For the light-induced N_2 reduction, however, the significantly negative potential required for the first electron transfer (E^O = –4.16 V) is a major obstacle (**eqs 9** and **10**), although the overall ammonia/ammonium

formation is thermodynamically favorable (**eqs 11** and **12**).[371] Thus, efforts need to be directed toward preparation of catalysts to lower the kinetic barrier of the N_2 activation, as well as photoactive materials to satisfy the reduction potentials of the catalysts by absorbing visible light.

$$N_2 + e^- \rightarrow N_2^- \quad E^O = -4.16\ V\ (\textbf{eq 9})$$

$$N_2 + H^+ + e^- \rightarrow N_2H \quad E^O = -3.2\ V\ (\textbf{eq 10})$$

$$N_2 + 6H^+ + 6e^- \rightarrow 2NH_3 \quad E^O = 0.55\ V\ (\textbf{eq 11})$$

$$N_2 + 8H^+ + 6e^- \rightarrow 2NH_4^+ \quad E^O = 0.27\ V\ (\textbf{eq 12})$$

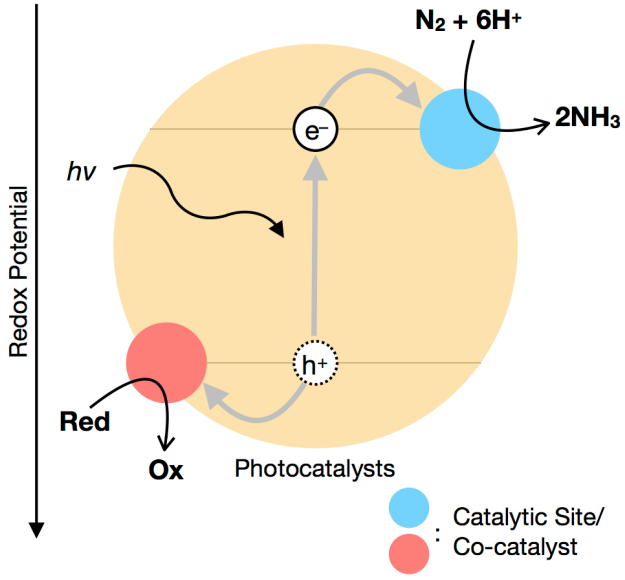

Figure 28. Schematic description of photocatalytic N_2 reduction. Abbreviation: Red, reducing agents; Ox, oxidized products of Red.

Kanatzidis and coworkers used a biomimetic approach by utilizing synthetic metal sulfur clusters as precursors of porous materials. Their early findings in this effort were the synthesis of porous chalcogenide aerogels (chalcogels) by using $[MQ_4]^{4-}$, $[M_2Q_6]^{4-}$, and $[M_4Q_{10}]^{4-}$ (M = Ge, Sn; Q = S, Se)[373] linkers, as well as the application of the linkers to assemble synthetic $[Fe_4S_4]$ or $[MoFe_3S_4]_2$ clusters into photoactive H_2-evolving and CO_2-reducing chalcogels.[374,375,376] A Ru-based photosensitizer ($[Ru(bpy)_3]^{2+}$; bpy = 2,2'-bipyridyl) was often incorporated through cation exchange for efficient photocatalytic behaviors,[374,376,377] but simpler chalcogels consisting of $[Fe_4S_4]$ or $[MoFe_3S_4]_2$ clusters

linked by $[Sn_2S_6]^{4-}$ exhibited photo-induced N_2 reduction without the requirement for a light-harvesting additive. The active materials were synthesized through salt-metathesis reactions of Cl-supported clusters (*i.e.* $[Fe_4S_4Cl_4]^{2-}$ and $[(MoFe_3S_4Cl_3)_2(\mu\text{-SPh})_3]^{3-}$) with $Na_4[Sn_2S_6]$ (**Figure 29**).[378,379] This gelation process proceeded slowly, and took a week or longer for complete solidification; the resultant porous materials exhibited high surface areas (>118 m^2/g) as determined by N_2 adsorption/desorption measurements. Kanatzidis *et al.* speculated that $[Fe_4S_4]$ and $[MoFe_3S_4]$ core structures remained intact in each chalcogel matrix, based on the extrusion of the Fe-S or Mo-Fe-S clusters from the solid materials in the presence of excess PhSH. Unlike the corresponding small-molecule clusters, these chalcogels are stable against hydrolysis, enabling their applications in aqueous media.

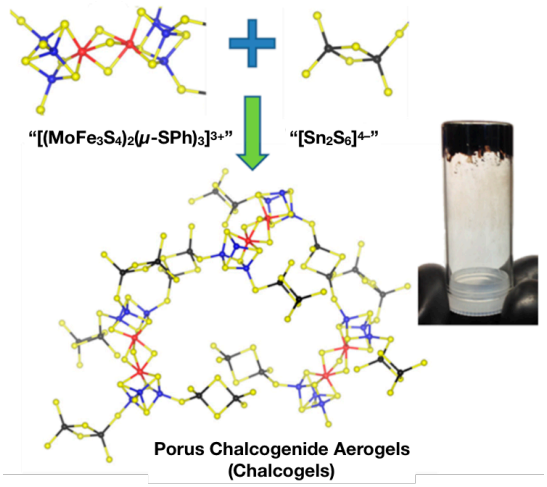

Figure 29. Schematic description of chalcogel synthesis. An example of a combination of $[(MoFe_3S_4)_2(\mu\text{-SPh})_3]^{3+}$ and $[Sn_2S_6]^{4-}$ is displayed. A picture of the material is shown at right. Color legend: Black, Sn; blue, Fe; red, Mo; yellow, S. Reprinted with permission from Banerjee, A.; Yuhas, B. D.; Margulies, E. A.; Zhang, Y.; Shim, Y.; Wasielewski, M. R.; Kanatzidis, M. G. *J. Am. Chem. Soc.* **2015**, *137*, 2030–2034. Copyright 2015 American Chemical Society.

A standard N_2 reduction assay was carried out under continuous N_2 flow and light irradiation (150-W Xe lump at 100 mW/cm^{-1}) in the presence of sodium ascorbate (5 mM) as a sacrificial reductant and pyridinium hydrochloride (50 mM) as a proton source. Ammonia production was detected by

the indophenol method[380,381] as well as the ^{1}H NMR observation of NH_4^+. In contrast, a series of blank experiments in the absence of Fe-S or Mo-Fe-S components, light, or N_2 flow showed no detectable amount of ammonia. An additional proof for the conversion of N_2 was provided from the assay under a $^{15}N\equiv^{14}N$ atmosphere, where the amounts of both $^{15}NH_4^+$ and $^{14}NH_4^+$ increased proportional to the irradiation time. These results strongly indicated the involvement of synthetic Fe-S or Mo-Fe-S clusters in the photoinduced reduction of N_2. Interestingly, the $[Fe_4S_4]$ chalcogel (FeS-SnS) outperformed those from the $[MoFe_3S_4]_2$ cluster or a mixture of both clusters (FeMoS-SnS and FeMoS-FeS-SnS, respectively). The NH_3 yields of 48-h reactions using 150 mg of Fe-S-SnS, FeMoS-SnS, and FeMoS-FeS-SnS were 160, 105, and 53 μg, respectively.

The binding behavior of N_2 to the chalcogels under light irradiation was monitored by *in situ* diffuse-reflectance Fourier transform infrared spectroscopy (DRIFTS). Two infrared absorption bands assigned to N-N stretches, at 1753 and 1746 cm^{-1}, appeared for FeMoS-FeS-SnS under N_2-flowing and light-irradiating conditions, indicating the accommodation of N_2 on the $[MoFe_3S_4]$ and $[Fe_4S_4]$ moieties, respectively. As the latter band red-shifted to 1724 cm^{-1} in the presence of D_2O, the N_2 species trapped by the $[Fe_4S_4]$ moiety was suggested to form hydrogen bonds with water. Facile protonation of N_2 by the FeS-SnS chalcogel is in accordance with the higher TON of N_2 reduction, while the larger surface area of FeS-SnS (148 m^2/g) should also provide more chances for N_2 binding than FeMoS-SnS. The reason behind the difference in the catalytic activities of the $[Fe_4S_4]$ and $[MoFe_3S_4]$ moieties remains unclear.

Among typical metal sulfide materials, cadmium sulfide (CdS) has been of intense interest as a photocatalyst[382] and a fluorescence probe,[383] because it absorbs visible light and shows a high quantum efficiency and photostability. Application of CdS in photocatalytic N_2 reduction was first reported in 1980,[384] when a CdS film made from a commercially available powder was found to reduce N_2 into NH_3 under irradiation with a mercury lamp, furnishing 10.6 μmol/g_{cat} of NH_3 after 5 h at 38˚C. Improvement of the catalytic activity of CdS semiconductor was attained by incorporation of heterometal dopants. Thus, $Zn_{0.1}Sn_{0.1}Cd_{0.8}S$, $Zn_{0.1}Mo_{0.1}Cd_{0.8}S$, $Ni_{0.1}Sn_{0.1}Cd_{0.8}S$, [385] and $Mo_{0.1}Ni_{0.1}Cd_{0.8}S$ [386] were synthesized and tested by Hu and coworkers, resulting in the NH_3 production rates of 279, 220, 88, and 190 μmol/(g_{cat}·h), respectively. While powder X-ray diffraction (XRD) patterns of $Zn_{0.1}Sn_{0.1}Cd_{0.8}S$ and $Mo_{0.1}Ni_{0.1}Cd_{0.8}S$ indicated the crystal lattice of CdS, elemental analyses of these materials exhibited lower sulfur contents than those estimated from their

compositions, which indicates partial vacancies of S sites in the CdS lattice. Using the differences between the calculated and found S contents as indexes of the concentrations of vacancies, the authors found a linear correlation between the rate of ammonia production and the vacancy concentration (**Figure 30**). Thus, it was proposed that heterometal doping leads to the generation of surface sulfur vacancies, which should provide N_2 binding sites. This claim was supported by comparisons between the as-prepared and O_2-calcined materials of $Zn_{0.1}Sn_{0.1}Cd_{0.8}S$ or $Mo_{0.1}Ni_{0.1}Cd_{0.8}S$. In both cases, calcination significantly decreased the rates of ammonia production (<18 μmol/(g_{cat}·h)) due to oxygenation of the sulfur vacancies. Involvement of the sulfur vacancies in the N_2 activation was also indicated by temperature-programmed desorption (TPD) studies, where the peak at ~270˚C related to the chemisorbed N_2 was found only for the as-prepared material.

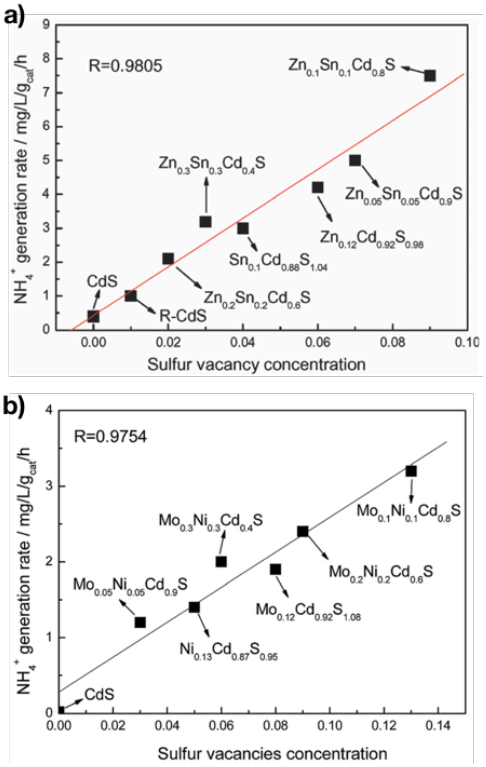

Figure 30. Dependence of photocatalytic N_2 fixation performance on the concentration of sulfur vacancies in CdS-based materials doped with a) Zn and Sn or b) Mo and Ni. For a), reprinted with permission from Hu, S.; Chen, X.; Li, Q.; Zhao, Y.; Mao, W. *Catal. Sci. Technol.* **2016**, *6*, 5884–5890. Copyright 2016 Royal Society of Chemistry. For b), reprinted with permission from Fan, Z.; Wang, Q.; Lu, G.; Cao, Y.; Hu, S.; Li, F.; Bai, J. *RSC Adv.* **2016**, *6*, 49862–49867. Copyright 2016 Royal Society of Chemistry.

The heterometal-doped materials were further combined with graphitic carbon nitride (g-C_3N_4) to prepare heterojunction photocatalysts. Nanocomposites of $Zn_{0.1}Sn_{0.1}Cd_{0.8}S$ [387] or $Zn_{0.1}Mo_{0.1}Cd_{0.8}S$[388] with g-$C_3N_4$ improved the rates of photocatalytic N_2 reduction by 1.6 fold for $Zn_{0.1}Sn_{0.1}Cd_{0.8}S$/g-$C_3N_4$ or 1.75 fold for $Zn_{0.1}Mo_{0.1}Cd_{0.8}S$/g-$C_3N_4$ (**Figure 31a**), while the retention of spectroscopic features and physical properties of the components was indicated by EPR, powder XRD, and TPD measurements. The beneficial contribution of g-C_3N_4 to the catalytic activities could be attributed to the inhibition of charge carrier recombination by efficient separation of electron-hole pairs. As g-C_3N_4 has valence and conduction bands lying slightly above the heterometal-doped

CdS photocatalysts, the composites led to an effective accumulation of electrons to the CdS moiety and holes to the g-C_3N_4 counterpart (**Figure 31b**).[389] Decreased photoluminescence (PL) intensities of the nanocomposites are consistent with the proposed separation of electrons and holes. An analogous strategy was applied by Lashgari and Zeinalkhani for the combination of pyrite (FeS_2) and carbon nanotubes (CNTs),[390] which exhibited higher N_2 reducing activity and lower PL intensity upon formation of the nanocomposite (**Figure 32**), indicating an effective electron-hole separation of the excited species.

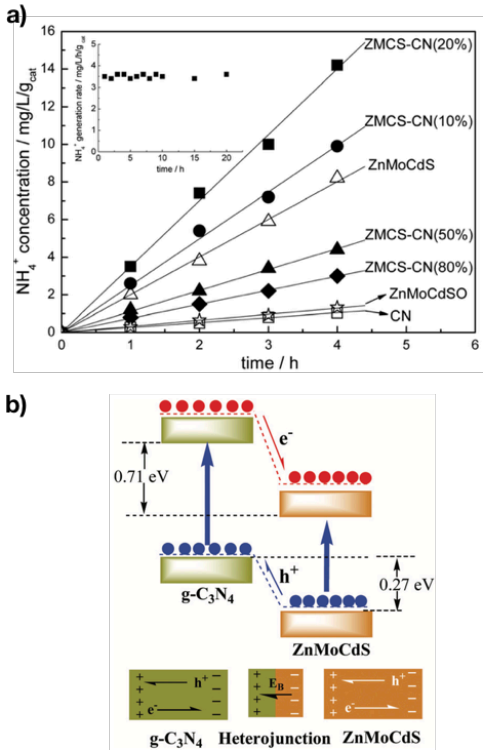

Figure 31. a) Photocatalytic N_2-reducing performance of as-prepared $Zn_{0.12}Mo_{0.12}Cd_{0.9}S_{1.14}$ (ZMCS) and heterojunction of ZMCS and graphitic carbon nitride (termed as g-C_3N_4 or CN) denoted as ZMCS-CN(*x*%), where x% stands for the mass % of CN. An inset of a) shows the steady catalytic performance of ZMCS-CN(20%) under prolonged light irradiation. b) Schematic description of electron-hole separation/transport at the interface of the ZMCS-CN heterojunction. Reprinted with permission from Zhang, Q.; Hu, S.; Fan, Z.; Liu, D.; Zhao, Y.; Ma, H.; Li, F. *Dalton Trans.* **2016**, *45*, 3497–3505. Copyright 2016 Royal Society of Chemistry.

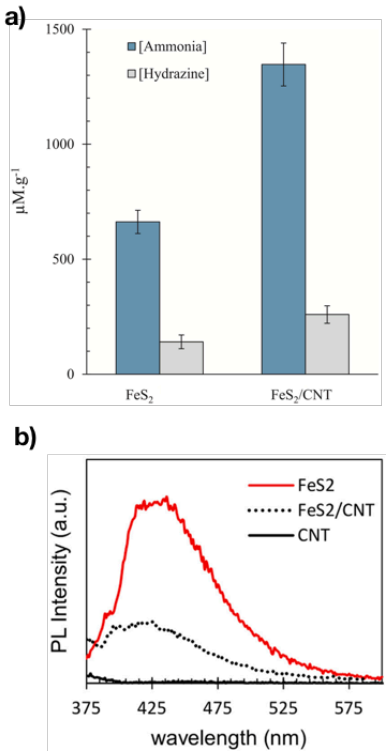

Figure 32. a) Photocatalytic NH_3/N_2H_4 production from N_2 mediated by FeS_2 and FeS_2/carbon nanotube (CNT) composites after 1 h light irradiation. b) Photoluminescence of FeS_2 and FeS_2/CNT. Reprinted with permission from Lashgari, M.; Zeinalkhani, P. *Nano Energy* **2018**, *48*, 361–368. Copyright 2018 Elsevier.

CdS can also act as a donor of excited electrons to assist co-existing catalytic systems. A notable example is a mixture of photoactive $CdS/Pt/RuO_2$ particles and $[Ru(Hedta)(N_2)]^-$ (edta = ethylenediamine-tetraacetate) (**Figure 33a**),[391] which generated NH_3 at up to 6.8 mol/(mol_{Ru}·h) (mol_{Ru} = mole of Ru complex) in aqueous solutions with irradiation by visible light (λ = 505 nm) and ambient conditions (30˚C and 1 atm N_2), while bulk electrolysis in the absence of $CdS/Pt/RuO_2$ showed significantly decreased catalytic activity. Accommodation of the Ru species on the particles might play a crucial role achieving this catalytic activity, because both the Ru-N_2 complex and the $CdS/Pt/RuO_2$ particles appeared to be essential for the N_2 reduction, whereas the detailed mechanisms remain unclear. Formation of a composite of $Cd_{0.5}Zn_{0.5}S$ photosensitizer and a catalytic component has also been investigated. $Cd_{0.5}Zn_{0.5}S$ nanoparticles decorated with 0.5 mol% of Ni_2P

($Ni_2P/Cd_{0.5}Zn_{0.5}S$) were found to catalyze light-induced N_2 reduction under irradiation by visible light at wavelengths of 420, 450, 500, and 550 nm (**Figure 33b**).[392] The catalytic rate reached 254 µmol/ (g_{cat}·h) with the highest apparent quantum efficiency of 4.32% with 420 nm irradiation. Similarly, the loading of Ni_2P onto the surface of $Cd_{0.5}Zn_{0.5}S$ particles led to the efficient separation of electron-hole pairs and improved electron mobility, as indicated by the long lifetime of the charge carriers (τ = 1.13 ns for $Ni_2P/Cd_{0.5}Zn_{0.5}S$, τ = 0.97 ns for $Cd_{0.5}Zn_{0.5}S$). The N_2-reducing activities reported thus far do not exceed ~300 µmol/ (g_{cat}·h), implying that unknown factors currently inhibit maximal reaction rates.

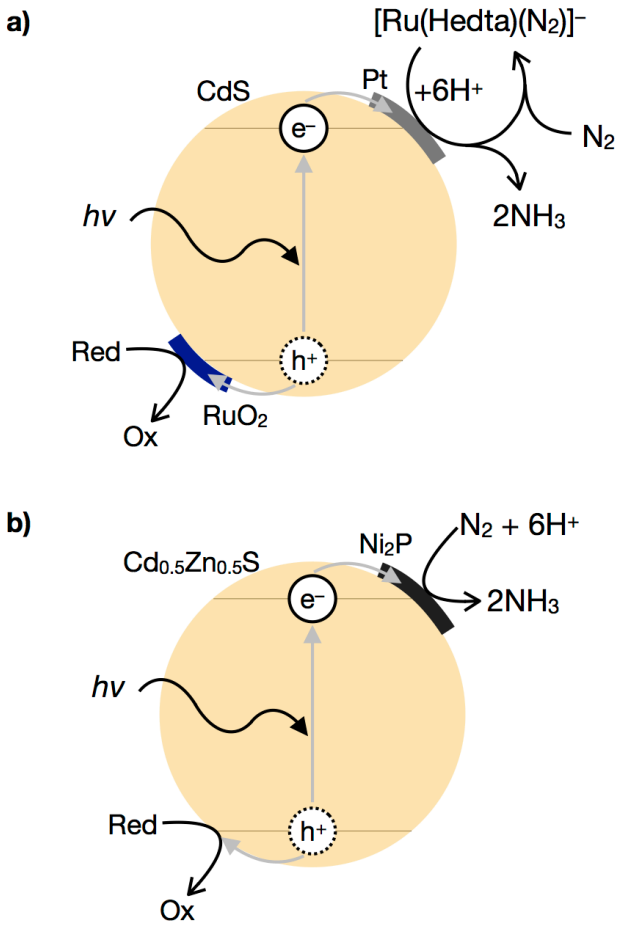

Figure 33. Schematic descriptions of photocatalytic N_2 reduction by composites of a) $CdS/Pt/RuO_2$ particles and $[Ru(Hedta)(N_2)]^-$ (edta = ethylenediamine-tetraacetate) and b) $Cd_{0.5}Zn_{0.5}S$ nanoparticles and Ni_2P. Abbreviation: Red, reducing agents; Ox, oxidized products of Red.

A unique example in the application of photoactive CdS is the integration of the Mo-nitrogenase to furnish an N_2-reducing *biohybrid* material.[393] In analogy to the method to assemble CdS or CdTe with hydrogenase for photoinduced H_2 production,[394,395] King and coworkers used water-soluble CdS nanorods (d≈ 38 ± 5 Å, l ≈ 168 ± 16 Å) to adsorb the Mo-nitrogenase. The CdS nanorods showed a sufficiently negative potential (–0.8 V vs. NHE)[395] to reduce the Mo-nitrogenase (–0.31 V).[396] Thus, the CdS/Mo-nitrogenase *biohybrid* material photocatalytically reduced N_2 into NH_3 under visible light irradiation (405 nm) at 25˚C (**Figure 34**). The photocatalytic NH_3 production rate reached 315±55 nmol/(mg Mo-nitrogenase)·min (= 18900 μmol/(g Mo-nitrogenase)·h), which is 63% of native enzyme activity. A prominent feature of this *biohybrid* material is that it does not require the specific electron carrier (Fe protein) or ATP, which are both indispensable for the enzymatic reaction.[2] It should also be noted that other reported examples of ATP-independent reactions of Mo-nitrogenase have not been able to catalyze N_2 reduction. [135,136,146,397] Given that the relatively strong Eu^{II} reductants (*i.e.* –1.2 V vs. NHE for Eu^{II}-DTPA; DTPA = diethylenetriaminepentaacetic acid) cannot facilitate N_2 reduction by Mo-nitrogenase, [135,136] the specific observation of N_2 reduction in the biohybrid material may imply that the interaction of Mo-nitrogenase with CdS nanorods induces a conformational change to a state suitable for N_2 reduction, which is normally achieved by binding of the Fe protein. The negatively charged amino acids on the surface of Mo-nitrogenase (seven Glu and one Asp residues) have been postulated to participate in the interaction with the Fe protein,[9] and these residues might form analogous interactions with CdS nanorods, as the surface of the nanorod has high affinity to anionic species.[383]

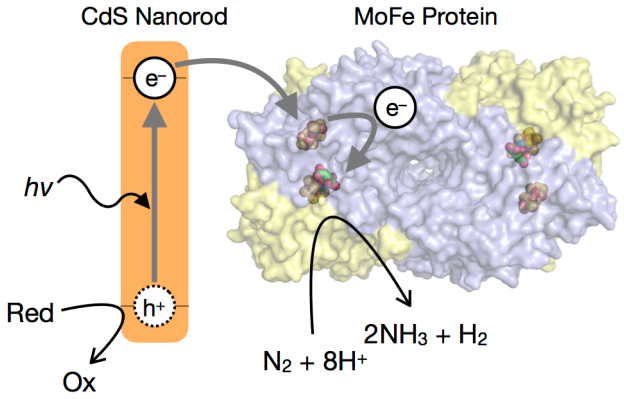

Figure 34. Schematic illustration of N_2 reduction to NH_3 catalyzed by a CdS/Mo-nitrogenase (MoFe protein) biohybrid under light irradiation. Abbreviation: Red, reducing agents; Ox, oxidized products of Red.

Metal sulfide semiconductors for the photocatalytic reduction of N_2 are not limited to CdS-based materials. Ultrathin and hexagonal MoS_2 was recently found to catalyze the photoinduced reduction of N_2 at the rate of up to 325 μmol/(g_{cat}·h), under simulated sunlight irradiation and at room temperature in 0.5 M Na_2SO_4 aq. (pH = 3.5).[398] Based on the correlation to the catalytic activities, Wang and coworkers proposed the importance of negative photoconductivity, which is a prominent feature of ultrathin MoS_2 semiconductor.

4.3 Metal Sulfides in Electrocatalytic N_2 Reduction

Electrocatalytic reduction of N_2 to generate NH_3, which has been summarized elsewhere,[399,400,401] sometimes employs metal sulfides as electrodes. **Table 2** summarizes activities of metal-sulfide materials for electrochemical N_2 reduction. In an early study by Furuya and Yoshida, various metal sulfides were tested under ambient conditions using gas-diffusion electrodes.[402] However, the current efficiencies at –1.0 V (vs. reversible hydrogen electrode (RHE)) were less than 1% (*e.g.* 0.098% for MoS and 0.105% for FeS). Chen, Tang, Sun, and their coworkers improved the activity of the Mo-based material by using a MoS_2 nanosheet grown on carbon cloth, and achieved a faradic efficiency of 1.17% and the NH_3 yield of 8.08 x 10^{11} mol/s·cm_{cat} at –0.5 V (vs. RHE) in 0.1 M Na_2SO_4 aq.[403] With regard to Fe-sulfides, Mu, Fu, and their coworkers developed Fe_3S_4 nanosheets that improved to 6.45% faradic efficiency, and the yield of NH_3 reached to 75.4 μg/h·mg_{cat} at –0.4 V (vs.

RHE) at room temperature in 0.1 M HCl (**Figure 35**).[404] The Fe_3S_4 nanosheet appeared to be robust and retained its full catalytic activity for at least 20 h. The synthetic procedure for Fe_3S_4, which is a solvothermal reaction in a mixture of poly(ethyleneglycol)-200 and thiourea, is also applicable to the synthesis of CoS_2 and NiS_2 analogues, but their activities were lower by more than one order of magnitude. Improved catalytic activity of CoS_2 was achieved by Wu and coworkers. They used hybrid materials consisting of CoS_x (x = 1 - 2) nanoparticles and nitrogen- and sulfur-doped reduced graphene, and attained a faradic efficiency of 25.9% at –0.05 V (vs. RHE) and the NH_3 yield of 25.0 $\mu g/h \cdot mg_{cat}$ at –0.2 V (vs. RHE) with the CoS_2-based material.[405] FeS_x- and NiS_x-based materials can be similarly prepared, although their catalytic activities were lower than the CoS_x-based materials. The high catalytic activity of CoS_x-graphene hybrid was attributed to the strong binding of uniformly grown CoS_x nanoparticles to graphene through many Co-N and S-C bonds at the interface, which was indicated by the soft X-ray absorption near-edge spectra (XANES), showing characteristic features in carbon and nitrogen K-edge spectra and cobalt and sulfur L-edge spectra. Doping of electrons to the π* (C=C) state of graphene was suggested to introduce sp^3-interactions through the formation of additional bonds out of the graphene layer.

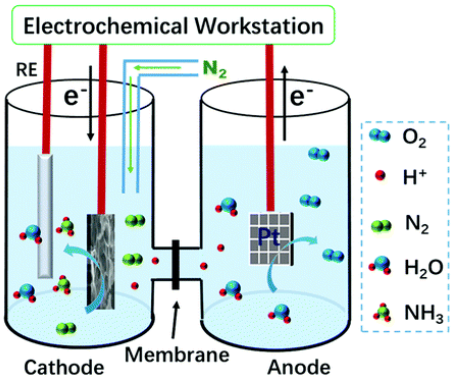

Figure 35. Schematic illustration of electrocatalytic N_2 reduction reactions. In the figure, Fe_3S_4 nanosheets are used as the cathodic materials. Reprinted with permission from Zhao, X.; Lan, Z.; Yu, D.; Fu, H.; Liu, Z.; Mu, T. *Chem. Commun.* **2018**, *54*, 13010-13013. Copyright 2018 Royal Society of Chemistry.

Table 2. Electrochemical N_2 reduction by metal-sulfide based catalysts.

Material	Electrolyte	Temp. (˚C)	Potential (V vs. RHE)	NH_3 yield ($mol \cdot s^{-1} \cdot cm^{-2}$)	Faradaic Efficiency (%)	Refs.
ZnS	1 M KOH	25	–1.0	$5.65 \cdot 10^{-9}$ [d]	0.964	402
NiS	1 M KOH	25	–1.0	$3.87 \cdot 10^{-9}$ [d]	0.849	402
CdS	1 M KOH	25	–1.0	$4.14 \cdot 10^{-9}$ [d]	0.741	402
CuS	1 M KOH	25	–1.0	$1.01 \cdot 10^{-9}$ [d]	0.182	402
Bi_2S_3	1 M KOH	25	–1.0	$1.57 \cdot 10^{-9}$ [d]	0.172	402
FeS	1 M KOH	25	–1.0	$3.03 \cdot 10^{-9}$ [d]	0.105	402
MoS	1 M KOH	25	–1.0	$1.24 \cdot 10^{-9}$ [d]	0.098	402
Sb_2S_3	1 M KOH	25	–1.0	$6.63 \cdot 10^{-9}$ [d]	0.096	402
SnS	1 M KOH	25	–1.0	$1.21 \cdot 10^{-9}$ [d]	0.085	402
MnS	1 M KOH	25	–1.0	$4.35 \cdot 10^{-9}$ [d]	0.040	402
PbS	1 M KOH	25	–1.0	$3.14 \cdot 10^{-9}$ [d]	0.031	402
PdS	1 M KOH	25	–1.0	$7.63 \cdot 10^{-9}$ [d]	0.031	402
AgS	1 M KOH	25	–1.0	$4.56 \cdot 10^{-9}$ [d]	0.024	402
CoS	1 M KOH	25	–1.0	$1.75 \cdot 10^{-9}$ [d]	0.015	402
MoS_2/CC [a]	0.1 M Na_2SO_4	rt [c]	–0.5	$8.08 \cdot 10^{-11}$	1.17	401
	0.1 M HCl	rt [c]	–1.0	$8.48 \cdot 10^{-11}$	0.096	401
Fe_3S_4 nanosheets	0.1M HCl	rt [c]	–0.4	~$3.7 \cdot 10^{-10}$ [d]	6.45	402
CoS_2/NS-G [b]	0.05 M H_2SO_4	rt [c]	–0.05	-	25.9	403
			–0.2	25.0 ($\mu g \cdot h^{-1} \cdot mg_{cat}^{-1}$) [e]	-	403
CoS/NS-G [b]	0.05 M H_2SO_4	rt [c]	–0.05	-	15.6	403
			–0.2	5.7 ($\mu g \cdot h^{-1} \cdot mg_{cat}^{-1}$) [e]	-	403

[a] CC = carbon cloth. [b] NS-G = nitrogen- and sulfur-doped reduced graphene. [c] rt = room temp. [d] Original values are reported using different units (*i.e.* $\mu g \cdot h^{-1} \cdot mg_{cat}^{-1}$) and are converted. [e] Values cannot be converted due to undescribed details.

5 Summary and Future Outlook

This review has summarized studies of the static and dynamic properties of synthetic metal-sulfur (M-S) compounds from three different viewpoints: multi-nuclear M-S clusters, mono- and di-nuclear metal complexes supported by S-containing ligands, and metal sulfide-based solid materials. **Section 2** addressed synthetic chemistry and reactivity studies of M-S clusters relevant to the nitrogenase cofactors. Attempts to artificially synthesize the active sites of nitrogenases began even prior to the precise structural determination of FeM'co (M' = Mo, V), and various strategies have been taken for this purpose. In this review, we summarized representative synthetic studies by categorizing the strategies as follows: structural conversion of cuboidal [M_4S_4] clusters, template-based synthetic approaches using [(L)MS_3] (M = Mo, W) complexes with a multi-dentate ligand L, assembly of metal and sulfur atoms under non-ionic conditions, and incorporation of light atoms into M-S inorganic cores. With regard to the reactivity studies of M-S clusters, catalytic N_2 conversion still remains a challenge, while sub-stoichiometric N_2 reduction has been recently achieved. Some other nitrogense-related reactions, *e.g.* catalytic reductions of C_2H_2, MeN=NMe, N_2H_4, CO, and CO_2, have been achieved with synthetic M-S clusters electrochemically and/or in the presence of reducing equivalents. **Section 3** highlighted the N_2 and N_2H_x (x = 2, 4) chemistry of sulfur-supported transition metal complexes, with a focus on mono- and di-nuclear Fe complexes. Detailed studies of their coordination behaviors and physicochemical properties revealed some representative features of S-based ligands, *e.g.* their relatively strong electron donating ability leading to efficient π-back bonding from the d orbital of metals to the π^* orbital of metal-bound N_2 and hydrogen bonding between thiolates and the N_2H_x species on metals. Reduction and disproportionation of N_2H_x species have also been reported, whereas the conversion of metal-bound N_2 remained scarce when it came to sulfur-supported transition metal complexes. In **Section 4**, a variety of metal sulfide materials involved in the reduction of N_2 were discussed. In the context of ancient chemical evolution, the N_2-reducing activities of iron-sulfides have been of interest, and a limited production of NH_3 has been achieved by the FeS-based systems. Some other materials were reported to perform photocatalytic reduction of N_2 with or without co-catalysts. Atomic arrangement and/or sulfur vacancies in the metal sulfide materials were suggested to affect their performance as catalysts and/or light harvesters.

As a future outlook of this field, we would like to point out three issues that have not been well

addressed, but might advance comprehension of biological/pre-biotic N_2 fixation and drive the development of artificial alternatives corresponding to the native systems: (1) better M-S cluster models of nitrogenase active sites, (2) elucidation of the possible roles of sulfur atoms in N_2 fixation, and (3) studies of sulfur-based materials inspired by the chemistry of nitrogenases. With regard to issue (1), what remains elusive is the precise chemical synthesis of M-S clusters that reproduce FeM'co of nitrogenases, particularly those with eight transition metals (Fe and Mo/V) encapsulating a carbon atom. Given the idiosyncrasy of the μ_6-C atom in the nitrogenase cofactors, a more complete understanding of its chemical behavior could unveil the significance of Fe-C interactions in physiological N_2 reduction in sulfur-rich environments. Since recent studies on the biosynthesis of FeMoco have revealed that a methyl group from *S*-adenosyl methionine is the source of the carbon atom that is eventually encapsulated by two cuboidal [Fe_4S_4] precursors,[6,36,77] relevant carbon-insertion reactions of metal-sulfur clusters could represent one of the possible approaches. In relation to issue (2), the catalytic cycle of N_2 fixation by nitrogenase has been proposed to involve protonated sulfur atom(s) in key intermediates.[17] As these protons on sulfur atoms would serve as the proton source of NH_3, further studies of chemical actions of S-based ligands may provide a better understanding of the enzymatic system. New approaches encompassing such features on S atoms will also be beneficial in a broader perspective of small-molecule activation. In the context of issue (3), metal sulfide materials in previous studies have not been linked well to the chemistry of M-S clusters and nitrogenase active sites. Assuming that nanoscopic structures of metal sulfides determine their chemical behaviors, one can extend the synthetic strategies of M-S clusters, *e.g.* utilization of FeMoco models as building blocks, to furnish nano-sized materials with structural homogeneity or narrow structural diversity, which would help to examine the relationships between the nano-structures and the N_2 fixation abilities. It would also provide possible insights into pre-biotic N_2 fixation.

Given the abundance of M-S clusters as metallo-cofactors, especially in enzymes promoting the reduction of N_2, CO_2, H^+, and N_2O, participation of S atoms could not only be a relic from pre-biotic chemical evolution but also an intrinsic advantage under physiological reducing conditions. Further insights into how metals and S atoms can cooperatively function for the reduction of substrates may contribute to developing artificial and bio-inspired catalysts that are comparable or even superior to the biological systems employing M-S cofactors.

Author Information

Notes

The authors declare no competing financial interest.

Biography

Yasuhiro Ohki received his Bachelor degree from Department of Applied Chemistry at Tokyo Institute of Technology in 1995 and Master degree from the same institute in 1997, under the guidance of Prof. Hiroharu Suzuki. After working for a year at the research center of TOTO co. ltd., he joined the Suzuki group again as a researcher of CREST, Japan Science and Technology Corporation. His Ph.D. degree was given in 2002 from Tokyo Institute of Technology. He was appointed to an assistant professor in 2000 and was promoted to an associate professor in 2008 at Department of Chemistry, Nagoya University, where he worked with Prof. Kazuyuki Tatsumi until 2013. In 2006, he took a sabbatical leave at the University of British Columbia, where he worked with Prof. Michael D. Fryzuk. His research interest is centered on the development of new synthetic methodologies for inorganic molecules, regarding bio-inorganic chemistry, organometallic chemistry, and molecular-based material candidates.

Kazuki Tanifuji received his B.Sc from the Department of Chemistry at Nagoya University in 2009 and a Ph.D. degree from the same institute in 2014 under the supervision of Prof. Yasuhiro Ohki and Prof. Kazuyuki Tatsumi. After a short period of working as a postdoctoral scholar in the Tatsumi group, he moved to the U.S. in 2014 to join the group of Prof. Markus W. Ribbe in the Department of Molecular Biology and Biochemistry at UC Irvine. In recognition of his postdoctoral work, he was awarded the Barbara K. Burgess fellowship and Dean's Early Career Award from the School of Biosciences at UC Irvine. His research involves development of bio-analytical tools by combining biochemistry of metalloproteins with synthetic inorganic chemistry.

Acknowledgments

This work was financially supported by Grant-in-Aids for Scientific Research (19H02733 and 18H04246) from the Japanese Ministry of Education, Culture, Sports, Science and Technology

(MEXT), the Takeda Science Foundation, and the Yazaki Memorial Foudation. We are grateful to Dr. Akira Katayama (Nagoya Institute of Technology), Dr. Megan P. Newcomb, and Dr. Andrew J. Jasniewski (University of California, Irvine) for useful comments on this paper.

Table of contents (TOC) graphic

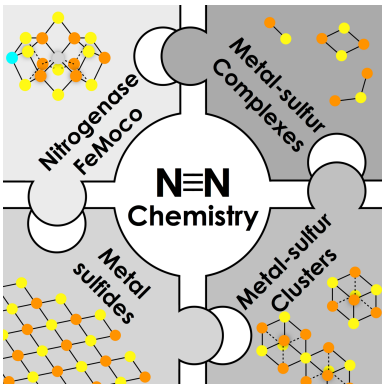

References

(1) Canfield, D. E.; Glazer, A. N.; Falkowski, P. G. The Evolution and Future of Earth's Nitrogen Cycle. *Science* **2010**, *330*, 192–196.

(2) Georgiadis, M. M.; Komiya, H.; Chakrabarti, P.; Woo, D.; Komuc, J. J.; Rees, D. C. Crystallographic Structure of the Nitrogenase Iron Protein from Azotobacter vinelandli. *Science* **1992**, *257*, 1653-1659.

(3) Jasniewski, A. J.; Sickerman, N. S.; Hu, Y.; Ribbe, M. W. The Fe Protein: An Unsung Hero of Nitrogenase. *Inorganics* **2018**, *6*, 25.

(4) Peters, J. W.; Stowell, M. H. B.; Soltis, S. M.; Finnegan, M. G.; Johnson, M. K.; Rees, D. C. Redox-Dependent Structural Changes in the Nitrogenase P-Cluster. *Biochemistry* **1997**, *36*, 1181–1187.

(5) Mayer, S. M; Lawson, D. M.; Gomal, C. A.; Roe, S. M.; Smith, B. E. New Insights into Structure-function Relationships in Nitrogenase: A 1.6 Å Resolution X-ray Crystallographic Study of Klebsiella pneumoniae MoFe-protein. *J. Mol. Biol.* **1997**, *292*, 871-891.

(6) Spatzal, T.; Aksoyoglu, M.; Zhang, L.; Andrade, S. L. A.; Schleicher, E.; Weber, S.; Rees, D. C.; Einsle, O. Evidence for Interstitial Carbon in Nitrogenase FeMo Cofactor. *Science* **2011**, *334*, 940–940.

(7) Lancaster, K. M.; Roemelt, M.; Ettenhuber, P.; Hu, Y.; Ribbe, M. W.; Neese, F.; Bergmann, U.; DeBeer, S. X-ray Emission Spectroscopy Evidences a Central Carbon in the Nitrogenase Iron-Molybdenum Cofactor. *Science* **2011**, *334*, 974–977.

(8) Wiig, J. A.; Hu, Y.; Lee, C. C.; Ribbe, M. W. Radical SAM-dependent Carbon Insertion into the Nitrogenase M-cluster. *Science* **2012**, *337*, 1672–1675.

(9) Schindelin, H.; Kisker, C.; Schlessman, J. L.; Howard, J. B.; Rees, D. C. Structure of ADP-AlF_4^- stabilized nitrogenase complex and its implications for signal transduction. *Nature* **1997**, *387*, 370-376.

(10) Tezcan, F. A.; Kaiser, J. T.; Mustafi, D.; Walton, M. Y.; Howard, J. B.; Rees, D. C. Nitrogenase Complexes: Multiple Docking Sites for a Nucleotide Switch Protein. *Science* **2005**, *309*, 1377-1380.

(11) Danyal, K.; Dean, D. R.; Hoffman, B. M.; Seefeldt, L. C. Electron transfer within Nitrogenase: Evidence for a Deficit-spending Mechanism. *Biochemistry* **2011**, *50*, 9255–9263.

(12) Sippel, D.; Einsle, O. The structure of vanadium nitrogenase reveals an unusual bridging ligand. *Nat. Chem. Biol.* **2017**, *13*, 956–960.

(13) Sippel, D.; Rohde, M.; Netzer, J.; Trncik, C.; Gies, J.; Grunau, K.; Djurdjevic, I.; Decamps, L.; Andrade, S. L. A.; Einsle, O. A bound reaction intermediate sheds light on the mechanism of nitrogenase. *Science* **2018**, *359*, 1484–1489.

(14) Eady, R. R. Structure−Function Relationships of Alternative Nitrogenases. *Chem. Rev*. **1996**, *96*, 3013–3030.

(15) Krahn, E.; Weiss, B. J. R.; Kröckel, M.; Groppe, J.; Henkel, G.; Cramer, S. P.; Trautwein, A. X.; Schneider, K.; Müller, A. The Fe-only nitrogenase from *Rhodobacter capsulatus*: identification of the cofactor, an unusual, high-nuclearity iron-sulfur cluster, by Fe *K*-edge EXAFS and ^{57}Fe Mössbauer spectroscopy *J. Biol. Inorg. Chem.* **2002**, *7*, 37-45.

(16) Burgess, B. K.; Lowe, D. J. Mechanism of Molybdenum Nitrogenase. *Chem. Rev*. **1996**, *96*, 2983–3012.

(17) Hoffman, B. M.; Lukoyanov, D.; Yang, Z.; Dean, D. R.; Seefeldt, L. C. Mechanism of Nitrogen Fixation by Nitrogenase: The Next Stage. *Chem. Rev*. **2014**, *114*, 4041–4062.

(18) Yang, Z. –Y.; Khadka, N.; Lukoyanov, D.; Hoffman, B. M.; Dean, D. R.; Seefeld, L. C. On reversible H_2 loss upon N_2 binding to FeMo-cofactor of nitrogenase *Proc. Natl. Acad. Sci. U.S.A.* **2013**, *110*, 16327-16332.
(19) Lukoyanov, D.; Yang, Z. –Y.; Khadka, N.; Dean, D. R.; Seefeldt, L. C.; Hoffman, B. M. Identification of a Key Catalytic Intermediate Demonstrates That Nitrogenase Is Activated by the Reversible Exchange of N_2 for H_2. *J. Am. Chem. Soc.* **2015**, *137*, 3610-3615.
(20) Chatt, J.; Pearman, A. J.; Richards, R. L. Conversion of dinitrogen in its molybdenum and tungsten complexes into ammonia and possible relevance to the nitrogenase reaction. *J. Chem. Soc., Dalton Trans*. **1977**, 1852–1860.
(21) Pickett, C. J. The Chatt cycle and the mechanism of enzymic reduction of molecular nitrogen. *J. Biol. Inorg. Chem.* **1996**, *1*, 601-606.
(22) Burford, R. J.; Fryzuk, M. D. Examining the relationship between coordination mode and reactivity of dinitrogen. *Nat. Rev. Chem*. **2017**, *1*, 0026.
(23) Dilworth, M. J.; Eady, R. R. Hydrazine is a product of dinitrogen reduction by the vanadium-nitrogenase from Azotobacter chroococcum. *Biochem. J*. **1991**, *277*, 465–468.
(24) Dilworth, M. J.; Eldridge, M. E.; Eady, R. R. The molybdenum and vanadium nitrogenases of Azotobacter chroococcum: effect of elevated temperature on N_2 reduction. *Biochem. J*. **1993**, *289*, 395–400.
(25) Deng, H.; Hoffmann, R. How N_2 Might Be Activated by the FeMo-Cofactor in Nitrogenase. *Angew. Chem. Int. Ed*. **1993**, *32*, 1062–1065.
(26) Kästner, J.; Blöchl, P. E. Ammonia Production at the FeMo Cofactor of Nitrogenase: Results from Density Functional Theory. *J. Am. Chem. Soc*. **2007**, *129*, 2998–3006.
(27) Varley, J. B.; Wang, Y.; Chan, K.; Studt, F.; Nørskov, J. K. Mechanistic insights into nitrogen fixation by nitrogenase enzymes *Phys. Chem. Chem. Phys*. **2015**, *17*, 29541–29547.
(28) Siegbahn, P. E. M. Is there computational support for an unprotonated carbon in the E_4 state of nitrogenase? *J. Comput. Chem*. **2018**, *39*, 743–747.
(29) Dance, I. How feasible is the reversible S-dissociation mechanism for the activation of FeMo-co, the catalytic site of nitrogenase? *Dalton Trans*. **2019**, *48*, 1251–1262.
(30) Cao, L.; Ryde, U. Extremely large differences in DFT energies for nitrogenase models. *Phys. Chem. Chem. Phys*. **2019**, *21*, 2480–2488.
(31) McWilliams, S. F.; Holland, P. L. Dinitrogen Binding and Cleavage by Multinuclear Iron Complexes. *Acc. Chem. Res*. **2015**, *48*, 2059–2065.
(32) Nishibayashi, Y. Recent Progress in Transition-Metal-Catalyzed Reduction of Molecular Dinitrogen under Ambient Reaction Conditions. *Inorg. Chem*. **2015**, *54*, 9234–9247.
(33) van der Ham, C. J. M.; Koper, M. T. M.; Hetterscheid, D. G. H. Challenges in reduction of dinitrogen by proton and electron transfer. *Chem. Soc. Rev*. **2014**, *43*, 5183–5191.
(34) Shah, V. K.; Brill, W. J. Isolation of an iron-molybdenum cofactor from nitrogenase. *Proc. Natl. Acad. Sci. U. S. A*. **1977**, *74*, 3249–3253.
(35) Fay, A. W.; Blank, M. A.; Lee, C. C.; Hu, Y.; Hodgson, K. O.; Hedman, B.; Ribbe, M. W. Characterization of Isolated Nitrogenase FeVco. *J. Am. Chem. Soc*. **2010**, *132*, 12612–12618.
(36) Kaiser, J. T.; Hu, Y.; Wiig, J. A.; Rees, D. C.; Ribbe, M. W. Structure of Precursor-Bound NifEN: A Nitrogenase FeMo Cofactor Maturase/Insertase. *Science* **2011**, *331*, 91–94.
(37) Fay, A. W.; Blank, M. A.; Lee, C. C.; Hu, Y.; Hodgson, K. O.; Hedman, B.; Ribbe, M. W. Spectroscopic Characterization of the Isolated Iron–Molybdenum Cofactor (FeMoco) Precursor

from the Protein NifEN. *Angew. Chem. Int. Ed*. **2011**, *50*, 7787–7790.
(38) Lee, S. C.; Holm, R. H. The Clusters of Nitrogenase: Synthetic Methodology in the Construction of Weak-Field Clusters. *Chem. Rev*. **2004**, *104*, 1135–1158.
(39) Seino, H.; Hidai, M. Catalytic functions of cubane-type M_4S_4 clusters. *Chem. Sci.* **2011**, *2*, 847-857.
(40) Ohki, Y.; Tatsumi, K. New Synthetic Routes to Metal-Sulfur Clusters Relevant to the Nitrogenase Metallo-Clusters. *Z. Anorg. Allg. Chem*. **2013**, *639*, 1340–1349.
(41) Lee, S. C.; Lo, W.; Holm, R. H. Developments in the Biomimetic Chemistry of Cubane-Type and Higher Nuclearity Iron–Sulfur Clusters. *Chem. Rev*. **2014**, *114*, 3579–3600.
(42) Holm, R. H.; Lo, W. Structural Conversions of Synthetic and Protein-Bound Iron–Sulfur Clusters. *Chem. Rev.* **2016**, *116*, 13685-13713.
(43) Ohta, S.; Ohki, Y. Impact of ligands and media on the structure and properties of biological and biomimetic iron-sulfur clusters. *Coord. Chem. Rev*. **2017**, *338*, 207–225.
(44) Sickerman, N. S.; Tanifuji, K.; Hu, Y.; Ribbe, M. W. Synthetic Analogues of Nitrogenase Metallocofactors: Challenges and Developments. *Chem. Eur. J.* **2017**, *23*, 12425–12432.
(45) Tanifuji, K.; Ohki, Y. Recent Advances in the Chemical Synthesis of Nitrogenase Model Clusters. In *Structure and Bonding*; Ribbe, M. W., Ed.; Springer, Berlin, Heidelberg: Berlin, Heidelberg, 2019.
(46) Wolff, T. E.; Berg, J. M.; Warrick, C.; Hodgson, K. O.; Holm, R. H.; Frankel, R. B. The molybdenum-iron-sulfur cluster complex $[Mo_2Fe_6S_9(SC_2H_5)_8]^{3-}$. A synthetic approach to the molybdenum site in nitrogenase. *J. Am. Chem. Soc.* **1978**, *100*, 4630–4632.
(47) Christou, G.; Garner, C. D.; Mabbs, F. E., A molybdenum derivative of a four-iron ferredoxin type centre, *Inorg. Chim. Acta* **1978**, *28*, L189-L190.
(48) Christou, G.; Garner, C. D.; Mabbs, F. E.; Drew, M. G. B., Thiol Exchange Reactions of Iron-Molybdenum-Sulphur Clusters ; Preparation and X-Ray Crystal Structure of $[Et_4N]_3[Fe_6Mo_2S_8(SCH_2CH_2OH)_9]$, a Water Soluble Iron-Molybdenum-Sulphur Cluster, *J. Chem. Soc., Chem. Commun.* **1979**, 91-93.
(49) Wolff, T. E.; Berg, J. M.; Hodgson, K. O.; Frankel, R. B.; Holm, R. H., Synthetic Approaches to the Molybdenum Site in Nitrogenase. Preparation and Structural Properties of the Molybdenum-Iron-Sulfur "Double-Cubane" Cluster Complexes $[Mo_2Fe_6S_8(SC_2H_5)_9]^{3-}$ and $[Mo_2Fe_6S_9(SC_2H_5)_8]^{3-}$ *J. Am. Chem. Soc.* **1979**, *101*, 4140-4150.
(50) Wolff, T. E.; Power, P. P.; Frankel, R. B.; Holm, R. H. Synthesis and electronic and redox properties of "double-cubane" cluster complexes containing $MoFe_3S_4$ and WFe_3S_4 cores. *J. Am. Chem. Soc.* **1980**, *102*, 4694-4703.
(51) Wolff, T. E.; Berg, J. M.; Power, P. P.; Hodgson, K. O.; Holm, R. H., Structural characterization of the iron-bridged "double-cubane" cluster complexes $[Mo_2Fe_7S_8(SC_2H_5)_{12}]^{3-}$ and $[M_2Fe_7S_8(SCH_2C_6H_5)_{12}]^{4-}$ (M = Mo, W) containing MFe_3S_4 cores, *Inorg. Chem.* **1980**, *19*, 430–437.
(52) Palermo, R. E.; Singh, R.; Bashkin, J. K.; Holm, R. H. Molybdenum atom ligand substitution reactions of molybdenum-iron-sulfur (MoFe3S4) cubane-type clusters: synthesis and structures of clusters containing molybdenum-bound pseudosubstrates of nitrogenase. *J. Am. Chem. Soc*. **1984**, *106*, 2600–2612.
(53) Kim, J.; Rees, D. C. Structural Models for the Metal Centers in the Nitrogenase Molybdenum-iron Protein. *Science* **1992**, *257*, 1677–1682.
(54) Barclay, J. E.; Evans, D. J.; Garcia, G.; Santana, M. D.; Torralba, M. C.; Yago, J. M. Binding of the $\{MoFe_3S_4\}^{3+}$ core by a tridentate thiolate and chemical analogues of the molybdenum co-ordination

environment in the iron–molybdenum cofactor of nitrogenase. *J. Chem. Soc. Dalton Trans*. **1995**, 1965–1971.
(55) Demadis, K. D.; Coucouvanis, D. Synthesis, structural characterization, and properties of new single and double cubanes containing the $MoFe_3S_4$ structural unit and molybdenum-bound polycarboxylate ligands. Clusters with a molybdenum-coordination environment similar to that in the iron-molybdenum cofactor of nitrogenase. *Inorg. Chem*. **1995**, *34*, 436–448.
(56) Kovacs, J. A.; Holm, R. H., Assembly of Vanadium-Iron-Sulfur Cubane Clusters from Mononuclear and Linear Trinuclear Reactants *J. Am. Chem. Soc*. **1986**, *108*, 340–341.
(57) Kovacs, J. A.; Holm, R. H., Heterometallic Clusters: Synthesis and Reactions of Vanadium-Iron-Sulfur Single- and Double-Cubane Clusters and the Structure of $[V_2Fe_6S_8Cl_4(C_2H_4S_2)_2]^{4-}$, *Inorg. Chem.* **1987**, *26*, 702-711.
(58) Kovacs, J. A.; Holm, R. H., Structural Chemistry of Vanadium-Iron-Sulfur Clusters Containing the Cubane-Type $[VFe_3S_4]^{2+}$ Core, *Inorg. Chem*. **1987**, *26*, 711–718.
(59) Carney, M. J.; Kovacs, J. A.; Zhang, Y. P.; Papaefthymiou, G. C.; Spartalian, K.; Frankel, R. B.; Holm, R. H., Comparative Electronic Properties of Vanadium-Iron-Sulfur and Molybdenum-Iron-Sulfur Clusters Containing Isoelectronic Cubane-Type $[VFe_3S_4]^{2+}$ and $[MoFe_3S_4]^{3+}$ Cores *Inorg. Chem*. **1987**, *26*, 719–724.
(60) Huang, J.; Mukerjee, S.; Segal, B. M.; Akashi, H.; Zhou, J.; Holm, R. H., Molybdenum-Iron Sulfide-Bridged Double Cubanes, *J. Am. Chem. Soc*. **1997**, *119*, 8662–8674.
(61) Einsle, O.; Tezcan, F. A.; Andrade, S. L. A.; Schmid, B.; Yoshida, M.; Howard, J. B.; Rees, D. C. Nitrogenase MoFe-Protein at 1.16 Å Resolution: A Central Ligand in the FeMo-Cofactor. *Science* **2002**, *297*, 1696–1700.
(62) Demadis, K. D.; Campana, C. F.; Coucouvanis, D. Synthesis and Structural Characterization of the New $Mo_2Fe_6S_8(PR_3)_6(Cl_4\text{-cat})_2$ Clusters. Double Cubanes Containing Two Edge-Linked $[MoFe_3S_4]^{2+}$ Reduced Cores. *J. Am. Chem. Soc.* **1995**, *117*, 7832-7833.
(63) Tyson, M. A.; Coucouvanis, D. New Fe/Mo/S Clusters with $MoFe_3S_3$ Cuboidal Cores Similar to the One in the Fe/Mo Cofactor of Nitrogenase. Synthesis and Structural Characterization of the $(C1_4\text{-cat})MoFe_3S_3(PEt_3)_2(CO)_6$ and $(C1_4\text{-cat})Mo(O)Fe_3S_3(PEt_3)_3(CO)_5$ Clusters. *Inorg. Chem*. **1997**, *36*, 3808–3809.
(64) Coucouvanis, D.; Han, J.; Moon, N. Synthesis and Characterization of Sulfur-Voided Cubanes. Structural Analogues for the $MoFe_3S_3$ Subunit in the Nitrogenase Cofactor. *J. Am. Chem. Soc*. **2002**, *124*, 216–224.
(65) Han, J.; Beck, K.; Ockwig, N.; Coucouvanis, D. Synthetic Analogs for the $MoFe_3S_3$ Subunit of the Nitrogenase Cofactor: Structural Features Associated with the Total Number of Valence Electrons and the Possible Role of M–M and Multiple M–S Bonding in the Function of Nitrogenase. *J. Am. Chem. Soc.* **1999**, *121*, 10448–10449.
(66) Chu, C. T.-W.; Dahl, L. F. Structural characterization of $[AsPh_4]^+[Fe_4(NO)_7(\mu_3\text{-}S)_3]^-$. Stereochemical and bonding relationship of the Roussin black monoanion with the red ethyl ester, $Fe_2(NO)_4(\mu_2\text{-}SC_2H_5)_2$, and $Fe_4(NO)_4(\mu_3\text{-}S)_4$. *Inorg. Chem*. **1977**, *16*, 3245–3251.
(67) Butler, A. R.; Glidewell, C.; Li, M. –H., Nitrosyl Complexes of Iron-Sulfur Clusters. *Adv. Inorg. Chem.* **1988**, *32*, 335-393.
(68) Fritsch, J.; Scheerer, P.; Frielingsdorf, S.; Kroschinsky, S.; Friedrich, B.; Lenz, O.; Spahn, C. M. T. The crystal structure of an oxygen-tolerant hydrogenase uncovers a novel iron-sulphur centre. *Nature* **2011**, *479*, 249-252.

(69) Shomura, Y.; Yoon, K.-S.; Nishihara, H.; Higuchi, Y. Structural basis for a [4Fe-3S] cluster in the oxygen-tolerant membrane-bound [NiFe]-hydrogenase. *Nature* **2011**, *479*, 253–256.
(70) Wiig, J. A.; Hu, Y.; Ribbe, M. W., Refining the pathway of carbide insertion into the nitrogenase M-cluster, *Nat. Commun.* **2015**, *6*, 8034.
(71) Ribbe, M. W.; Hu, Y.; Hodgsonm, K. O.; Hedman, B., Biosynthesis of Nitrogenase Metalloclusters. *Chem. Rev.* **2014**, *114*, 4063-4080.
(72) Hu, Y.; Ribbe, M. W., Biosynthesis of the Metalloclusters of Nitrogenases. *Annu. Rev. Biochem.* **2016**, *85*, 455-483.
(73) Sickerman, N. S.; Ribbe, M. W.; Hu, Y., Nitrogenase Cofactor Assembly: An Elemental Inventory. *Acc. Chem. Res.* **2017**, *50*, 2834-2841.
(74) Hu, Y.; Fay, W. W.; Lee, C. C.; Ribbe, M. W., P-cluster maturation on nitrogenase MoFe protein, *Proc. Natl. Acad. Sci. U.S.A.* **2007**, *104*, 10424-10429.
(75) Cotton, M. S.; Rupnik, K.; Broach, R. B.; Hu, Y.; Fay, A. W.; Ribbe, M. W.; Hales, B. J., VTVH-MCD Study of the ΔnifBΔnifZ MoFe Protein from Azotobacter vinelandii, *J. Am. Chem. Soc.* **2009**, *131*, 4558-4559.
(76) Lee, C. C.; Blank, M. A.; Fay, A. W.; Yoshizawa, J. M.; Hu, Y.; Hodgson, K. O.; Hedman, B.; Ribbe, M. W., Stepwise formation of P-cluster in nitrogenase MoFe protein, *Proc. Natl. Acad. Sci. U.S.A.* **2009**, *106*, 18474-18478.
(77) Tanifuji, K.; Lee, C. C.; Sickerman, N. S.; Tatsumi, K.; Ohki, Y.; Hu, Y.; Ribbe, M. W., Tracing the '9th Sulfur' of the nitrogenase cofactor via a semi-synthetic approach, *Nat. Chem*. **2018**, *10*, 568–572.
(78) Osterloh, F.; Sanakis, Y.; Staples, R. J.; Münck, E.; Holm, R. H. A Molybdenum-Iron-Sulfur Cluster Containing Structural Elements Relevant to the P-Cluster of Nitrogenase. *Angew. Chem. Int. Ed*. **1999**, *38*, 2066–2070.
(79) Osterloh, F.; Achim, C.; Holm, R. H. Molybdenum–Iron–Sulfur Clusters of Nuclearities Eight and Sixteen, Including a Topological Analogue of the P-Cluster of Nitrogenase. *Inorg. Chem*. **2001**, *40*, 224–232.
(80) Zhang, Y.; Zuo, J. L.; Zhou, H. C.; Holm, R. H. Rearrangement of Symmetrical Dicubane Clusters into Topological Analogues of the P Cluster of Nitrogenase: Nature's Choice? *J. Am. Chem. Soc.* **2002**, *124*, 14292–14293.
(81) Zhang, Y.; Holm, R. H. Synthesis of a Molecular $Mo_2Fe_6S_9$ Cluster with the Topology of the P^N Cluster of Nitrogenase by Rearrangement of an Edge-Bridged $Mo_2Fe_6S_8$ Double Cubane. *J. Am. Chem. Soc.* **2003**, *125*, 3910–3920.
(82) Zuo, J. –L.; Zhou, H. –C.; Holm, R. H. Vanadium–Iron–Sulfur Clusters Containing the Cubane-type $[VFe_3S_4]$ Core Unit: Synthesis of a Cluster with the Topology of the P^N Cluster of Nitrogenase. *Inorg. Chem.* **2003**, *42*, 4624-4631.
(83) Zhang, Y.; Holm, R. H. Structural Conversions of Molybdenum–Iron–Sulfur Edge-Bridged Double Cubanes and P^N-Type Clusters Topologically Related to the Nitrogenase P-Cluster. *Inorg. Chem*. **2004**, *43*, 674–682.
(84) Berlinguette, C. P. Holm, R. H. Edge-Bridged $Mo_2Fe_6S_8$ to P^N-Type $Mo_2Fe_6S_9$ Cluster Conversion: Structural Fate of the Attacking Sulfide/Selenide Nucleophile. *J. Am. Chem. Soc.* **2006**, *128*, 11993-12000.
(85) Hlavinka, M. L.; Miyaji, T.; Staples, R. J.; Holm, R. H. Hydroxide-Promoted Core Conversions of

Molybdenum−Iron−Sulfur Edge-Bridged Double Cubanes: Oxygen-Ligated Topological P^N Clusters. *Inorg. Chem.* **2007**, *46*, 9192-9200.
(86) Pesavento, R. P.; Berlinguette, C. P.; Holm, R. H. Stabilization of Reduced Molybdenum−Iron−Sulfur Single- and Double-Cubane Clusters by Cyanide Ligation. *Inorg. Chem*. **2007**, *46*, 510–516.
(87) Zheng, B.; Chen, X. D.; Zheng, S. L.; Holm, R. H. Selenium as a Structural Surrogate of Sulfur: Template-Assisted Assembly of Five Types of Tungsten–Iron–Sulfur/Selenium Clusters and the Structural Fate of Chalcogenide Reactants. *J. Am. Chem. Soc.* **2012**, *134*, 6479–6490.
(88) Ohki, Y.; Tanifuji, K.; Yamada, N.; Cramer, R. E.; Tatsumi, K. Formation of a Nitrogenase P-cluster [Fe_8S_7] Core via Reductive Fusion of Two All-Ferric [Fe_4S_4] Clusters. *Chem. Asian J*. **2012**, *7*, 2222–2224.
(89) Ohki, Y.; Sunada, Y.; Honda, M.; Katada, M. Synthesis of the P-Cluster Inorganic Core of Nitrogenases. *J. Am. Chem. Soc*. **2003**, *125*, 4052–4053.
(90) Ohki, Y.; Imada, M.; Murata, A.; Sunada, Y.; Ohta, S.; Honda, M.; Sasamori, T.; Tokitoh, N.; Katada, M. Synthesis, Structures, and Electronic Properties of [8Fe-7S] Cluster Complexes Modeling the Nitrogenase P-Cluster. *J. Am. Chem. Soc*. **2009**, *131*, 13168–13178.
(91) Keable, S. M.; Zadvornyy, O. A.; Johnson, L. E.; Ginovska, B.; Rasmussen, A. J.; Danyal, K.; Eilers, B. J.; Prussia, G. A.; LeVan, A. X.; Raugei, S.; Seefeldt, L. C.; Peters, J. W. Structural characterization of the P^{1+} intermediate state of the P-cluster of nitrogenase. *J. Biol. Chem*. **2018**, *293*, 9629–96354.
(92) The RMSD values were calculated by using the PyMOL software package (ver. 2.0.6). PyMol is freely available from https://pymol.org/2.
(93) McLean, P. A.; Papaefthymiou, V.; Orme-Johnson, W. H.; Münck, E. Isotopic hybrids of nitrogenase. Mössbauer study of MoFe protein with selective ^{57}Fe enrichment of the P-cluster. *J. Biol. Chem.* **1987**, *262*, 12900–12903.
(94) Surerus, K. K.; Hendrich, M. P.; Christie, P. D.; Rottgardt, D.; Orme-Johnson, W. H.; Münck, E. Moessbauer and integer-spin EPR of the oxidized P-clusters of nitrogenase: P^{OX} is a non-Kramers system with a nearly degenerate ground doublet. *J. Am. Chem. Soc*. **1992**, *114*, 8579–8590.
(95) Kawaguchi, H.; Yamada, K.; Lang, J.; Tatsumi, K. A New Entry into Molybdenum/Tungsten Sulfur Chemistry: Synthesis and Reactions of Mononuclear Sulfido Complexes of Pentamethylcyclopentadienyl-Molybdenum(VI) and -Tungsten(VI). *J. Am. Chem. Soc.* **1997**, *119*, 10346–10358.
(96) Lang, J.; Ji, S.; Xu, Q.; Shen, Q.; Tatsumi, K. Structural aspects of copper(I) and silver(I) sulfide clusters of pentamethylcyclopentadienyl trisulfido tungsten(VI) and molybdenum(VI). *Coord. Chem. Rev.* **2003**, *241*, 47–60.
(97) Seino, H.; Arai, Y.; Iwata, N.; Nagao, S.; Mizobe, Y.; Hidai, M. Preparation of Mononuclear Tungsten Tris(sulfido) and Molybdenum Sulfido−Tetrasulfido Complexes with Hydridotris(pyrazolyl)borate Coligand and Conversion of the Former into Sulfido-Bridged Bimetallic Complex Having Pt(μ-S)$_2$WS Core. *Inorg. Chem*. **2001**, *40*, 1677–1682.
(98) Fomitchev, D. V.; McLauchlan, C. C.; Holm, R. H., Heterometal Cubane-Type MFe_3S_4 Clusters (M = Mo, V) Trigonally Symmetrized with Hydrotris(pyrazolyl)borate(1-) and Tris(pyrazolyl)methanesulfonate(1-) Capping Ligands, *Inorg. Chem.* **2002**, *41*, 958-966.
(99) Christou, G.; Holm, R. H.; Sabat, M.; Ibers, J. A. A hexanuclear iron-sulfide-thiolate cluster: assembly and properties of [Fe_6S_9(S-tert-C_4H_9)$_2$]$^{4-}$ containing three types of bridging sulfur atoms. *J. Am. Chem. Soc.* **1981**, *103*, 6269−6271.

(100) Christou, G.; Sabat, M.; Ibers, J. A.; Holm, R. H. A new structural type in iron-sulfide-thiolate chemistry: preparation, properties, and structure of the hexanuclear cluster $[Fe_6S_9(S\text{-}tert\text{-}C_4H_9)_2]^{4-}$. *Inorg. Chem.* **1982**, *21*, 3518−3526.
(101) Henkel, G.; Strasdeit, H.; Krebs, B. $[Fe_6S_9(SCH_2C_6H_5)_2]^{4-}$: A Hexanuclear Iron-Sulfur Cluster Anion Containing the Square-Pyramidal $[(\mu_4\text{-}S)Fe_4]$ Unit. *Angew. Chem. Int. Ed.* **1982**, *21*, 201−202.
(102) Strasdeit, H.; Krebs, B.; Henkel, G. Synthetic route to $[Fe_6S_9(SR)_2]^{4-}$ clusters (R = alkyl). Their spectroscopic and magnetic properties and the solid-state structures of $[Fe_6S_9(SCH_2Ph)_2]^{4-}$ and $[(Fe_6S_9(SMe)_2)_2Na_2]^{6-}$. *Inorg. Chem.* **1984**, *23*, 1816−1825.
(103) Strasdeit, H.; Krebs, B.; Henkel, G. $[Fe_6Se_6(SR)_2]^{4-}$ Clusters (R = Me, CH_2Ph): Synthesis and Characterization, and the X-Ray Structure of $(PhCH_2NEt_3)_4[Fe_6Se_9(SMe)_2]$. *Z. Naturforsch.* **1987**, *42b*, 565–572.
(104) Zhou, H.; Su, W.; Achim, C.; Rao, P. V.; Holm, R. H. High-Nuclearity Sulfide-Rich Molybdenum−Iron−Sulfur Clusters: Reevaluation and Extension. *Inorg. Chem*. **2002**, *41*, 3191–3201.
(105) Partyka, D. V.; Staples, R. J.; Holm, R. H., Nucleophilic Reactivity and Oxo/Sulfido Substitution Reactions of $M^{VI}O_3$ Groups (M = Mo, W), *Inorg. Chem.* **2003**, *42*, 7877-7886.
(106) Majumdar, A.; Holm, R. H. Specific Incorporation of Chalcogenide Bridge Atoms in Molybdenum/Tungsten-Iron-Sulfur Single Cubane Clusters. *Inorg. Chem*. **2011**, *50*, 11242–11251.
(107) Tanifuji, K.; Sickerman, N.; Lee, C. C.; Nagasawa, T.; Miyazaki, K.; Ohki, Y.; Tatsumi, K.; Hu, Y.; Ribbe, M. W. Structure and Reactivity of an Asymmetric Synthetic Mimic of Nitrogenase Cofactor. *Angew. Chem. Int. Ed.* **2016**, *55*, 15633–15636.
(108) Xu, G.; Wang, Z.; Ling, R.; Zhou, J.; Chen, X.; Holm, R. H. Ligand metathesis as rational strategy for the synthesis of cubane-type heteroleptic iron–sulfur clusters relevant to the FeMo cofactor. *Proc. Natl. Acad. Sci. U. S. A.* **2018**, *115*, 5089–5092.
(109) Chen. X. –D.; Duncan, J. S.; Verma, A. K.; Lee, S. C., Selective Syntheses of Iron-Imide-Sulfide Cubanes, Including a Partial Representation of the Fe-S-X Environment in the FeMo Cofactor *J. Am. Chem. Soc.* **2010**, *132*, 15884-15886.
(110) Chen, X. –D.; Zhang, W.; Duncan, J. S.; Lee, S. C., Iron–Amide–Sulfide and Iron–Imide–Sulfide Clusters: Heteroligated Core Environments Relevant to the Nitrogenase FeMo Cofactor, *Inorg. Chem.* **2012**, *51*, 12891-12904.
(111) Churchill, M. R.; Wormald, J.; Knight, J.; Mays, M. J. Synthesis and Crystallographic Characterization of Bis(tetramethylammonium) Carbidohexadecacarbonylhexaferrate, a Hexanuclear Carbidocarbonyl Derivative of Iron. *J. Am. Chem. Soc.* **1971**, *93*, 3073−3074. (b)
(112) Churchill, M. R.; Wormald, J. Crystal and Molecular Structure of Tetramethylammonium Carbidohexadecacarbonylhexaferrate(2−), $[Me_4N]_2[Fe_6(CO)_{16}C]$, a Hexanuclear Iron Cluster Complex with an Encapsulated Six-Co-ordinate Carbon Atom. *J. Chem. Soc., Dalton Trans.* **1974**, 2410−2415.
(113) Liu, L.; Rauchfuss, T. B.; Wood, T. J., Iron-Carbide-Sulfide Carbonyl Clusters, *Inorg. Chem.* **2019**, 58, 8271-8274.
(114) Bogdan, P. L.; Sabat, M.; Sunshine, S. A.; Woodcock, C.; Shriver, D. F. Anionic Iron Carbido Carbonyl Clusters with Sulfur Dioxide Ligands. *Inorg. Chem.* **1988**, *27*, 1904−1910.
(115) Ohki, Y.; Ikagawa, Y.; Tatsumi, K. Synthesis of New [8Fe-7S] Clusters: A Topological Link between the Core Structures of P-Cluster, FeMo-co, and FeFe-co of Nitrogenases. *J. Am. Chem. Soc.* **2007**, *129*, 10457–10465.

(116) Hashimoto, T.; Ohki, Y.; Tatsumi, K. Synthesis of Coordinatively Unsaturated Mesityliron Thiolate Complexes and Their Reactions with Elemental Sulfur. *Inorg. Chem.* **2010**, *49*, 6102–6109.
(117) O'Sullivan, T.; Millar, M. M. Synthesis and study of an analog for the [Fe4S4]3+ center of oxidized high potential iron-sulfur proteins. *J. Am. Chem. Soc.* **1985**, *107*, 4096−4097.
(118) Ohki, Y.; Tanifuji, K.; Yamada, N.; Imada, M.; Tajima, T.; Tatsumi, K. Synthetic analogues of $[Fe_4S_4(Cys)_3(His)]$ in hydrogenases and $[Fe_4S_4(Cys)_4]$ in HiPIP derived from all-ferric $[Fe_4S_4\{N(SiMe_3)_2\}_4]$. *Proc. Natl. Acad. Sci. U.S.A.* **2011**, *108*, 12635−12640.
(119) Tanifuji, K.; Yamada, N.; Tajima, T.; Sasamori, T.; Tokitoh, N.; Matsuo, T.; Tamao, K.; Ohki, Y.; Tatsumi, K. A Convenient Route to Synthetic Analogues of the Oxidized Form of High-Potential Iron–Sulfur Proteins. *Inorg. Chem.* **2014**, *53*, 4000-4009.
(120) Moula, G.; Matsumoto, T.; Miehlich, M. E.; Meyer, K.; Tatsumi, K. Synthesis of an All-Ferric Cuboidal Iron–Sulfur Cluster $[Fe^{III}_4S_4(SAr)_4]$, *Angew. Chem. Int. Ed.* **2018**, *57*, 11594-11597.
(121) Spatzal, T.; Schlesier, J.; Burger, E. M.; Sippel, D.; Zhang, L.; Andrade, S. L. A.; Rees, D. C.; Einsle, O. Nitrogenase FeMoco investigated by spatially resolved anomalous dispersion refinement. *Nat. Commun*. **2016**, *7*, 10902.
(122) Lee, H. I.; Hales, B. J.; Hoffman, B. M. Metal-Ion Valencies of the FeMo Cofactor in CO-Inhibited and Resting State Nitrogenase by ^{57}Fe Q-Band ENDOR. *J. Am. Chem. Soc.* **1997**, *119*, 11395–11400.
(123) Bjornsson, R.; Lima, F. A.; Spatzal, T.; Weyhermüller, T.; Glatzel, P.; Bill, E.; Einsle, O.; Neese, F.; DeBeer, S. Identification of a spin-coupled Mo(III) in the nitrogenase iron–molybdenum cofactor. *Chem. Sci*. **2014**, *5*, 3096–3103.
(124) Siemann, S.; Schneider, K.; Drötboom, M.; Müller, A., The Fe-only nitrogenase and the Mo nitrogenase from *Rhodobacter capsulatus*: A comparative study on the redox properties of the metal clusters present in the dinitrogenase components *Eur. J. Biochem.* **2002**, *269*, 1650-1661.
(125) Orme-Johnson, W. H.; Hamilton, W. D.; Jones, T. L.; Tso, M. –Y. W.; Burris, R. H.; Shah, V. K.; Brill, W. J., Electron Paramagnetic Resonance of Nitrogenase and Nitrogenase Components from *Clostridium pasteurianum W5* and *Azotobacter vinelandii OP*, *Proc. Natl. Acad. Sci. U.S.A.* **1972**, *69*, 3142-3145.
(126) Smith, B. E.; Lowe, D. J.; Bray, R. C., Studies by electron paramagnetic resonance on the catalytic mechanism of nitrogenase of *Klebsiella pneumonia*, *Biochem. J.* **1973**, *135*, 331-341.
(127) Lowe, D. J.; Eady, R. R.; Thorneley, R. N. F., Electron-paramagnetic-resonance studies on nitrogenase of *Klebsiella pneumoniae*. Evidence for acetylene- and ethylene-nitrogenase transient complexes, *Biochem. J.* **1978**, *173*, 277-290.
(128) Hu, Y.; Fay, A. W.; Ribbe, M. W. *Proc. Natl. Acad. Sci. U. S. A*. **2005**, *102*, 3236–3241.
(129) Ohta, S.; Ohki, Y.; Hashimoto, T.; Cramer, R. E.; Tatsumi, K. A Nitrogenase Cluster Model $[Fe_8S_6O]$ with an Oxygen Unsymmetrically Bridging Two Proto-Fe_4S_3 Cubes: Relevancy to the Substrate Binding Mode of the FeMo Cofactor. *Inorg. Chem*. **2012**, *51*, 11217–11219.
(130) Smith, B. E.; Durrant, M. C.; Fairhurst, S. A.; Gormal, C. A.; Grönberg, K. L. C.; Henderson, R. A.; Ibrahim, S. K.; Le Gall, T.; Pickett, C. J., Exploring the reactivity of the isolated iron-molybdenum cofactor of nitrogenase, *Coord. Chem. Rev.* **1999**, *185–186*, 669–687.
(131) For organic substrates of nitrogenases, see: Seefeldt, L. C.; Yang, Z. Y.; Duval, S.; Dean, D. R. Nitrogenase reduction of carbon-containing compounds. *Biochim. Biophys. Acta* **2013**, *1827*, 1102–1111.
(132) Brown, K. A.; Harris, D. F.; Wilker, M. B.; Rasmussen, A.; Khadka, N.; Hamby, H.; Keable, S.;

Dukovic, G.; Peters, J. W.; Seefeldt, L. C.; King, P. W. Light-driven dinitrogen reduction catalyzed by a CdS:nitrogenase MoFe protein biohybrid. *Science* **2016**, *352*, 448–450.
(133) Barney, B. M.; McClead, J.; Lukoyanov, D.; Laryukhin, M.; Yang, T. C.; Dean, D. R.; Hoffman, B. M.; Seefeldt, L. C. Diazene (HN=NH) Is a Substrate for Nitrogenase: Insights into the Pathway of N_2 Reduction. *Biochemistry* **2007**, *46*, 6784–6794.
(134) Davis, L. C. Hydrazine as a substrate and inhibitor of Azotobacter vinelandii nitrogenase. *Arch. Biochem. Biophys*. **1980**, *204*, 270–276.
(135) Danyal, K.; Rasmussen, A. J.; Keable, S. M.; Inglet, B. S.; Shaw, S.; Zadvornyy, O. A.; Duval, S.; Dean, D. R.; Raugei, S.; Peters, J. W.; Seefeldt, L. C. Fe Protein-Independent Substrate Reduction by Nitrogenase MoFe Protein Variants. *Biochemistry* **2015**, *54*, 2456–2462.
(136) Danyal, K.; Inglet, B. S.; Vincent, K. A.; Barney, B. M.; Hoffman, B. M.; Armstrong, F. A.; Dean, D. R.; Seefeldt, L. C. Uncoupling Nitrogenase: Catalytic Reduction of Hydrazine to Ammonia by a MoFe Protein in the Absence of Fe Protein-ATP. *J. Am. Chem. Soc*. **2010**, *132*, 13197–13199.
(137) Dilworthl, M. J.; Thorneley, R. N. F. Nitrogenase of *Klebsiella pneumoniae*. Hydrazine is a product of azide reduction. *Biochem. J*. **1981**, *193*, 971–983.
(138) Rubinson, J. F.; Burgess, B. K.; Corbin, J. L.; Dilworthl, M. J. Nitrogenase reactivity: azide reduction. *Biochemistry* **1985**, *24*, 273–283.
(139) Jensen, B. B.; Burris, R. H. Nitrous oxide as a substrate and as a competitive inhibitor of nitrogenase. *Biochemistry* **1986**, *25*, 1083–1088.
(140) Vaughn, S. a; Burgess, B. K. *Biochemistry* **1989**, *28*, 419–424.
(141) Rebelein, J. G.; Hu, Y.; Ribbe, M. W. Differential Reduction of CO_2 by Molybdenum and Vanadium Nitrogenases. *Angew. Chem. Int. Ed*. **2014**, *53*, 11543–11546.
(142) Yang, Z.-Y.; Moure, V. R.; Dean, D. R.; Seefeldt, L. C. Carbon dioxide reduction to methane and coupling with acetylene to form propylene catalyzed by remodeled nitrogenase. *Proc. Natl. Acad. Sci. U. S. A*. **2012**, *109*, 19644–19648.
(143) Seefeldt, L. C.; Ensign, S. A.; Rasche, M. E. Carbonyl sulfide and carbon dioxide as new substrates, and carbon disulfide as a new inhibitor, of nitrogenase. *Biochemistry* **1995**, *34*, 5382–5389.
(144) Hu, Y.; Lee, C. C.; Ribbe, M. W. Extending the Carbon Chain: Hydrocarbon Formation Catalyzed by Vanadium/Molybdenum Nitrogenases. *Science* **2011**, *333*, 753–755.
(145) (a) Li, J.; Burgess, B. K.; Corbin, J. L. Nitrogenase reactivity: cyanide as substrate and inhibitor. *Biochemistry* **1982**, *21*, 4393–4402. (b) Kelly, M.; Postgate, J. R.; Richards, R. L. Reduction of Cyanide and Isocyanide by Nitrogenase of *Azotobacter chroococcum*. *Biochem. J.* **1967**, *102*, 1C–3C.
(146) Roth, L. E.; Tezcan, F. A. ATP-Uncoupled, Six-Electron Photoreduction of Hydrogen Cyanide to Methane by the Molybdenum–Iron Protein. *J. Am. Chem. Soc*. **2012**, *134*, 8416–8419.
(147) Miller, R. W.; Eady, R. R. Cyanamide: a new substrate for nitrogenase. *Biochim. Biophys. Acta* **1988**, *952*, 290-296.
(148) Rubinson, J. F.; Corbin, J. L.; Burgess, B. K. Nitrogenase reactivity: methyl isocyanide as substrate and inhibitor. *Biochemistry* **1983**, *22*, 6260–6268.
(149) Rasche, M. E.; Seefeldt, L. C. Reduction of Thiocyanate, Cyanate, and Carbon Disulfide by Nitrogenase: Kinetic Characterization and EPR Spectroscopic Analysis. *Biochemistry* **1997**, *36*, 8574–8585.
(150) Fuchsman, W. H.; Hardy, R. W. F. Nitrogenase-catalyzed acrylonitrile reductions. *Bioinorg. Chem*. **1972**, *1*, 195–213.

(151) Lee, C. C.; Hu, Y.; Ribbe, M. W. Unique features of the nitrogenase VFe protein from *Azotobacter vinelandii. Proc. Natl. Acad. Sci. U. S. A*. **2009**, *106*, 9209–9214.
(152) Lee, C. C.; Hu, Y.; Ribbe, M. W. Vanadium Nitrogenase Reduces CO. *Science* **2010**, *329*, 642.
(153) Schneider, K.; Müller, A. In Catalyst for Nitrogen Fixation: Nitrogenases, Relevant Chemical Models, and Commercial Processes; Scmith, B. E., Richards, R, L., Newton, W. E., Eds.; Springer-Science+Business Media Dordrecht: Berlin/Heidelberg, 2004; pp 281–307.
(154) Zheng, Y.; Harris, D. F.; Yu, Z.; Fu, Y.; Poudel, S.; Ledbetter, R. N.; Fixen, K. R.; Yang, Z. Y.; Boyd, E. S.; Lidstrom, M. E.; Seefeldt, L. C.; Harwood, C. S. A pathway for biological methane production using bacterial iron-only nitrogenase. *Nat. Microbiol*. **2018**, *3*, 281–286.
(155) Lee, C. C.; Hu, Y.; Ribbe, M. W. Catalytic Reduction of CN^-, CO, and CO_2 by Nitrogenase Cofactors in Lanthanide ‐ Driven Reactions. *Angew. Chem. Int. Ed*. **2015**, *54*, 1219–1222.
(156) Lee, C. C.; Hu, Y.; Ribbe, M. W. ATP-Independent Formation of Hydrocarbons Catalyzed by Isolated Nitrogenase Cofactors. *Angew. Chem. Int. Ed*. **2012**, *51*, 1947–1949.
(157) Lee, C. C.; Hu, Y.; Ribbe, M. W. Insights into Hydrocarbon Formation by Nitrogenase Cofactor Homologs. *MBio* **2015**, *6*, e00307-15.
(158) Lee, C. C.; Hu, Y.; Ribbe, M. W. Reduction and Condensation of Aldehydes by the Isolated Cofactor of Nitrogenase. *ACS Cent. Sci*. **2018**, *4*, 1430–1435.
(159) Shah, V. K.; Chisnell, J. R.; Brill, W. J. Acetylene reduction by the iron-molybdenum cofactor from nitrogenase. *Biochem. Biophys. Res. Commun*. **1978**, *81*, 232–236.
(160) Bazhenova, T. A.; Bazhenova, M. A.; Mironova, S. A.; Petrova, G. N.; Shilova, A. K.; Shuvalova, N. I.; Shilov, A. E. Catalytic reduction of acetylene in the presence of molybdenum and iron clusters, including FeMo cofactor of nitrogenase. *Inorg. Chim. Acta* **1998**, *270*, 221–226.
(161) Bazhenova, T. A.; Bazhenova, M. A.; Petrova, G. N.; Shilova, A. K.; Shilov, A. E. Catalytic reduction of acetylene and dinitrogen with the participation of the iron-molybdenum cofactor of nitrogenase and synthetic polynuclear molybdenum(iii) complexes. *Russ. Chem. Bull*. **1998**, *47*, 861–867.
(162) Bazhenova, T. A.; Bazhenova, M. A.; Petrova, G. N.; Mironova, S. A.; Strelets, V. V. Catalytic behavior of the nitrogenase iron-molybdenum cofactor extracted from the enzyme in the reduction of C_2H_2 under nonenzymatic conditions. *Kinet. Catal*. **2000**, *41*, 499–510.
(163) Bazhenova, T. A.; Bardina, N. V.; Petrova, G. N.; Borovinskaya, M. A. Effect of the potential of an external electron donor on C_2H_2 reduction catalyzed by the nitrogenase active center (FeMoco) isolated from the enzyme. *Russ. Chem. Bull*. **2004**, *53*, 1646–1654.
(164) Mori, H.; Seino, H.; Hidai, M.; Mizobe, Y. Isolation of a Cubane-Type Metal Sulfido Cluster with a Molecular Nitrogen Ligand. *Angew. Chem. Int. Ed*. **2007**, *46*, 5431–5434.
(165) Osman, R.; Pattison, D. I.; Perutz, R. N.; Bianchini, C.; Casares, J. A.; Peruzzini, M. Photochemistry of $M(PP_3)H_2$ (M = Ru, Os; $PP_3 = P(CH_2CH_2PPh_2)_3$): Preparative, NMR, and Time-Resolved Studies. *J. Am. Chem. Soc*. **1997**, *119*, 8459–8473.
(166) Ohki, Y.; Uchida, K.; Tada, M.; Cramer, R. E.; Ogura, T.; Ohta, T. N_2 activation on a molybdenum–titanium–sulfur cluster. *Nat. Commun*. **2018**, *9*, 3200.
(167) Pearce, R. A. R.; Levin, I. W.; Harris, W. C., Raman spectra and vibrational potential function of polycrystalline azomethane and azomethane-d_6. *J. Chem. Phys.* **1973**, *59*, 1209–1216.
(168) Gulaczyk, I.; Kreglewski, M.; Valentin, A., The N-N stretching band of hydrazine. *J. Mol. Spectr.* **2003**, *220*, 132–136.
(169) Almenningen, A.; Anfinsen, I. M.; Haaland, A., An electron diffraction study of azomethane,

CH_3NNCH_3, *Acta Chem. Scand.* **1970**, *24*, 1230–1234.
(170) Ohki, Y.; Uchida, K.; Hara, R.; Kachi, M.; Fujisawa, M.; Tada, M.; Sakai, Y.; Sameera, W. M. C. Cubane-Type $[Mo_3S_4M]$ Clusters with First‐Row Groups 4–10 Transition-Metal Halides Supported by C_5Me_5 Ligands on Molybdenum. *Chem. Eur. J.* **2018**, *24*, 17138-17147.
(171) Ohki, Y.; Hara, R.; Munakata, K.; Tada, M.; Takayama, T.; Sakai, Y.; Cramer, R. E. Synthesis of $[Mo_3S_4]$ Clusters from Half-Sandwich Molybdenum(V) Chlorides and Their Application as Platforms for $[Mo_3S_4Fe]$ Cubes. *Inorg. Chem.* **2019**, *58*, 5230-5240.
(172) Takei, I.; Suzuki, K.; Enta, Y.; Dohki, K.; Suzuki, T.; Mizobe, Y.; Hidai, M., Synthesis of a New Family of Heterobimetallic Tetranuclear Sulfido Clusters with $Mo_2Ni_2S_x$ (x = 4 or 5) or $Mo_3M'S_4$ (M' = Ru, Ni, Pd) Cores, *Organometallics* **2003**, *22*, 1790-1792.
(173) Takei, I.; Wakebe, Y.; Suzuki, K.; Enta, Y.; Suzuki, T.; Mizobe, Y.; Hidai, M., Synthesis of ubane-Type Mo_3NiS_4 Clusters and Their Catalytic Activity for the Cyclization of Alkynoic Acids to Enol Lactones *Organometallics* **2003**, *22*, 4639-4641.
(174) Takei, I.; Dohki, K.; Kobayashi, K.; Suzuki, T.; Hidai, M., Cleavage of Hydrazine N-N Bonds by $RuMo_3S_4$ Cubane-Type Clusters, *Inorg. Chem.* **2005**, *44*, 3768-3770.
(175) Takei, I.; Enta, Y.; Wakebe, Y.; Suzuki, T.; Hidai, M., Intramolecular Cyclization of Aminoalkynes Catalyzed by $PdMo_3S_4$ Cubane Clusters, *Chem. Lett.* **2006**, *35*, 590-591.
(176) Chen, P.; Chen, Y.; Zhou, Y.; Peng, Y.; Qu, J.; Hidai, M., Heterometallic cubane-type clusters $[M'Mo_3S_4]$ (M' = Au, Ag and Cu): synthesis, structures and electrochemical properties, *Dalton Trans.* **2010**, *39*, 5658-5663.
(177) Rink, B.: Brorson, M.; Scowen, I. J., New Heterometallic Cubane-Like Clusters $[\{(\eta^5\text{-}Cp)Mo\}_3S_4\{M'(CO)_3\}](pts)$ (M' = Cr, Mo, W; pts = *p*-Toluenesulfonate) Obtained by Ligand Substitution Reactions and Insertion of $\{M'(CO)_3\}$ Fragments, *Organometallics* **1999**, *18*, 2309-2313.
(178) Herbst, K.; Rink, B.; dahlenburg, L.; Brorson, M., Heterobimetallic Cubane-like Cluster Compounds Prepared as the Homologous Series $[(\eta^5\text{-}Cp')_3Mo_3S_4M'(PPh_3)]^+$ (M' = Ni, Pd, Pt). Crystal Structures Show that Platinum Is Smaller than Palladium, *Organometallics* **2001**, *20*, 3655-3660.
(179) Herbst, K.; Monari, M.; Brorson, M., Heterobimetallic, Cubane-like Mo_3S_4M' Cluster Cores Containing the Noble Metals M' = Ru, Os, Rh, Ir. Unprecedented Tri(μ-carbonyl) Bridge Between Ruthenium Atoms in $[\{(\eta^5\text{-}Cp')_3Mo_3S_4Ru\}_2(\mu\text{-}CO)_3]^{2+}$, *Inorg. Chem.* **2001**, *40*, 2979-2985.
(180) Herbst, K.; Monari, M.; Brorson, M., Molecular Metal Sulfide Cluster Model for Substrate Binding to Oil-Refinery Hydrodesulfurization Catalysts, *Inorg. Chem.* **2002**, *41*, 1336-1338.
(181) Herbst, K.; Monari, M.; Brorson, M., Facile formation of a heterobimetallic cluster with a cubane-like $[Mo_3S_4Cu]^{5+}$ core, *Inorg. Chim. Acta* **2004**, *357*, 895-899.
(182) Herbst, K.; Söderhjelm, E.; Nordlander, E.; Dahlenburg, L.; Brorson, M., Variation of the electron population by four units in the cluster series $[(\eta^5\text{-}Cp')_3Mo_3S_4Co(L)]^{n+}$ (L = I, CO, PPh_3, NO; n = 0, 1), *Inorg. Chim. Acta* **2007**, *360*, 2697-2703.
(183) Tanifuji, K.; Tajima, S.; Ohki, Y.; Tatsumi, K. Interconversion between $[Fe_4S_4]$ and $[Fe_2S_2]$ Clusters Bearing Amide Ligands. *Inorg. Chem.* **2016**, *55*, 4512-4518.
(184) Scott, T. A; Berlinguette, C. P; Holm, R. H; Zhou, H. –C, Initial synthesis and structure of an all-ferrous analogue of the fully reduced $[Fe_4S_4]^0$ cluster of the nitrogenase iron protein. *Proc. Natl. Acad. Sci. U.S.A.* **2005**, *102*, 9741–9744.
(185) Deng, L.; Holm, R. H., Stabilization of fully reduced iron-sulfur clusters by carbene ligation: the $[Fe_nS_n]^0$ oxidation levels (n = 4, 8). *J. Am. Chem. Soc.* **2008**, *130*, 9878–9886.

(186) Ogino, H.; Inomata, S.; Tobita, H. Abiological Iron-Sulfur Clusters, *Chem. Rev.* **1998**, *98*, 2093-2121.
(187) Luo, Y. –R. *in* Comprehensive Handbook of Chemical Bond Energies; CRC Press; Taylor & Francis: Boca Raton, FL, 2007.
(188) Harris, D. F.; Lukoyanov, D. A.; Kallas, H.; Trncik, C.; Yang, Z. -Y.; Compton, P.; Kelleher, N.; Einsle, O.; Dean, D. R.; Hoffman, B. M. et al. Mo-, V-, and Fe-Nitrogenases Use a Universal Eight-Electron Reductive-Elimination Mechanism To Achieve N_2 Reduction. *Biochemistry* **2019**, *58*, 3293-3301.
(189) Herskovitz, T.; Averill, B. A.; Holm, R. H.; Ibers, J. A.; Phillips, W. D.; Weiher, J. F. Structure and Properties of a Synthetic Analogue of Bacterial Iron-Sulfur Proteins. *Proc. Natl. Acad. Sci. U. S. A*. **1972**, *69*, 2437–2441.
(190) Schrauzer, G. N.; Kiefer, G. W.; Tano, K.; Doemeny, P. A. Chemical evolution of a nitrogenase model. VII. Reduction of nitrogen. *J. Am. Chem. Soc*. **1974**, *96*, 641–652.
(191) Schrauzer, G. N.; Robinson, P. R.; Moorehead, E. L.; Vickrey, T. M. The chemical evolution of a nitrogenase model. XI. Reduction of molecular nitrogen in molybdocyanide systems. *J. Am. Chem. Soc*. **1976**, *98*, 2815–2820.
(192) Schrauzer, G. N., Nonenzymatic Simulation of Nitrogenase Reactions and the Mechanism of Biological Nitrogen Fixation, *Angew. Chem. Int. Ed.* **1975**, *14*, 514-522.
(193) van Tamelen, E. E.; Gladysz, J. A.; Miller, J. S. Nonenzymic nitrogen fixation by an iron-molybdenum model for nitrogenase. *J. Am. Chem. Soc*. **1973**, *95*, 1347–1348.
(194) van Tamelen, E. E.; Gladysz, J. A.; Brúlet, C. R. Biological and abiological nitrogen fixation by molybdenum-bound N2/4Fe-4S cluster systems. *J. Am. Chem. Soc*. **1974**, *96*, 3020–3021.
(195) Brûlet, C. R.; van Tamelen, E. E. Ammonia formation from molybdenum-bound dinitrogen under weakly reducing protic conditions. *J. Am. Chem. Soc*.**1975**, *97*, 911–912.
(196) Balch, A. L. Electron-Transfer Series Involving Sulfur-Rich, Polynuclear Iron Dithiolene Complexes. *J. Am. Chem. Soc.* **1969**, *91*, 6962-6967.
(197) Tanaka, K.; Hozumi, Y.; Tanaka, T. Dinitrogen Fixation Catalyzed by the reduced Species of $[Fe_4S_4(SPh)_4]^{2-}$ and $[Mo_2Fe_6S_8(SPh)_9]^{3-}$. *Chem. Lett*. **1982**, 1203–1206.
(198) Bazhenova, T. A.; Shilov, A. E., Nitrogen fixation in solution, *Coord. Chem. Rev*. **1995**, *144*, 69–145.
(199) Shilov, A. E., Catalytic reduction of molecular nitrogen in solutions, *Russ. Chem. Bull.* **2003**, *52*, 2555-2562.
(200) Henderson, R. A., Mechanistic Studies on Synthetic Fe-S-Based Clusters and Their Relevance to the Action of Nitrogenases, *Chem. Rev.* **2005**, *105*, 2365-2437.
(201) Cramer, S. P.; Hodgson, K. O.; Gillum, W. O.; Mortenson, L. E. The Molybdenum Site of Nitrogenase. Preliminary Structural Evidence from X-Ray Absorption Spectroscopy *J. Am. Chem. Soc*. **1978**, *100*, 3398–3407.
(202) Madden, M. S.; Krezel, A. M.; Allen, R. M.; Ludden, P. W.; Shah, V. K. Plausible structure of the iron-molybdenum cofactor of nitrogenase *Proc. Natl. Acad. Sci*. **1992**, *89*, 6487–6491.
(203) McMillan, R. S.; Renaud, J.; Reynolds, J. G.; Holm, R. H. Biologically Related Iron-sulfur Clusters as Reaction Centers. Reduction of Acetylene to Ethylene in Systems Based on $[Fe_4S_4(SR)_4]^{3-}$ *J. Inorg. Biochem*. **1979**, *11*, 213–227.
(204) Grönberg, K. L.; Henderson, R. A.; Oglieve, K. E. A Unified Mechanism for the Stoichiometric Reduction of H^+ and C_2H_2 by $[Fe_4S_4(SPh)_4]^{3-}$ in MeCN *J. Chem. Soc., Dalton Trans*. **1998**, 3093–3104.

(205) Nakamura, A.; Kamada, M.; Sugihashi, K.; Otsuka, S. Molybdenum–sulfur Chelates as Catalysts in the Reductive Cleavage of Azobenzene by Electron Donors in Protic Media *J. Mol. Catal*. **1980**, *8*, 353–367.
(206) Yoshimoto, K.; Yatabe, T.; Matsumoto, T.; Tran, V. –H.; Robertson, A.; Nakai, H.; Asazawa, K.; Tanaka, H.; Ogo, S. Inorganic clusters with a $[Fe_2MoOS_3]$ core - a functional model for acetylene reduction by nitrogenases. *Dalton Trans.* **2016**, *45*, 14620-14627.
(207) Tanaka, K.; Tanaka, T. Reduction of Acetylene to Ethylene Catalyzed by the Reduced Species of $[Fe_4S_4(SPh)_4]^{2-}$ and $[Mo_2Fe_6S_9(SPh)_8]^{3-}$: A Model Reaction to Nitrogenase *Chem. Lett*. **1981**, 895–898.
(208) Tanaka, K.; Nakamoto, M.; Tsunomori, M.; Tanaka, T. Raman Spectra of the Adducts of Reduced Species of $[Fe_4S_4(SPh)_4]^{2-}$ and $[Mo_2Fe_6S_8(SPh)_9]^{3-}$ with Acetylene *Chem. Lett*. **1987**, 613–616.
(209) Tanaka, K.; Honjo, M.; Tanaka, T. Catalytic Reduction of Acetylene by the Reduced Species of $[Fe_4S_4L_4]^{2-}$ (L = SCH_2CH_2OH, SPh), $[Mo_2Fe_6S_8(SC_2H_5)_3(SCH_2CH_2OH)_6]^{3-}$ and $[Mo_2Fe_6S_8(SPh)_9]^{3-}$ *J. Inorg. Biochem*. **1984**, *22*, 187–199.
(210) Tanaka, M.; Tanaka, K.; Tanaka, T. Absorption of Dihydrogen by $[Fe_4S_4(SPh)_4]^{2-}$and $[Mo_2Fe_6S_8(SPh)_9]^{3-}$, and the H–D Exchange Reaction between H_2 and D_2 Catalyzed by the Reduced Species of These Clusters. *Chem. Lett*. **1982**, 767–770.
(211) Hozumi, Y.; Imasaka, Y.; Tanaka, K.; Tanaka, T. Catalytic Reduction of Hydrazine to Ammonia by the Reduced Species of $[Mo_2Fe_6S_8L_9]^{3-}$ and $[Fe_4S_4L_4]^{2-}$ (L = SPh, SCH_2CH_2OH) *Chem. Lett*. **1983**, 897–900.
(212) Tanaka, K.; Imasaka, Y.; Tanaka, M.; Honjo, M.; Tanaka, T. Reduction of CH_3NC and CH_3CN by the Reduced Species of $[Fe_4S_4(SPh)_4]^{2-}$ and $[Mo_2Fe_6S_8(SPh)_9]^{3-}$: Model Reactions to Nitrogenase *J. Am. Chem. Soc*. **1982**, *104*, 4258–4260.
(213) Imasaka, Y.; Tanaka, K.; Tanaka, T. The Catalytic Reduction of N^{3-} to NH_3 by the Reduced Species of $[Fe_4S_4L_4]^{2-}$, $[Mo_2Fe_6S_8L_9]^{3-}$ (L = SCH_2CH_2OH), and a Related Anion in H_2O or in MeOH/THF: Evidence for the Formation of N_2H_2 and N_2H_4 as Intermediates *Chem. Lett*. **1983**, 1477–1480.
(214) Tanaka, K.; Kuwabata, S.; Denno, S.; Tanaka, T. Reduction of N^{3-} by $[Mo_2Fe_6S_8(SPh)_9]^{3-}$ Modified Glassy Carbon Electrode—Model Study of Nitrogenase *Bull. Chem. Soc. Jpn*. **1989**, *62*, 1561–1566.
(215) Kuwabata, S.; Hozumi, Y.; Tanaka, K.; Tanaka, T. Multielectron Reduction of Alkylazide by a $(n\text{-}Bu_4N)_3[Mo_2Fe_6S_8(SPh)_9]$-modified Glassy Carbon Electrode *Chem. Lett*. **1985**, 401–404.
(216) Kuwabata, S.; Tanaka, K.; Tanaka, T. Multielectron Reductions of Alkyl Azides with $[Mo_2Fe_6S_8(SPh)_9]^{3-}$ and $[Mo_2Fe_6S_8(\mu\text{-}SEt)_3(SCH_2CH_2OH)_6]^{3-}$ in Homogeneous Systems and with a $(Bu_4N)_3[Mo_2Fe_6S_8(SPh)_9]$ Modified Glassy-carbon Electrode in Water *Inorg. Chem*. **1986**, *25*, 1691–1697.
(217) Kuwabata, S.; Uezumi, S.; Tanaka, K.; Tanaka, T. Assimilatory and Dissimilatory Reduction of NO^{3-} and NO^{2-} with an $(n\text{-}Bu_4N)_3[Mo_2Fe_6S_8(SPh)_9]$ Modified Glassy-Carbon Electrode in Water *Inorg. Chem*. **1986**, *25*, 3018–3022.
(218) Coucouvanis, D.; Mosier, P. E.; Demadis, K. D.; Patton, S.; Malinak, S. M.; Kim, C. G.; Tyson, M. A. The Catalytic Reduction of Hydrazine to Ammonia by the $MoFe_3S_4$ Cubanes and Implications Regarding the Function of Nitrogenase. Evidence for Direct Involvement of the Molybdenum Atom in Substrate Reduction *J. Am. Chem. Soc*. **1993**, *115*, 12193–12194.
(219) Coucouvanis, D.; Demadis, K. D.; Malinak, S. M.; Mosier, P. E.; Tyson, M. A.; Laughlin, L. J.

Catalytic and Stoichiometric Multielectron Reduction of Hydrazine to Ammonia and Acetylene to Ethylene with Clusters that Contain the MFe_4S_4 Cores (M = Mo, V). Relevance to the Function of Nitrogenase *J. Mol. Catal. A Chem*. **1996**, *107*, 123–135.
(220) Thorhallsson, A. T.; Bjornsson, R. Computational Mechanistic Study of $[MoFe_3S_4]$ Cubanes for Catalytic Reduction of Nitrogenase Substrates *Inorg. Chem*. **2019**, *58*, 1886–1894.
(221) Mosier, P. E.; Kim, C. G.; Coucouvanis, D. Synthesis, Structural Characterization, and Properties of Singly Bridged Double Cubanes Containing Two $[(Cl_4\text{-cat})MoFe_3S_4Cl_3]^{2-}$ Subunits and Hydrazine or Pyrazine Bridges *Inorg. Chem*. **1993**, *32*, 2620–2621.
(222) Coucouvanis, D.; Challen, P. R.; Koo, S. man; Davis, W. M.; Butler, W.; Dunham, W. R. Stepwise Synthesis and Structural Characterization of The $\{[MoFe_3S_4Cl_2(Cl_4cat)]_2(\mu_2\text{-}S)_2\}^{6-}$ And $\{[MoFe_3S_4Cl_2(Cl_4cat)]_2(\mu_2\text{-}S)(\mu_2\text{-}OH)\}_5$-Doubly Bridged Double Cubanes Obtained By the Coupling of $[MoFe_3S_4]$ Clusters *Inorg. Chem*. **1989**, *28*, 4181–4183.
(223) Challen, P. R.; Koo, S. M.; Kim, C. G.; Dunham, W. R.; Coucouvanis, D. Nitrogenase Substrates as Intercluster Bridging Units between the Mo Atoms in Doubly Bridged, Double Cubanes. The Synthesis and Characterization of the $[\{MoFe_3S_4Cl_2(Cl_4cat)\}_2(\mu_2\text{-}S)(\mu_2\text{-}L)]^{n-}$ Anions ($L = N_2H_4$, $n = 4$; $L = CN^-$, $n = 5$) *J. Am. Chem. Soc*. **1990**, *112*, 8606–8607.
(224) Demadis, K. D.; Malinak, S. M.; Coucouvanis, D. Catalytic Reduction of Hydrazine to Ammonia with $MoFe_3S_4$−Polycarboxylate Clusters. Possible Relevance Regarding the Function of the Molybdenum-Coordinated Homocitrate in Nitrogenase *Inorg. Chem*. **1996**, *35*, 4038–4046.
(225) Spatzal, T.; Perez, K. A.; Einsle, O.; Howard, J. B.; Rees, D. C. Ligand binding to the FeMo-cofactor: Structures of CO-bound and reactivated nitrogenase. *Science* **2014**, *345*, 1620-1623.
(226) Malinak, S. M.; Demadis, K. D.; Coucouvanis, D. Catalytic Reduction of Hydrazine to Ammonia by the VFe_3S_4 Cubanes. Further Evidence for the Direct Involvement of the Heterometal in the Reduction of Nitrogenase Substrates and Possible Relevance to the Vanadium Nitrogenases *J. Am. Chem. Soc*. **1995**, *117*, 3126–3133.
(227) Malinak, S. M.; Simeonov, A. M.; Mosier, P. E.; McKenna, C. E.; Coucouvanis, D. Catalytic Reduction of *cis*-Dimethyldiazene by the $[MoFe_3S_4]^{3+}$ Clusters. The Four-electron Reduction of a N=N Bond by a Nitrogenase-relevant Cluster and Implications for the Function of Nitrogenase *J. Am. Chem. Soc*. **1997**, *119*, 1662–1667.
(228) Laughlin, L. J.; Coucouvanis, D. Use of $[MoFe_3S_4]^{3+}$ Single Cubanes in the Catalytic Reduction of Acetylene to Ethylene and Ethane. Identification of Molybdenum and Iron Atoms as Catalytic Sites during Substrate Reduction and Implications of Nitrogenase Action. *J. Am. Chem. Soc.* **1995**, *117*, 3118-3125.
(229) Tezuka, M.; Yajima, T.; Tsuchiya, A.; Matsumoto, Y.; Uchida, Y.; Hidai, M. Electroreduction of Carbon Dioxide Catalyzed by Iron-Sulfur Clusters $[Fe_4S_4(SR)_4]^{2-}$ *J. Am. Chem. Soc*. **1982**, *104*, 6834–6836.
(230) Tomohiro, T.; Uoto, K.; Okuno, H. Electrochemical reduction of carbon dioxide catalysed by macrocyclic Fe_4S_4 iron–sulphur clusters *J. Chem. Soc., Chem. Commun.* **1990**, 194-195.
(231) Kuwabata, S.; Uezumu, S.; Tanaka, K.; Tanaka, T. Reduction of NO_3^- Giving NH_3 Using a $(Bu^n{}_4N)_3[Mo_2Fe_6S_8(SPh)_9]$-modified Glassy Carbon Electrode *J. Chem. Soc., Chem. Commun*. **1986**, 135-136.
(232) Tanaka, K.; Matsui, T.; Tanaka, T. Assimilatory and Dissimilatory Reductions of NO_n^- (n = 2, 3) Catalyzed by MoFeS Cluster *Chem. Lett*. **1989**, 1827–1830.
(233) Tanaka, K.; Wakita, R.; Tanaka, T. Carbon Dioxide Fixation Coupled with Nitrite Reduction,

Catalyzed by 4Fe4S Cluster *Chem. Lett*. **1987**, 1951–1954.
(234) Tanaka, K.; Wakita, R.; Tanaka, T. Electrochemical Carboxylation Coupled with Nitrite Reduction Catalyzed by $[Fe_4S_4(SPh)_4]^{2-}$ and $[Mo_2Fe_6S_8(SPh)_9]^{3-}$ *J. Am. Chem. Soc*. **1989**, *111*, 2428–2433.
(235) Tanaka, K.; Matsui, T.; Tanaka, T. Catalytic Formation of α-Keto Acids by Artificial CO_2 Fixation *J. Am. Chem. Soc*. **1989**, *111*, 3765–3767.
(236) Komeda, N.; Nagao, H.; Matsui, T.; Adachi, G.; Tanaka, K. Electrochemical Carbon Dioxide Fixation to Thioesters Catalyzed by $[Mo_2Fe_6S_8(SEt)_9]^{3-}$ *J. Am. Chem. Soc*. **1992**, *114*, 3625–3630.
(237) Nagao, H.; Miyamoto, H.; Tanaka, K. Carbon Dioxide Fixation Competed with Proton Addition to Methyl Acrylate *Chem. Lett*. **1991**, 323–326.
(238) Rebelein, J. G.; Stiebritz, M. T.; Lee, C. C.; Hu, Y. Activation and Reduction of Carbon Dioxide by Nitrogenase Iron Proteins *Nat. Chem. Biol*. **2016**, *13*, 147–149.
(239) Stiebritz, M. T.; Hiller, C. J.; Sickerman, N. S.; Lee, C. C.; Tanifuji, K.; Ohki, Y.; Hu, Y. Ambient Conversion of CO_2 to Hydrocarbons by Biogenic and Synthetic $[Fe_4S_4]$ Clusters *Nat. Catal*. **2018**, *1*, 444–451.
(240) Hill, C. L.; Renaud, J.; Holm, R. H.; Mortenson, L. E. Synthetic Analogues of the Active Sites of Iron-sulfur Proteins. 15. Comparative Polarographic Potentials of the $[Fe_4S_4(SR)_4]^{2-,3-}$ and *Clostridium pasteurianum* Ferredoxin Redox Couples *J. Am. Chem. Soc*. **1977**, *99*, 2549–2557.
(241) Barclay, J. E.; Davies, S. C.; Evans, D. J.; Hughes, D. L.; Longhurst, S. Lattice Effects in the Mössbauer Spectra of Salts of $[Fe_4S_4\{S(CH_2)_nOH\}_4]^{2-}$. Crystal Structures of $[PPh_4]_2[Fe_4S_4\{S(CH_2)_nOH\}_4]$ (n = 2, 3 and 4) *Inorg. Chim. Acta* **1999**, *291*, 101–108.
(242) Ye, M.; Thompson, N. B.; Brown, A. C.; Suess, D. L. M. A Synthetic Model of Enzymatic $[Fe_4S_4]$ –Alkyl Intermediates. *J. Am. Chem. Soc.* **2019**, *141*, 13330-13335.
(243) Hagen, K. S.; Watson, A. D.; Holm, R. H. Synthetic Routes to Fe_2S_2, Fe_3S_4, Fe_4S_4, and Fe_6S_9 Clusters from the Common Precursor $[Fe(SC_2H_5)_4]^{2-}$: Structures and Properties of $[Fe_3S_4(SR)_4]^{3-}$ and $[Fe_6S_9(SC_2H_5)_2]^{4-}$, Examples of the Newest Types of Fe–S–SR Clusters *J. Am. Chem. Soc*. **1983**, *105*, 3905–3913.
(244) Sickerman, N. S.; Tanifuji, K.; Lee, C. C.; Ohki, Y.; Tatsumi, K.; Ribbe, M. W.; Hu, Y. Reduction of C_1 Substrates to Hydrocarbons by the Homometallic Precursor and Synthetic Mimic of the Nitrogenase Cofactor *J. Am. Chem. Soc*. **2017**, *139*, 603–606.
(245) Tanifuji, K.; Lee, C. C.; Ohki, Y.; Tatsumi, K.; Hu, Y.; Ribbe, M. W. Combining a Nitrogenase Scaffold and a Synthetic Compound into an Artificial Enzyme, *Angew. Chem. Int. Ed* **2015**, *54*, 14022-14025.
(246) Hernandez-Molina, R.; Sokolov, M. N.; Sykes, A. G. Behavioral Patterns of Heterometallic Cuboidal Derivatives of $[M_3Q_4(H_2O)_9]^{4+}$ (M = Mo, W; Q = S, Se) *Acc. Chem. Res*. **2001**, *34*, 223–230.
(247) Llusar, R.; Uriel, S. Heterodimetallic Chalcogen-bridged Cubane-type Clusters of Molybdenum and Tungsten Containing First-row Transition Metals *Eur. J. Inorg. Chem*. **2003**, 1271–1290.
(248) Hidai, M.; Kuwata, S.; Mizobe, Y. Synthesis and Reactivities of Cubane-type Sulfido Clusters Containing Noble Metals *Acc. Chem. Res*. **2000**, *33*, 46–52.
(249) Seino, H.; Masumori, T.; Hidai, M.; Mizobe, Y. Synthesis of Bimetallic Cubane-type $Mo_2M_2S_4$ Clusters (M = Ir, Rh, Ru) and Reductive Cleavage of the N-N Bond of 1,1-Methylphenylhydrazine Affording *N*-methylaniline Using $Mo_2Ir_2S_4$ and $Mo_2Rh_2S_4$ Clusters as Catalyst Precursors *Organometallics* **2003**, *22*, 3424–3431.
(250) Yandulov, D. V.; Schrock, R. R. Catalytic Reduction of Dinitrogen to Ammonia at a Single

Molybdenum Center. *Science* **2003**, *301*, 76-78.
(251) Arashiba, K.; Miyake, Y.; Nishibayashi, Y. A molybdenum complex bearing PNP-type pincer ligands leads to the catalytic reduction of dinitrogen into ammonia. *Nat. Chem.* **2011**, *3*, 120-125.
(252) Anderson, J. S.; Rittle, J.; Peters, J. C. Catalytic conversion of nitrogen to ammonia by an iron model complex. *Nature* **2013**, 501, 84–87.
(253) Del Castillo, T. J.; Thompson, N. B.; Peters, J. C. A Synthetic Single-Site Fe Nitrogenase: High Turnover, Freeze-Quench ^{57}Fe Mössbauer Data, and a Hydride Resting State *J. Am. Chem. Soc.* **2016**, *138*, 5341-5350.
(254) Chalkley, M. J.; Del Castillo, T. J.; Matson, B. D.; Roddy, J.; Peters, J. C. Catalytic N_2-to-NH_3 Conversion by Fe at Lower Driving Force: A Proposed Role for Metallocene-Mediated PCET. *ACS Cent. Sci.* **2017**, *3*, 217-223.
(255) Arashiba, K.; Eizawa, A.; Tanaka, H.; Nakajima, K.; Yoshizawa, K. and Nishibayashi, Y. Catalytic Nitrogen Fixation via Direct Cleavage of Nitrogen–Nitrogen Triple Bond of Molecular Dinitrogen under Ambient Reaction Conditions. *Bull. Chem. Soc. Jpn.* **2017**, *90*, 1111-1118.
(256) Ashida, Y.; Arashiba, K.; Nakajima, K.; Nishibayashi, Y. Molybdenum-Catalysed Ammonia Production with Samarium Diiodide and Alcohols or Water. *Nature* **2019**, *568***,** 536-540.
(257) Kraatz, H. B.; Jacobsen, H.; Ziegler, T.; Boorman, P. M. π-Acidity of thioethers and selenoethers: truth or fiction? A comparative density functional study. *Organometallics* **1993**, *12*, 76–80.
(258) Sellmann, D.; Sutter, J. In Quest of Competitive Catalysts for Nitrogenases and Other Metal Sulfur Enzymes. *Acc. Chem. Res*. **1997**, *30*, 460–469.
(259) Stiefel, E. I. *in* Transition Metal Sulfur Chemistry: Biological and Industrial Significance and Key Trends. In *Transition Metal Sulfur Chemistry*; Stiefel, E. I., Matsumoto, K. Eds.; ACS Symposium Series; American Chemical Society: Washington, DC, 1996.
(260) (a) Pauleta, S. R.; Dell'Acqua, S.; Moura, I. Nitrous oxide reductase, *Coord. Chem. Rev.* **2013**, *257*, 332-349. (b) Johnson, B. J.; Antholine, W. E.; Lindeman, S. V.; Graham, M. J.; Mankad, N. P. A One-Hole Cu_4S Cluster with N_2O Reductase Activity: A Structural and Functional Model for Cu_Z, *J. Am. Chem. Soc.* **2016**, *138*, 13107-13110.
(261) Rodriguez, M. M.; Bill, E.; Brennessel, W. W.; Holland, P. L. N_2 Reduction and Hydrogenation to Ammonia by a Molecular Iron-Potassium Complex. *Science* **2011**, 334, 780–783.
(262) Hazari. N. Homogeneous iron complexes for the conversion of dinitrogen into ammonia and hydrazine. *Chem. Soc. Rev.*, **2010**, *39*, 4044–4056.
(263) Sacco, A.; Aresta, M. Nitrogen fixation: hydrido-and hydrido-nitrogen-complexes of iron (II). *Chem. Commun.* **1968**, 1223-1224.
(264) Bart, S. C.; Lobkovsky, E.; Bill, E.; Wieghardt, K.; Chirik, P. J. Neutral-Ligand Complexes of Bis(imino)pyridine Iron: Synthesis, Structure, and Spectroscopy. *Inorg. Chem*. **2007**, *46*, 7055–7063.
(265) Takaoka, A.; Mankad, N. P.; Peters, J. C. Dinitrogen Complexes of Sulfur-Ligated Iron. *J. Am. Chem. Soc*. **2011**, *133*, 8440–8443.
(266) Lee, Y.; Mankad, N. P.; Peters, J. C. Triggering N_2 uptake via redox-induced expulsion of coordinated NH_3 and N_2 silylation at trigonal bipyramidal iron. *Nat. Chem.* **2010**, *2*, 558-565.
(267) Zhang, F.; Song, H.; Zhuang, X.; Tung, C.; Wang, W. Iron-Catalyzed 1,2-Selective Hydroboration of N-Heteroarenes. *J. Am. Chem. Soc*. **2017**, *139*, 17775–17778.
(268) Gu, N. X.; Oyala, P. H.; Peters, J. C. An S = 1/2 Iron Complex Featuring N_2, Thiolate, and

Hydride Ligands: Reductive Elimination of H_2 and Relevant Thermochemical Fe–H Parameters. *J. Am. Chem. Soc*. **2018**, *140*, 6374–6382.
(269) Creutz, S. E.; Peters, J. C. Diiron Bridged-Thiolate Complexes That Bind N_2 at the $Fe^{II}Fe^{II}$, $Fe^{II}Fe^{I}$, and $Fe^{I}Fe^{I}$ Redox States. *J. Am. Chem. Soc*. **2015**, *137*, 7310–7313.
(270) Čorić, I.; Mercado, B. Q.; Bill, E.; Vinyard, D. J.; Holland, P. L. Binding of dinitrogen to an iron–sulfur–carbon site. *Nature* **2015**, *526*, 96–99.
(271) Speelman, A. L.; Čorić, I.; Stappen, C. V.; DeBeer, S.; Mercado, B. Q.; Holland, P. L. Nitrogenase-Relevant Reactivity of a Synthetic Iron–Sulfur–Carbon Site, *J. Am. Chem. Soc.* **2019**, *141*, 13148-13157.
(272) Araake, R.; Sakadani, K.; Tada, M.; Sakai, Y.; Ohki, Y. [Fe_4] and [Fe_6] Hydride Clusters Supported by Phosphines: Synthesis, Characterization, and Application in N_2 Reduction. *J. Am. Chem. Soc*. **2017**, *139*, 5596–5606.
(273) Ohki, Y.; Araki, Y.; Tada, M.; Sakai, Y. Synthesis and Characterization of Bioinspired [Mo_2Fe_2]–Hydride Cluster Complexes and Their Application in the Catalytic Silylation of N_2. *Chem. Eur. J*. **2017**, *23*, 13240–13248.
(274) Siedschlag, R. B.; Bernales, V.; Vogiatzis, K. D.; Planas, N.; Clouston, L. J.; Bill, E.; Gagliardi, L.; Lu, C. C. Catalytic Silylation of Dinitrogen with a Dicobalt Complex. *J. Am. Chem. Soc.* **2015**, *137*, 4638-4641.
(275) Sellmann, D.; Hautsch, B.; Rösler, A.; Heinemann, F. W. [$Ru(N_2)(PiPr_3)(`N_2Me_2S_2')$]: Coordination of Molecular N_2 to Metal Thiolate Cores under Mild Conditions. *Angew. Chem. Int. Ed*. **2001**, *40*, 1505–1507.
(276) Sellmann, D.; Hille, A.; Rösler, A.; Heinemann, F. W.; Moll, M. Phosphane effects on formation and reactivity of [$Ru(L)(PR_3)(`N_2Me_2S_2')$] complexes with L = N_2, N_2H_4, NH_3, and CO. *Inorg. Chim. Acta* **2004**, *357*, 3336–3350.
(277) Sellmann, D.; Hille, A.; Heinemann, F. W.; Moll, M.; Rösler, A.; Sutter, J.; Brehm, G.; Reiher, M.; Brehm, G.; Reiher, M. *et al*. Metal thiolate complexes binding molecular nitrogen under mild conditions: [μ-N_2{$Ru(P^iPr_3)(N_2Me_2S_2)$}$_2$], the first dinuclear example. *Inorg. Chim. Acta* **2003**, *348*, 194–198.
(278) Sellmann, D.; Hille, A.; Rösler, A.; Heinemann, F. W.; Moll, M.; Brehm, G.; Schneider, S.; Reiher, M.; Hess, B. A.; Bauer, W. Binding N_2, N_2H_2, N_2H_4, and NH_3 to Transition-Metal Sulfur Sites: Modeling Potential Intermediates of Biological N_2 Fixation. *Chem. Eur. J*. **2004**, *10*, 819–830.
(279) Cruz-Garritz, D.; Torrens, H.; Leal, J.; Richards, R. L. The reactions of *mer*-[$OsCl_2(N_2)(PMe_2Ph)_3$] with sulphur-containing ligands: X-ray structure of *mer*-[$OsCl(SC_6F_5)(N_2)(PMe_2Ph)_3$. *Transit. Met. Chem*. **1983**, *8*, 127–128.
(280) Cruz-Garritz, D.; Gelover, S.; Torrens, H.; Leal, J.; Richards, R. L. Dinitrogen complexes of osmium(II) with thiolate co-ligands: X-ray structure of *mer*-[$OsCl(SC_6F_5)(N_2)(PMe_2Ph)_3$]. *Dalton Trans.* **1988**, 2393–2396.
(281) Fernández, P.; Sousa-Pedrares, A.; Romero, J.; Durán, M. L.; Sousa, A.; Pérez-Lourido, P.; García-Vázquez, J. A. Synthesis and Structural Characterization of Cobalt, Nickel and CopperPhosphanylthiolato Complexes. *Eur. J. Inorg. Chem*. **2010**, 814–823.
(282) Laplaza, C. E.; Cummins, C. C. Dinitrogen Cleavage by a Three-Coordinate Molybdenum(III) Complex. *Science* **1995**, *268*, 861–863.
(283) Yandulov, D. V.; Schrock, R. R. Reduction of Dinitrogen to Ammonia at a Well-Protected Reaction Site in a Molybdenum Triamidoamine Complex. *J. Am. Chem. Soc*. **2002**, *124*, 6252–6253.

(284) Chatt, J.; Crabtree, R. H.; Dilworth, J. R.; Richards, R. L. Tris(dimethylphenylphosphine)(dinitrogen)(dithiocarbamato)rhenium complexes and their reactions with hydrogen halides. *J. Chem. Soc., Dalton Trans*. **1974**, 2358–2362.
(285) Chatt, J.; Crabtree, R. H.; Jeffrey, E. A.; Richards, R. L. The basic strengths of some dinitrogen complexes of molybdenum(0), tungsten(0), rhenium(I), and osmium(II). *J. Chem. Soc., Dalton Trans*. **1973**, 1167-1172.
(286) Pombeiro, A. J. L.; Hitchcock, P. B.; Richards, R. L. Preparation of isocyanide and mixed dinitrogen–isocyanide complexes of rhenium(I) from reactions of *trans*-[ReCl(N_2)(PMe_2Ph)$_4$], *mer*-[Re(S_2PPh_2)(N_2)(PMe_2Ph)$_3$], or *mer*-[Re(S_2CNEt_2)(N_2)(PMe_2Ph)$_3$] with methyl isocyanide; crystal structure of *mer*-[Re(S_2PPh_2)(N_2)(CNMe)(PMe_2Ph)$_3$]. *Dalton Trans*. **1987**, 319–325.
(287) Dilworth, J. R.; Hu, J.; Thompson, R. M.; Hughes, D. L. A d^4-thiolato–dinitrogen complex. The synthesis and crystal structure of [Re(N_2)(SC_6H_2-2,4,6-Pr^i_3)$_3$(PPh_3)]. *Chem. Commun*. **1992**, 551–553.
(288) Dilworth, J. R.; Hu, J.; Miller, J. R.; Hughes, D. L.; Zubieta, J. A.; Chen, Q. Syntheses and structures of [Re($SC_6H_3Me_2$-2,6)$_3$(PPh_3)], [Re($SC_6H_3Me_2$-2,6)$_3$(Bu^tNC)$_2$], [Re($SC_6H_2Pr^i_3$-2,4,6)$_3$L(PPh_3)](L = N_2 or CO) and [ReH_4(PPh_3)$_4$][ReO($SC_6H_2Pr^i_3$-2,4,6)$_4$]. *Dalton Trans*. **1995**, 3153–3164.
(289) Aresta, M.; Sacco, A. Nitrogen-Fixation 3. Dinitrogen-Complexes, Carbonyl-Complexes, and Hydrido-Complexes of Molybdenum, *Gazz. Chim. Ital.* **1972**, *102*, 755-759.
(290) Morris, R. H.; Ressner, J. M.; Sawyer, J. F.; Shiralian, M. A sulfur-ligated molybdenum complex that reduces dinitrogen to ammonia. The crystal and molecular structure of the dinitrogen-molybdenum complex *trans*-Mo(N_2)$_2$($PMePh_2$)$_2$($PPh_2CH_2CH_2SMe$). *J. Am. Chem. Soc*. **1984**, *106*, 3683–3684.
(291) Yoshida, T.; Adachi, T.; Kaminaka, M.; Ueda, T.; Higuchi, T. A novel molybdenum(0) dinitrogen complex containing crown thio ether as the sole auxiliary ligand: trans-Mo(N_2)$_2$$Me_8$[16]ane$S_4$ (Me_8[16]aneS_4 = 3,3,7,7,11,11,15,15-octamethyl-1,5,9,13-tetrathiacyclohexadecane). *J. Am. Chem. Soc*. **1988**, *110*, 4872–4873.
(292) Seymore, S. B.; Brown, S. N. Kinetic Effects in Heterometallic Dinitrogen Cleavage. *Inorg. Chem*. **2006**, *45*, 9540–9550.
(293) Seymore, S. B.; Brown, S. N. Polar Effects in Nitride Coupling Reactions. *Inorg. Chem*. **2002**, *41*, 462–469.
(294) O'Regan, M. B.; Liu, A. H.; Finch, W. C.; Schrock, R. R.; Davis, W. M. A study of high-oxidation-state complexes of the type [W(η^5-C_5Me_5)Me_2X]$_2$(μ-N_2), including x-ray structures of [W(η^5-C_5Me_5)Me_2(OC_6F_5)]$_2$(μ-N_2) and [W(η^5-C_5Me_5)Me_2(S-2,4,6-$C_6H_2Me_3$)]$_2$(μ-N_2). *J. Am. Chem. Soc.* **1990**, *112*, 4331-4338.
(295) Dilworth, J. R.; Harrison, S. J.; Henderson, R. A.; Walton, D. R. M. The use of $(Me_3Si)_2NN(SiMe_3)_2$ as a reagent for the synthesis of μ-dinitrogen complexes or as a homogeneous one-electron reducing agent. *J. Chem. Soc., Chem. Commun.* **1984**, 176-177.
(296) Dilworth, J. R.; Henderson, R. A.; Hills, A.; Hughes, D. L.; Macdonald, C.; Stephens, A. N.; Walton, D. R. M. The chemistry of niobium and tantalum dithiocarbamato-complexes. Part 1. Synthesis, structure, and protonation of dinitrogen-bridged complexes. *Dalton Trans*. **1990**, 1077–1085.
(297) Schrock, R. R.; Wesolek, M.; Liu, A. H.; Wallace, K. C.; Dewan, J. C. Thiolato dinitrogen (or hydrazido(4-)) complexes, [Ta(SAr)$_3$(THF)]$_2$(μ-N2) (Ar = 2,6-C_6H_3-iso-Pr_2, 2,4,6-C_6H_2-iso-Pr_3), and phenoxide analogs. A structural comparison of [Ta(S-2,6-C_6H_3-iso-Pr_2)$_3$(THF)]$_2$(μ-N_2), and [Ta(O-2,6-

C_6H_3-iso-$Pr_2)_3$(THF)]$_2$(μ-N_2). *Inorg. Chem.* **1988**, *27*, 2050-2054.
(298) Wiberg, N.; Fischer, G.; Bachhuber, H. Darstellung, Struktur und Thermolyse von Diimin. *Chem. Ber.* **1974**, *107*, 1456-1471.
(299) Tang, H. R.; Stanbury, D. M. Direct Detection of Aqueous Diazene: Its UV Spectrum and Concerted Dismutation. *Inorg. Chem.* **1994**, *33*, 1388-1391.
(300) Sellmann, D.; Kunstmann, H.; Knoch, F.; Moll, M. Transition-metal complexes with sulfur ligands. Part 37. Iron, molybdenum, and ruthenium complexes with pentadentate OS4 and NHS_4 ligands combining thiolato, thioether, and ether or amine donor functions: synthesis, structures, and reactivity of carbon monoxide, nitric oxide, trimethylphosphine and hydrazine derivatives. *Inorg. Chem.* **1988**, *27*, 4183-4190.
(301) Sellmann, D.; Soglowek, W.; Knoch, F.; Moll, M. Nitrogenase Model Compounds: [µ-N_2H_2{Fe("N_HS_4")}$_2$], the Prototype for the Coordination of Diazene to Iron Sulfur Centers and Its Stabilization through Strong N-H···S Hydrogen Bonds. *Angew. Chem. Int. Ed*. **1989**, *28*, 1271–1272.
(302) Sellmann, D.; Friedrich, H.; Knoch, F.; Moll, M. Transition Metal Complexes with Sulfur Ligands, C. Unexpectedly Facile Formation of Diazene Complexes and a New Type of Diastereomerism: [µ-N_2H_2{Fe(PPr_3)('S_4')}$_2$] and Analogous Complexes with [FeS]-Centers. ('S_4' = 1,2-Bis(2-mercaptophenylthio)ethane(2-)). *Z. Naturforsch.* **1994**, *49b*, 76–88.
(303) Sellmann, D.; Hennige, A. Direct Proof of *trans*-Diazene in Solution by Trapping and Isolation of the Trapping Products. *Angew. Chem. Int. Ed*. **1997**, *36*, 276–278.
(304) Sellmann, D.; Blum, D. C. F.; Heinemann, F. W. Transition metal complexes with sulfur ligands. Part CLV. Structural and spectroscopic characterization of hydrogen bridge diastereomers of [µ-N_2H_2{Fe(PR_3)('tpS_4')}$_2$] diazene complexes ('tpS_4'$^{2-}$=1,2-bis(2-mercaptophenylthio)phenylene(2−)). *Inorg. Chim. Acta* **2002**, *337*, 1–10.
(305) Sellmann, D.; Hennige, A.; Heinemann, F. W. Transition metal complexes with sulfur ligands part CXXIX. Retention and reactivity of the [Fe=NH=NH=Fe] chromophore in the iron sulfur diazene complex [µ-N_2H_2{Fe(PPr_3)('S_4')}$_2$] in exchange and oxidation processes. ('S_4'$^{2-}$ = 1,2-bis (2-mercaptophenylthio)ethane(2−)). *Inorg. Chim. Acta* **1998**, *280*, 39–49.
(306) Chen, Y.; Zhou, Y.; Chen, P.; Tao, Y.; Li, Y.; Qu, J. Nitrogenase Model Complexes [Cp*Fe(µ-$SR^1)_2$(µ-η^2-R^2N=NH)FeCp*] (R^1 = Me, Et; R^2 = Me, Ph; Cp* = η^5-C_5Me_5): Synthesis, Structure, and Catalytic N−N Bond Cleavage of Hydrazines on Diiron Centers. *J. Am. Chem. Soc.* **2008**, *130*, 15250–15251.
(307) Chen, Y.; Liu, L.; Peng, Y.; Chen, P.; Luo, Y.; Qu, J. Unusual Thiolate-Bridged Diiron Clusters Bearing the *cis*-HN-NH Ligand and Their Reactivities with Terminal Alkynes. *J. Am. Chem. Soc.* **2011**, *133*, 1147-1149.
(308) Li, Y.; Li, Y.; Wang, B.; Luo, Y.; Yang, D.; Tong, P.; Zhao, J.; Luo, L.; Zhou, Y.; Chen, S. *et al*. Ammonia formation by a thiolate-bridged diiron amide complex as a nitrogenase mimic. *Nat. Chem*. **2013**, *5*, 320–326.
(309) Yuki, M.; Miyake, Y.; Nishibayashi, Y. Synthesis of Sulfur- and Nitrogen-Bridged Diiron Complexes and Catalytic Behavior toward Hydrazines. *Organometallics* **2012**, *31*, 2953–2956.
(310) Sellmann, D.; Kreutzer, P.; Huttner, G.; Frank, A. N_2H_4 Coordination on Iron Sulfur Centres: Synthesis and Structure of [$N(C_4H_9)_4]_2$[µ-N_2H_4{Fe($S_2C_6H_4)_2$}$_2$]. *Z. Naturforsch*. **1978**, *33b*, 1341–1346.
(311) Sellmann, D.; Friedrich, H.; Knoch, F. Transition Metal Complexes with Sulfur Ligands, CI*. Synthesis and Structure of N_2H_5[Fe(N_2H_4)($S_2C_6H_4)_2$]·1,33N_2H_4. *Z. Naturforsch*. **1994**, *49b*, 660–664.

(312) Sellmann, D.; Sogiowek, W.; Knoch, F.; Ritter, G.; Dengier, J. Transition-metal complexes with sulfur ligands. 88. Dependence of spin state, structure, and reactivity of [Fe^{II}(L)('NH)S_4']] complexes on the coligand L (L = CO, N_2H_2, N_2H_4, NH_3, pyridine, $NHCH_3NH_2$, CH_3OH, THF, $P(OCH_3)_3$, $P(OPh)_3$): model complexes for iron nitrogenases ('$NHS_4'^{2-}$ = dianion of 2,2'-bis[(2-mercaptophenyl)thio]diethylamine). *Inorg. Chem*. **1992**, *31*, 3711–3717.
(313) Sellmann, D.; Blum, N.; Heinemann, F. W. Transition Metal Complexes with Sulphur Ligands, Part 151 [1]. Ligand Enforced Configurations and Low-Spin States of [$FeNS_4$] Cores in [Fe^{II}(L)('pyS_4')] Complexes with σ and σ-π Ligands (L = N_2H_4, pyridine, PMe_3, $PnPr_3$; '$pyS_4'^{2-}$ = 2,6-bis(2-mercaptophenylthiomethyl)pyridine(2-)). *Z. Naturforsch*. **2001**, *56b*, 581–588.
(314) Chang, Y. H.; Chan, P. M.; Tsai, Y. F.; Lee, G. H.; Hsu, H. F. Catalytic Reduction of Hydrazine to Ammonia by a Mononuclear Iron(II) Complex on a Tris(thiolato)phosphine Platform. *Inorg. Chem*. **2014**, *53*, 664–666.
(315) Liminga, R.; Olovsson, I. The crystal structure of hydrazine monohydrate. *Acta Crystallogr*. **1964**, *17*, 1523-1528.
(316) Collin, R. L.; Lipscomb, W. N. The crystal structure of hydrazine. *Acta Crystallogr*. **1951**, *4*, 10-14.
(317) Vela, J.; Stoian, S.; Flaschenriem, C. J.; Münck, E.; Holland, P. L. A Sulfido-Bridged Diiron(II) Compound and Its Reactions with Nitrogenase-Relevant Substrates. *J. Am. Chem. Soc*. **2004**, *126*, 4522–4523.
(318) Rodriguez, M. M.; Stubbert, B. D.; Scarborough, C. C.; Brennessel, W. W.; Bill, E.; Holland, P. L. Isolation and Characterization of Stable Iron(I) Sulfide Complexes. *Angew. Chem. Int. Ed*. **2012**, *51*, 8247–8250.
(319) Anderson, J. S.; Peters, J. C. Low-Spin Pseudotetrahedral Iron(I) Sites in Fe_2(μ-S) Complexes. *Angew. Chem. Int. Ed.* **2014**, *53*, 5978-5981.
(320) Roussin, M. J. Recherches sur les nitrosulfures doubles de fer (nouvelle classe de sels.). *Ann. Chim. Phys.* **1858**, *52*, 285-303.
(321) Sanina, N. A.; Chuev, I. I.; Aldoshin, S. M.; Ovanesyan, N. S.; Strelets, V. V.; Geletii, Y. V. Synthesis, crystal structures, Mössbauer spectra, and redox properties of binuclear and tetranuclear iron-sulfur nitrosyl clusters. *Russ. Chem. Bull.* **2000**, *49*, 444-451.
(322) Lu, T. –T.; Huang, H. –W.; Liaw, W. –F. Anionic Mixed Thiolate–Sulfide-Bridged Roussin's Red Esters $[(NO)_2Fe(\mu\text{-}SR)(\mu\text{-}S)Fe(NO)_2]^-$ (R = Et, Me, Ph): A Key Intermediate for Transformation of Dinitrosyl Iron Complexes (DNICs) to [2Fe-2S] Clusters. *Inorg. Chem.* **2009**, *48*, 9027-9035.
(323) Arnet, N. A.; Dugan, T. R.; Menges, F. S.; Mercado, B. Q.; Brennessel, W. W.; Bill, E.; Johnson, M. A.; Holland, P. L. Synthesis, Characterization, and Nitrogenase-Relevant Reactions of an Iron Sulfide Complex with a Bridging Hydride. *J. Am. Chem. Soc*. **2015**, *137*, 13220–13223.
(324) Arnet, N. A.; McWilliams, S. F.; DeRosha, D. E.; Mercado, B. Q.; Holland, P. L. Synthesis and Mechanism of Formation of Hydride–Sulfide Complexes of Iron. *Inorg. Chem.* **2017**, *56*, 9185-9193.
(325) Stubbert, B. D.; Vela, J.; Brennessel, W. W.; Holland, P. L. A Sulfide-Bridged Diiron(II) Complex with a N_2H_4 Ligand. *Z. Anorg. Allg. Chem*. **2013**, *639*, 1351–1355.
(326) DeRosha, D. E.; Arnet, N. A.; Mercado, B. Q.; Holland, P. L., A [2Fe−1S] Complex That Affords Access to Bimetallic and Higher- Nuclearity Iron−Sulfur Clusters, *Inorg. Chem.* **2019**, *58*, 8829-8834.
(327) DeRosha, D. E.; Chilkuri, V. G.; Stappen, C. V.; Bill, E.; Mercado, B. Q.; DeBeer, S.; Neese, F.; Holland, P. L. Planar three-coordinate iron sulfide in a synthetic [4Fe-3S] cluster with biomimetic reactivity, *Nat. Chem.* **2019**, *11*, 1019-1025.

(328) Zdilla, M. J.; Verma, A. K.; Lee, S. C. Reactivity of a Sterically Hindered Fe(II) Thiolate Dimer with Amines and Hydrazines. *Inorg. Chem*. **2008**, *47*, 11382–11390.
(329) Verma, A. K.; Lee, S. C. Reductive Cleavage of the N–N Bond: Synthesis of Imidoiron(III) Cubanes. *J. Am. Chem. Soc.* **1999**, *121*, 10838-10839.
(330) Zdilla, M. J.; Verma, A. K.; Lee, S. C. Iron-Mediated Hydrazine Reduction and the Formation of Iron-Arylimide Heterocubanes. *Inorg. Chem*. **2011**, *50*, 1551–1562.
(331) Soong, S. –L.; Haln, J. H.; Millar, M. Jr.; Koch, S. A. Nitrosyl Displacement Reactions, C-H Activation, and M-H-C Interactions in Ruthenium Thiolate Compounds. *Organometallics* **1988**, *7*, 556-557.
(332) Xie, M. –H.; Wang, M.; Wu, C. –D. Catalytic Alkenylation of Phenylpyridines with Terminal Alkynes by a [12]Metallacrown-6 Ruthenium(II) Compound. *Inorg. Chem.* **2009**, *48*, 10477-10479.
(333) Sellmann, D.; Böhlen, E.; Waeber, M.; Huttner, G.; Zsolnai, L. [μ-N_2H_2{Ru(PPh_3)dttd}$_2$], the First Diazene Complex with Sulfur-Coordinated Transition Metal Centers (dttd = 2,3,8,9-Dibenzo-1,4,7,10-tetrathiadecane(2⁻)). *Angew. Chem. Int. Ed*. **1985**, *24*, 981–982.
(334) Sellmann, D.; Engl, K.; Heinemann, F. W.; Sieler, J. Coordination of CO, NO, N_2H_2, and Other Nitrogenase Relevant Small Molecules to Sulfur-Rich Ruthenium Complexes with the New Ligand 'tpS_4' = 1,2-Bis(2-mercaptophenylthio)phenylene(2⁻). *Eur. J. Inorg. Chem*. **2000**, 1079–1089.
(335) Sellmann, D.; Kaeppler, J.; Moll, M.; Knoch, F. Transition metal complexes with sulfur ligands. 95. Diazene, hydrazine, ammine and azido complexes with sulfur dominated [Ru(PPh_3)('buS_4')] fragments ('buS_4'$^{2-}$ = 1,2-bis(2-mercapto-3,5-di-tert-butylphenylthio)ethanato(2-)). *Inorg. Chem*. **1993**, *32*, 960–964.
(336) Back, R. A. The preparation, properties and reactions of diimide. *Rev. Chem. Intermed.* **1984**, *5*, 293-323.
(337) Sellmann, D.; Böhlen, E. Syntheses and Reactions of Sulfur Coordinated Ruthenium Complexes. *Z. Naturforsch.* **1982**, *37b*, 1026–1033.
(338) Kawano, M.; Hoshino, C.; Matsumoto, K. Synthesis, properties, and crystal structure of a novel μ-hydrazine-bridged mixed-valence ruthenium(II,III) complex stabilized by hydrazine hydrogen bonds, [RuCl(TMP)$_2$]$_2$(μ-Cl)(μ-N_2H_4)(μ-S_2) (TMP = trimethyl phosphite). *Inorg. Chem*. **1992**, *31*, 5158–5159.
(339) Matsumoto, K.; Koyama, T.; Koide, Y. Oxidation of the Sulfide Ligands to SO_4^{2-} in the Dinuclear Complex {RuCl[P(OMe)$_3$]$_2$}$_2$(μ-S_2)(μ-Cl)(μ-N_2H_4): Synthesis and Characterization of {RuCl[P(OMe)$_3$]$_2$}$_2$(μ-S_2)(μ-Cl)(μ-N_2H_4)$^+$$HSO_4^-$, {RuCl$_2$[P(OMe)$_3$]$_2$}$_2$(μ-S)(μ-$N_2H_4$), and {RuCl[P(OMe)$_3$]$_2$}$_2$(μ-$S_2O_5$)(μ-$N_2H_4$). *J. Am. Chem. Soc*. **1999**, *121*, 10913–10923.
(340) Matsumoto, K.; Hiroyuki, U.; Kawano, M. A Novel Diruthenium(II,III) Complex, [{Ru(AN)(TMP)$_2$}$_2$(μ-S_2)(μ-NH_2NH_2)$_2$](CF_3SO_3)$_3$·Et_2O, with Two Hydrazine Bridges (AN = acetonitrile, TMP = P(OMe)$_3$). *Chem. Lett*. **1994**, *23*, 1215–1218.
(341) Furuhashi, T.; Kawano, M.; Koide, Y.; Somazawa, R.; Matsumoto, K. Structural Studies of the Hydrazine and Ammine Complexes of the Dinuclear Ruthenium Polysulfide Complexes. *Inorg. Chem*. **1999**, *38*, 109–114.
(342) Matsumoto, K.; Matsumoto, T.; Kawano, M.; Ohnuki, H.; Shichi, Y.; Nishide, T.; Sato, T. Syntheses and Crystal Structures of Disulfide-Bridged Binuclear Ruthenium Compounds: The First UV–Vis, Raman, ESR, and XPS Spectroscopic Characterization of a Valence-Averaged Mixed-Valent $Ru^{III}SSRu^{II}$ Core. *J. Am. Chem. Soc*. **1996**, *118*, 3597–3609.

(343) Fátima, M.; Guedes Da Suva, C.; Pombeiro, A. J. L.; Geremia, S.; Zangrando, E.; Calligaris, M.; Zinchenko, A. V.; Kukushkin, V. Y. Unusual pathways for the reaction between [$MCl_2(Me_2SO)_4$] (M = Os, Ru) and hydrazine dihydrochloride: deoxygenation of sulfoxides vs. coordination of hydrazinium. *J. Chem. Soc., Dalton Trans*. **2000**, 1363–1371.
(344) Mashima, K.; Kaneyoshi, H.; Kaneko, S.; Tani, K.; Nakamura, A. Combined Effect of Bulkiness and NH···S Hydrogen Bonding Controls the Formation of Terminal and Bridging Hydrazine Ruthenium(II) Complexes with Thiolate Ligands. *Chem. Lett*. **1997**, *26*, 569–570.
(345) Mashima, K.; Kaneko, S. I.; Tani, K.; Kaneyoshi, H.; Nakamura, A. Synthesis and reactions of coordinatively unsaturated 16-electron chalcogenolate complexes, $Ru(EAr)_2(\eta^6$-arene) and cationic binuclear chalcogenolate complexes, [(η^6-arene)Ru(μ-EPh)$_3$Ru(η^6-arene)]PF_6. *J. Organomet. Chem.* **1997**, *545–546*, 345–356.
(346) Mashima, K.; Kaneyoshi, H.; Kaneko, S.; Mikami, A.; Tani, K.; Nakamura, A. Chemistry of Coordinatively Unsaturated Bis(thiolato)ruthenium(II) Complexes (η^6-arene)$Ru(SAr)_2$ [SAr = 2,6-Dimethylbenzenethiolate, 2,4,6-Triisopropylbenzenethiolate; $(SAr)_2$ = 1,2-Benzenedithiolate; Arene = Benzene, *p*-Cymene, Hexamethylbenzene]. *Organometallics* **1997**, *16*, 1016–1025.
(347) Herberhold, M.; Yan, H.; Milius, W. The 16-electron dithiolene complexes (*p-cymene*)M[$S_2C_2(B_{10}H_{10})$] (M = Ru, Os) containing both η^6-(*p-cymene*) and η^2-(ortho-carborane-dithiolate): adduct formation with Lewis bases, and X-ray crystal structures of (*p-cymene*)Ru[$S_2C_2(B_{10}H_{10})$](L) (L = PPh_3) and {(*p-cymene*)Ru[$S_2C_2(B_{10}H_{10})$]}$_2$(μ-LL) (LL = $Ph_2PCH_2CH_2PPh_2$ and N_2H_4). *J. Organomet. Chem*. **2000**, *598*, 142–149.
(348) Cheung, W. M.; Chiu, W. H.; Williams, I. D.; Leung, W. H. Ruthenium η^6-Hexamethylbenzene Complexes Containing Dichalcogenoimidodiphosphinate Ligands. *Eur. J. Inorg. Chem*. **2009**, *6*, 792–798.
(349) Zhang, Q. F.; Zheng, H.; Wong, W. Y.; Wong, W. T.; Leung, W. H. Ruthenium(II) Ammine and Hydrazine Complexes with $[N(Ph_2PQ)_2]^-$ (Q = S, Se) Ligands. *Inorg. Chem*. **2000**, *39*, 5255–5264.
(350) Pereira, I. A. C.; Lane, N.; Sousa, F. L.; Landan, G.; Nelson-Sathi, S.; Allen, J. F.; Thiergart, T.; Martin, W. F. Early Bioenergetic Evolution. *Phil. Trans. R. Soc. B* **2013**, *368*, 20130088.
(351) Goldford, J. E.; Hartman, H.; Smith, T. F.; Segrè, D. Remnants of an Ancient Metabolism without Phosphate. *Cell* **2017**, *168*, 1126–1134.
(352) Bada, J. L.; Lazcano, A. Some Like It Hot, but not the First Biomolecules. *Science* **2002**, *296*, 1982–1983.
(353) Wächtershäuser, G. From Volcanic Origins of Chemoautotrophic Life to Bacteria, Archaea and Eukarya. *Philos. Trans. R. Soc. B* **2006**, *361*, 1787–1806.
(354) Barge, L. M.; White, L. M. Experimentally Testing Hydrothermal Vent Origin of Life on Enceladus and Other Icy/Ocean Worlds. *Astrobiology* **2017**, *17*, 820–833.
(355) Huber, C.; Wächtershäuser, G. Activated Acetic Acid by Carbon Fixation on (Fe,Ni)S Under Primordial Conditions. *Science* **1997**, *276*, 245–247.
(356) Huber, C.; Wächtershäuser, G. *α*-Hydroxy and *α*-Amino Acids Under Possible Hadean, Volcanic Origin-of-Life Conditions. *Science* **2006**, *314*, 630–632.
(357) Cody, G. D.; Boctor, N. Z.; Filley, T. R.; Hazen, R. M.; Scott, J. H.; Sharma, A.; Yoder Jr., H. S. Primordial Carbonylated Iron-sulfur Compounds and the Synthesis of Pyruvate. *Science* **2000**, *289*, 1337–1339.
(358) Hennet, R. J.-C.; Holm, N. G.; Engel, M. H. Abiotic Synthesis of Amino Acids under Hydrothermal Conditions and the Origin of Life: A Perpetual Phenomenon? *Naturwissenschaften*

1992, *79*, 361-365.
(359) Schulte, M.; Shock, E. Thermodynamics of Strecker Synthesis in Hydrothermal Systems. *Orig. Life Evol. Biosph*. **1995**, *25*, 161-173.
(360) Huber, C.; Wächtershäuser, G. Peptides by Activation of Amino Acids with CO on (Ni,Fe)S Surfaces : Implications for the Origin of Life. *Science* **1998**, *281*, 670–672.
(361) Stüeken, E. E.; Buick, R.; Guy, B. M.; Koehler, M. Isotopic evidence for biological nitrogen fixation by molybdenum-nitrogenase from 3.2 Gyr. *Nature* **2015**, *520*, 666-669.
(362) Kasting, J. F. Earth's Early Atmosphere. *Science* **1993**, *259*, 920-926.
(363) Kasting, J. F.; Sifert, J. L. The Nitrogen Fix. *Nature* **2001**, *412*, 26–27.
(364) Brandes, J. A.; Boctor, N. Z.; Cody, G. D.; Cooper, B. A.; Hazen, R. M.; Yoder, H. S. Jr Abiotic nitrogen reduction on the early Earth. *Nature* **1998**, *395*, 365–367.
(365) Rickard, D.; Luther III, G. W. Chemistry of Iron Sulfides, *Chem. Rev.* **2007**, *107*, 514-562.
(366) Raymond, J.; Siefert, J. L.; Staples, C. R.; Blankenship, R. E. The natural history of nitrogen fixation. *Mol. Biol. Evol*. **2004**, *21*, 541–554.
(367) Drobner, E.; Huber, H.; Wächtershäuser, G.; Rose, D.; Stetter, K. O. Pyrite formation linked with hydrogen evolution under anaerobic conditions. *Nature* **1990**, *346*, 742–744.
(368) Schoonen, M. A. A.; Xu, Y. Nitrogen Reduction Under Hydrothermal Vent Conditions: Implications for the Prebiotic Synthesis of C-H-O-N Compounds. *Astrobiology* **2001**, *1*, 133–142.
(369) Dörr, M.; Käßpbohrer, J.; Grunert, R.; Kreisel, G.; Brand, W. A.; Werner, R. A.; Geilmann, H.; Apfel, C.; Robl, C.; Weigand, W. A Possible Prebiotic Formation of Ammonia from Dinitrogen on Iron Sulfide Surfaces. *Angew. Chem. Int. Ed*. **2003**, *42*, 1540–1543.
(370) Niño, M. A.; Flores, E.; Sánchez, C.; Rojo, J. M. Reactivity of a FeS Surface under Room Temperature Exposure to Nitrogen and H_2S. *J. Phys. Chem. B* **2018**, *122*, 705–712.
(371) Medford, A. J.; Hatzell, M. C. Photon-Driven Nitrogen Fixation: Current Progress, Thermodynamic Considerations, and Future Outlook. *ACS Catal*. **2017**, *7*, 2624–2643.
(372) Chen, X.; Li, N.; Kong, Z.; Ong, W. J.; Zhao, X. Photocatalytic fixation of nitrogen to ammonia: state-of-the-art advancements and future prospects. *Mater. Horizons* **2018**, *5*, 9–27.
(373) Bag, S.; Trikalitis, P. N.; Chupas, P. J.; Armatas, G. S.; Kanatzidis, M. G. Porous Semiconducting Gels and Aerogels from Chalcogenide Clusters. *Science* **2007**, *317*, 490–493.
(374) Yuhas, B. D.; Smeigh, A. L.; Samuel, A. P. S.; Shim, Y.; Bag, S.; Douvalis, A. P.; Wasielewski, M. R.; Kanatzidis, M. G. Biomimetic Multifunctional Porous Chalcogels as Solar Fuel Catalysts. *J. Am. Chem. Soc.* **2011**, *133*, 7252–7255.
(375) Yuhas, B. D.; Prasittichai, C.; Hupp, J. T.; Kanatzidis, M. G. Enhanced Electrocatalytic Reduction of CO_2 with Ternary Ni-Fe_4S_4 and Co-Fe_4S_4-Based Biomimetic Chalcogels. *J. Am. Chem. Soc*. **2011**, *133*, 15854–15857.
(376) Yuhas, B. D.; Smeigh, A. L.; Douvalis, A. P.; Wasielewski, M. R. ; Kanatzidis, M. G. Photocatalytic Hydrogen Evolution from FeMoS-Based Biomimetic Chalcogels. *J. Am. Chem. Soc.* **2012**, *134*, 10353–10356.
(377) Shim, Y.; Yuhas, B. D.; Dyar, S. M.; Smeigh, A. L.; Douvalis, A. P.; Wasielewski, M. R.; Kanatzidis, M. G. Tunable Biomimetic Chalcogels with Fe_4S_4 Cores and $[Sn_nS_{2n+2}]^{4-}$(n = 1, 2, 4) Building Blocks for Solar Fuel Catalysis. *J. Am. Chem. Soc.* **2013**, *135*, 2330–2337.
(378) Banerjee, A.; Yuhas, B. D.; Margulies, E. A.; Zhang, Y.; Shim, Y.; Wasielewski, M. R.; Kanatzidis, M. G. Photochemical Nitrogen Conversion to Ammonia in Ambient Conditions with FeMoS-Chalcogels *J. Am. Chem. Soc.* **2015**, *137*, 2030–2034.

(379) Liu, J.; Kelley, M. S.; Wu, W.; Banerjee, A.; Douvalis, A. P.; Wu, J.; Zhang, Y.; Schatz, G. C.; Kanatzidis, M. G. Nitrogenase-mimic iron-containing chalcogels for photochemical reduction of dinitrogen to ammonia. *Proc. Natl. Acad. Sci*. **2016**, *113*, 5530–5535.
(380) Scheiner, D. Determination of ammonia and Kjeldahl nitrogen by indophenol method. *Water Res*. **1976**, *10*, 31−36.
(381) Searle, P. L. The berthelot or indophenol reaction and its use in the analytical chemistry of nitrogen. A review. *Analyst* **1984**, *109*, 549−568.
(382) Li, X.-B.; Tung, C.-H.; Wu, L.-Z. Semiconducting quantum dots for artificial photosynthesis, *Nat. Rev. Chem*. **2018**, *2*, 160–173.
(383) Zhou, J.; Yang, Y.; Zhang, C. Y. Toward Biocompatible Semiconductor Quantum Dots: From Biosynthesis and Bioconjugation to Biomedical Application. *Chem. Rev*. **2015**, *115*, 11669–11717.
(384) Miyama, H.; Fujii, N.; Nagae, Y. Heterogeneous photocatalytic synthesis of ammonia from water and nitrogen. *Chem. Phys. Lett*. **1980**, *74*, 523–524.
(385) Hu, S.; Chen, X.; Li, Q.; Zhao, Y.; Mao, W. Effect of sulfur vacancies on the nitrogen photofixation performance of ternary metal sulfide photocatalysts. *Catal. Sci. Technol*. **2016**, *6*, 5884–5890.
(386) Cao, Y.; Hu, S.; Li, F.; Fan, Z.; Bai, J.; Lu, G.; Wang, Q. Photofixation of atmospheric nitrogen to ammonia with a novel ternary metal sulfide catalyst under visible light. *RSC Adv*. **2016**, *6*, 49862–49867.
(387) Hu, S.; Li, Y.; Li, F.; Fan, Z.; Ma, H.; Li, W.; Kang, X. Construction of g-C_3N_4/$Zn_{0.11}Sn_{0.12}Cd_{0.88}S_{1.12}$ Hybrid Heterojunction Catalyst with Outstanding Nitrogen Photofixation Performance Induced by Sulfur Vacancies. *ACS Sustainable Chem. Eng*. **2016**, *4*, 2269–2278.
(388) Zhang, Q.; Hu, S.; Fan, Z.; Liu, D.; Zhao, Y.; Ma, H.; Li, F. Preparation of g-C_3N_4/ZnMoCdS hybrid heterojunction catalyst with outstanding nitrogen photofixation performance under visible light via hydrothermal post-treatment. *Dalton Trans*. **2016**, *45*, 3497–3505.
(389) Lu, M.; Pei, Z.; Weng, S.; Feng, W.; Fang, Z.; Zheng, Z.; Huang, M.; Liu, P. Constructing atomic layer g-C_3N_4–CdS nanoheterojunctions with efficiently enhanced visible light photocatalytic activity. *Phys. Chem. Chem. Phys*. **2014**, *16*, 21280–21288.
(390) Lashgari, M.; Zeinalkhani, P. Ammonia photosynthesis under ambient conditions using an efficient nanostructured FeS_2/CNT solar-energy-material with water feedstock and nitrogen gas. *Nano Energy* **2018**, *48*, 361–368.
(391) Khan, M. M. T.; Bhardwaj, R. C.; Bhardwaj, C. Catalytic Fixation of Nitrogen by the Photocatalytic CdS/Pt/RuO_2 Particulate System in the Presence of Aqueous [Ru(Hedta)N_2]⊖ Complex. *Angew. Chem. Int. Ed*. **1988**, *27*, 923–925.
(392) Ye, L.; Han, C.; Ma, Z.; Leng, Y.; Li, J.; Ji, X.; Bi, D.; Xie, H.; Huang, Z. Ni_2P loading on $Cd_{0.5}Zn_{0.5}S$ solid solution for exceptional photocatalytic nitrogen fixation under visible light. *Chem. Eng. J*. **2017**, *307*, 311–318.
(393) Brown, K. A.; Harris, D. F.; Wilker, M. B.; Rasmussen, A.; Khadka, N.; Hamby, H.; Keable, S.; Dukovic, G.; Peters, J. W.; Seefeldt, L. C. *et al*. Light-driven dinitrogen reduction catalyzed by a CdS:nitrogenase MoFe protein biohybrid. *Science* **2016**, *352*, 448–450.
(394) Brown, K. A.; Rumbles, G.; Dayal, S.; Ai, X.; King, P. W. Controlled Assembly of Hydrogenase-CdTe Nanocrystal Hybrids for Solar Hydrogen Production. *J. Am. Chem. Soc.* **2010**, *132*, 9672–9680.
(395) Brown, K. A.; Wilker, M. B.; Boehm, M.; Dukovic, G.; King, P. W. Characterization of Photochemical Processes for H_2 Production by CdS Nanorod–[FeFe] Hydrogenase Complexes. *J.*

Am. Chem. Soc. **2012**, *134*, 5627–5636.
(396) Lanzilotta, W. N.; Seefeldt, L. C. Changes in the Midpoint Potentials of the Nitrogenase Metal Centers as a Result of Iron Protein−Molybdenum-Iron Protein Complex Formation. *Biochemistry* **1997**, *36*, 12976–12983.
(397) Roth, L. E.; Nguyen, J. C.; Tezcan, F. A. ATP- and Iron−Protein-Independent Activation of Nitrogenase Catalysis by Light. *J. Am. Chem. Soc*. **2010**, *132*, 13672–13674.
(398) Sun, S.; Li, X.; Wang, W.; Zhang, L.; Sun, X. Photocatalytic robust solar energy reduction of dinitrogen to ammonia on ultrathin MoS_2. *Appl. Catal. B: Environmental* **2017**, *200*, 323-329.
(399) Kyriakou, V.; Garagounis, I.; Vasileiou, E.; Vourros, A.; Stoukides, M. Progress in the Electrochemical Synthesis of Ammonia. *Catal. Today* **2017**, *286*, 2-13.
(400) Guo, C.; Ran, J.; Vasileff, A.; Qiao, S. –Z. Rational design of electrocatalysts and photo(electro)catalysts for nitrogen reduction to ammonia (NH_3) under ambient conditions. *Energy Environ. Sci.* **2018**, *11*, 45-56.
(401) Liu, H.; Wei, L.; Liu, F.; Pei, Z.; Shi, J.; Wang, Z. –J.; He, D.; Chen, Y. Homogeneous, Heterogeneous, and Biological Catalysts for Electrochemical N_2 Reduction toward NH_3 under Ambient Conditions. *ACS Catal.* **2019**, *9*, 5245-5267.
(402) Furuya, N.; Yoshiba, H. Electroreduction of nitrogen to ammonia on gas-diffusion electrodes loaded with inorganic catalyst. *J. Electroanal. Chem.* **1990**, *291*, 269-272.
(403) Zhang, L.; Ji, X.; Ren, X.; Ma, Y.; Shi, X.; Tian, Z.; Asiri, A. M.; Chen, L.; Tang, B.; Sun, X. Electrochemical Ammonia Synthesis via Nitrogen Reduction Reaction on a MoS_2 Catalyst: Theoretical and Experimental Studies. *Adv. Mater.* **2018**, *30*, 1800191.
(404) Zhao, X.; Lan, Z.; Yu, D.; Fu, H.; Liu, Z.; Mu, T. Deep eutectic-solvothermal synthesis of nanostructured Fe_3S_4 for electrochemical N_2 fixation under ambient conditions. *Chem. Commun.* **2018**, *54*, 13010-13013.
(405) Chen, P.; Zhang, N.; Wang, S.; Zhou, T.; Tong, Y.; Ao, C.; Yan, W.; Zhang, L.; Chu, W.; Wu, C. *et al*. Interfacial engineering of cobalt sulfide/graphene hybrids for highly efficient ammonia electrosynthesis. *Proc. Natl. Acad. Sci. U.S.A.* **2019**, *116*, 6635-6640.